Investigating Clonal Interactions and Field Effects in Colorectal Adenomas

Viola Walther

Thesis submitted for the degree of Doctor of Philosophy at the University of London

Primary supervisor: Dr. Stuart McDonald

Secondary supervisor: Dr. Trevor A. Graham

Institute/Department: Barts Cancer Institute, Centre for Tumour Biology

University: Barts and The London School of Medicine and Dentistry, Queen Mary University of London, UK

Declaration

I, Viola Walther, confirm that the work presented in this thesis is my own. Where information has been derived from other sources, I confirm that this has been indicated in the thesis.

Viola Walther
November 2018

Abstract

According to the somatic mutation theory of carcinogenesis, tumours are derived from a single mutated cell that clonally expands into a neoplasm. However, studies on familial adenomatous polyposis (FAP) colonic adenomas and some sporadic microadenomas have revealed tumours that are *polyclonal in origin* – they are derived from more than one clone. This has questioned the current dogma of how colonic tumours are initiated; however the mechanisms of how polyclonality is generated are unknown. Studies using chimeric mice have suggested that polyclonal adenomas arise through crosstalk between unique clones in close physical proximity. In this project, the local microenvironment surrounding human adenomas was characterised by investigating the non-dysplastic crypts in close proximity to adenomas, in particular their mutation burden, DNA damage status, crypt stem cell dynamics and the cellular makeup of the stroma.

Immunohistochemistry was used to quantify cell proliferation (Ki67), DNA damage (γH2AX) and Wnt signalling status (nuclear β-catenin) in non-dysplastic crypts, stratified according to their physical distance from the nearest dysplastic crypt. Normal crypts within 250μm of an adenoma displayed increased cell proliferation, DNA damage and Wnt signalling. These effects were associated with an increase in T cell, macrophage and fibroblast infiltrate in the non-dysplastic stroma, however the concentration of intraepithelial CD8 T cells in dysplastic crypts showed a significant decrease. Furthermore, cytochrome *c* oxidase histochemistry (a marker of mitochondrial DNA (mtDNA) mutations - a proxy for mutation pressure on crypts) was used to demonstrate that crypts neighbouring an adenoma contained a higher mutation burden. Furthermore, the proximity of a crypt to an adenoma also affected stem cell dynamics: using somatic mtDNA mutations to trace clonal lineages, it was found that human intestinal stem cell evolution in adenomas and surrounding normal crypts followed neutral drift dynamics.

The effects of an adenoma on gene expression in normal epithelium were investigated using murine organoid cultures. Wild type (WT) organoids when grown in the presence of fibroblasts previously exposed to mutant $Apc^{1322/+}$ organoids demonstrated a significant upregulation of the MAPK, JAK/STAT and Wnt pathway when compared to WT only. Moreover, *Tnf-α*, *MMP9* and collagen genes were found to be upregulated in exposed WT.

To conclude, clonal interactions between dysplastic and non-dysplastic epithelium driving clonal expansion were demonstrated: adenomas create a field effect, dysplastic crypts exert mutagenic pressure, and crypt-to-crypt crosstalk between adenomatous and immune cells takes place leading to a pro-tumourigenic environment. This work has made a significant contribution to the understanding of the initiation of cancer in the human colon.

Acknowledgments

I would like to thank my supervisor Stuart McDonald for giving me the opportunity to carry out my PhD project in his lab, and for his guidance, technical assistance, intellectual support and continuous optimism. I would also like to thank Trevor Graham, my second supervisor, for the inspiring conversations throughout the PhD. I am grateful to all members of the McDonald/Graham lab for their invaluable support and input over the last years, particularly to Ann-Marie Baker, Biancastella Cereser, Laura Gay, Weini Huang and Nina Moderau. You have been a great source of knowledge and your advice has helped me ever so often to make a blurry image become clear. Thank you for your patience, your friendship and for making me laugh countless times.

I would also like to thank Hayley Davis for showing me how to set up organoids and the Barts Histopathology core facility for the processing of tissue samples. I want to thank the Barts Cancer Institute for providing the facilities to carry out my research. I was very lucky to have had the opportunity to carry out my PhD at the Centre of Tumour Biology. It has been such a friendly, collaborative and welcoming environment to work in.

Special thanks goes to my beloved family - my Dad Robert, my Mum Claudia and my sister Saskia for their kindness, endless support and the encouragement they have given me throughout my PhD and my life in general. Thank you for believing in me.

Massive thanks to Christian Owusu for analysing the RNAseq data, but more importantly for being my friend. Thank you for always being there for me, your kindness, limitless understanding and honesty.

Thanks to all my friends, near and far, for your moral support, friendship, and distraction when I needed it. Particularly I would like to thank Nikola Schröder for always having an open ear and your loyal friendship for the last 27 years and also to my other girls from home, Anna-Lena Dilcher, Kristina Mühlstädt, Alicia and Esther Arroyo, Rabea Schmidt, Maggie Bertelmann, Caro Gatzmaga, und Carmen Umlauf for your unwavering support during the times of personal difficulties and always having my back.

Isabel Raabe, I am thankful for your warm and honest friendship and very pleased that by chance we ended up living close to each other during our PhD years.

Nicola Di Marco, I still remember the day you walked into the lab. I am very grateful for that day and the resulting friendship.

Thanks to Miriam Tenderini, Yasmine Tanner and Rachel Rosenthal – our writing retreat has made the process of writing lighter and a lot more enjoyable.

Finally, I acknowledge support from Cancer Research UK for funding my studentship.

List of abbreviations

ABC	ATP-binding cassette
ACF	Aberrant crypt foci
AFAP	Attenuated familial adenomatous polyposis
ANOVA	Analysis of variance
APC	Adenomatous polyposis coli
ATP	Adenosine triphosphate
BMP	Bone morphogenic protein
CAF	Cancer associated fibroblast
CBC	Crypt base columnar
CCO	Cytochrome *c* oxidase
cDNA	Complementary DNA
CIMP	CpG island methylation phenotype
CIN	Chromosomal instability
CRC	Colorectal cancer
DAB	Diaminobenzidine
DNA	Deoxyribonucleic acid
dNTPs	Deoxynucleotide triphosphates
DSB	Double strand break
DVL	Dishevelled
ECM	Extracellular matrix
EDTA	Ethylenediaminetetraacetic acid
EGF	Epidermal Growth Factor
ERK	Extracellular signal–regulated kinase
ES	Enrichment score
FABP1	Fatty Acid-Binding Protein 1
FAP	Familial adenomatous polyposis
FBS	Fetal bovine serum
FDR	False discovery rate
FFPE	Formalin-fixed paraffin embedded
FZD	Frizzled
G6PD	Glucose-6-phosphate dehydrogenase

GAPDH	Glyceraldehyde 3-phosphate dehydrogenase
GSEA	Gene Set Enrichment Analysis
H&E	Hematoxylin and Eosin
HBSS	Hank's Balanced Salt Solution
HLA	Human leukocyte antigen
HNPCRC	Hereditary non-polyposis colorectal cancer
IBD	Inflammatory bowl disease
IELs	Intraepithelial lymphocytes
IGV	Integrative Genomics Viewer
IHC	Immunohistochemistry
IPA	Ingenuity Pathway Analysis
ISC	Intestinal stem cell
ISH	*In situ* hybridisation
ITH	Intratumour heterogeneity
JNK	c-Jun N-terminal kinase
KS	Kolmogorov-Smirnov
KW	Kruskal-Wallis
LCM	Laser capture microdissection
Lgr5	Leucine-rich repeat-containing G-protein coupled receptor 5
LOH	Loss of heterozygosity
MAPK	Mitogen activated protein kinase
MMR	Mismatch repair
MSI	Microsatellite instability
mtDNA	Mitochondrial DNA
NBT	NitroBlue Tetrazolium
NES	Normalised enrichment score
NGS	Next generation sequencing
PBS	Phosphate-buffered saline
PBST	Phosphate-buffered saline Triton X
PCA	Principal component analysis
PCR	Polymerase chain reaction
PFA	Paraformaldehyde
PPAR	Peroxisome proliferator-activated receptor

qRT-PCR	Quantitative reverse transcriptase polymerase chain reaction
RIN	RNA Integrity Number
RNA	Ribonucleic acid
ROS	Reactive oxygen species
SDH	Succinate Dehydrogenase
SMA	Smooth muscle actin
TA cells	Transit-amplifying cells
TAE	Tris-acetate-EDTA
TAM	Tumour-associated macrophage
TCF	T-cell factor
TEF	Tumour-exposed fibroblast
TGF-β	Transforming growth factor-β
VAF	Variant allele frequency
WES	Whole-exome sequencing
WGS	Whole-genome sequencing
WT	Wild type

Contents

List of Tables

List of Figures

1 Chapter I: Introduction

1.1 General introduction

The development of cancer is a process of clonal evolution due to somatic mutation and selection based on the effect of these mutations on the cell. Understanding cancer from an evolutionary perspective has extensive clinical implications for neoplastic progression, prevention and therapy (Greaves *et al*. 2012, Merlo *et al*. 2006). In 1976, Peter Nowell's landmark paper highlighted clonal evolution of tumour cell populations (Nowell 1976). The "somatic mutation theory" now states that each tumour is derived from a single mutated cell that clonally expands into a neoplasm acquiring additional mutations with each cell division (*monoclonal-in-origin*). Subsequent progression to invasive cancer is due to further evolution within the neoplasm, as a series of mutations in oncogenes and tumour suppressor genes accumulate over time (Kinzler *et al*. 1996), with each additional mutation providing the mutated cell and its progeny with a growth or survival advantage, and so driving expansion of the tumour (Baker *et al*. 2013).

The monoclonal origin of cancer has long been accepted in the scientific community. However, recent evidence has shown that tumours can be derived from multiple independently transformed cells, thus being *polyclonal-in-origin* (Merritt *et al*. 1997, Novelli *et al*. 2003, Novelli *et al*. 1996, Thirlwell *et al*. 2010, Thliveris *et al*. 2005). The mechanism that generates polyclonal tumours is unknown, as is the importance of polyclonality in driving tumour progression. Short-range interactions between multiple initiated clones within one or two crypt diameters of each other have been suggested to lead to the formation of polyclonal tumours. These clonal interactions might be critical, if not necessary, for initiation, growth, and progression of tumourigenesis.

This thesis describes how clonal interactions between dysplastic and non-dysplastic epithelium drives clonal expansion and alters stem cell dynamics. In addition, it provides an insight into the gene expression changes between normal epithelium and normal epithelium in close proximity to adenomas.

Hence, this chapter will focus on introducing the macroscopic and microscopic biology of colorectal cancer, the process that initiates and drives tumourigenesis, the stem cell dynamics, and the development and progression to cancer.

1.2 Anatomy of the human intestine

The colon (large intestine) is part of the digestive system that functions to absorb water and salt from waste material, and to transport it from the small intestine to the rectum. The entire adult colon is five to six feet long, and comprises the caecum, ascending colon, transverse colon, descending colon, sigmoid colon and rectum (Figure 1.1). The tube like structure of the colon is made up of three layers: the outer layer comprises sheets of innervated smooth muscle (muscularis externa), the middle layer is composed of connective tissue (submucosa) and the inner layer is a sheet of cuboidal epithelial cells termed the mucosa, processing and absorbing nutrients, and compacting the stool. While in the small intestine, absorption is increased through villi and crypts of Lieberkühn (invaginations into the submucosa), in the large intestine, there are only crypts, and instead of villi a flat surface epithelium (Figure 1.2) (Sancho *et al*. 2004).

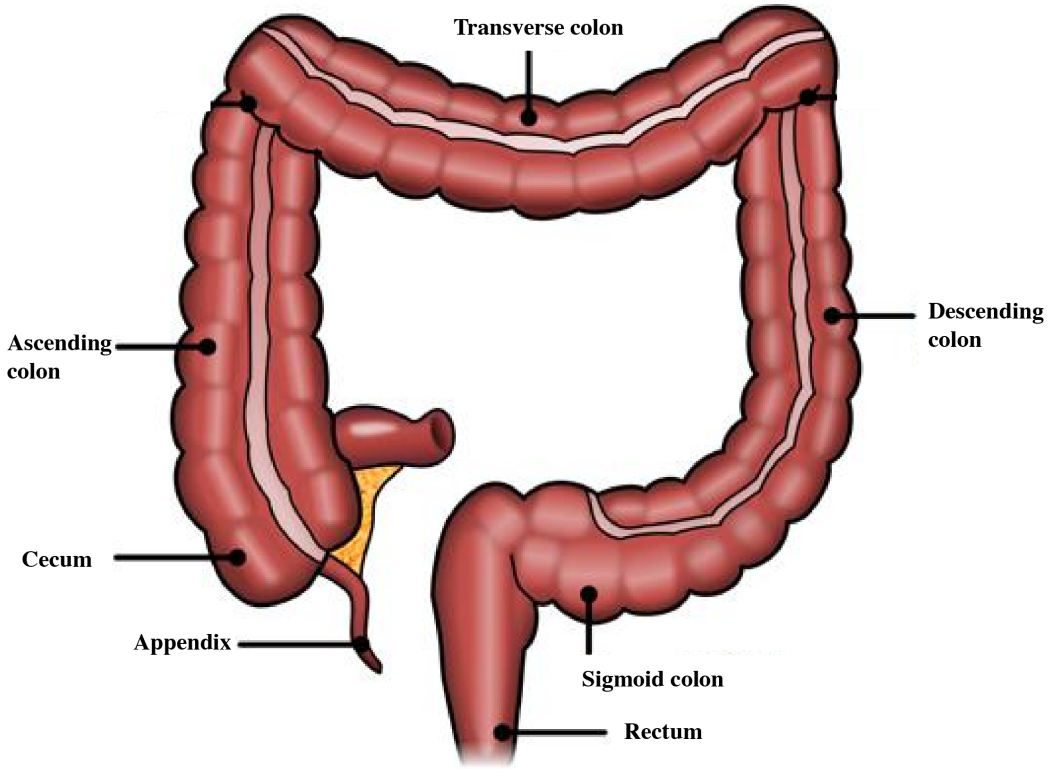

Figure 1.1: Anatomy of the human large intestine.
The colon is divided into five major anatomic segments: the caecum, ascending colon, transverse colon, descending colon, sigmoid colon and rectum. Adapted from http://www.crcftlauderdale.com.

1.3 Intestinal epithelium

The colonic epithelium is pitted with millions of cylinder like structures called crypts. The crypt is considered to be the smallest functional unit of the colorectal mucosa (Figure 1.2) (Clevers 2013, Humphries *et al*. 2008). The opening of the crypt is at the luminal surface of the mucosa and the base of the crypt lies superior to the muscularis mucosae.

Human intestinal crypts are clonal populations, derived from a single stem cell (Barker *et al*. 2007, Gutierrez-Gonzalez *et al*. 2009, Ponder *et al*. 1985, Taylor *et al*. 2003). Each crypt has a population of stem cells at their base that generates epithelial cell lineages. However, intestinal stem cells (ISCs) do not directly form differentiated cells; they rather contribute to an intermediate pool, known as transit-amplifying (TA) cells. These proliferative cells are confined to the bottom third of the crypt. TA cells divide approximately every 12 – 18 hours, 4 – 6 times prior to fully differentiating into the main epithelial lineages within the crypt: goblet cells, enteroendocrine cells and enterocytes (Heath 1996). Goblet cells protect the mucous lining, enteroendocrine cells secrete gastrointestinal hormones, and enterocytes absorb nutrients and make up the majority of epithelial cells (Sancho *et al*. 2004).

TA cells, resulting from stem cell divisions, then migrate upwards towards the luminal surface where they differentiate while losing their proliferative capacity, eventually undergoing apoptosis (Crosnier *et al*. 2006, Potten 1998). Cells reach the top of the villus after around 5 days (van der Flier *et al*. 2009). Turnover of the entire epithelial lining is rapid, taking 7 days to replace it (Brittan *et al*. 2002). However, TA cells can dedifferentiate back into stem cells if the stem cell population is lost (Ritsma *et al*. 2014).

Specific features for the murine small intestine are the presence of Paneth cells and intestinal villi. Paneth cells, although differentiated, reside at the crypt base and secrete antimicrobial peptides as well as growth factors, such as Wnt, EGF and Notch ligands, to maintain the stem cell niche (Figure 1.2A) (Farin *et al*. 2012, Sato *et al*. 2011).

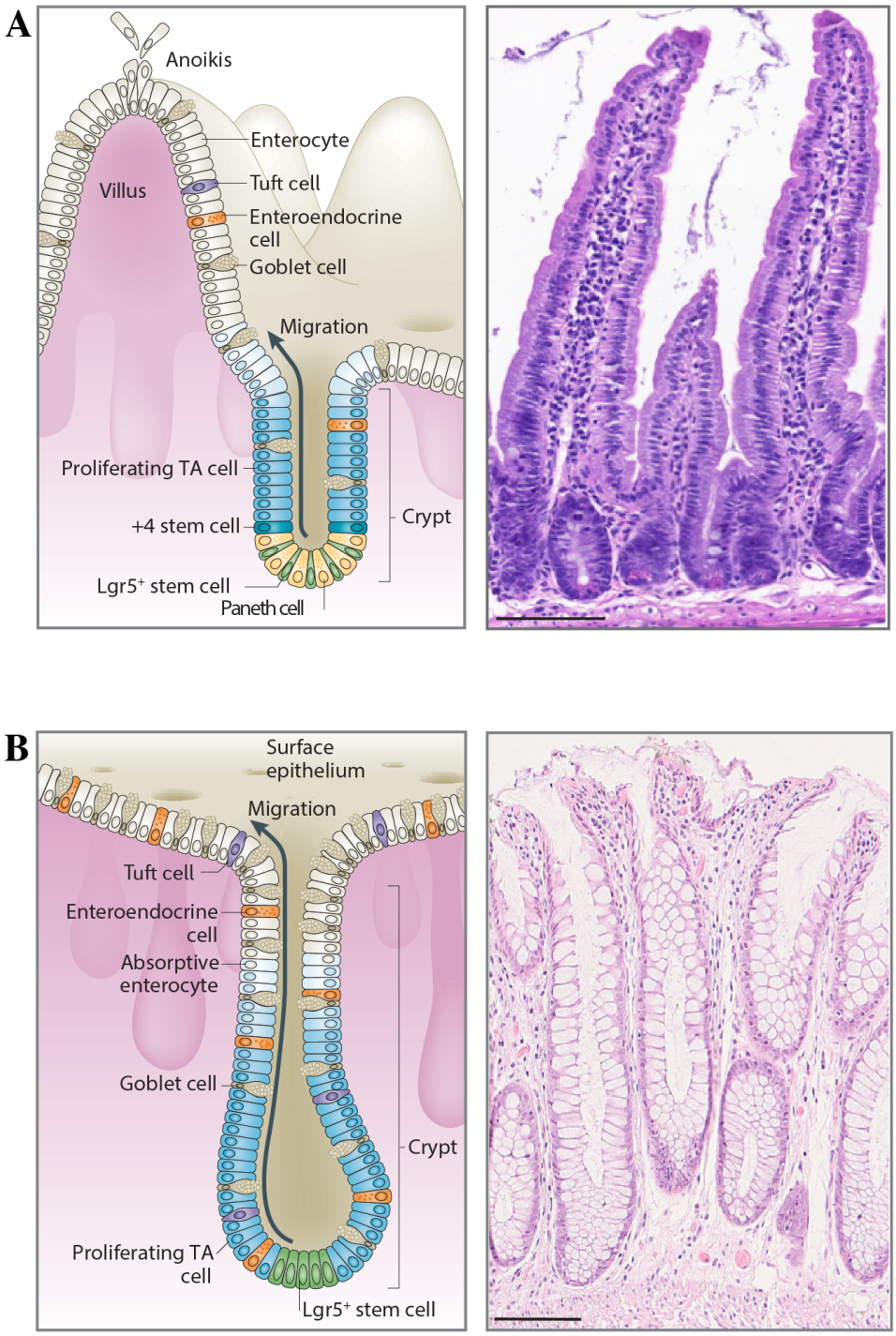

Figure 1.2: The crypt–villus structure of the small intestine and the structure of a crypt of the large intestine.

A) In the murine small intestine, LGR5$^+$ stem cells are intermingled with Paneth cells at the crypt base. The +4 'reserve' stem cells occupy the fourth position from the crypt base. The stem cells generate transit-amplifying (TA) cells. TA cells differentiate into various functional cells on the villi including goblet cells, enteroendocrine cells, tuft cells and enterocytes to replace epithelial cells, which are lost via anoikis at the villus tip (left panel). H&E staining of a crypt and villus (right panel). B) In the human colon, LGR5$^+$ stem cell compartment resides at the base of the crypt, generating rapidly proliferating TA cells, which subsequently differentiate into the cells of the colon (goblet cells, absorptive enterocyte, enteroendocrine cells, and tuft cells) (left panel). H&E staining of a crypt in the large intestine (right panel). Scale bar = 100μm. Adapted from Barker 2014.

Moreover, Paneth cells are the exception to this rapid self-renewal, as they are renewed every 3 – 6 weeks (Ireland *et al*. 2005). Paneth cells are absent in the colon, but $Reg4^+$ deep crypt secretory cells function as an epithelial niche for stem cells (Rothenberg *et al*. 2012, Sasaki *et al*. 2016).

Intestinal villi are finger-like structures covered in simple columnar epithelium, projecting into the intestinal lumen to maximise the surface area for digestion and absorption (Barker 2014).

1.4 Stem cells

1.4.1 Stem cells are housed within a basal niche

Stem cells are defined functionally by their potential for self-renewal and multipotency, generating all the differentiated cells found in the colonic crypt (Barker *et al*. 2008).

Stem cells are located within the stem cell niche (Williams *et al*. 1992). The stem cell niche is defined as the local microenvironment that supports stem cells and molecular signals, and regulates their behaviour during tissue homeostasis and regeneration (Smith *et al*. 2017). The niche consists of the stem cells themselves and surrounding mesenchymal cells, including subepithelial myofibroblasts, fibroblasts, pericytes, endothelial cells, immune cells, neural cells, and smooth muscle cells (Tan *et al*. 2018). In addition to providing structural support, they have been shown to be involved in cross-talk with the intestinal epithelium (Powell *et al*. 2011).

Wnt signalling is critical for stem cell maintenance, cell polarity and cell fate determination (Logan *et al*. 2004). Given that Wnt signalling is an essential pathway for stem cell maintenance, the Wnt ligand-producing cells therefore represent an important part of the niche. Wnt signalling can activate three distinct pathways: the canonical Wnt/β-catenin pathway, the non-canonical Wnt/β-catenin pathway and the Wnt/Ca^{2+} pathway (Logan *et al*. 2004), of which the canonical pathway is the most relevant pathway in the context of ISCs (Figure 1.3).

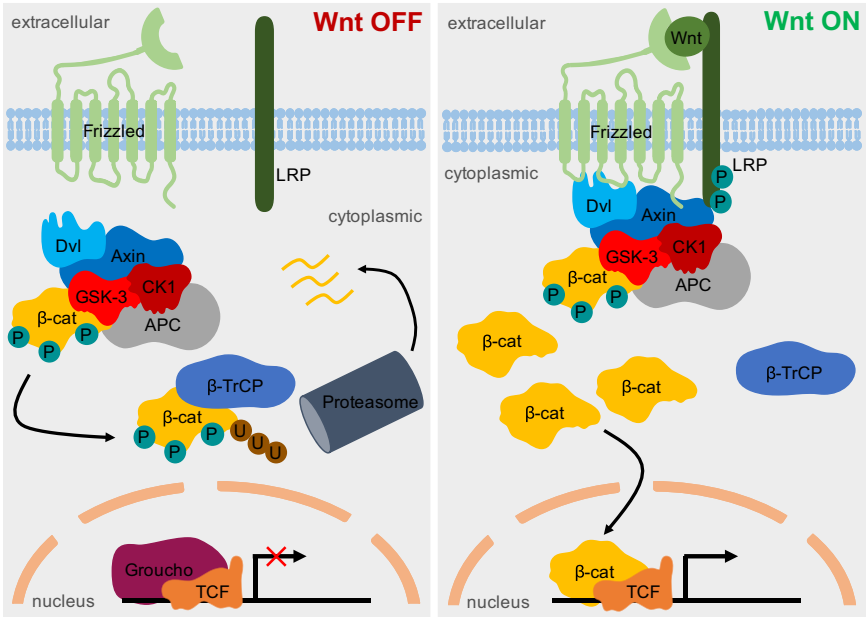

Figure 1.3: Canonical Wnt-*β*-catenin signalling pathway.
The Wnt signalling pathway is shown in the "OFF" (left hand side) and "ON" (right hand side) states. In the absence of a Wnt signal, the destruction complex phosphorylates and ubiquinates *β*-catenin, therefore being destroyed by the proteasome. In the presence of a Wnt signal, as the dishevelled protein (Dvl) recruits Axin2 and inhibits GSK-3, *β*-catenin is not phosphorylated and therefore not destroyed. It can translocate to the nucleus and activate transcription genes (Kretzschmar *et al*. 2017).

The canonical Wnt signalling pathway is initiated when WNT ligands bind to the Frizzled (FZD)/LRP5/6 co-receptor complex, interacting with cytoplasmic Dishevelled (DVL), that leads to its phosphorylation (Janda *et al*. 2012, Li *et al*. 2012). This receptor activation also induces phosphorylation of LRP by protein kinases CK1γ1 and GSK3β, allowing AXIN to be sequestered from the β-catenin destruction complex (Clevers *et al*. 2014). This results in an accumulation of β-catenin in the cytoplasm, which then translocates into the nucleus (Kretzschmar *et al*. 2017). In the nucleus, Groucho is displaced from T-cell factor (TCF) transcription factor and thus activating the transcription of WNT target genes (Roose *et al*. 1998, van de Wetering *et al*. 1991), such as *Axin2* (Lustig *et al*. 2002) and *Lgr5* (Leucine-rich repeat-containing G-protein coupled receptor 5) (Van der Flier et al. 2007). In general, nuclear translocation of β-catenin is used as an indicator for Wnt activity. Whereas Axin2 is a weak negative feedback regulator, Lgr5 amplifies Wnt signalling (Carmon *et al*. 2017). When Lgr5 (or Lgr4 and Lgr6) binds to its secreted ligand R-spondin, they form a complex with Znrf3 and Rnf43, thereby preventing Fzd receptor degradation resulting in enhanced accumulation of β-catenin (de Lau *et al*. 2011, Hao *et al*. 2016, Koo *et al*. 2012).

Studies on the transcription mechanism downstream of Wnt signalling in $Lgr5^+$ ISCs identified *Ascl2* is the master regulatory transcription factor maintaining crypt stemness. Deletion of *Ascl2* resulted in a loss of $Lgr5^+$ ISCs, whereas its overexpression caused expansion, leading to hyperplastic crypts (van der Flier *et al*. 2009). In addition, *Ascl2* can co-occupy DNA with TCF4/β-catenin to activate a stem cell gene expression (Schuijers *et al*. 2015). These studies indicate the mechanisms by which Wnt activates specific transcriptional processes through *Ascl2*.

Wnt ligands act as short-range signals and can be produced by any of the cell types present in the niche (Willert *et al*. 2003). The production of mature Wnt ligands and their transport to the membrane for secretion depends on two proteins: Porcupine (Porcn) and Wntless (Wls). Porcn enables functional Wnt ligands through catalysing palmitoylation (Kadowaki *et al*. 1996, van den Heuvel *et al*. 1993), and Wls enables the transport of the Wnt ligands to the vesicular membrane (Banziger *et al*. 2006).

In normal intestinal crypts, Wnt signals are expressed as a gradient, in which they predominate at the crypt base in order to maintain normal stem cell behaviour and begin to differentiate as they migrate upward (Farin *et al*. 2016). Therefore, the

level of Wnt signalling must be tightly controlled. For instance, WNT receptor turnover is mediated by ZNRF3/RNF43 E3 ubiquitin ligases and deletion of these two E3 ubiquitin ligases in the intestinal epithelium led to adenoma formation and expansion of $Lgr5^+$ ISCs, demonstrating the importance of balanced Wnt signalling (Hao *et al*. 2012, Koo *et al*. 2012).

The level of Wnt signalling is also modulated by the WNT ligand gradient in the murine intestinal crypt (Van der Flier *et al*. 2007). Wnt responsive cells are stimulated by soluble ligands that are released from surrounding mesenchymal and epithelial cells (Crosnier *et al*. 2006). For instance, Paneth cells produce high levels of Wnt3 that act locally on stem cells by promoting stemness and the further away cells are from this signal, the more differentiated they become. Furthermore, frizzled receptors bind to Wnt on the stem cell membrane, which is diluted through cell division and thus, shaping the epithelial Wnt gradient (Farin *et al*. 2012). R-spondin engages Lgr4-Lgr6, RNF43 and ZNRF3 receptor classes enforcing the canonical Wnt/β-catenin signalling pathway, which induces intestinal organoid growth *in vitro* and $Lgr5^+$ ISCs *in vivo*. A recent study by Yan *et al*. (2017) has identified the functional roles of Wnt and R-spondin ligands in the stem cell niche. By default, $Lgr5^+$ ISCs differentiate, unless both R-spondins and Wnt ligands are present. Self-renewal of $Lgr5^+$ ISCs is an active process requiring Wnt as a priming and R-spondin as a self-renewal factor. Strikingly, Wnt proteins are unable to induce $Lgr5^+$ ISCs self-renewal as they maintain R-spondin receptor expression instead, which then enables R-spondin ligands to actively drive stem cell expansion. This cooperative interaction between Wnt and R-spondin ligands has important implications in tissue homeostasis (Yan *et al*. 2017).

Another key component of the niche are Paneth cells, and together with myofibroblasts, they provide essential factors for the survival of crypt base stem cells such as Wnt3a, epidermal growth factor (EGF) and BMP antagonists (Worthley *et al*. 2010). Paneth cells play a unique role in the stem cell niche. Unlike other differentiated cells, they migrate down to the crypt base, where they persist for approximately three to six weeks. They are arranged in a way that a Paneth cell is always surrounding a crypt base columnar (CBC) cell and vice versa, and a crypt contains about 14±2 CBC cells and 10 Paneth cells (Snippert *et al*. 2010). *In-vitro* studies have shown that the removal of Paneth cells led to loss of stem cells. Sato *et al*. (2011) concluded that Paneth cells constitute the niche for stem cells in intestinal

crypts, because Paneth cells elaborate important signalling molecules such as Wnt3 and EGF and *in vitro* organoid formation by stem cells was enhanced by co-culture with a Paneth cell–enriched population (Sato *et al*. 2011). Therefore, it seems essential for a Paneth cell to be in physical contact with a stem cell in order to maintain stemness, and it appears that the number of Paneth cells must be strictly controlled, which is accomplished through strong Wnt signals.

However, in a different study it has been shown that ablating Paneth cells had no effect on the maintenance of functional stem cells (Kim *et al*. 2012), implying that other cell populations are involved in producing niche factors necessary for maintaining ISCs (Durand *et al*. 2012, Kim *et al*. 2012). Indeed, stromal cell populations function as stem cell niches secreting important WNT ligands (San Roman *et al*. 2014, Valenta *et al*. 2016). In fact, a recent study has demonstrated that stromal cells expressing the transcription factor Foxl1 play an essential role in the ISC niche component. Diphtheria toxin- mediated ablation of these stromal cells led to crypt cell arrest (Aoki *et al*. 2016). Myofibroblasts are the first layer of subepithelial cells interacting with stem cells, modulating stem cell behaviour by activating conserved signalling pathways, including Wnt, bone morphogenic protein (BMP), Hedgehog and the Delta/Notch families (Clevers *et al*. 2012).

BMP signalling has a critical role in intestinal development, controls ISC replication and is further needed for terminal differentiation of mature cell lineages (Auclair *et al*. 2007). As opposed to Wnt signalling, an opposite gradient is observed for BMP signalling, with the highest level at the luminal surface. BMP expression is regulated by its antagonists Gremlin1 and Gremlin2. BMP signalling also suppresses Wnt, thus inhibiting self-renewal of ISCs (He *et al*. 2004).

The Notch signalling pathway plays an important role in lineage specification of differentiated cells, regulates intestinal proliferation, and maintains intestinal homeostasis (Pellegrinet *et al*. 2011). It is also essential for maintenance of stem cell number and function, and for its regulation of cell fate decision between absorptive and secretory cell types (VanDussen *et al*. 2012). Recently, it has been shown that Notch signalling regulates fast- and slow cycling stem cells in colorectal cancer (CRC), making sure these two populations are in balance (Srinivasan *et al*. 2016).

The Hedgehog signalling pathway controls tissue polarity and is critical for the development and homeostasis of many tissues (Varjosalo *et al*. 2008). The main Hedgehog protein, Indian hedgehog, is secreted in a paracrine manner by

differentiated epithelial cells to act on mesenchymal cells, where it maintains homeostasis of mesenchymal cells. It further regulates epithelial cell proliferation through negative feedback to ensure proliferation of CBC cells through BMP signalling (Buller *et al*. 2012). Specifically, to promote differentiation of intestinal epithelial cells, stromal cells respond to Hedgehog signalling by producing the BMP4 ligand, which antagonises Wnt signalling to inhibit stem cell expansion and to allow differentiation (He *et al*. 2004, Miyazono *et al*. 2010). To protect ISCs from BMP signalling activation, the pericryptal myofibroblasts and smooth muscle cells express the BMP inhibitors Gremlin1 and Gremlin2 (Kosinski *et al*. 2007). To conclude, these studies have shown that major developmental signalling pathways co-ordinately mediate mesenchymal and epithelial interactions to maintain proper crypt homeostasis.

Therefore, activation of the Wnt and Notch cascade signalling pathways is required to maintain the undifferentiated 'stem-like' state (Fevr *et al*. 2007, van Es *et al*. 2005). Along with BMP antagonists Gremlin 1 and Gremlin 2, shown to be secreted by myofibroblasts (Kosinski *et al*. 2007), they are involved in the maintenance of the stem cells, cell migration and differentiation (Batlle *et al*. 2002, Crosnier *et al*. 2006, van Es *et al*. 2005). These signalling pathways are not only important for intestinal homeostasis, but have also been implicated in forming and sustaining the stem cell niche.

1.4.2 Identifying intestinal stem cells

Much evidence for the organisation of the intestinal crypt has come from murine labelling experiments using somatic mutations or chimeric mice, where one parent strain carries a marker.

Evidence that the intestinal crypt is supported by a number of stem cells residing in a niche first came from Cheng and Leblond (Cheng *et al*. 1974) and Bjerknes and Cheng (Bjerknes *et al*. 1981). In these studies, mice were injected with ^{3}H-thymidine-labelled cells. Labelled DNA was incorporated during cell division and were found at the crypt base after 30h post injection, but had migrated towards position +1 and +4 after 66h, indicating that stem cells lie within the CBC cell population. Later on, Williams *et al*. (1992) marked crypt cells via mutagen-induced

loss of the X-linked enzyme glucose-6-phosphate dehydrogenase (G6PD), and compared the time-course of mutated phenotypes in both, the small and large intestine. Shortly after administration of the mutagen, partially mutated crypts were observed, which over time developed into fully mutated crypts. They concluded that stem cells within a crypt niche could explain the observed effect, and that the number of stem cells may differ between the small and large colon, with a greater number of niche stem cells in the small intestine (Williams *et al*. 1992). Since then, further studies have shown that the intestinal crypt is maintained by a stem cell niche in both mouse and human (Barker *et al*. 2007, Bjerknes *et al*. 1999, Yatabe *et al*. 2001).

It is not possible to morphologically differentiate stem cells from other cells within the crypt, however using the unique ability of stem cells, once clonally-marked, to re-populate the crypt with clonal descendants in all cell lineages, a number of markers has been proposed to label stem cells. Two positions are suggested for ISCs: CBC cells at the base of the crypt and at position +4 from the crypt base (Takeda *et al*. 2011). CBC cells are rapid cycling, whereas the +4 cells are quiescent or slow cycling (Carlone *et al*. 2012).

By analysing the differential expression profiles of Wnt targets to identify those genes with restricted crypt base expression, the Leucine-rich repeat-containing G-protein coupled receptor 5 (*Lgr5*) gene was found to be specifically expressed on the surface of crypt base stem cells, and found throughout the entire gastrointestinal tract (Barker *et al*. 2009, Barker *et al*. 2007). Lineage tracing in transgenic mice expressing the Wnt target gene *Lgr5* revealed that *Lgr5*$^{+}$ cells could generate all cell types of the small intestine, and moreover, fulfilled all the requirements of being a functional stem cell: self-renewal, long-term maintenance, and production of specialised cell types (Barker *et al*. 2007). Thus, CBC cells were identified as stem cells at the crypt base in mouse intestine and colon. Not only do *Lgr5*$^{+}$ stem cells maintain crypt homeostasis, they are also involved in mediating Wnt signal transduction by interacting with R-spondins, thus maintaining the stemness potential (Takashima *et al*. 2011).

Further experiments studying the clonogenic capacity of Lgr5^{+} cells confirmed its expression as a specific intestinal stem cell marker (Sato *et al*. 2009). Single Lgr5^{+} cells isolated from mouse small intestine were able to generate long-lived organised crypt-villus structures in culture that contained all differentiated cell types. They concluded that a non-epithelial niche is not required for the formation of

a small intestinal crypt (Sato *et al*. 2009). The same group further challenged the role of the myofibroblasts in maintaining stem cells by showing evidence that Paneth cells in the mouse colon produce Wnt and other essential niche signals for stem cell maintenance (Sato *et al*. 2011). In addition to *Lgr5*, *Ascl2* is also a marker for highly proliferative CBC cells (van der Flier *et al*. 2009).

Subsequent to the discovery of Lgr5, other stem cell markers have been identified and validated with lineage-tracing experiments. B cell specific Moloney murine leukemia virus integration site 1 (*Bmi1*$^+$) cells are located at the +4 cell position and have been found to serve as a reserve stem cell pool (Sangiorgi *et al*. 2008). *Bmi1*$^+$ intestinal cells act as secretory precursors of Paneth and enteroendocrine cells during normal homeostasis (Buczacki *et al*. 2013). Precursors of the absorptive enterocytes have the capacity to replace lost Lgr5$^+$ stem cells (Tetteh *et al*. 2016). Moreover, *Tert* expression was found more broadly along the crypt axis marking slow cycling ISCs. They also exist alongside Lgr5$^+$ populations (Montgomery *et al*. 2011). *Hopx* is also a specific marker for +4 cells. Cells expressing *Hopx* can develop into all intestinal cell lineages (Takeda *et al*. 2011). In addition, the Notch ligand Dll1 has been identified as a stem cell marker. Lineage tracing of Dll1 knock-in mice showed that Dll1 cells produced all four cell types found in the intestinal crypt (van Es *et al*. 2012).

While *Lgr5* cells divide approximately once a day, cells in the +4 position are quiescent and slow cycling (Buczacki *et al*. 2013, Takeda *et al*. 2011). Together, these two stem cell populations follow a bidirectional relationship and are not completely mutually exclusive. *Lgr5*$^+$ ISCs are considered to be the primary ISC pool, while cells at the +4 position remain as a quiescent reserve of stem cells with the ability to reconstitute crypt integrity, also indicating crypt cell plasticity (Smith *et al*. 2017). *Lgr5*$^+$ are responsible for homeostatic self-renewal, whereas *Bmi1*$^+$ stem cells are part of the injury-induced regeneration (Tian *et al*. 2011), further indicating that mammals use more than one stem cell population to maintain homeostasis in the small intestine (Sangiorgi *et al*. 2008).

1.5 Stem cell dynamics

The discovery of *Lgr5* made it possible to study stem cells and their dynamics. The behaviour of stem cells determines the dynamics and differentiation potential within a colonic crypt. They continuously transfer their genetic information to the next generation. The current technique to assess stem cell activity is clonal lineage tracing (Blanpain *et al*. 2013). In this technique, a stem cell is labelled with a permanent genetic marker, such as the expression of a fluorescent protein, and this marker is inherited by all of the descendants of that cell. When multiple cell types of a single traced clone can then be detected that persist over the entire lifetime of the organism, multipotency and self-renewal capabilities of the original labelled cell have been proven.

Snippert *et al*. (2010) investigated how homeostatic self-renewal is controlled and how crypts drift towards clonality over time. Crossing Lgr5-EGFP-Ires-Cre^{ERT2} mice to a R26R-Confetti reporter, individual *Lgr5* stem cells were lineage-traced and the behaviour of clones developing from *Lgr5* cells investigated. The short-term clonal tracing revealed an overall expansion of clone size of a few clones, balanced out by ongoing extinction of other clones, so that clones became larger and less frequent over time. Long-term lineage tracing (up to 30 weeks) documented the drift towards clonality of a few, but larger clones occupying a whole crypt. Starting out with a highly heterogeneous pattern, a significant expansion was observed at later time points, demonstrating stem cell loss and expansion of neighbouring clones until crypts became fully labelled by one colour on average after 3 months. This reflects neutral drift dynamics in normal crypt homeostasis: stem cells remain their numbers and a clone reaches fixation (Snippert *et al*. 2010). Additional data to support this model was derived from pulse-chase experiments. It was shown that stem cells form an equipotent population at which stem cell multiplication is compensated by the loss of a neighbour, resulting in neutral drift dynamics. Clones expand and take over the crypt or become lost at random (Lopez-Garcia *et al*. 2010).

Neutral drift dynamics lead to neutral competition among stem cells (Kozar *et al*. 2013, Snippert *et al*. 2010). Neutral drift is defined as a stochastic process in which each stem cell is equally prone to become extinct over time and has the chance to produce zero, one or two stem cells. If a stem cell produces zero stem cells but

instead TA cells, then the stem cell clone information is lost and the stem cell is replaced by a neighbouring stem cell. Therefore, symmetric cell division is essential for homeostatic conditions in the crypt, and that homeostasis is maintained by neutral competition at the population level (Lopez-Garcia *et al*. 2010). Thus, new lineages appear randomly, and by chance a single stem cell lineage can persist and occupy the entire crypt (= niche succession) (Ro *et al*. 2001). An individual stem cell is capable of replacing other stem cells in the niche. Niche succession occurs on average every 8 years in the normal human colon (Yatabe *et al*. 2001). Eventually, the entire crypt will be colonised with its mutant progeny, a process called monoclonal conversion (Humphries *et al*. 2008). This is a slow process, as fully mutated crypts are rarely observed before the age of 40 and only in 80 year olds clonal conversion is only observed in 15% of all colonic crypts (Taylor *et al*. 2003). Cooperation among different cell types within and around the niche has been observed, for instance, Lgr5 stem cells receive niche support from Paneth cells (Sato *et al*. 2011).

ISCs are characterised by a bi-compartmental organisation, meaning one compartment is responsible for regeneration, whilst the other one controls the stem cell niche. Ritsma *et al*. (2014) have shown that there are two groups of stem cells in the niche: border stem cells and central stem cells. Together they collaborate to maintain tissue homeostasis. Central stem cells are located in the middle of the stem cell niche (position +1 and +2) and are mostly responsible for controlling the number of stem cells. Furthermore, central stem cells tend to maintain their population and produce border cells. Border stem cells are located between the central stem cells and the TA cells (position +3 and +4) and are responsible for regulating the number of non-stem cells. They tend to produce mainly cells on the border region and rarely contribute to the central stem cell population. Moreover, Ritsma and colleagues have shown that the probability of differentiation of border stem cells is 0.5, while the probability of proliferation is 0.2. In contrast, the offspring of central stem cells are stem cells, and the probability of division is 0.3. Division of a central stem cell led to the displacement of neighbouring cells, which could lead to a nearby cell being pushed out of the stem cell niche. Thus, central stem cells are in the "Goldilocks spot" (Walther *et al*. 2014) (Figure 1.4), as their chance of being displaced from the stem cell niche is minimised. However, they also observed occasional migration from border stem cells to central stem cells (Ritsma *et al*. 2014).

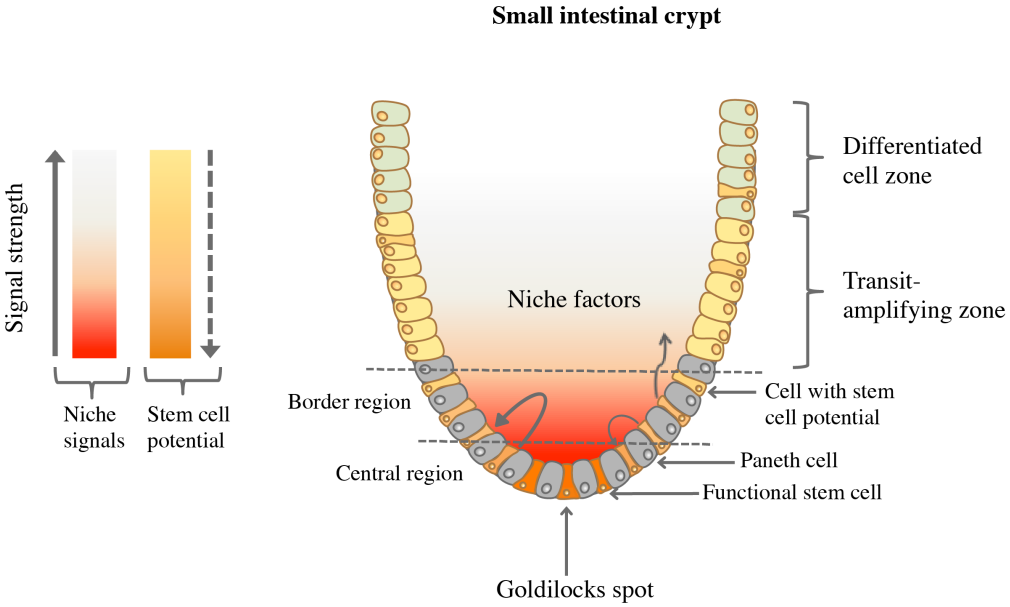

Figure 1.4: The stem cell niche.
Long-term functional stem cell behaviour (orange cells) is maintained when a cell with stem cell potential is located within the niche. Through cell divisions at the crypt base and the resulting placing of the progeny, cell positions are shuffled around: cells that are located in the central region (the Goldilocks spot) are more likely to remain in the basal region of the crypt and function as stem cells, whereas cells in the border region are more likely to be displaced and lost from the niche. Adopted from Walther *et al*. 2014.

Thus, stem cells are highly plastic and its long-term functioning is mainly determined by their position within the niche. Central stem cells are those with long-lived lineages, whereas border stem cells are biased for loss. Therefore, only a small number of stem cells are functional.

This was previously shown by Kozar *et al*. (2013) who detected only five or six functioning stem cells in each crypt by using a continuous clonal labelling approach based on a mutation-induced clonal mark that allowed measuring the rate of mutation together with neutral drift dynamics. This approach quantified the dynamics of stem cell replacement and thereby allowed tracing stem cells over a lifetime *in vivo*. They concluded that Lgr5 expression may be enough to assume stem cell potential, but the actual number of functional stem cells is smaller and cannot be determined using the stem cell marker (Kozar *et al*. 2013). This was further confirmed by Vermeulen *et al*. (2013), who estimated the number of functional stem cells to be five with a rate of replacement equal to 0.1 per stem cell per day. They further confirmed that a sizable fraction of $Lgr5^+$ cells are more committed progenitor cells and thus, do not function as stem cells in homeostasis (Vermeulen *et al*. 2013).

Shahriyari *et al*. (2017) have developed a model to investigate the spread of mutants within the stem cell niche. They have shown that the probability for a mutant clone to become fixed is independent of the type of stem cell division as long as stem cells do not fully divide asymmetrically. Furthermore, the progeny of central stem cells have a much higher change to take over the entire niche as compared to border stem cells. Interestingly, they found that the migration of border stem cells to central stem cells will delay the spread of mutant clones (Shahriyari *et al*. 2017).

ISCs divide daily to produce new ISCs and differentiated cells, while maintaining their numbers. The immediate progeny of $Lgr5^+$ ISCs produce absorptive and secretory lineages via lateral inhibition, a means for reciprocal cell specification (Pellegrinet *et al*. 2011, Stamataki *et al*. 2011). Kim *et al*. (2016) characterised the earliest cells to exit the stem cell compartment *in vivo* by measuring stem- and lineage-specific transcripts in single $Lgr5^+$ cells. Two distinct cell populations were identified, one expressing stem cell markers, the other one simultaneously expressing stem cell markers as well as mature absorptive and secretory cell markers, concluding only one activates terminal cell markers. They demonstrated multilineage priming, as markers for both the absorptive and secretory

daughter lineages were present in the earliest progeny of $Lgr5^+$ ISCs. The earliest cells to leave the ISC compartment activate genes of both intestinal lineages, detected on the basis of single-cell RNAseq (Kim *et al*. 2016). Producing precise numbers of functional differentiated cells is crucial to maintain crypt homeostasis. In fact, ISCs differentiate early to form a precise 1:3 ratio of secretory (goblet cells) to absorptive cells (enterocytes), which is surprising given the small number of functional stem cells in the colonic crypt (Tóth *et al*. 2017).

1.6 Investigating stem cell dynamics in normal human tissue

Stem cell dynamics have been well defined in transgenic mice experiments using clonal lineage tracing techniques. These methods are impractical in humans, and stem cell dynamic studies have been based on rare hereditary changes, such as X-inactivation in glucose-6-phosphate dehydrogenase (G6PD) heterozygotes (Novelli *et al*. 2003), polymorphisms in the gene coding for the enzyme *O*-acetyltransferase (Fuller *et al*. 1990), and an isolated patient with XO/XY chimerism (Novelli *et al*. 1996). More recently, stem cell dynamic observations were based on somatic mitochondrial DNA (mtDNA) mutations to trace clonal lineages. MtDNA mutations are naturally occurring and can thus be used as clonal markers to uniquely identify clonal expansion of a population of cells with the same ancestry in human epithelial tissue (Fellous *et al*. 2009). The mitochondrial genome is prone to non-pathological mutations (passenger mutations), conferring no evolutionary constraints, thus they can be considered as neutral markers (Walther *et al*. 2016).

Mitochondria are intracellular organelles, found in all nucleated human cells. They generate ATP by oxidative phosphorylation, incorporate the electron-transferring respiratory chain (complexes I-IV) and the ATP synthase (complex V). Mitochondria contain the only non-chromosomal DNA in human cells; they contain their own mtDNA (Taylor *et al*. 2005) and are thus under the dual control of nuclear and mitochondrial DNA (Taylor *et al*. 2003). Unlike the nuclear DNA, the mtDNA is permanently turning over and not integrated in the cell cycle (=relaxed replication) (Elson *et al*. 2001). The mitochondrial genome is polyploid: each cell harbours several thousand copies (Stewart *et al*. 2015). Inheritance of mtDNA differs from

Mendelian genetics, as mtDNA is strictly inherited through the maternal line and mtDNA lineages are therefore clonal. The mitochondrial genome is subject to homoplasmy, where all copies of the genome are identical, and heteroplasmy, described as mixed mitochondrial genotypes. Mutations in the mitochondrial genome can thus either be homoplasmic (= identical mutations affecting all copies of the mitochondrial genome) or heteroplasmic (= a mixture of mutated and wild type). The transmission of mutant mtDNA together with the high mutation rate leads to the accumulation of new mtDNA mutations within the population (Chinnery *et al*. 2000, Taylor *et al*. 2005).

The mitochondrial genome has a higher mutation rate compared to the nuclear genome, which can be explained by its lack of protective histones – instead they are packed into chromosome-like organellar nuclei termed nucleoids (Lee *et al*. 2017), by its lack of DNA repair mechanisms (He *et al*. 2002, Taylor *et al*. 2001), and by its production of high levels of reactive oxygen species (ROS) triggering apoptosis (Proietti *et al*. 2017, Richter *et al*. 1988). The overall amount of mtDNA mutations is low (<2%), but individual cells may contain high levels of mutant mtDNA (Elson *et al*. 2001). Based on a mathematical simulation, mtDNA mutations arise in the stem cells through random genetic drift with a mutation rate in humans *in vivo* of 5 x 10^{-5} mutations/genome/day (Taylor *et al*. 2003). Over time, a mutation can evolve from a heteroplasmic state into a homoplasmic or near-homoplasmic state (Figure 1.5A-D).

Unsurprisingly, this process of genetic drift can take up to many years, implying that only stem cells are sufficiently long lived to acquire the near-homoplasmic state, enabling detection by the lack of an encoded protein: cytochrome *c* oxidase (CCO) (Zeki *et al*. 2012). CCO-deficient cells in humans increase with age, and only few mutants are seen before the age of 40 in the human colon (Greaves *et al*. 2006). This also enables to estimate the time required for homoplasmy to occur and for neutral competition between stem cells to take over the niche. Moreover, it provides evidence that stem cells are the source of these mutations, as whole crypts become clonally mutated and these mutations get passed on to their daughter cells. Hence, lineage tracing mtDNA mutations provide a method of tracing the stem cell progeny.

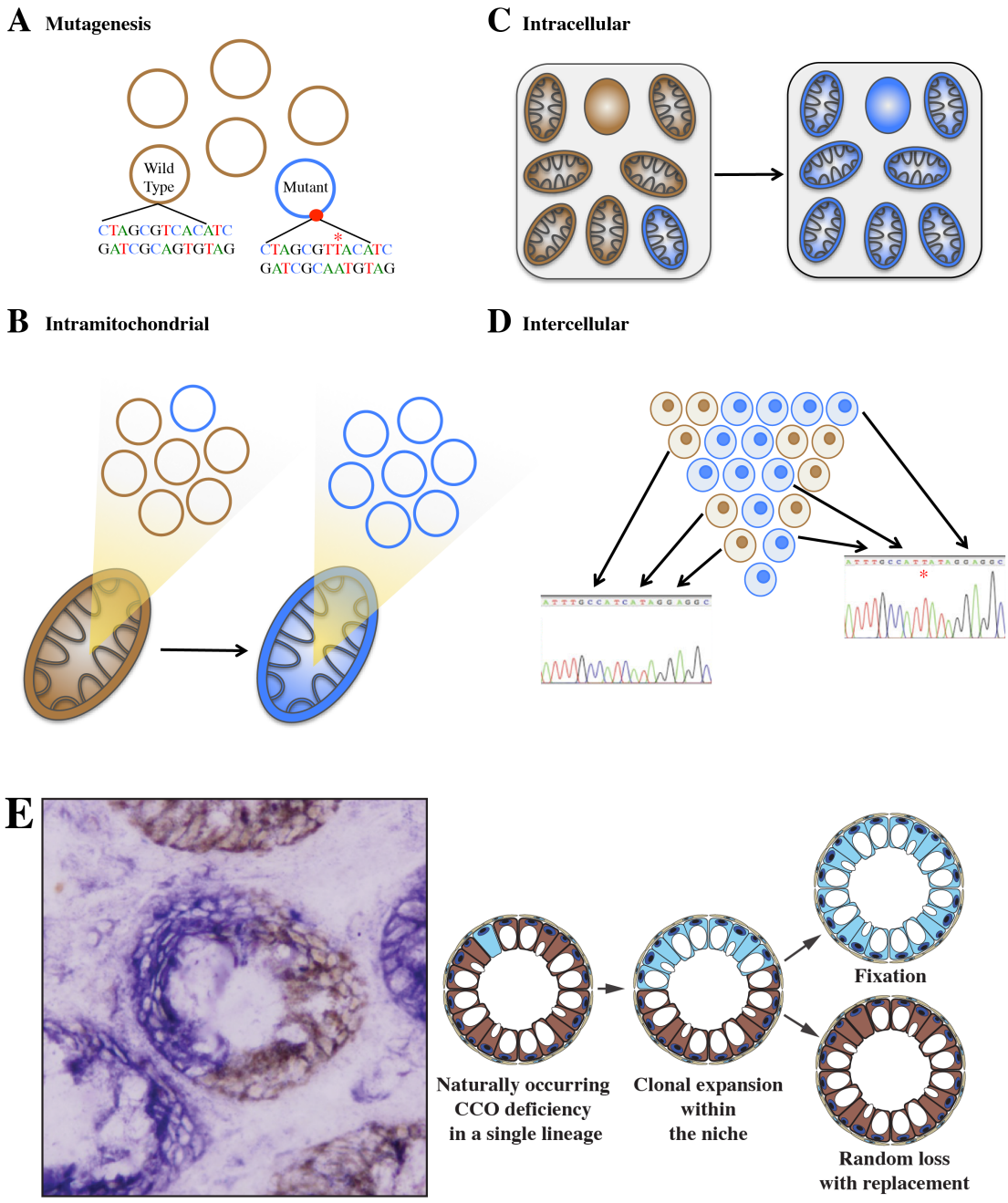

Figure 1.5: Lineage tracing in human epithelial tissues using mitochondrial DNA (mtDNA). A) MtDNA mutations can occur spontaneously in a single circular genome and B) through genome duplication and turnover become visible within a single mitochondrion and then C) through the many mitochondria in a single cell, evolving from a heteroplasmic state to a near-homoplasmic state. A cell in which at least 80% of its mtDNA is mutated results in cytochrome c oxidase (CCO) deficiency: CCO-proficient cells will stain brown, whereas CCO-deficient cells will stain blue. D) Sequencing of blue and brown cells can identify mutations. If all CCO-negative cells in a patch harbour an identical mutation, the population is considered to be clonal. E) Dual-colour cytochrome *c* oxidase (CCO) /succinate dehydrogenase (SDH) histochemistry can detect partially mutated colonic crypts, which indicate the presence of multiple stem cells within the crypt. Taken from Walther *et al*. 2016.

CCO is primarily a mitochondrial-encoded enzyme (Nooteboom *et al*. 2010), and a major regulatory site for oxidative phosphorylation. It is thus essential for the assembly and respiratory function of the enzyme complex. CCO-deficiency in the cells leads to a compromised mitochondrial membrane potential, decreased ATP levels, and essentially to apoptosis (Li *et al*. 2006).

CCO-deficient cells are known to contain high levels of mutated mtDNA, but importantly these are essentially passenger mutations conferring little to no selective advantage to normal colonic crypts. Mutations in the mtDNA *CCO* gene arise spontaneously and are detectable when > 80% are mutated in a cell (Nooteboom *et al*. 2010). Cells expressing CCO stain brown and cells deficient in CCO stain blue (Figure 1.5E). Distinctive CCO-deficient areas suggest cells have a common origin, but without sequencing the mtDNA genome of several of those clones, it remains speculation. If all cells within a CCO-deficient patch possess identical mutations, then a clonal population presumably with its origin in stem cells has been identified. Presence of multiple cell lineages within a CCO negative clone demonstrates multipotentiality (Humphries *et al*. 2013). Therefore, using somatic mtDNA mutations allows tracing clonally derived cell populations, to identify the location of their stem cell niche and to demonstrate stemness (Fellous *et al*. 2009).

The efficiency of tracing lineages of human stem cells using mtDNA mutations has already been proven successful in the intestine (Greaves *et al*. 2006, Gutierrez-Gonzalez *et al*. 2009, Humphries *et al*. 2013, Taylor *et al*. 2003), stomach (Gutierrez-Gonzalez *et al*. 2011, McDonald *et al*. 2008), Barrett's oesophagus (Nicholson *et al*. 2012), prostate (Gaisa *et al*. 2011) and in various other tissues (Fellous *et al*. 2009) and has led to a better understanding of how tumours evolve and how mutations spread. Moreover, sequencing of CCO-proficient and CCO-deficient clones has revealed that colorectal adenomas are clonal and maintained by multipotent stem cells, as the same mutation was detected in all deficient crypts, but not in the surrounding normal CCO-proficient crypts (Humphries *et al*. 2013). Partially mutated crypts were identified in the intestine indicating that these crypts contain multiple stem cell lineages (Gutierrez-Gonzalez *et al*. 2009). Furthermore, CCO-deficient crypts were found in clusters and the size of these patches increased with age (Greaves *et al*. 2006).

To investigate stem cell dynamics *in vivo* in human colonic crypts, Baker *et al*. (2014) have reconstructed crypt maps from serial *en face* sections of partially

mutated mtDNA crypts and generated clonal ribbon images, called 'Wiggles'. They have recognised that the width of the clonal ribbon reflects mtDNA mutated stem cell expansion and contraction infers temporal evolutionary dynamics from a single time point. Expansion of the ribbon equals expansion of the mutant cell pool, whereas contraction equals lineage death. By analysing the size and distribution of the changes is clone size, they have shown that human ISCs follow neutral drift dynamics and the number of functional, symmetrically dividing stem cells is five to six (Baker *et al*. 2014); similar to what has been observed in the mouse small intestine (Kozar *et al*. 2013).

A recent study by Winton's group investigated stem cell dynamics and the timing by which somatic mutations become fixed in the adult human colonic epithelium (Nicholson *et al*. 2018). As opposed to Baker *et al*. (2014), they have found that crypts are maintained by approximately 7 stem cells, of which one stem cell is replaced on average every 9 months, and a replacement rate that is between 0.65 and 2.7 stem cell replacements per crypt per year. This was further validated using various different clonal markers. This contradicts heavily the stem cell replacement rate in mice, which is almost 100-fold faster (Kozar *et al*. 2013), as well as the estimate calculated by Baker *et al*. (2014). According to Nicholson *et al*., such fast replacement is not compatible with observed times to monoclonality described for human crypts (Kim *et al*. 2002, Yatabe *et al*. 2001). Moreover, they found other processes, such as variation in the number of amplifying cells and lateral expansion of mutant clones due to crypt fission to generate large patches within the epithelium, which can explain the slower replacement rate. Furthermore, they have estimated the rate of monoclonal conversion to take many years - 13 years for 90% conversion. Similarly to Baker *et al*. (2014), they have confirmed biased behaviour for both fixation and expansion in age-related mutation burden (Nicholson *et al*. 2018).

Interestingly, another recent study using age-related mitochondrial oxidative phosphorylation defects to trace clonal lineages in human colonic crypts have found approximately 5 functional stem cells, and a stem cell replacement rate ranging from 0.14 to 1.7 per crypt per year, thus showing similar results as the Nicholson study (Stamp *et al*. 2018).

As seen in transgenic mice experiments, the ability to identify stem cells and their progeny is leading to a better and clearer understanding of stem cell evolution.

However, the underlying mechanisms why the dynamics of clonal expansion are faster in mice than in human colonic crypts remain to be established.

1.7 Clonal expansion in the normal intestine

Clones expand by crypt fission, where a crypt bifurcates from its base and divides into two independent crypts (Cheng *et al*. 1986, Wong *et al*. 2002). The crypt fission rate in the human normal colon was estimated to be every 30-40 years. This number was estimated based on the patch size distribution of CCO-deficient crypts in normal epithelium. The low basal rate of crypt fission in the adult human colon is comparable to the murine small intestine (Li *et al*. 1994). With different approaches, the rate of crypt fission ranged between 3% and 22% (Baker *et al*. 2014, Totafurno *et al*. 1987), however a recent estimate of 0.7% (Nicholson *et al*. 2018) is consistent with genomic methylation pattern studies, suggesting that most crypts can survive adult life without undergoing fission (Kim *et al*. 2002, Kim *et al*. 2004).

The underlying mechanism controlling how crypt fission is regulated in the normal intestine depends on the arrangement of Paneth cells and $Lgr5^+$ cells in the stem cell niche. Whilst Paneth cells shape the crypt base, $Lgr5^+$ cells can proliferate to expand into daughter crypts. The site of where crypt fission occurs depends on the stiffness and adhesiveness of Paneth cells. A cluster of $Lgr5^+$ cells located between at least two Paneth cells can initiate fission (Langlands *et al*. 2016).

Recently, the existence of crypt fusion has been discovered in adult mouse intestines. This phenomenon is almost exactly the reverse to crypt fission, in which two parental crypts fuse to one daughter crypt. Using *in vivo* imaging, Bruens *et al*. (2017) have found that while 3.5% of all crypts were undergoing fission, 4.1% were in the process of fusion, suggesting that fusion counteracts fission and is a counterbalancing mechanism for crypt birth. They speculated that crypt fission and crypt fusion regulate crypt and ISC numbers during the lifetime of a mouse (Bruens *et al*. 2017). However, using stochastic simulations to investigate such effect of crypt fusion, Nicholson *et al*. (2018) have shown that the observed patch size is due to crypt fission rather than crypt fusion for both, neutral and advantageous mutations (Nicholson *et al*. 2018).

1.8 Colorectal cancer

Colorectal cancer (CRC) is the third most common cancer worldwide (Amaro *et al*. 2016), and the second most common cause of cancer death in Europe (Roseweir *et al*. 2017). In 2012, CRC accounted for 9.7% of all cancers with a subsequently high global mortality rate (Ferlay *et al*. 2015). The incidence and mortality rate has declined over the last two decades. The decline in incidence in Western countries is likely to be explained by the improvement in prevention (Siegel *et al*. 2014). CRC death can be prevented by early detection, usually through colonoscopy (Brenner *et al*. 2014, Citarda *et al*. 2001). Such preventative interventions allow the detection of polyps and adenomas in an early stage, which can then be removed surgically (Amaro *et al*. 2016). Patients diagnosed with early stage CRC have a five-year survival rate of greater than 90%. Patients diagnosed with locally advanced or metastatic disease only have a 11% survival rate, and patients with metastatic CRC have a median survival of only two years, despite multiple available treatment modalities (Anderson *et al*. 2011).

1.9 Sporadic CRC

The majority of CRC cases are considered sporadic (about 95% of cases) in that they develop spontaneously typically after 50 years of age, and approximately 70% develop in the distal colon (Yamagishi *et al*. 2016). In these cases, somatic mutations occur by chance.

Sporadic CRCs develop through the accumulation of somatic genetic and epigenetic clonal events, including loss-of-function defects among tumour suppressor genes and gain-of-function defects in oncogenes (Vogelstein *et al*. 2013). These defects may confer a selective growth advantage to a cell, which characterises it as a "driver" event. It was estimated that for the ~20,000 identified human genes there are 138 driver genes (74 tumour suppressor genes and 64 oncogenes) (Vogelstein *et al*. 2013). However, a typical sporadic CRC consists of 2 - 8 driver gene alterations and "passenger" gene defects, which have no effect on neoplastic

progression (Tomasetti *et al*. 2015). This explains why each patient's tumour is genetically and epigenetically unique (Network 2012).

Sporadic CRCs can be grouped into two categories: hypermutated (15% of sporadic CRCs) and non-hypermutated (85% of sporadic CRCs) (Network 2012). Hypermutated CRCs are characterised by microsatellite instability and CpG island methylation phenotype (CIMP) resulting from DNA mismatch repair (MMR) deficiency, specifically due to the hypermethylation of the *MLH1* promoter. Other common genetic mutations in hypermutated tumours are *APC, TGF-β*, and *POLE*, as well as *MSH2, MSH3, and MSH6* of the DNA MMR genes. Most mutations occur in intrinsic coding microsatellites. Non-hypermutated tumours are usually microsatellite stable and characterised by aneuploidy, somatic copy number alterations, tumour suppressor gene mutations coupled with loss of heterozygosity (LOH) and oncogene activation. *APC, TP53, KRAS*, *PIK3CA* and *SMAD4* among others are commonly mutated at high frequency in non-hypermutated tumours (Fearon 2011, Grady *et al*. 2008).

Although hypermutated and non-hypermutated tumours progress through different sequences of genetic events, there is some overlap. For instance, *APC* is mutated in both, hypermutated and non-hypermutated tumours. Loss of *APC* is responsible for 90% of sporadic CRC cases (Shih *et al*. 2001). In total, there are ~25 genes commonly affected by somatic mutations in sporadic CRCs, whereby tumour suppressor genes and oncogenes occur at a 4:1 ratio (Network 2012). It has been shown that defects in driver genes affect general cell functions, such as cell fate, cell survival and genome maintenance, thus affecting pathways such as DNA damage control, transcriptional regulation, APC, MAPK and STAT among others (Carethers *et al*. 2015, Vogelstein *et al*. 2013). Detailed analysis revealed that in 93% of all sporadic tumours Wnt signalling was activated. Additionally, in nearly 100% of sporadic CRCs changes in MYC transcriptional targets were detected, indicating its important role in the development of sporadic CRCs (Network 2012).

1.10 Familial adenomatous polyposis

Familial CRCs account for 5% of the total number of CRC cases (Centelles 2012). Hereditary CRCs are broadly divided into non-polyposis colorectal cancers (Hereditary Non-Polyposis Colorectal Cancer, HNPCC; or Lynch syndrome), and polyposis cancers (Familial Adenomatous Polyposis, FAP; and Attenuated Familial Adenomatous Polyposis, AFAP), both of which are autosomal dominant (Takane *et al*. 2016). Patients with inherited conditions are of much higher risk to develop cancer early in life (Giglia *et al*. 2016). Lynch syndrome is the most common form of hereditary CRC with 90% of mutations caused by MMR genes, e.g. *MHL1*, *MSH2*, and *MSH6 (*Nagy *et al*. *2004,* Wells *et al*. *2017)*. Mutations in these genes can cause microsatellite instability (MSI) affecting cell growth and apoptosis, thus leading to tumour initiation and progression (Jacob *et al*. 2002).

FAP is the second most common hereditary CRC and patients with FAP have a 100% lifetime risk of developing CRC (Leoz *et al*. 2015). FAP has an incidence of 0.6 – 2.3 per million and accounts for about 0.5% - 1% of all CRCs, resulting in a heterogeneous genetic syndrome that is characterised by the development of > 100 colorectal adenomatous polyps during adolescence and the development of CRC by an average age of 40 years (Esplin *et al*. 2014, Wells *et al*. 2017). The condition when patients presenting with fewer than 100 polyps and having a later onset of CRC (an average of 59 years) is termed AFAP. These patients are typically offered prophylactic colectomy due to a high risk of cancer (Miyaki *et al*. 1994).

FAP and AFAP are caused by a mutation in the adenomatous polyposis coli (*APC*) gene, located on chromosome 5q21, and these germline mutations have been associated with 80% of patients (Groden *et al*. 1991, Kwong *et al*. 2009). The *APC* gene has been called a "gatekeeper gene" and is responsible for maintaining homeostasis in the intestinal epithelium. Loss of *APC* function causes immediate alterations of the intestinal epithelium: cells proliferate rapidly, migrate slowly and fail to differentiate, and eventually lead to tumour growth (Sansom *et al*. 2004). Patients with FAP carry an inactivating mutation in one copy of their *APC* gene, and loss of the remaining wild-type allele (either by mutation or LOH) is sufficient to initiate polyposis. Deletions at codon 1309 and truncating mutations at codons 1250 and 1464 are associated with an aggressive phenotype with early onset of polyposis.

Mutations located between codon 157 and 1595 are associated with intermediate polyposis (Wells *et al*. 2017).

In 1971, Knudson formulated the 'two-hit hypothesis' of tumourigenesis. Based on work undertaken on retinoblastomas, it was found that this cancer appeared to be caused by two mutational events; if the patient had an inherited predisposition, one mutation was germline and the second mutation was somatic, otherwise both mutations were somatic (Knudson 1971). This principle applies to *APC* mutations in FAP, where patients have one inherited mutant *APC* gene, and loss of function of the other allele will initiate tumourigenesis. Powell *et al*. (1992) demonstrated that every tumour they analysed contained *APC* mutations. This implies that loss of function of the *APC* gene is one of the earliest events occurring in tumourigenesis (Powell *et al*. 1992). The location of the second mutation depends on the location of the original germline mutation (Lamlum *et al*. 1999).

1.11 Colorectal tumourigenesis

1.11.1 The adenoma-carcinoma sequence and molecular pathways for CRC

Traditionally, colorectal tumourigenesis has been defined by Vogelstein's adenoma-carcinoma sequence (Fearon *et al*. 1990), which describes a stepwise tumour progression from normal to pre-invasive stages to carcinoma with the capacity to metastasise due to the increasing accumulation of genetic alterations (Figure 1.6A) (Fearon 2011, Leslie *et al*. 2002). This sequence also allows studying the timing of genetic alterations and the accompanying cancer-related signalling pathways. Genes involved in these genetic alterations are oncogenes, tumour suppressor genes and DNA repair genes. APC mutations are the initiating factor in the adenoma-carcinoma sequence and their frequency remains similar throughout tumour progression. LOH occurs also at early stages, but its frequency increases with tumour progression. Following *APC* initiation, LOH and mutations in *AXIN2* and *CTBNN1*, oncogenic *KRAS* mutations, and mutations in *SMAD2* and *SMAD4* appear as the tumour progresses.

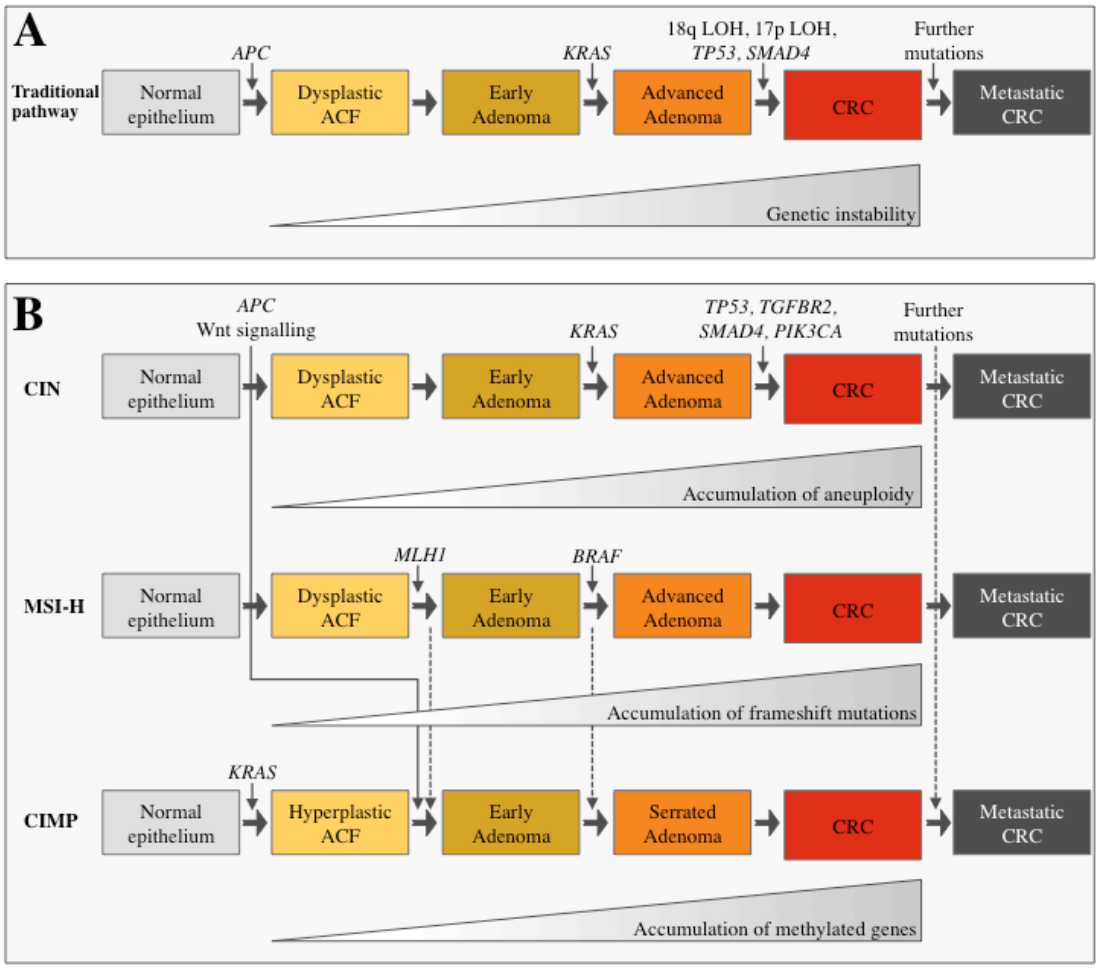

Figure 1.6: Traditional and alternative genetic pathways for CRC.
A) The traditional pathway. APC mutations are required for the initiation of most sporadic CRCs, followed by KRAS mutations also occurring early in the adenoma development. B) Alternative genetic pathways. Wnt signalling is the gatekeeper for all 3 pathways. The CIMP pathway contributes to both the MSI-H (through hypermethylation of *MLH1*) and CIN pathways, and specifically characterises a serrated pathway. CIN, chromosomal instability; MSI-H, microsatellite instability-high; CIMP, CpG island methylation phenotype. Adapted from (Carethers *et al*. 2015).

As the sequence progresses to a solid adenoma, more hits are acquired, such as *TP53* mutations and loss of apoptosis, along with increasing genomic instability, eventually leading to CRC. In addition to the adenoma-carcinoma sequence, three major distinct genetic pathways have been described after which sporadic CRCs develop: chromosomal instability (CIN; non-hypermutated), microsatellite instability (MSI; hypermutated), and CpG island methylation phenotype (CIMP; both hypermutated and non-hypermutated) (Figure 1.6B).

Approximately 85% of sporadic CRCs are non-hypermutated and follow the chromosomal instability pathway, a process that generates gene deletions, gene duplications, and chromosomal rearrangements, which usually results in aneuploidy and LOH (Pino *et al*. 2010, Puccini *et al*. 2017). CIN tumours can be distinguished by the accumulation of specific mutations in oncogenes and tumour suppressor genes (Fearon *et al*. 1990, Pino *et al*. 2010). *APC* mutations together with LOH appear to be the initial event in tumour initiation, followed by KRAS mutations (Stephens *et al*. 2011). Mutant KRAS causes increased proliferation and an increase in tumour size and moreover, is part of the ERBB/KRAS/BRAF/MAPK signalling axis. KRAS mutations were found in 41% of CIN CRCs and overall 55% of all CRCs showed KRAS and BRAF mutations (Cancer Genome Atlas Network, 2012). CIN tumours also show genetic alterations in *TGFBR1, TGFBR2, SMAD2, SMAD3* and *SMAD4* genes as part of the TGF-β signalling pathway (Jung *et al*. 2009). Mutations and LOH in TP53 initiates the conversion from benign to malignancy in CIN tumours (Starzynska *et al*. 1992), and 60% of TP53 alterations were found in CIN tumours conferring poor prognosis for the patient (Jorgensen *et al*. 2015).

15% of CRCs develop following the microsatellite instability (MSI) pathway (Azzoni *et al*. 2011, Koi *et al*. 2018). Microsatellites are sequence repeats located in both coding and non-coding regions (Subramanian *et al*. 2003). MSIs are insertion or deletion mutations at microsatellites, and these structures are prone to DNA replication. Consequently, these stretches of DNA microsatellites are not repaired due to a defect in the MMR system (Centelles 2012). Thus, MSI is caused by DNA MMR deficiency and is characterised by frequent mutations at simple nucleotide repeat sequences (Lengauer *et al*. 1998). MMR deficiency in these hypermutated sporadic cases is mainly due to the *MLH1* gene (>80% of cases) (Network 2012, Weisenberger *et al*. 2006), preventing its gene transcription (Veigl *et al*. 1998). MSI

cases are classified according to the altered size of various mono- and di-nucleotide repeat sequences (Umar *et al*. 2004). CRCs with more than two altered repeat sequences are defined as MSI-high, as opposed to MSI-low types that typically only have one altered repeat sequence. MSI-high tumours are usually associated with frameshift mutations in genes, such as *TGFBR2*, *IGF2R*, *MSH6*, *MSH3*, and *CASP5* (Markowitz *et al*. 1995, Schwartz *et al*. 1999, Souza *et al*. 1996, Yamamoto *et al*. 1997). These frameshift mutations result in a stop codon creating neo-antigenic proteins to the patient's immune system, while inactivating pathways controlling cell proliferation (Schwitalle *et al*. 2008). Moreover, in MSI-high tumours, *APC* and *BRAF* are often mutated, but *KRAS* mutations and LOH are rare. Interestingly, MSI-high tumours are mostly located on the proximal side of the colon and show better prognosis (Jenkins *et al*. 2007, Kim *et al*. 1994).

The third pathway, the CpG island methylation phenotype (CIMP), is also described as epigenetic instability that influences CRC pathogenesis (Hughes *et al*. 2012, Puccini *et al*. 2017). CIMP is characterised by an excess of epigenetic methylation of genetic loci that contain CpG islands typically in the promoter region, thus affecting gene transcription (Tahara *et al*. 2014). CIMP can be subdivided into CIMP-high and CIMP-low tumours based on the number of markers positive for methylation. CIMP-high tumours occur in ~20% of sporadic CRCs. These tumours show mostly $BRAF^{V600E}$ mutations as well as hypermethylation of *MLH1*, and are classified as hypermutated tumours (Levine *et al*. 2016, Tahara *et al*. 2014). CIMP-low tumours occur also in ~20% of sporadic CRCs, but these are mostly microsatellite stable, containing *KRAS* mutations, and are classified as non-hypermutated tumours (Luo *et al*. 2014). However, one has to notice that this classification is not absolute and CIMP CRCs overlap with MSI-H and CIN CRC pathways.

In summary, there are multiple genetic pathways involved in colorectal tumourigenesis and Wnt signalling is the gatekeeper. Importantly, these three genetic pathways are not mutually exclusive (Wong *et al*. 2011). For instance, the CIMP pathway contributes to MSI-high tumours through *MLH1* promoter methylation and the CIN pathway. Furthermore, MSI CRCs can show signs of CIN (Simons *et al*. 2013).

1.11.2 Role of stem cells in tumour initiation

It is generally believed that the earliest event in tumourigenesis occurs in the stem cell compartment, since only stem cells live long enough to acquire sufficient mutations to initiate the tumour process.

While we are now confident that cancers can be traced back to genetic events in the normal adult crypt stem cells, demonstrating this in humans has been a challenge. According to the *bottom-up* model, dysplasia arises in stem cells at the base of the crypt and their dysplastic progeny migrate upwards along the length of the crypt (Preston *et al*. 2003), as opposed to the *top-down* model, which assumes that early adenomatous lesions develop on the luminal surface without being in contact with the stem cell niche and is observed largely in advanced in adenomas. Murine studies have strongly supported the *bottom-up* model: Wnt-activating *Apc* mutations induced in $Lgr5^{+}$ CBC cells result in adenoma development and sustained growth, whereas inducing the same mutations in the TA-cells shows limited adenoma growth and eventual loss (Barker *et al*. 2009).

1.11.3 Altered Wnt signalling in tumourigenesis

Intestinal homeostasis depends on functional Wnt signalling. It is therefore unsurprisingly that mutations commonly occur in components of this pathway in CRC. In 80% of the cases, mutations in the *APC* gene lead to the activation of the Wnt/β-catenin pathway and subsequently the formation of adenomas (Cerami *et al*. 2012, Clevers 2006). Loss of function of the Wnt signalling pathway, particularly caused by APC, has been linked to CIN (Aoki *et al*. 2007). Adenomas that do not have an APC mutation often have oncogenic mutations in the β-catenin gene (*CTNNB1*) (Harada *et al*. 1999, Morin *et al*. 1997). Therefore, most CRCs have mutations in components that activate the Wnt/β-catenin pathway. In addition, in some CRCs, FZD and Wnt ligands are overexpressed and thus also modulate the Wnt pathway (Vincan 2004, Zhan *et al*. 2017). Moreover, mutations in R-spondin/Lgr5/RNF43 have been shown to drive Wnt-dependent tumour growth (Eto *et al*. 2018). For instance, R-spondin3 mutations have been described in 10% (Seshagiri *et al*. 2012) and deleterious RNF43 mutations in 19% of CRC cases

(Giannakis *et al*. 2014). RNF43 mutations are mutually exclusive to APC mutations, but depend on Wnt secretion (van de Wetering *et al*. 2015).

As opposed to the WNT-OFF state (absence of a Wnt ligand and degradation of β-catenin; see section 1.4.1), in the WNT-ON state the pathway becomes active upon Wnt binding (Figure 1.3). Following Wnt binding to Frizzled and its co-receptor LRP, the intra-cellular domain of LRP is phosphorylated, which causes the destruction complex to transduce the signal. Ubiquitylation of β-catenin is then inhibited, which enables β-catenin to escape degradation. Thus, it accumulates in the cytoplasm and eventually translocates into the nucleus where it replaces Groucho and forms a complex with the transcription factors TCF/LEF, thus initiating the expression of Wnt/β-catenin target genes involved in cell proliferation, differentiation and apoptosis (Daniels *et al*. 2005, Reya *et al*. 2005). Of note, deficiency of Tcf4 results in a lack of ISCs during the development, as it switches off Wnt signalling (Korinek *et al*. 1997). Once the Wnt pathway is mutated, the adenoma cells can maintain their progenitor status and persist for many years allowing for further mutations to be acquired (Reya *et al*. 2005). It has been shown that elevated β-catenin expression in the cytoplasm and nucleus is a biomarker for metastasis and poor prognosis (Cheah *et al*. 2002, Wong *et al*. 2004). β-catenin is mainly expressed in the membrane of normal cells, whereas in adenocarcinomas its nuclear expression is increased (Hao *et al*. 1997, Wong *et al*. 2004).

However, it is important to note that it is rather the fold change of the β-catenin level than the absolute amount in the nucleus that leads to Wnt signalling activation and dictates the outcome (Goentoro *et al*. 2009). There is a Wnt gradient throughout the intestine (Leedham *et al*. 2013), which supports the "just right" hypothesis or led to the "Goldilocks" model of Wnt signalling (Albuquerque *et al*. 2002, Driehuis *et al*. 2017).

Interestingly, different APC mutations cause distinct levels of Wnt activity and are associated with characteristic tumour locations within the large intestine for both, human CRC samples and murine tumours (Buchert *et al*. 2010, Christie *et al*. 2013). Dow *et al*. (2015) have shown that if the APC function is restored, adenomas could regress, thus indicating the importance of continuous Wnt signalling for tumour maintenance (Dow *et al*. 2015). A recent study has shown that even subtle alterations in Wnt signalling levels can reduce the fitness of ISCs (Young *et al*. 2018). Using an *Apc2*$^{-/-}$ mouse model, increased levels of nuclear β-catenin were

detected indicating that *Apc2* regulates Wnt signalling in the murine small intestine. Furthermore, *Apc2* deficiency caused an increase in Lgr5 expression, but did not lead to an increase in the stem cell number, however it affected the function and maintenance of intestinal homeostasis in $Apc2^{-/-}$ organoids. Apc2 is a homolog of Apc, but less efficient. Nevertheless Apc2 is able to form a destruction complex capable of binding β-catenin (Schneikert *et al*. 2013, van Es *et al*. 1999). This study highlights that even small changes in Wnt signalling can compromise the function and fitness of ISCs (Young *et al*. 2018).

Moreover, the tumour microenvironment also influences the Wnt pathway, indicating a more complex regulation of tumourigenesis (Brabletz *et al*. 2001). In fact, most CRCs have shown heterogeneity regarding the expression of β-catenin levels (Fodde *et al*. 2007). High Wnt activity has been observed in tumour cells that are located close to stromal myofibroblasts and myofibroblast-secreted factors can activate β-catenin dependent transcription, and thus inducing stemness features in CRC cells (Vermeulen *et al*. 2010).

1.11.4 The development of adenomas and carcinomas

The earliest observation in the development of adenomas in the colon is the monocryptal adenoma where a single dysplastic or hyperplastic crypt is seen. There has been a debate on whether dysplastic cells develop through a *top-down* mechanism to invade and colonise adjacent crypts (Shih *et al*. 2001), or whether they develop through a *bottom-up* model, where the monocryptal adenoma spreads by crypt fission (Preston *et al*. 2003) (see section 1.11.2). Clonal expansion by crypt fission has been accepted to be the prominent mode of spread of an adenomatous crypt (Wong *et al*. 2002).

Clonal crypt structures are maintained within adenomas (Humphries *et al*. 2013), and so it is important to appreciate that the crypt is the basic unit of natural selection in the colon even after the initiation of tumour growth (Barker *et al*. 2009). A somatic mutation in the tumour suppressor gene *APC* is thought to be the initial genetic change in most colorectal adenomas, resulting in a stem cell niche that is $APC^{+/-}$ (Kim *et al*. 2002).

Monocryptal adenomas are the earliest detectable lesions in the adenoma-carcinoma sequence. These clonal lesions frequently occur in FAP patients (Novelli *et al*. 1996) and have been observed in sporadic patients (Woda *et al*. 1977), but are difficult to detect due to the size of the human mucosa. It is thought that $APC^{+/-}$ cells appear normal, and become dysplastic after the second *APC* hit (Lamlum *et al*. 2000), and as a result monocryptal adenomas are often dysplastic. Loss of APC in stem cells appears to confer an ability to divide by fission at a greater rate than WT crypts resulting in a field of dysplastic crypts: the microadenoma (Park *et al*. 1995, Wong *et al*. 2002).

Stem cells that possess the second hit in *APC* colonise the base of the crypt before taking over and replacing the non-mutant cells in the stem cell niche, a process called niche succession (Humphries *et al*. 2008). Niche succession can take place as a result of symmetric stem cell divisions (Kim *et al*. 2002). $APC^{-/-}$ cells colonise the niche with mutant stem cells, which then migrate up the crypt and the crypt becomes filled with its progeny. Niche succession and monoclonal conversion results in a dysplastic $APC^{-/-}$ crypt in an otherwise normal tissue, giving rise to a monocryptal adenoma (Figure 1.7) (Nakamura *et al*. 1984).

The next step in the progression from a monocryptal adenoma is the development of a microadenoma or aberrant crypt focus (ACF). ACF are defined as small numbers of histologically, abnormal crypts, considered to be the first morphological change of the pathway that leads to the formation of adenomas (Jass *et al*. 2002).

There are two types of ACF: dysplastic and non-dysplastic ACF. Although non-dysplastic ACF are associated with the formation of hyperplastic polyps, their role in colorectal tumourigenesis remains unclear. They appear to be initiated by mutations in the *KRAS* gene (Takayama *et al*. 2001). Dysplastic ACF are easily recognisable in the mucosa of FAP and non-FAP patients. Studies of FAP lesions have shown that all dysplastic ACF contain *APC* mutations, whereas in sporadic lesions mutations in the *KRAS* gene are much more frequent (Otori *et al*. 1998, Takayama *et al*. 2001). Thus, a single dysplastic crypt can arise and expand via crypt fission to become an established adenoma. During adenomatous growth the normal crypt hierarchy appears to be maintained, but rates of crypt fission are increased.

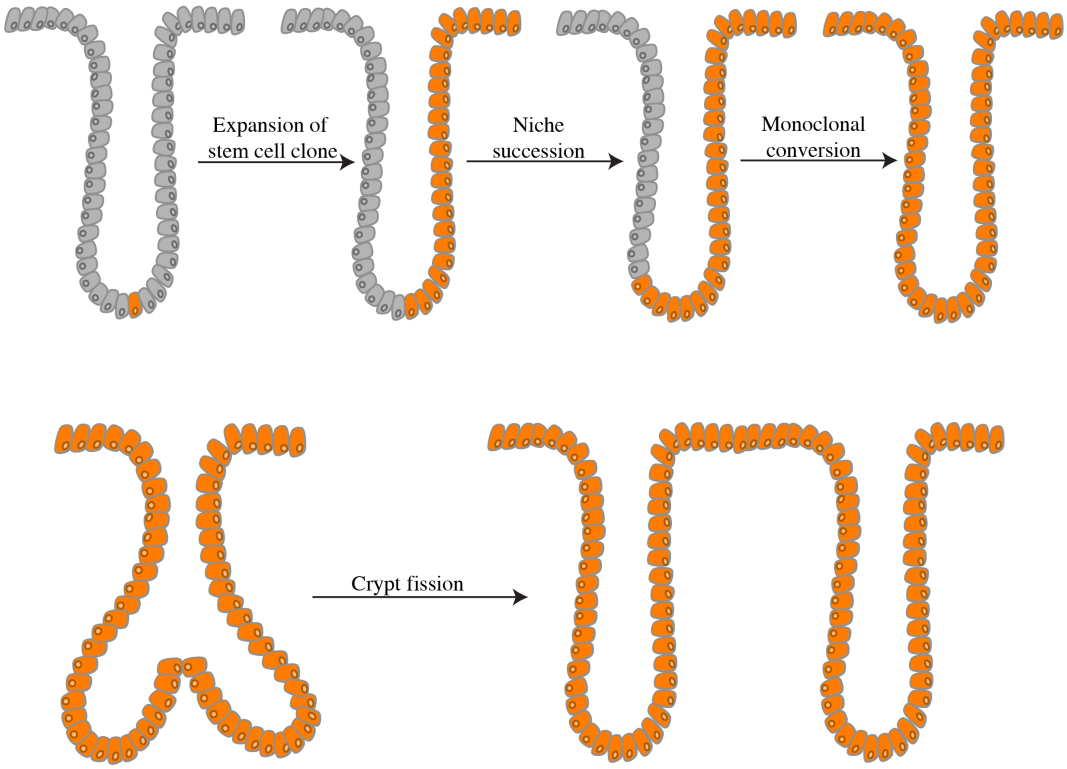

Figure 1.7: Niche succession and crypt fission.
Stem cells reside at the crypt base. A mutated stem cell (highlighted in orange) within the stem cell niche is able to expand via niche succession. Subsequently, all progeny of that stem cell lineage take over the crypt, known as monoclonal conversion, resulting in a monocryptal adenoma. The mutated crypt then clonally expands by crypt fission forming a microadenoma.

Development of a large adenoma usually requires further mutations, for instance in *KRAS* or *BRAF* oncogenes, and progression to carcinoma usually involves acquisition of mutations in the transforming growth factor-β (TGF-β) and p53 pathways (Luebeck *et al*. 2002). The progression to a malignant colorectal tumour is thought to take many years. CRC is characterised by genomic instability, which is an early event in the progression to cancer. It is thought to be caused by a defect in cell cycle checkpoints, DNA damage or a non-repaired mutation and can manifest itself as CIN and MSI (see section 1.11.1) (Horvat *et al*. 2011).

The evolutionary events behind the progression from adenomas to carcinomas remain largely unknown. Multi-region sequencing of benign and malignant colorectal tumours has shed light on the evolutionary fitness landscape of those tumours. The fitness landscape is a concept to understand the relationship between genotypes and, in this case, the fitness of sub-clones. The fitness landscape of adenomas evolved wavy-like, whereas with carcinomas, the fitness landscape showed sharper peaks, most likely due to stabilising selection. While adenomas were found to frequently harbour sub-clonal driver mutations and to have high genetic heterogeneity, carcinomas showed chromosomal abnormalities that evolved due to a punctuated manner (Cross *et al*. 2018). In a recent study using whole-exome sequencing, the somatic mutation landscape of premalignant adenomas was characterised. A gene panel of 20 genes was identified with which colorectal adenomas can be distinguished from adenocarcinomas. This could potentially be of help for targeted surveillance programmes and preventive interventions to reduce the number of patients with adenomas progressing to CRC (Lin *et al*. 2018).

Intratumour heterogeneity (ITH) has been well documented in CRC and occurs when distinct subclones carry genomic and epigenomic alterations that are not present in the bulk of the tumour or other subclones. Genomic instability, a hallmark of many cancers, is thought to generate ITH and is a feature of CRC (Amaro *et al*. 2016). The big bang model best explains the mutation pattern observed in CRC: after initiation, the tumour grows predominantly as a single expansion. Mutations are acquired early followed by a flat evolution with limited expansion resulting in ITH. Mutations that arise later in the process are only present in small regions of the tumour. This finding supports their hypothesis that some precursor lesions might be 'born to be bad' and early events dictate later events in tumour growth and

progression (Sottoriva *et al*. 2015). Another study by Kang and colleagues has shown that by measuring point mutations, chromosome copy number alterations and DNA methylation patterns from individual glands of opposite ends in colorectal adenomas, ITH was present between tumour sides and individual glands, but private mutations were side-specific and subdivided the adenoma into two major subclones. The methylation studies have shown that glands were diverse and relatively old populations, indicating that mutations detected in ITH arose during the first few divisions and expanded into a star-like tree with co-clonal expansion (Kang *et al*. 2015). In addition, by analysing sub-clonal genetic divergence from multi-region sequencing, it is possible to distinguish tumours that are driven by strong selection from those that are under weak selection, having implications on how tumours progress and accumulate ITH (Sun *et al*. 2017).

A recent study has examined the role of early tumour cell mobility regarding the shaping of private mutations detected in the "final tumour". Using computational models, they have shown that early cell mixing in the first tumour gland resulted in private mutations that can be detected on both sides of the tumour, whereas lack of early cell mixing led to distinguished mutation patterns. This was further validated using single gland data from human colorectal tumours, showing evidence of abnormal cell mobility in 60% of invasive colorectal carcinomas, while none were found in benign adenomas. This indicates that the start of benign and some malignant tumours can be differentiated, and that abnormal cell mobility, which is required for invasion, is already present at the early stages of tumour growth (Ryser *et al*. 2018).

1.11.5 Niche succession by tumour clones

Through symmetrical divisions and random apoptosis of stem cells, a stem cell lineage can via neutral drift or via a selective advantage become dominant in a niche - a process termed *niche succession* (Kim *et al*. 2002). The progeny of this stem cell will then occupy the whole crypt - a process known as *monoclonal conversion*.

The work done by Shibata and colleagues has given substantial insights into the mechanisms of niche succession in the human colonic epithelium (Kim *et al*. 2002, Nicolas *et al*. 2007, Yatabe *et al*. 2001). They proposed that the progeny of stem cell lineages might be distinguished by analysing their methylation pattern,

since it is known to increase with age even in the normal colon (Issa 2000). Methylation at CpG loci become polymorphic with age, inferring that stem cell lineages that are closely related should exhibit similarities in epigenetic signatures, as they are not subjected to selective pressure. Therefore, cell histories can be inferred by comparing epigenetic tags between cell populations. This further indicates that niche succession cycles occur as a consequence of stem cell divisions and neutral drift dynamics within the colonic niche (Simons *et al*. 2011).

During the process of niche succession and monoclonal conversion, mutations become fixed (see Figure 1.7). Stem cells are prone to genetic drift and a single mutated stem cell can dominate the entire niche as a result of stochastic non-selective events. Therefore, neutral mutations can become fixed over time without affecting the fitness of a cell in a population. These neutral alterations can be detected, as they expand through the crypt by clonal expansions driven by selection or drift (Stratton 2011). Occasionally, mutations can have a selective growth advantage, especially mutations in tumour suppressor genes, such as *APC*. This allows speeding up the process of niche succession and monoclonal conversion, and the mutated stem cell progeny can occupy the whole crypt.

It is assumed that mutant clones expand by natural selection and genetic drift, whereby the fitness of neoplasms is dependent on their interactions with other cells and their microenvironment (Greaves *et al*. 2012). Mutations can be defined as drivers when they confer a selective advantage to the cell, and passengers when they do not alter fitness but occur in a cell that has already acquired a driver mutation (Bozic *et al*. 2010). The progressive accumulation of mutations may result in a selective sweep, which is defined as a process where natural selection rapidly drives the advantageous clone to fixation (Greaves *et al*. 2012).

Even though it has been established that *KRAS* and *APC* mutations have a competitive advantage over WT clones, this does not necessarily infer that a clone will become fixed. The proportion of a mutant $Apc^{-/-}$ clone to become fixed in an $Apc^{+/-}$ background is ~55%. The majority of $Apc^{+/-}$ mutant stem cells will be replaced by WT stem cells through a stochastic, albeit biased process and thus disappear from the tissue, indicating that the accumulation of mutations is actually a very inefficient process (Vermeulen *et al*. 2013). Another cellular defence mechanism is senescence and apoptosis, which also minimises the accumulation of mutations (Vermeulen *et al*. 2014).

1.11.6 Crypt fission is the mechanism of clonal expansion in the gastrointestinal tract

Progression and expansion from a monocryptal adenoma to an established adenoma within the colon is due to crypt fission (Wong *et al*. 2002) (see Figure 1.7). In the normal adult colon, crypt fission is rare, but in response to epithelial damage, such as inflammation, the proportion of crypt fission increases (Cheng *et al*. 1986, Snippert *et al*. 2014, Wong *et al*. 2002).

Crypt fission is generally accepted as the most important mechanism for clonal expansion in early adenomas (Wong *et al*. 2002). Current dogma states that adenomas are monoclonal and therefore are derived from a single crypt. Therefore, crypt fission results in patches of related crypts and is frequently observed in normal colon increasing with age. Mechanistically, an adenomatous crypt would start dividing at the crypt base in the stem cell region and bifurcate into two adenomatous crypts (Greaves *et al*. 2006).

There is evidence that *APC* mutant crypts show an increased ability to undergo fission. In FAP patients, the crypt fission rate is increased compared to normal mucosa and further evidence suggests that *APC* mutations cause expansion of the crypt base cell populations, indicating that $APC^{+/-}$ crypts are able to expand at a faster rate than normal crypts (Wasan *et al*. 1998). The crypt fission rate of non-dysplastic colon of FAP and AFAP patients was comparable to the crypt fission rate of normal colon. However, the estimated crypt fission rate within $APC^{-/-}$ adenomas increased drastically, thus providing a plausible explanation for the expansion of mutant clones (Baker *et al*. 2014). Genetic lineage tracing studies in mice have shown the crypt fission rate is increased 30-fold by an oncogenic *KRAS* mutation compared to the normal murine colon (Snippert *et al*. 2014). Crypt fission is also increased in conditions of inflammation and adenomas resulting in extensive clonal expansion (Cheng *et al*. 1986, Galandiuk *et al*. 2012, Leedham *et al*. 2009).

Crypt fission is thought to be the mechanism for field cancerization, which is defined as the replacement of the normal cell population by a non-dysplastic mutant clone predisposed to tumour development (Hawthorn *et al*. 2014). The concept of "field cancerization" was first described by Slaughter *et al*. in 1953 as the "preconditioning of an area of epithelium to cancer growth by a carcinogenic agent"

to explain the development of primary tumours and recurrent cancer types (Slaughter *et al*. 1953).

Thus, the mutant clone grows into large patches, or fields, of cells, which eventually progress to a neoplasm (Braakhuis *et al*. 2003). Over time, the clone with the fittest phenotype will dominate the cancerized field (Driessens *et al*. 2012). In addition, the surrounding microenvironment is altered by the cancerized field, and thus the interplay between the microenvironment and the mutant cells determines the selection of mutations (Curtius *et al*. 2018). The cancerized field can vary in size, starting from a single lineage, which evolves to cancer over time (Garcia *et al*. 1999).

A characteristic of a cancerized field is the mutational diversity existing within the field and genetic drift. Mutational diversity is likely to be a substrate for natural selection and the fittest clone will dominate the field (Simons *et al*. 2011). Furthermore, changes in the microenvironment, such as of stromal cells, can also promote field cancerization. However, a study in the skin has shown that stromal cells provide selective pressure for a tumour to form, but are unable to actually cause the formation of a tumour (Hu *et al*. 2012). As the stroma does not transform into a tumour, it is not considered to be cancerized.

Mutations that are important for generating a field are recognised as driver mutations. In the skin, a high density of driver mutations (~140 per cm^2) has been found (Martincorena *et al*. 2015) and more interestingly, driver mutations were found in small patches of morphologically normal skin compared to skin basal cell carcinoma (Bonilla *et al*. 2016). In the inflamed small intestine, TP53 is a driver mutation for field cancerization (Vermeulen *et al*. 2013), indicating that the interplay between the microenvironment and the mutant clones provides a growth advantage. However, multiple driver mutations are necessary for a field to progress to cancer (Weaver *et al*. 2014). Field cancerization has also been shown in the colon (Hawthorn *et al*. 2014, Leedham *et al*. 2009), in Crohn's disease (Galandiuk *et al*. 2012), the stomach (Gutierrez-Gonzalez *et al*. 2011), and the skin (Hafner *et al*. 2010).

The altered microenvironment enables field cancerization due to changes of fitness effects of mutations in epithelial cells. As a consequence, cancerized lineages can expand (Elinav *et al*. 2013). It is not surprising that a cancerized clone is found in a specific microenvironment. Clones need to adapt to the selective pressures

emanating from the microenvironment in order to progress to malignancy. Gatenby and Gillies identified six microenvironmental challenges a clone had to overcome to develop into a malignant phenotype: apoptosis, inadequate growth promotion, senescence, hypoxia, acidosis and ischaemia (Gatenby *et al*. 2008). Thus, clonal adaptation and the generation of a cancerized field can only occur if such microenvironmental challenges are met.

Three evolutionary measures – genetic diversity, the quantification of mutation rates and rates of clonal expansion – are factors with prognostic value for sensitive detection of a cancerized field that is of high risk (Curtius *et al*. 2018). Genetic diversity is a proxy measure for indicating that a more diverse field is more likely to have adapted to new selective pressures (Greaves *et al*. 2012). Quantifying the mutation rates indicates at what speed new adaptive lineages are produced. Clonal expansion shows how quickly a clone can grow, thus assessing the size of a cancerized field. Clonal expansion is also providing evidence for positive selection of those growing clones within the field, which has been shown to have prognostic value in ulcerative colitis (Salk *et al*. 2009).

Understanding the evolutionary dynamics of cells within a cancerized field is crucial in accurately determining the clinical risk of cancer development from a cancerized lesion, as cancerized fields are common but only a few do actually progress to cancer (Welch *et al*. 2010).

1.12 Stem cell dynamics in tumourigenesis

ISCs and CRC are closely linked in that ISCs are the cells of origin for CRC (Vermeulen *et al*. 2014). Thus visualising their behaviour is necessary for monitoring tumour progression. The effect of oncogenic mutations in ISC behaviour describes the basis of tumourigenesis in the gut. Various methods have been described to investigate stem cell dynamics in murine and human tissue. For murine tissue, the approach of using the lineage tracing technique is the most informative. Stem cell lineage tracing enables to trace the progeny of a stem cell (Blanpain *et al*. 2013).

The stem cell marker Lgr5 has also been proven useful to label stem cells in adenomatous crypts. Schepers *et al*. (2012) have used the multicolor Cre-reporter

R26R-Confetti to study the behaviour of Lgr5^{+} cells within *Apc*-mutant adenomas and demonstrated that adenomas developed from *Apc*-depleted Lgr5 stem cells (Schepers *et al*. 2012). This indicates that Lgr5 also labels a subpopulation of adenomatous stem cells. Moreover, these Lgr5^{+} cells were found to be intermingled with Paneth cells at the base of the crypt, which is similar to what has been observed in the normal crypt base architecture (Sato *et al*. 2011), indicating an adenoma stem cell niche. This was also shown using markers enriched in normal colon Lgr5^{+} stem cells to detect stem cell population in CRC, which were also shown to reside at the base of the crypt resembling normal crypts (Merlos-Suarez *et al.* 2011). The presence of such Lgr5^{+} stem cells and their differentiated lineages was confirmed using single cell polymerase chain reaction (PCR) (Dalerba *et al.* 2011).

Clonogenic analyses from Lgr5-GFP^{hi} and Lgr5-GFP^{lo} cells from 30-day-old adenomas showed that Lgr5-GFP^{hi} stem cells grew out into organoids with an efficiency that was 20 times higher than for Lgr5-GFP^{lo} stem cells, implying multipotent stem cells (Schepers *et al.* 2012). Only 5 to 10% of the adenoma cells were Lgr5-GFP^{hi} , which is again similar to number of stem cells in the niche of normal crypts (Kozar *et al.* 2013, Vermeulen *et al.* 2013). Kozar *et al*. (2013) applied a continuous clonal labelling approach to quantify the dynamics of such clonogenic stem cell replacement, but found a lower number of nine functional stem cells per adenomatous crypt. Furthermore, these stem cells were replaced at a lower rate as well, indicating that the purpose of tumour stem cell division is to replace stem cell loss (Kozar *et al*. 2013).

Snippert *et al*. (2014) used a tamoxifen- induced Cre-LoxP transgenic system to induce activating *Kras*^{G12D} mutations in Lgr5^{+} ISCs in mice to trace lineages via expression of β−galactosidase (β-gal) or confetti expression. After only 3 days post tamoxifen injection, β-gal clones in *Kras* mice were significantly larger and had more *Lgr5*$^{+}$ cells than WT mice. After 14 days a higher frequency of those clones was identified and many crypts became entirely β-gal^{+} (fixation), which was not observed in WT clones induced using similar methods. Concurrently, clonal extinction occurred less frequent in *Kras* mutant stem cells compared to WT clones, indicating that stem cells with *Kras* mutations have a survival advantage. It has been shown that labelled clones in the stem cell compartment expand or contract due to the frequency of loss and replacement (Snippert *et al*. 2014).

To determine the mechanism and rate of how such mutations affect intra-crypt stem cell competition, Snippert *et al*., (2014) applied a model of neutral drift to commonly observed mutations. This model is based on the stem cell number in a crypt and calculating the loss (displacement from the niche) and replacement rate to predict clone size distributions. Their model also assumed that a mutant clone can expand through stochastic stem cell division replacing a WT clone at a higher rate to account for the observed survival advantage over WT clones. It was found that *Kras* mutant clones have a 4-5 larger survival probability than WT clones. This competitive survival advantage mutant clones have over WT clones was partly explained by a faster cell cycle rate in *Kras* mutant epithelia, however, mutant clones expanded faster due to increased crypt fission rates to up to 30-fold (Snippert *et al*. 2014).

Understanding stem cell differentiation is important in understanding disease progression. Stem cells can interact and sense their neighbouring cells, and cell-cell interactions are important factors in determining the progeny of a daughter cell (Smith *et al*. 2015). In a mouse model with activated *Kras* mutations, clones have an advantage as they expand and become fixed more rapidly as compared to WT lineages. In the Snippert *et al*. study, $Kras^{G12D}$ mutant stem cell clones replaced the WT crypt stem cell population in approximately 80% of the experiments, based on biased drift. In mice with an inactivating heterozygous *APC* mutation, the mutated stem cell replaced the WT stem cell in 62% of the time, whereas inactivating homozygous *Apc* mutations conferred a 79% advantage over WT clones. Moreover, $Apc^{-/-}$ stem cells had a 69% clonal benefit over $Apc^{+/-}$ stem cells under neutral competition, although clones harbouring a mutation in *Apc* clearly had an advantage over WT clones (Vermeulen *et al*. 2013).

The functional role of ISCs in CRC initiation has recently been defined in mice with $Apc^{min/+}$ and $Kras^{LSL\text{-}G12D}$ mutations labelled with *Lgr5* that express a diphtheria toxin (DT) receptor fused to an enhanced green fluorescent protein (eGFP) (AKL model) (de Sousa e Melo *et al*. 2017). To further imitate the classical CRC progression, *Trp53* (AKPL model) and *Smad4* (AKSL model) gene mutations were introduced in these mice. Organoid cultures were established and subcutaneously transplanted into animals expressing WT Lgr5. Moderate growth was observed in AKL and AKPL mice, whereas in AKSL mice tumours grew exponentially, thus mimicking gradual disease progression as seen in patients. Lgr5

cells were shown to mark tumour-initiating cells, as a higher fraction of *Lgr5*$^{+}$ cells was found in mice with increased tumourigenic potential. Interestingly, ablation of *Lgr5*$^{+}$ stem cells with DT does not lead to tumour regression. Instead, the tumour remained static and maintained by proliferative *Lgr5*$^{-}$ cells upon treatment was stopped, which then led to a rapid re-initiation of tumour growth, indicating that *Lgr5*$^{+}$ cells are required for tumour progression and that the *Lgr5*$^{+}$ cell state is reversible (de Sousa e Melo *et al*. 2017).

Clonal outgrowth has not only been attributed to Lgr5, but also to colon cancer cells with high MAPK activity, also providing evidence for cellular hierarchy (Blaj *et al*. 2017). A recent study using multicolour lineage tracing in colon cancer xenografts has shown that clonal expansion starts at the leading edge of the tumour with tumour cells competing for outgrowth towards the tumour centre, indicating that the position of tumour cells may be more important for a lineage to persist than the tumour cell phenotype (Lamprecht *et al*. 2017).

In conclusion, a complex interplay between mutations and clonal dynamics is involved in the evolution of cancer. Oncogenic mutations alter the fate of a clone, thus giving it a competitive advantage that can persist and colonise the entire crypt and tissue, posing an increased risk for cancer development.

1.12.1 Investigating stem cell dynamics in human tumourigenic tissue

Genetic lineage-tracing studies in human tumours are unfeasible and the inference of stem cell dynamics relies on so called 'molecular clocks', which are essentially any stable and detectable neutral mutation occurring at a rather high rate. An example of a molecular clock is the use of CCO activity in mtDNA mutations, which has revealed that adenomatous crypts are predominantly clonal (Humphries *et al*. 2013).

Lineage tracing has been a powerful tool in understanding tumour evolution over time. Investigating stem cell dynamics *in vivo* using somatic mtDNA mutations to trace clonal lineages in human colonic crypts of FAP and AFAP patients has revealed that *APC*$^{+/-}$ and *APC*$^{-/-}$ adenomatous crypts follow a neutral drift type process. The functional stem cell number was calculated to be between five and six in FAP patients. Interestingly, in *APC*$^{-/-}$ adenomatous crypts a 2-fold increase in both the number of functional stem cells and the loss/replacement rate was observed

(Baker *et al*. 2014). This is the first study to show that APC mutations have a distinct role in regulating stem cell dynamics in the human colon.

Two recent studies implemented CRISPR-Cas9 gene-editing technology to insert cassettes into the *LGR5* locus in organoids from patients with CRC. Xenografts obtained from these organoids were used to study stem cell dynamics in tumours (Cortina *et al*. 2017, Shimokawa *et al*. 2017). Both experiments have identified that $Lgr5^+$ CRC produce progeny over long periods of time. Using a tamoxifen-inducible Cre knock-in allele of Lgr5 followed by selectively ablating $Lgr5^+$ in stem cells in organoids, the tumour ceased but re-grew when $Lgr5^+$ stem cells re-emerged (Shimokawa *et al*. 2017). The number of daughter cells produced by $Lgr5^+$ tumour cells was found to be proportional to the size of the xenografts (Cortina *et al*. 2017). These studies show that human CRCs are composed of heterogeneous cell populations organised into hierarchies, similar to that of the normal colonic epithelium. Using human organoids and xenografts allows quantifying stem cell dynamics in the human intestine.

Another approach to visualise stem cell dynamics in human intestinal tissue is through the analysis of methylation pattern diversity (Nicolas *et al*. 2007). Methylation events occur at CpG sites of non-expressed genes, which means that methylation is not strongly regulated and can occur randomly during DNA replication in stem cells. Thus, the resulting epigenetic signature to the stem cell lineage can be analysed to study dynamics and infer rates of clonal expansion (Ro *et al*. 2001). The number of methylated CpGs will increase with the longevity of stem cells, meaning that the older a stem cell lineage, the greater the chance of detecting methylation pattern diversity (Chu *et al*. 2007).

It has been proposed that age-related methylation predisposes a risk to CRC because methylation alters the physiology of aging cells and tissues (Issa *et al*. 2001, Kulis *et al*. 2010). Thus, higher levels of age related methylation signatures were associated with a greater risk of developing CRC. The clonal origin can be inferred by comparing the methylation signatures between any two cells. If two cells share similar methylation patterns, they are likely to share a recent common ancestor (clonal relationship). In a seminal study, Yatabe and colleagues investigated stem cell population dynamics in the crypt using methylation patterns (Yatabe *et al*. 2001). With the identification of individual crypts having a limited number of distinctive methylation signatures, they were able to prove that crypts housed multiple long-

lived stem cells. The rate of change of methylation status at CpG sites was estimated at approximately $2x10^{-5}$ per CpG site per division (Kim *et al*. 2002, Yatabe *et al*. 2001). Moreover, methylation pattern diversity within a crypt demonstrated that stem cells were challenging each other to remain within the niche (Nicolas *et al*. 2007, Yatabe *et al*. 2001). Similar niche dynamics have also been demonstrated within the small intestine (Kim *et al*. 2005).

The study of methylation patterns in the colon has revealed that age-related methylation is consistent with colonic crypts being maintained in niches that contain multiple related stem cells. This indicates that successive niche succession cycles take place in human colonic crypts, which is a natural consequence of stem cell divisions and neutral drift within the niche (Simons *et al.* 2011). This led to the estimation that every 8 years all stem cell lineages within a crypt niche except for one become extinct (Kim *et al.* 2002).

Methylation patterns also allow the study of clonal expansion of human intestinal crypts (Graham *et al*. 2011). By comparing the methylation patterns between clonal populations of adjacent CCO-deficient colonic crypts, clonality was established. The authors discovered that patches of related crypts had different methylation patterns and so did adjacent crypts, suggesting that clonal expansion rates are very slow in the normal gut. Even bifurcating crypts had different patterns, indicating that once a crypt has undergone fission, clone ancestry can no longer be followed. The observed dissimilarities in methylation pattern were most likely due to stem cell dynamics and epigenetic drift. Resulting from this observation is that epigenetically diverse tumours are likely to be old populations, while a similar methylation pattern within a clone suggests recent clonal expansion (Graham *et al*. 2011).

In another study, adenomas were shown to have diverse methylation patterns, indicating that each of the adenomas analysed had enough time to evolve distinct intra-tumour methylation patterns (Humphries *et al*. 2013). By comparing methylation patterns of adenomas with normal colon, the authors found that on average the growth rates did not differ significantly. Moreover, analysing methylation patterns revealed that adenomatous crypts have similar stem cell dynamics compared to normal crypts, suggesting that each crypt contains a number of stem cells, which are competing with one another for space within the niche.

Methylation pattern diversity has also been proven to be useful in distinguishing between tumour and normal breast, colon, liver and lung tissue (Hao *et al*. 2017). DNA methylation analysis distinguished cancer vs. normal tissue in more than 95% of the time, indicating the use of methylation biomarkers for molecular characterisation of cancer, thereby improving diagnosis and prognosis (Hao *et al*. 2017).

1.13 Genetic and environmental interactions

Increasing evidence suggests that in addition to genetic and epigenetic changes, environmental factors also drive tumour progression. Moreover, the evolution of CRC depends on reciprocal interactions between transformed epithelial cells and stromal cells that form the tumour microenvironment (Mroue *et al*. 2013). The stroma in healthy tissue acts as a barrier against tumourigenesis and maintains homeostasis, but the presence of tumour cells effects stromal cell gene expression changes that convert the microenvironment into one that supports tumourigenesis (Junttila *et al*. 2013). Inappropriate activation of the stroma implicates migration of stromal cells, ECM remodelling, reprogrammed metabolism, activated transcription, and expansion of the vasculature (Scherz-Shouval *et al*. 2014, Valencia *et al*. 2014). Regions under selective pressure influence tumour progression as well as environmental factors selecting for specific mutations that assure survival of cancer cells, which eventually lead to tumour heterogeneity (Meric-Bernstam *et al*. 2012). Once the stroma supports tumour progression, the stromal cells co-evolve with tumour cells: they become educated and modified by tumour cells to synthesise cytokines, chemokines and growth factors (Valkenburg *et al*. 2018).

The stroma constitutes a large fraction of solid tumours and in some carcinomas makes up more than 80% of the tumour mass. The tumour stroma is composed of infiltrating immune cells, and specialised fibroblasts (termed cancer-associated fibroblasts (CAFs)), blood vessels and muscle cells, all embedded in a network of extracellular matrix (ECM) proteins (Belov *et al*. 2010, Rupp *et al*. 2015).

1.13.1 The role of activated fibroblasts in colorectal carcinogenesis

Fibroblasts in the activated stroma are termed CAFs. CAFs form a favourable microenvironment for tumour cells, and have been shown to initiate and promote tumourigenesis in CRC (Nakagawa *et al*. 2004). They express high levels of extracellular factors, such as chemokines and insulin-like growth factor binding proteins, which leads to the formation of an inflammatory niche (Rupp *et al*. 2015, Torres *et al*. 2013). Fibroblasts can be activated through growth factors, cell-cell communications, and ROS among other factors (Kalluri *et al*. 2006). If they stay activated after the first mutational event, they start working together with other molecular pathways to enforce tumour initiation. CAFs then recruit inflammatory cells, and stimulate tumour cell proliferation by secreting growth factors, inducing angiogenesis, secreting cytokines and through mesenchymal-epithelial cell interactions (Kalluri *et al*. 2006).

A commonly used marker to identify CAFs is α-smooth muscle actin (SMA). In CRC, the number of positive stained myofibroblasts is increased compared to normal stroma, and α-SMA$^-$ fibroblasts change to α-SMA$^+$ ones (Adegboyega *et al*. 2002). CAFs are a useful marker for prognosis in CRC (Mukaida *et al*. 2016). Tumours with α-SMA positive cells have been associated with worse prognosis for stage II and III after CRC surgery (Tsujino *et al*. 2007). Patients with a high intra-tumour stroma proportion also show a shorter overall survival rate and metastasis (Henry *et al*. 2007). The prognostic value of CAFs can be recognised from the gene expression signature, as some genes predict recurrence in CRC patients with high accuracy (Berdiel-Acer *et al*. 2014). CRC subtypes with poor prognosis can be attributed to genes expressed by stromal cells. Especially CAFs increased the frequency of tumour initiating cells, which was further enhanced by TGF-β signalling (Calon *et al*. 2015). Another study has found a subtype of CRC also attributed to stromal cells rather than tumour epithelial cells, as unregulated genes were mostly expressed by stromal cells. High expression of CAFs was associated with poor prognosis in untreated CRC patients (Isella *et al*. 2015).

1.13.2 The role of immune cells in colorectal carcinogenesis

Progression of CRC also relies on infiltration of immune cells, providing a complex signalling environment. Inflammatory cells are a major component of the tumour stroma (Fridman *et al*. 2012), and their presence has been associated with a better prognosis for CRC patients, which is heavily dependent on the type of immune cells and their gene expression (Fridman *et al*. 2012).

The immune system is divided into an adaptive and innate immune system. The adaptive immune system contains T-cells and B-cells, while the innate immune system contains dendritic cells, natural killer cells, macrophages, granulocytes and mast cells (Angell *et al*. 2013). Immune cell types and their concentrations are heterogeneous between tumour types and between patients with the same tumour type. T cells can further be subdivided into T helper cells ($CD4^+$) and cytotoxic T cells ($CD8^+$). Specifically $CD8^+$ cells have been linked to a better clinical outcome, as opposed to regulatory T cells that can facilitate tumour immune avoidance or suppression (Quigley *et al*. 2015). In two pioneering studies, it has been demonstrated that high T cell infiltrates did correlate with improved overall survival in CRC patients (Galon *et al*. 2006), and that high number of tumour-infiltrating memory T cells do not show signs of metastasis (Pages *et al*. 2005). T cell infiltration is now an established prognostic marker in CRC (Funada *et al*. 2003, Halama *et al*. 2011, Reissfelder *et al*. 2015).

Tumour inflammatory infiltrate typically includes T and B cells, macrophages, dendritic cells, mast cells, and natural killer cells (Fridman *et al*. 2012). The tumour is able to alter its antigens, which can be presented to T cells, resulting in an adaptive immune response to the tumour consisting of helper T cells (CD4). $CD4^+$ cells then drive the expansion and differentiation of cytotoxic T cells (CD8), which leads to the influence of the tumour microenvironment on the T cell response and the generation of T regulator cells that aid the escape of the immune system (Chirica *et al*. 2015).

CD4 cells, important for anti-tumour immunity, stimulate cytotoxic CD8 cells, macrophages and B cells. They are subdivided in T helper-1 cells or T helper-2 cells. While T helper-1 cells drive the proliferation by producing IL-2 and IFNγ favouring cellular immunity, which acts on cytotoxic $CD8^+$ cells, NK cells and macrophages, T helper-2 cells produce IL-4, IL-5 and IL-13 favouring humoral immunity (Chirica *et al*. 2015, Fridman *et al*. 2012). Although a few studies in CRC have shown that

$CD4^+$ cells alone can initiate tumour elimination, in most cases it's the combination of $CD4^+$ and $CD8^+$ cells, as most CRC only express human leukocyte antigen (HLA) class I molecules, which are recognised by $CD8^+$ cells (Deschoolmeester *et al*. 2010). Another type of T helper cells, T 17 cells, produce IL-17 and IL-22 acting on epithelial and endothelial cells, fibroblasts and immune cells. $CD4^+$ T cells secrete IL-22, which acts through activation of STAT3 signalling to influence cancer stem cell stemness. When IL-22 signalling is neutralised, it can decrease and even reverse an inflammation driven mouse model of CRC (Kirchberger *et al*. 2013). A recent study has shown that CRC derived intra-tumoural T cells expressed FZD proteins as Wnt receptors and in addition, β-catenin levels were elevated. They found that enforced expression of β-catenin in $CD4^+$ cells increased IL-17a expression, and that those cells also enhanced proliferation, while apoptosis was inhibited, indicating a mechanism by which CRC derived Wnt ligands suppress T cell immunity in the tumour microenvironment (Sun *et al*. 2017).

CD8 cells have an important effector mechanism of anti-tumour immunity. They recognise antigens when expressed on HLA class I proteins and once activated they can mediate the tumour destruction (Deschoolmeester *et al*. 2010). An increased number of cytotoxic T lymphocytes has recently been shown to be associated with improved survival of CRC patients. Tumours with higher immune infiltration were characterised by MSI-high, CIMP-high or BRAF mutation status and greater infiltration was found in the proximal colon (Prizment *et al*. 2017).

$CD8^+$ cells are not only detectable in the stroma, but also in the epithelium of a crypt. These intraepithelial lymphocytes (IELs) are predominantly $CD8^+$ cells and, more importantly, are involved in the immune surveillance (Saurer *et al*. 2009). Approximately one IEL is found for every 30-50 intestinal epithelial cell in a healthy colon. Given the location of IELs, they are capable of rapid activation while keeping the epithelial lining intact (Baker *et al*. 2009).

Macrophages make up a great proportion in the tumour microenvironment (Badawi *et al*. 2015). There are two types of macrophages, M1 and M2 that were found to have dual functions in terms of tumour development and progression. M1 macrophages secrete pro-inflammatory cytokines, release reactive oxygen species, and have a pro-inflammatory role, whilst M2 macrophages have an anti-inflammatory role (Zhong *et al*. 2018). CD68 is a marker for tumour-associated macrophages (TAMs), recognising both M1 and M2 macrophages (Zhang *et al*.

2013). TAMs are able to switch between M1 and M2 phenotypes depending on the microenvironmental stimuli: they might exhibit pro-inflammatory M1 phenotypes in the beginning, but can convert to the M2 phenotype during progression (Chen *et al*. 2017). TAMs resemble M2 macrophages and function to promote tumour growth by secreting growth and angiogenic factors as well as enzymes necessary for cell invasion, thus escaping the immune surveillance (Hernandez *et al*. 2014).

Numerous studies have shown that high macrophage infiltration enables CRC growth, progression and is associated with poor survival (Franklin *et al*. 2014, Hamm *et al*. 2016). However, several studies have reported the opposite effect: heavy macrophage infiltration in the tumour microenvironment was associated with improved survival in CRC patients. In colorectal adenocarcinomas, higher TAM infiltration has been linked to better clinical outcome for CRC patients (Cavnar *et al*. 2017, Zhang *et al*. 2012). This was also confirmed in another study, shown that high CD68 counts correlated with improved overall survival in CRC cells and CD68 infiltration was associated with significantly less tumour budding (Koelzer *et al*. 2016).

The mechanisms of when macrophages are tumour promoting and when suppressing remain unclear. Further studies are required to understand the macrophage plasticity and how its phenotype changes with progression towards CRC (Zhong *et al*. 2018).

1.14 Polyclonality and clonal interactions

The traditional view of cancer is that initially a single transformed cell clonally expands to form a pre-cancerous lesion. Progression towards cancer is driven by somatic evolution within the population of neoplastic cells. However, there is now clear evidence that the traditional view of cancer as monoclonal-in-origin is rather simplistic, and instead a neoplasm can be derived from one or more independently transformed cells and the interaction between clones is a novel driver of tumourigenesis (Figure 1.8) (Marusyk *et al*. 2014, Wu *et al*. 2010). This has questioned the current dogma of how colonic tumours are initiated. The mechanisms causing a tumour to be fundamentally polyclonal-in-origin are unknown, as is how polyclonality drives neoplastic progression. Understanding polyclonality in tumour origins is fundamental for understanding the carcinogenic process, and also ultimately for preventing cancer initiation.

During the expansion of a dysplastic monoclonal adenoma, presumably clonal interactions between it and its surrounding non-dysplastic crypts occur (Figure 1.9). As a consequence, a new, independent clone within a stem cell of a neighbouring crypt arises that confers a selective advantage in order to persist and also colonises the entire crypt, resulting in a polyclonal adenoma (Figure 1.9A). The mutant clones then further expand by crypt fission (Figure 1.9B). Over time, a selective sweep may occur where the successful sub-clone outgrowths the other sub-clones and the lesion appears monoclonal once more (Figure 1.9C). Short-range interactions between multiple independent transformed cells have been suggested as a possible mechanism for survival and growth of the adenoma (see section 1.15). As time continues, new clones emerge generating ITH.

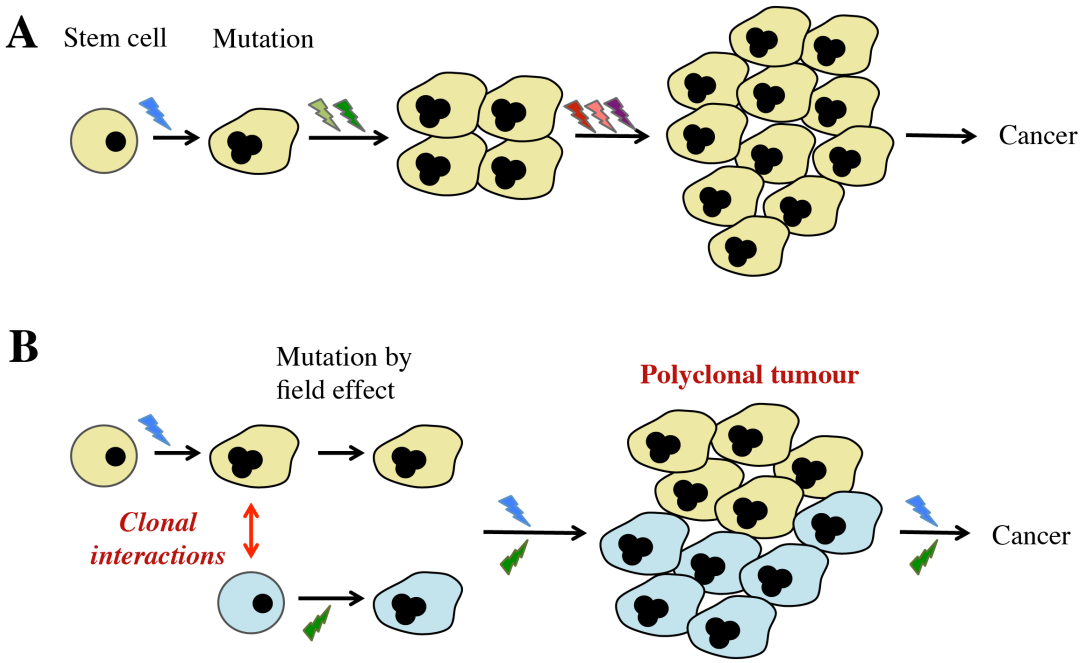

Figure 1.8: Monoclonal vs. polyclonal origins in cancers.
A) Monoclonal origin. A tumour is derived from a single somatic progenitor cell (stem cell) and as the tumour progresses from a benign to malignant form it accumulates a series of mutations in oncogenes and tumour suppressor genes. B) Polyclonal origin. Tumours are composed of at least two different progenitors. A spontaneous mutation in a single stem cell could generate a field of crypts composed entirely of cells carrying this mutation. The exposure of this field could then generate an additional independent mutation and consequently lead to a polyclonal tumour.

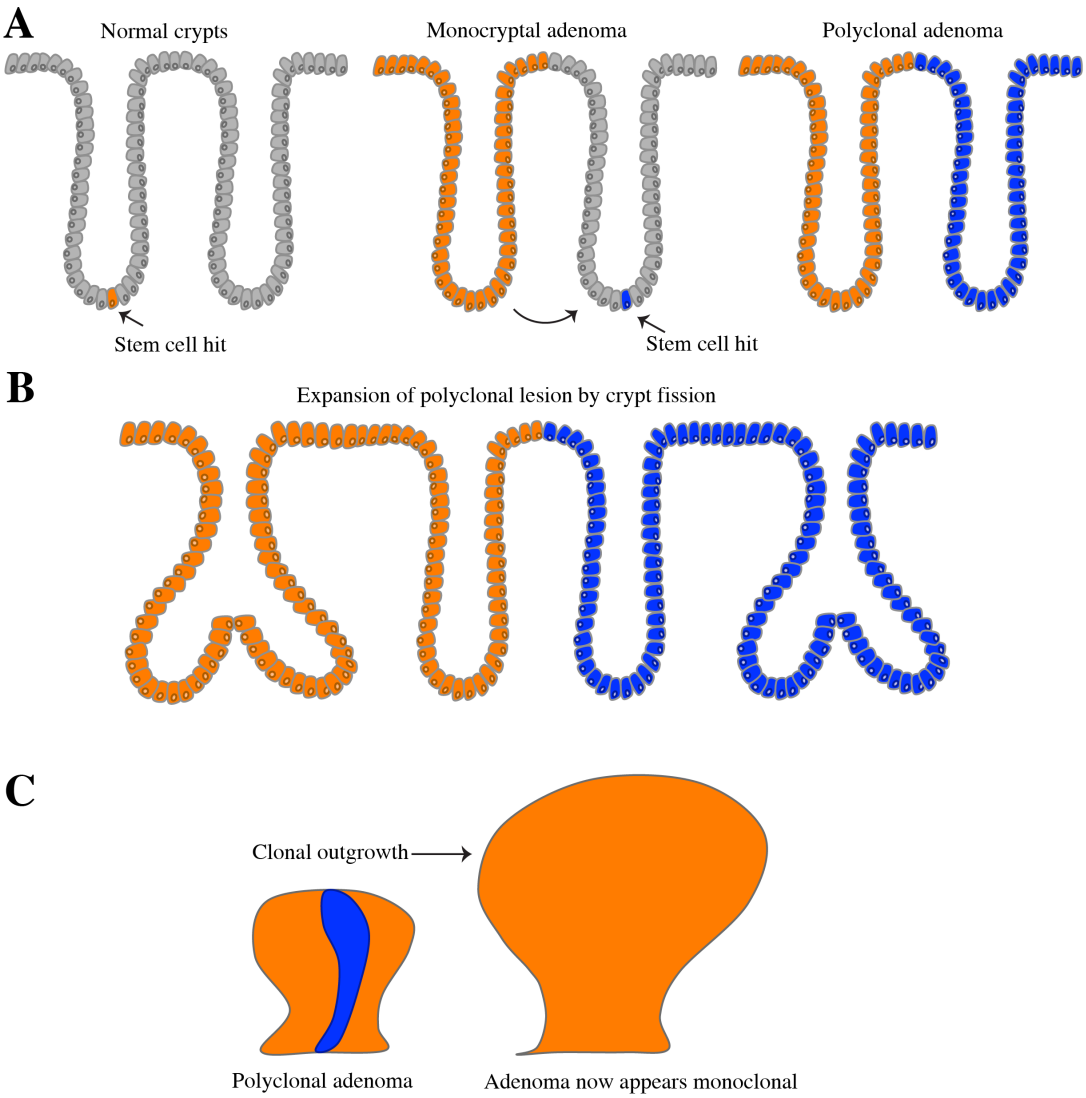

Figure 1.9: Development of a polyclonal adenoma.

A) A stem cell acquires a mutation, possibly in the *APC gene*, and colonizes the crypt with $APC^{-/-}$ cells to give rise to a monocryptal adenoma. There is evidence for short-range interactions in the development of polyclonality. In some way, possibly through altered signalling by the niche cells, known to form a network in the lamina propria, mutations are induced in an adjacent crypt(s), which also clonally converts, forming a polyclonal adenoma. B) The adenoma then expands by crypt fission, until eventually the expansion of a dominant clone leads to clonal outgrowth and the more advanced adenoma appears monoclonal C).

1.14.1 Evidence for polyclonality in human intestinal adenomas

In 1996, Novelli and his colleagues were the first to show that colorectal adenomas from a XO/XY mosaic male (20% of cells lack the X chromosome) with FAP were polyclonal. By using *in situ* hybridisation for the Y chromosome, which can determine patch size and tissue clonality in the large intestine, they reported that 94% were XY, 2% were XO, and 5% were mixtures of XY/XO crypts. Based on the overall frequencies of the XO and XY alleles, they estimated that 76% of colorectal microadenomas were polyclonal in origin (Novelli *et al*. 1996).

Due to the importance of *APC* mutations in colorectal tumourigenesis, it is typical that most polyclonality studies have used *APC* mutations as their marker (Thirlwell *et al*. 2010). Therefore, given the gatekeeper role of the *APC* gene, polyclonal tumours can also be identified by detecting clones with distinct *APC* mutations within the same tumour (Thirlwell *et al*. 2010); since *APC* mutations are considered sufficient for tumour growth in the intestine, a monoclonal-in-origin tumour would arise from crypts that share a common *APC* mutation. Thirwell *et al*. (2010) analysed polyps from the same XO/XY mosaic male and confirmed polyclonality. Clonality was analysed using X/Y chromosome fluorescence *in situ* hybridisation and analysis of *5q* loss of heterozygosity. Out of 55 adenomas, 51 were of XY, 1 was completely XO, and 3 adenomas were of mixed XO/XY crypts. In 13 additional microadenomas, 10 polyps showed no change in LOH, but 3 lesions showed heterogeneity in LOH, indicating somatic mutation polyclonality (Thirlwell *et al*. 2010).

Additionally, they analysed samples from patients with FAP and small sporadic adenomas. Clonality was assessed by analysing mutations in the *APC* gene. Out of 36 dissected crypts from 5 FAP patients, all showed two different somatic *APC* mutations in adjacent crypts, indicating that all FAP adenomas were polyclonal in origin (Figure 1.10). Remarkably, not only FAP associated adenomas, but also sporadic lesions are polyclonal in origin. Two out of 12 lesions were identified with a heterotypic *APC* mutation (Thirlwell *et al*. 2010).

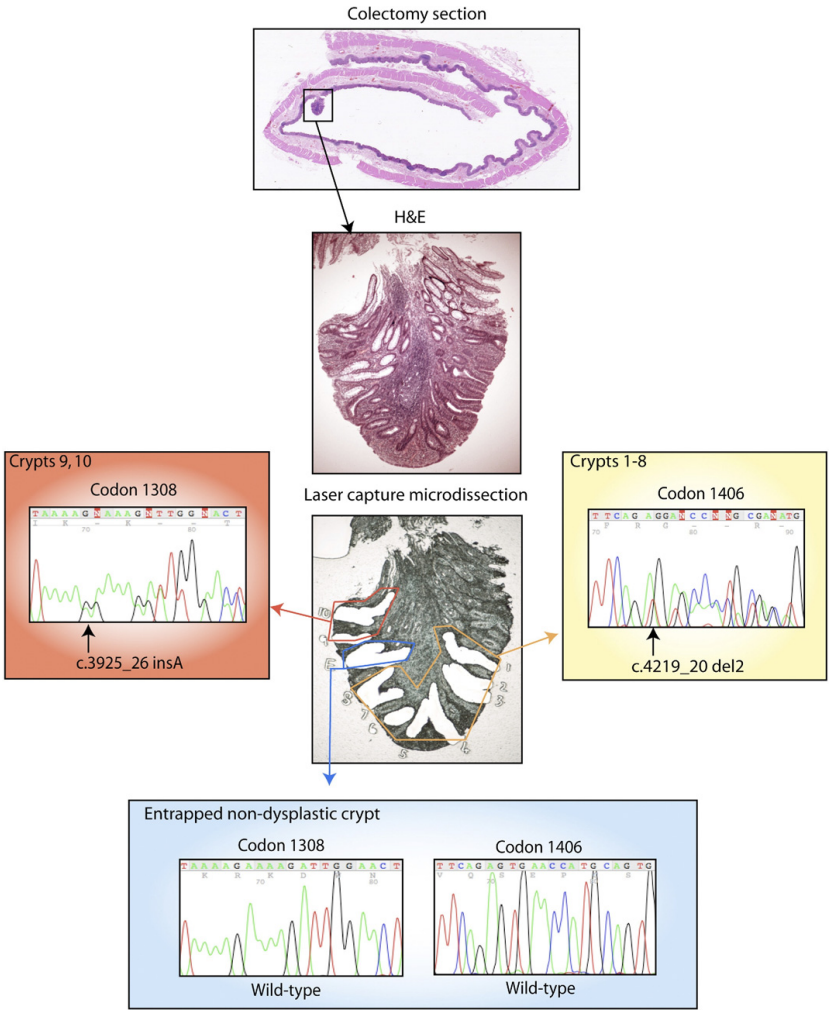

Figure 1.10: Polyclonal FAP with distinct *APC* mutations.
Laser-capture microdissection of individual crypts from around the polyp and somatic *APC* mutations sequencing revealed two clones with independent *APC* mutations surrounding an entrapped genotypically WT crypt. Taken from Thirlwell *et al*. 2010.

In a recent study, Gausachs *et al*. (2017) performed high-depth next-generation sequencing and SNP arrays in whole lesions of 37 FAP colorectal adenomas, and argued that by studying adenomas of FAP, the accumulation of multiple somatic events is sufficient to detect polyclonality, since these patients already have a germline *APC* mutation. Indeed, a second hit in *APC* was detected in 81% of adenomas and in 16% double somatic events in *APC* were observed. These were either two different mutations or a combination of one mutation associated with a 5q loss. Additionally, *KRAS* mutations were detected. Interestingly, two different *KRAS* and two *APC* mutations were found in one adenoma. Using colony analysis they were able to confirm that the somatic *APC* mutations were polyclonal (Gausachs *et al*. 2017).

Besides in human colorectal cancers, polyclonality has been evident in prostate cancer (Gaisa *et al*. 2011), melanomas (Lin *et al*. 2011), bladder tumours (Paiss *et al*. 2002), and breast adenomas (Kuijper *et al*. 2002) among others (Parsons 2008).

1.14.2 Clonality of murine intestinal adenomas

Merritt and colleagues (1997) developed a mouse model to assess the clonality of intestinal tumours knowing patch size and structure (Merritt *et al*. 1997). They investigated intestinal tumours from chimeric mice composed of $Apc^{Min/+}$ cells and $Apc^{Min/+}$ cells expressing ROSA26-driven LacZ expression. *Min* mice are heterozygous for a germline mutation in the *APC* gene and, like FAP patients, develop numerous intestinal tumours and adenoma formation requires loss of the remaining wild-type allele of *APC*. They reported that 22 out of 260 tumours were heterotypic being composed of $ROSA26^{-}$ (white) and $ROSA26^{+}$ (blue) neoplastic cells, indicating that a significant number of tumours were polyclonal. Further, after taking patch size into account, the authors estimated that 79% of the adenomas in this mouse model were actually polyclonal, remarkably similar to the ratio found in human FAP (Merritt *et al*. 1997, Novelli *et al*. 1996).

Thliveris *et al*. (2013) generated aggregation chimeras by fusing together embryos with unequal predisposition to tumour development. In a first experiment, $Apc^{Min/+}$ mice (develop on average 95 ± 53 tumours, n = 228) were fused together

with *Apc*$^{1638N/+}$*R26*$^{+}$ mice (develop on average 0.98 ± 1.17 tumours, n = 94). Out of 105 tumours, 97 were white homotypic, one was blue homotypic and 7 were heterotypic. To further contrast this result, aggregation chimeras were generated from *Apc*$^{Min/+}$ mice and *Apc*$^{+/+}$*R26*$^{+}$ mice, the latter developing no tumours. Strikingly, out of 54 tumours, 25 were homotypic white and 8 heterotypic, composed of blue and white neoplastic cells. This shows that polyclonal tumours are relatively common in aggregation chimeras generated from embryos with unequal tumour susceptibilities, even when one genetic component was highly resistant to spontaneous tumourigenesis in the intestine (Thliveris *et al*. 2013).

1.15 Mechanisms for the development of polyclonal tumours

Merritt *et al*. (1997) proposed four mechanisms to explain the heterotypic tumour formation: (1) the ROSA26 marker is lost within a ROSA26^{+} adenoma, but unlikely since ROSA26 does not show any mosaicism in *Apc*$^{Min/+}$ROSA26^{+} mice; (2) the ROSA26 marker is silenced epigenetically, again an unlikely mechanism to account for tumour formation, since these heterotypic tumours that were white did not carry the ROSA26 marker; (3) random collision between two or more distinct tumour; or (4) an active interaction between independently initiated clones (Merritt *et al*. 1997). Given the high tumour multiplicity in *Min* mice, it was difficult to eliminate the possibility that polyclonality was the result of random collision. To address the issue of multiplicity, Thliveris *et al*. (2005) analysed tumours from similar chimeric *Apc*$^{Min/+}$ mice, but which were additionally homozygous for the tumour resistance gene *Mom1* – these compound transgenic mice had a significantly lower tumour burden than a standard *Min* mouse. Despite a reduction of the number of intestinal tumour, 22% of the adenomas in *Apc*^{Min}/*Mom1* mouse were observed to be polyclonal in origin. Statistical analyses ruled out the random collision hypothesis, and further investigation of spatial distribution led the authors to the conclusion that short-range interactions of multiple initiated clones between one or two crypt diameters could best explain the observed frequency of polyclonal tumours (Thliveris *et al*. 2005). Indeed, a histological study of the crypts surrounding

intestinal tumours showed that they had full-length APC protein, but were grossly hyperplastic (Bjerknes *et al*. 1999). Similarly, in humans, Thirlwell *et al*. (2010) found the frequency of polyclonal tumour in FAP patients to be higher of what could be reasonably expected by random collision of independently initiated clones (Thirlwell *et al*. 2010).

Thliveris *et al*. (2013) sought to better understand the nature of clonal interactions. Two models, recruitment or cooperation, could explain the formation of a polyclonal tumour. Under recruitment, a single progenitor having lost Apc activity subsequently facilitates neoplastic transformation of one or more neighbouring clones. Alternatively, cooperation between multiple independently derived progenitor cells arising in close proximity could explain polyclonality. On the basis of aggregation chimeras from embryos with unequal tumour susceptibilities, it was found using a statistical approach that the recruitment model is much more likely to account for the formation of polyclonal tumours. It further strengthens the notion that polyclonal tumours arise because of an initial progenitor, following the loss of Apc activity, transforming one or more neighbouring cells. The range of this recruitment was best explained within 144μm of the initial transformed progenitor (Thliveris *et al*. 2013).

Wu *et al*. (2010) investigated how such interactions contribute to tumourigenesis using the model system *Drosophila melanogaster*. Two transgenic strains were created; one expressing the oncogenic protein RAS^{V12} and the other lacking the tumour suppressor gene *scribbled (scrib)*. Single mutant clones showed increased cell proliferation without any evident pathology. If both mutations were expressed within the same clone, large tumours developed. Interestingly, if single mutations were expressed within distinct cells adjacent to each other, large tumours developed, suggesting inter-clonal cooperation. If the JAK/STAT pathway was blocked, the tumours did not develop, signifying that this pathway was the mechanism behind this effect (Wu *et al*. 2010). Cleary *et al*. (2014) found that in tumours of a murine breast cancer model, tumour development required independent clones cooperating with each other to produce Wnt to maintain tumour growth (Cleary *et al*. 2014). A tumour cell population may be able to be maintained by a minor cell subpopulation, which drives proliferation in the whole tumour (Marusyk *et al*. 2014).

However, very little research has been done to understand these interactions

between mutated and normal clones. It is therefore clear that the standard model of tumourigenesis, of a single cell forming a tumour, is too simplistic and understanding how clones interact may determine risk of malignancy in adenomas.

1.15.1 Field cancerization as a mechanism of polyclonality

As described above, an active mechanism is likely to be responsible for the formation of polyclonal tumours. Field cancerization is an appealing mechanism in that the first mutated crypt produces signals that alter the behaviour of neighbouring stromal cells. This altered stromal field is then responsible for a second mutation occurring in neighbouring crypts (Graham *et al*. 2011). On the one hand, if the stromal field increases the size of the progenitor cell compartment, more cells susceptible to transformation would be produced, increasing the mutation rate, similar to what is observed as hyperplasia (Rubin 2011). As a consequence, signalling alters the cell-cell interactions in the epithelia. On the other hand, the stromal field might be a direct mutagenic environment, thus leading to polyclonal tumour formation (Graham *et al*. 2011).

1.16 The incidence of polyclonal tumours may be underestimated

Studies on the clonality of hereditary or sporadic colorectal cancers may have been underestimated because observing a polyclonal tumour depends on the size and structure of lineage patches throughout the intestinal epithelium. The patch size greatly influences the probability that a tumour will have a polyclonal origin especially, if interactions between initiated clones are limited to a short distance. In a region with very small patches, all crypts lie on borders between patches, thus polyclonal tumours are more likely to form. As the patch size increases, the percentage of crypts lying on borders decreases. Therefore, a tumour arising from interactions between initiated clones in a region would be much more likely to be homotypic (Halberg *et al*. 2007).

Most clonality studies were based on tumours in females that are mosaic for X-linked markers. In X-inactivation studies, a tumour can only be demonstrated to be

polyclonal if it is initiated at the border between two patches with different patterns of X-inactivation. Novelli *et al*. (2003) have analysed the size and structure of patches in the intestinal epithelium of humans from random inactivation of X-linked genes. Glucose-6- phosphate dehydrogenase (G6PD) expression in nine samples of normal intestinal tissue was analysed, but patches were relatively large, with only 8% of crypts lying on the border. They estimated that 43 adenomas must be shown to be monoclonal to exclude the possibility that all human colorectal tumours are polyclonal. Thus, assessing tumour clonality based on the analysis of mosaicism of X-linked genes in which patch size is large is heavily biased towards the conclusion that tumours are monoclonal because polyclonal tumours in this situation are likely to be homotypic (Novelli *et al*. 2003).

Mouse models for FAP allow studying clonality of intestinal tumours, since aggregation chimeras can be generated by fusing together embryos with different genotypes. Hence, the patch size and structure is known (Merritt *et al*. 1997), which permits accurate estimation of polyclonal tumours.

Together these studies suggest that polyclonality is common and the consequence of some active mechanism driving short-range interactions between neighbouring intestinal crypts.

1.17 Importance of clonal interactions for the development of polyclonal adenomas

It has been demonstrated that tumours can be derived from more than one independently initiated cell, but it remains unclear how polyclonal tumours develop and what are the underlying mechanisms responsible for the formation of a polyclonal tumour. Understanding the clonal origin of tumour development is important for the following reasons: (1) for developing an accurate scientific understanding of the initial events in carcinogenesis, (2) for improving cancer risk assessment, (3) for developing accurate mathematical models of tumour development, and (4) for more accurate insight regarding the merits of different therapeutic approaches (Parsons 2008).

Crosstalk between clones has been shown in Drosophila to initiate tumour growth (Wu *et al*. 2010). Clonal interactions between crypts and their neighbours remain the most plausible mechanism to explain polyclonal tumour formation. Thereby, interactions between multiple initiated clones could occur either between crypts promoting somatic LOH of *APC*, or cooperation between initiated clones that favour growth or survival (Thliveris *et al*. 2005). It is still unknown whether polyclonality is essential for the formation of adenomas and whether single, isolated transformed crypts are important progenitors (Thliveris *et al*. 2005). More specifically, it is unknown how one crypt could cause sufficient mutations in a neighbouring crypt to become initiated. Mitotic pressure might be involved in the process of how a mutated clone in one crypt transforms the neighbouring crypt. The cellular proliferation of normal neighbouring crypts could be influenced when a dysplastic crypt releases mitogenic factors. It can be hypothesised that growth factors are produced by the crypt with the mutated clone, so that cells within the neighbouring crypts, which respond to these factors, divide at a higher rate, and so are more likely to acquire a mutation. In fact, normal epithelium surrounded by a tumour is often hyperplastic (Bjerknes *et al*. 1999).

A further hypothesis on how one crypt could initiate mutations in its neighbours is that the mutated crypt could release a mutagenic signal, either through a direct inhibition of DNA repair in a neighbouring crypt, or through changes in the microenvironment resulting in an over abundance of mutagenic molecules, such as ROS or other inflammatory stresses. It is important to note that crypts are not directly in contact with their neighbours, and are separated by stroma containing fibroblasts, immune cells and blood vessels. The role of the stromal cells in these earliest phases of polyclonal lesions remains to be determined. However, it has been shown that genetic alterations occur in the stroma in early forms of tumourigenesis (Ishiguro *et al*. 2006). An initiated clone may induce local environmental changes affecting the proliferative rates in neighbouring clones. Further, the stroma may also initiate and drive cancer progression, but the mechanism by which these oncogenic signals enable the generation of malignant cells remains to be examined (Tlsty 2001). Pertinent to this project is the question of how the stroma responds to a dysplastic crypt in the epithelium, and whether these responses could induce transformation in secondary crypts (tumour-stroma interactions).

1.18 Aims

Short-range interactions have been suggested as the most plausible mechanism on how polyclonal tumours are formed in colonic adenomas. This investigation sought to better describe these clonal interactions in the context of adenomas and their surrounding non-dysplastic crypts and to determine the role of the stroma in this process.

Therefore, the three major aims were:

1. To demonstrate that clonal interactions between dysplastic and non-dysplastic colonic epithelium drive clonal expansion
2. To investigate the stem cell dynamics between dysplastic and non-dysplastic colonic epithelium
3. To investigate the underlying mechanisms responsible for the formation of a polyclonal tumour

2 Chapter II: Material & Methods

2.1 Tissue and cell specimens

2.1.1 Human

Fresh frozen FAP samples were obtained from patients undergoing colonic resection at the Academic Medical Centre, Amsterdam, The Netherlands, in accordance with their national ethics guidelines on the procurement of human tissue (local protocol-12). Sporadic adenoma samples (frozen and formalin-fixed, paraffin-embedded (FFPE)) were obtained from the University College Hospital, London and St. Marks Hospital London under ethical approval from the London Research Ethics Committee Stanmore (11/LO1613). Frozen FAP specimens from patients under 18 years old were obtained from St. Marks Hospital, London under ethical approval (MREC 10/H0604/72). All patients consented to the use of their tissue for research purposes.

2.1.2 Mice

Wild type (WT) and mutant *Apc*$^{1322/+}$ mice were housed at the animal unit at Functional Genomics Facility, Wellcome Trust Centre for Human Genetics, Oxford University, UK. WT ROSA$^{mT/mG}$ (membrane-Tomato/membrane-Green) mice were housed at the animal unit at the London Research Institute, Cancer Research UK, London, UK. All mice were derived on a C57BL/6J background. All procedures were carried out in accordance to Home Office UK regulations.

2.2 Protein analysis methods

2.2.1 Tissue sectioning

Frozen and FFPE sections were either cut on membrane slides (Zeiss, Oberkochen, Germany) for laser capture microdissection (LCM) (6-12μm thickness) or on normal charged glass slides (Fisher Scientific, Loughborough, UK) for general tissue histochemistry (4-6μm thickness).

2.2.2 Dual Cytochrome *c* Oxidase (CCO) and Succinate Dehydrogenase (SDH) enzyme histochemistry

Frozen human colon tissue sections were subjected to a two-colour enzyme histochemistry method used to detect mitochondrial DNA (mtDNA)-encoded CCO activity and nuclear DNA-encoded SDH activity to highlight CCO-deficiency. Cells deficient in CCO appeared blue on tissue sections and CCO-normal cells brown. Frozen sections were cut on membrane slides for LCM or on glass slides. Sections were air-dried for 30-60 min at room temperature before being incubated in CCO media (100mmol/l cytochrome c, 20μg/ml catalase, and 4mmol/l diaminobenzidine tetrahydrochloride in 0.2mol/l phosphate buffer, pH 7.0 (all from Sigma-Aldrich, Poole, UK)). Media was filtered through a 0.2μm syringe filter to remove particulate matter. 50-200μl of the CCO medium was then added to each tissue section, depending on section size, and was incubated at 37°C for up to 1 h, depending on tissue thickness, until a strong brown colour was obtained. Sections were then washed 3 times in phosphate-buffered saline (PBS), pH 7.4, for 3-5 min each and then incubated in SDH medium (130mmol/l sodium succinate, 200mmol/l phenazine methosulfate, 1mmol/l sodium azide, and 1.5mmol/l nitroblue tetrazolium in 0.2mol/l phosphate buffer, pH 7.0 (all from Sigma-Aldrich, UK)) for a maximum of 1 h at 37°C, or until a strong blue stain had developed. Sections were again washed 3 times in PBS and dehydrated in an increasing graded ethanol series: 70% for 2 min, 95% for 2 min, 100% for 2 min and a further 100% for 10 min. If sections were to be immediately cut on the LCM system, slides were left to air-dry for an hour before LCM. For normal tissue processing, sections were cleared with Histoclear (Lamb

Laboratory Supplies, Eastbourne, UK) and mounted with Eukitt mounting media (Sigma-Aldrich, UK).

2.2.3 Immunohistochemistry (IHC) on formalin-fixed, paraffin-embedded (FFPE) sections

FFPE sections were cut at a thickness of 4μm and allowed to air-dry overnight. Sections were then dewaxed in xylene for 5 min and rehydrated through decreasing alcohol concentrations (100% for 3 min, 90% for 3 min, 70% for 3 min) and placed into fresh water. Each section was subjected to a variety of antigen retrieval methods that were specific to each primary antibody (Table 2.1). Retrieval was performed either using 0.1M sodium citrate (pH 6.0) (Fisher Scientific, UK) or 1X ethylenediaminetetraacetic acid (tris-EDTA) (Sigma-Aldrich, UK). Each solution was brought to the boil, the slides were then added and then microwaved for 15 min. Sections were left to slowly cool for approximately 20 min before rinsing them twice in PBS/0.1% Tween (Sigma-Aldrich, UK) for 2 min. Sections were then blocked for endogenous peroxidase (3% hydrogen peroxide in ddH_2O; Sigma-Aldrich, UK) for 10 min, rinsed again twice in PBS/0.1% Tween for 2 min, and then blocked with Protein-Free block (Dako, Ely, UK) for 30 min at room temperature. Each primary antibody (Table 2.1) was diluted according to either the manufacturers recommendation or according to prior optimisation in PBS/0.1% Tween with 5% donkey serum, and applied to the section for 45 min at room temperature in a moist chamber. Sections again, washed 3 times in PBS/0.1% Tween for 5 min each, were then incubated for 30 min with appropriate secondary antibody conjugated to biotin at antibody-dependent concentrations in PBS/0.1% Tween with 5% donkey serum (Table 2.1). Sections were again washed 3 times in PBS/0.1% Tween for 5 min each and then incubated with HRP/Streptavidin (1:500 dilution in PBS/0.1% Tween with 5% donkey serum; Dako, UK) for 30 min. Sections were then washed in PBS/0.1% Tween (3 times x 5 min) and colour developed in a solution containing 4mmol/l diaminobenzidine and 0.2% hydrogen peroxide (DAB substrate, Vector labs, Peterborough, UK). Once a vivid brown colour was obtained, sections were rinsed in ddH_2O, placed in Gill's hematoxylin II (Sigma-Aldrich, UK) for 10 sec and then again rinsed in water. Sections were then dehydrated through ascending ethanol

concentrations (70% for 2 min, 95% for 2 min, 100% for 2 min, 100% for 10 min), cleared with xylene (Fisher Scientific, UK) and mounted with Eukitt mounting media (Sigma-Aldrich, UK).

Name	Species	Catalogue number	Clone number	Dilution	Antigen retrieval
Primary antibodies					
Ki67	Rabbit	ab92742	EPR3610	1:2000	Sodium citrate
β-catenin	Mouse	M3539	β-catenin-1	1:100	Tris-EDTA
γH2AX	Mouse	ab26350	9F3	1:100	Sodium citrate
CD4	Mouse	NCL-CD4-368	4B12	1:50	Tris-EDTA
CD8	Mouse	M7103	C8/144B	1:75	Sodium citrate
CD68	Mouse	M0876	PG-M1	1:100	Sodium citrate
SMA	Mouse	A-2547	1A4	1:6000	Sodium citrate
Secondary antibodies					
Biotin-anti-mouse	Rabbit	Dako E0354	n/a	1:300	n/a
Biotin-anti-rabbit	Goat	Dako E0432	n/a	1:400	n/a
Tertiary antibody					
HRP/Streptavidin		Dako P0397	n/a	1:500	n/a

Table 2.1: Antibodies used for immunohistochemistry.

2.3 Quantifying immunohistochemistry

2.3.1 Scanning and sectioning of images

Slides stained for epithelial and stromal cell markers using immunohistochemistry and an accompanying hematoxylin and eosin (H&E) stained section were scanned using a high-resolution scanner (Pannoramic 250 Flash III, 3DHISTECH, Budapest, Hungary). Dysplastic areas were identified on H&E slides by an experienced gastrointestinal pathologist (Dr Marnix Jansen, University College London Hospitals) using the Pannoramic Viewer software (Version 1.15.4). For each adenoma, surrounding mucosa (containing only non-dysplastic crypts) was

segregated into zones according to distance from adenoma: zone 1 included all non-dysplastic crypts less than 50μm away from the adenoma, zone 2 were those between 50-150μm, and zone 3 were those 150-250μm away from the adenoma (Thliveris *et al*. 2013).

Incomplete, damaged and crypts with weak staining were excluded. Crypts with nuclei that were excessively or incompletely stained, and consequently could not be discerned as positive or negative staining, were also excluded. Further, if there is an expected region of expression within a crypt (Ki67 is expressed in the lower third of each crypt) and no expression was detected, these crypts were also excluded.

2.3.2 Cell counting of epithelial markers

FAP and sporadic tissue sections were stained for cell proliferation (Ki67), DNA damage (γH2AX), Wnt-signalling (nuclear β-catenin), and intraepithelial lymphocytes (CD8) as per section 2.2.3. The annotation feature in the Pannoramic Viewer software was used to encircle the crypts in the adenoma and each zone in order to manually count the number of positively and negatively stained cells/crypt. The percentage of positively stained cells/crypt/zone was then calculated (Figure 2.1).

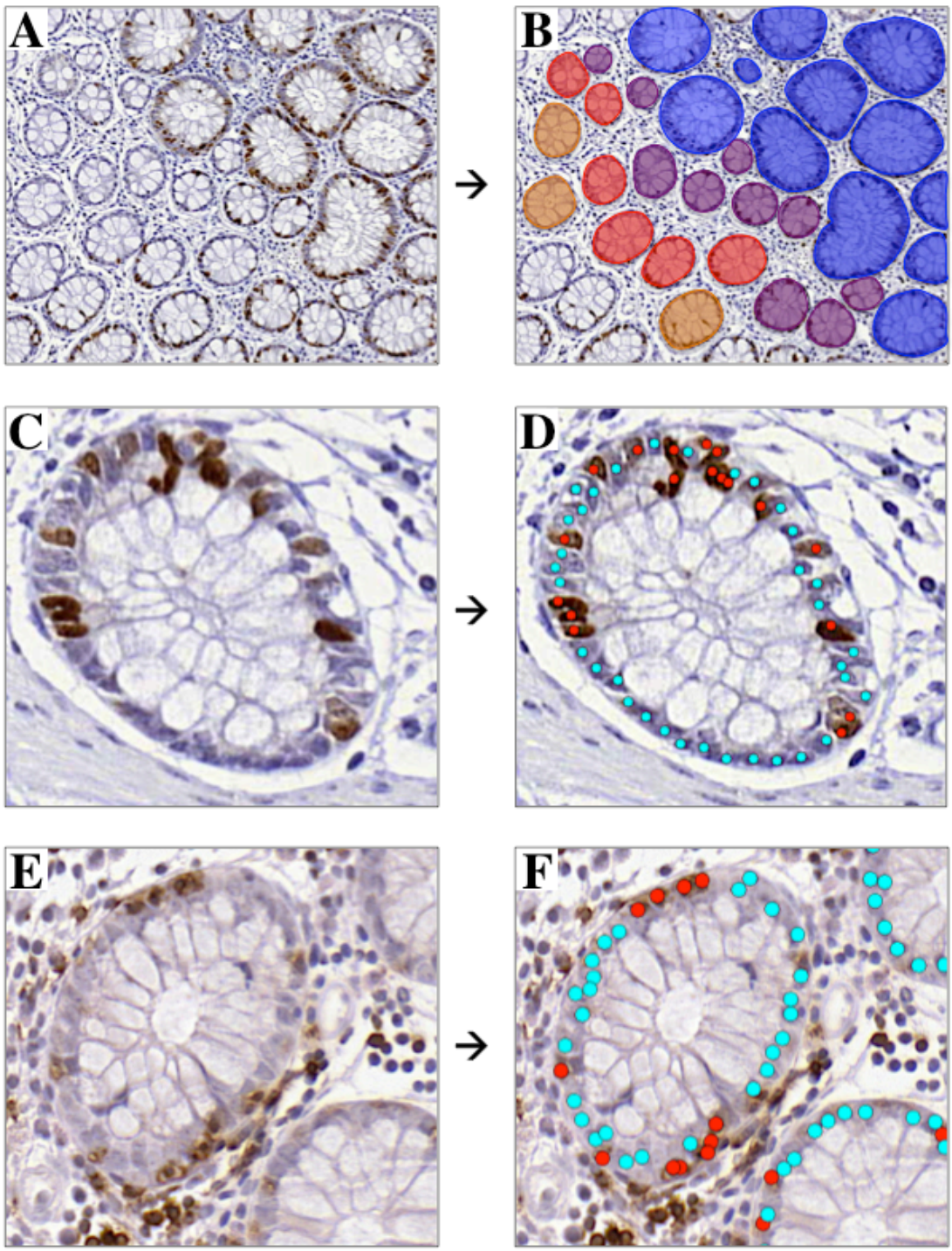

Figure 2.1: Identification of adenomas and cell counting.
A) Ki67 staining. B) Adenomas and non-dysplastic surrounding crypts were identified on H&E's of serial sections and divided into three zones: adenoma in blue, zone 1 (< 50μm) in purple, zone 2 (< 150μm) in red, and zone 3 (<250μm) in orange, shown for Ki67 staining. C) Single crypt stained for Ki67. D) Positive stained cells (red dots) and negative stained cells (turquoise dots) were manually counted. The percentage of positive stained cells within the crypts in each zone was calculated. E) Single crypt stained for CD8. CD8 stains for the cytotoxic T cells, but also for intraepithelial lymphocytes (IELs), which were counted (F) and the percentage of positive stained IELs calculated.

2.3.3 Semi-quantitative scoring system for stromal cells

FAP and sporadic tissue sections were stained for stromal markers that identify helper T cells (CD4), cytotoxic T cells (CD8), macrophages (CD68), and fibroblasts (α-smooth muscle actin (SMA)). A semi-quantitative scoring system was applied based on the number and intensity of stained cells (Figure 2.2). For each sample, the area around the adenoma and each zone was marked and a score given, based on the percentage of cells present (Table 2.2).

Score	Number of stained cells
0	No stained cells (0%)
1	Low number of stained cells (0 – 25%)
2	Medium number of stained cells (25 – 75%)
3	High number of stained cells (75 – 100%)

Table 2.2: Semi-quantitative scoring system for stromal markers.

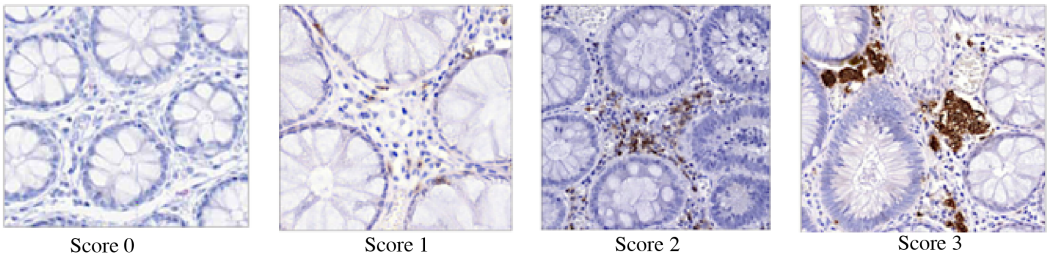

Figure 2.2: Illustration of semi-quantitative scoring of stromal markers.
Semi-quantitative scoring system for stromal markers CD4, CD8, CD68, and α-SMA based on positively stained cell number and intensity (CD68 staining shown here).

2.3.4 Assessing α-SMA$^+$ cell density

Intestinal subepithelial myofibroblasts were detected using α-SMA antibody. The density of myofibroblasts surrounding the adenoma and each zone was measured using the DensitoQuant application in the Pannoramic Viewer software. Myofibroblasts are difficult to individually count therefore densitometry was used as a proxy for cell number. An outer circle was manually drawn around the myofibroblasts and an inner circle around the crypt, the density of each circle then

assessed and the value of the inner circle subtracted from the outer circle to assess an overall measurement of myofibroblast density (Figure 2.3).

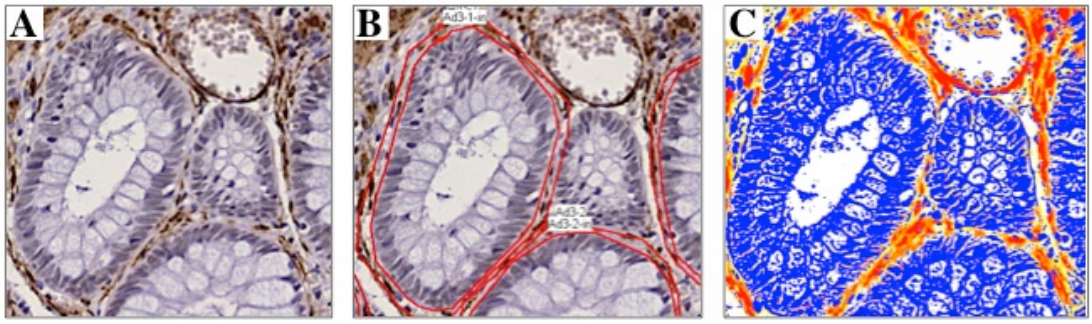

Figure 2.3: Assessing α-SMA$^+$ cell density.
A) α-SMA staining of a FAP patient of the colon. B) Zoning of the adenomatous crypts (red). An inner and outer circle was drawn manually around the crypt and the subepithelial myofibroblasts. C) Measuring α-SMA$^+$ cell density using the DensitoQuant application (Pannoramic Viewer software). Application measures the mean density of negative (blue), weak-positive (yellow), moderate-positive (orange), and strong-positive (red) pixels. Density was calculated by subtracting the sum of all positive pixels of the outer circle from the sum of all positive pixels in the inner circle.

2.3.5 Measuring crypt phenotypic characteristics

Crypt size (area per crypt in μm^2) and the density of nuclei in the dysplastic zone and surrounding non-dysplastic zones were measured in H&E sections to assess phenotypic characteristics. For each crypt in each zone, the size was measured using the annotation tool in the Pannoramic Viewer software. Depending on the angle the section was cut, some crypts may have appeared larger. To account for cutting artefacts, serial sections were cut. The density of nuclei was assessed per zone of the crypts using the DensitoQuant tool provided by the Pannoramic Viewer software.

2.3.6 CCO-mutant crypt counts

For FAP patient samples stained for CCO (see section 2.2.2), mutated (blue) and non-mutated (brown) of both normal and adenomatous crypts divided into each zone were manually counted and the percentage of mutated crypts/zone calculated (Figure 2.4).

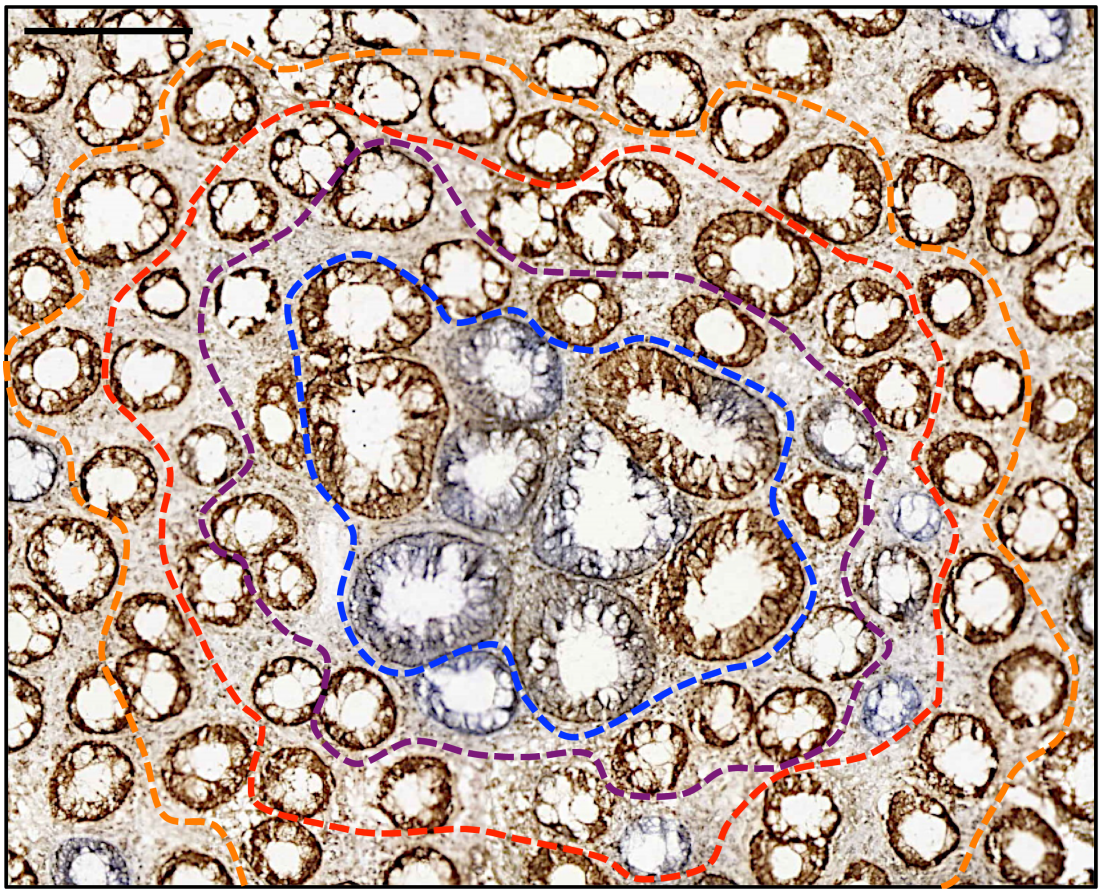

Figure 2.4: Assessing mutational burden using cytochrome *c* oxidase.
Section of a FAP patient stained for CCO/SDH. Identification and counting of CCO-deficient blue, and CCO-proficient brown crypts of both adenomatous and non-dysplastic crypts in zone 1 to zone 3. Adenomatous crypts are outlined by a blue dashed line, non-dysplastic crypts in zone 1 in purple, non-dysplastic crypts in zone 2 in red, and non-dysplastic crypts in zone 3 in orange.

2.4 Quantification of stem cell dynamics *in vivo*

2.4.1 Quantifying the change in clone size in CCO-deficient crypts between sequential sections

Partially mutated (crypts with both CCO-deficient and CCO-proficient cells) crypts in zone 1, zone 2, and zone 3 were identified in FAP, AFAP and non-dysplastic human tissue. The circumference of the blue and brown areas of a partially mutated crypt of interest were measured between serial sections using the Pannoramic Viewer software as previously described (Figure 2.5A-C). The difference in CCO-deficient clone fraction between serial sections was multiplied by the number of nuclei per crypt for that patient, to normalise for crypt size between adenomas and non-dysplastic crypts. The number of cell nuclei per crypt within zone 1, zone 2 and zone 3 were counted and the circumference of each crypt was measured from a serial *en face* H&E sections. For each patient, a minimum of 20 crypts for each zone was quantified and the mean number of cells per circumference calculated. Data on the mean number of cells per circumference for the adenoma and non-dysplastic crypts, as well as data for partially mutated crypts in the adenoma, in non-dysplastic FAP and AFAP tissue, and normal tissue was obtained from previously published data (Baker *et al*. 2014).

2.4.2 Crypt maps – tracking cell clones in the human colon

Crypts showing partial CCO/SDH staining were identified in *en face* serial sections taken from frozen FAP samples (Figure 2.5B). Digital, serial images were taken of every crypt of interest and the surrounding area, to ensure equal alignment of each section. Each crypt was followed all the way to its crypt base using serial sections. Crypt images from every serial section were stacked on top of each other and then BiaQIm software (http://www.bialith.com) (Figure 2.5F) (Fellous *et al*. 2009) orientated to a best fit orientation with the section above and below to form a crypt map. Each map is a representation of an entire 3D tubular crypt with colour enhancement post-processing to illustrate the contrast between CCO-deficient and CCO-normal staining as the clone expands and contracts over the time taken to migrate up the crypt (Figure 2.5A). In brief, the software aligned the digital, serial

images of a crypt to form a 3D reconstruction. The centre point and circumference of the serial, cross-sectioned image of each crypt was manually drawn. Then, in each cross-sectional image a line was marked out from the centre point to the perimeter of the crypt at a fixed angle for all images of the same crypt (Figure 2.5D, E). The oval cross-sectional profile of the crypt was then digitally cut and a straight profile generated. The average of the most basal pixels was taken and transformed into a pixel strip (Figure 2.5G), which was then aligned three-dimensionally to form a crypt map from the base of a crypt to the luminal surface (Figure 2.5H). Colour discrimination was then applied to isolate the blue colour. In the final crypt map, non-mutated brown areas appear black and mutated blue areas appear blue (Figure 2.5I). Thus, a crypt map is essentially a representation of the visual blue staining from the crypt base to the crypt surface (Fellous *et al*. 2009).

2.5 Next generation sequencing (NGS) of mitochondrial DNA

2.5.1 Laser Capture Microdissection

Frozen FAP sections were cut serially on membrane slides and stained with dual CCO/SDH enzyme histochemistry (see section 2.2.2). Crypts of interest were cut using a PALM Combisystem and collected in sterile 0.5ml adhesive opaque caps (both from Zeiss, Germany). DNA extraction from laser microdissected crypts was then performed.

2.5.2 Total DNA extraction

DNA was extracted from crypts that had been laser capture microdissected from frozen colon samples using a QiaAmp Micro Kit (Qiagen, Manchester, UK) following manufacturer's instructions. In brief, 15µl of ATL buffer and 10µl proteinase K was added to a laser-microdissected sample collected in a 0.2ml microcentrifuge tube and pulse-vortexed for 15 sec.

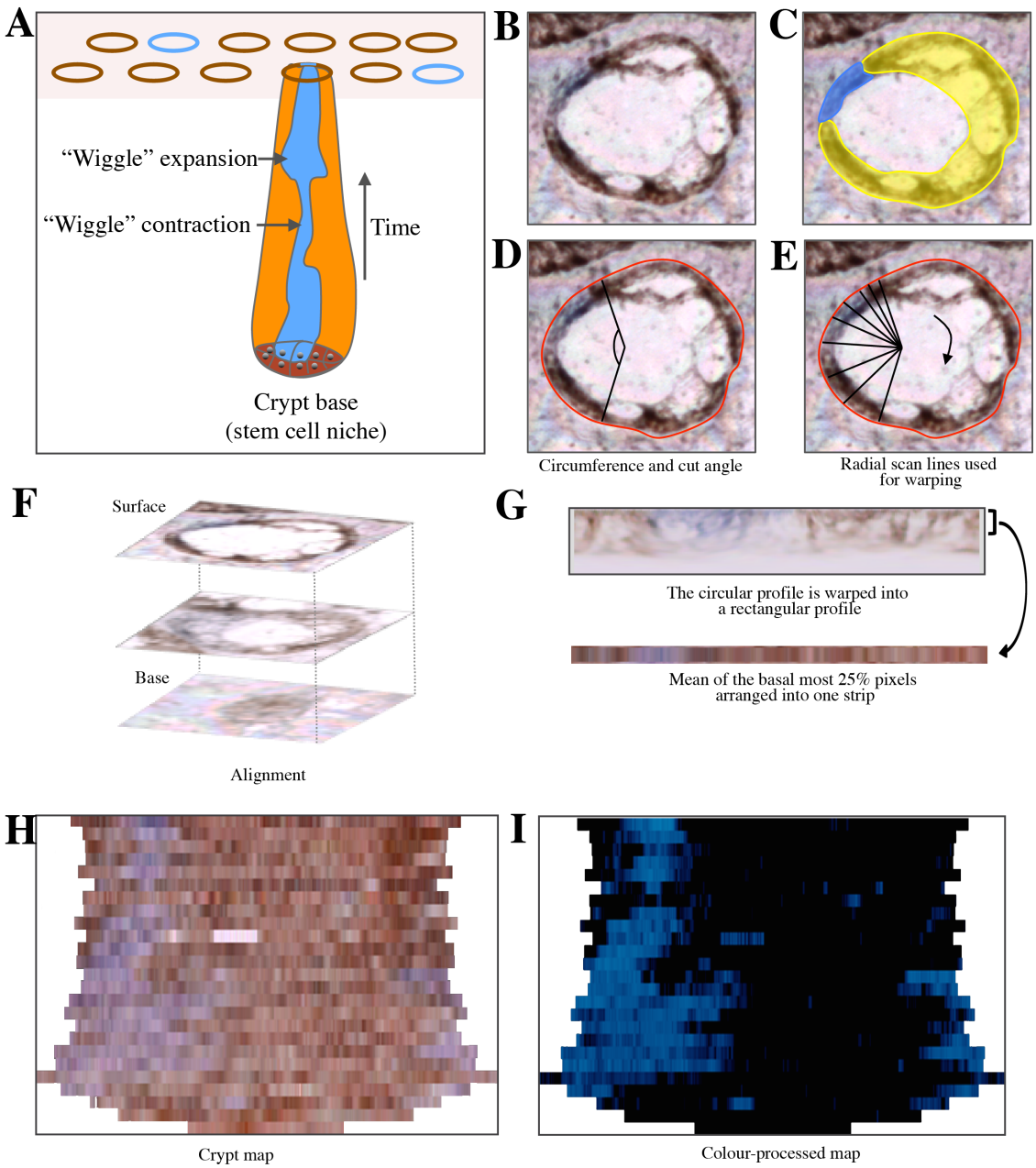

Figure 2.5: Measurement of CCO-deficient clone size and generation of a crypt map.
A) Schematic diagram showing the expansion and contraction of a CCO-deficient (blue) clone arising in the crypt base and its migration upwards as a narrow band of cells. B) Partial CCO-deficient crypts were identified in serial sections through the crypt. Displayed is a non-dysplastic, partially CCO-deficient crypt of zone 1 from a FAP patient. C) The circumference of blue vs. brown staining was measured. D) The circumference was delineated and a cut angle from the centre point was determined. E) For each image in the series, the approximately oval cross-sectional profile of the crypt is then digitally ''cut''. F) Serial sections were aligned and processed by the BiaQIm software to describe the position of the CCO-deficient cells in the crypt. G) The cross-sectional profile of the crypt was then warped into a straight profile. A single strip of an average of the first 10 pixels of the warped image was formed. H) Each single strip image was stacked from the base of the crypt to the surface forming a crypt map. I) A colour-processed representation of the original map (adapted from Baker *et al*. 2014, Fellous *et al*. 2009).

Tubes were then placed in a heat block and incubated at 56°C for 16 h. The incubation time may vary depending on the amount of tissue collected. After the incubation time, 25µl of ATL buffer and 50µl of AL buffer was added and mixed by pulse-vortexing for 15 sec. Then 50µl of 100% ethanol was added, thoroughly mixed by pulse-vortexing for 15 sec followed by a 5 min incubation time at room temperature. The mixture was then briefly centrifuged to remove drops from inside the lid. The entire lysate was transferred to a QIAamp MinElute column and centrifuged at 8000 rpm for 1 min before placed in a clean 2ml collection tube. The collection tube containing the flow-through was discarded. 500µl AW1 buffer was then added to a QIAamp MinElute column, centrifuged at 8000 rpm for 1 min and placed in a clean 2ml collection tube. The collection tube containing the flow-through was discarded. Then, 500µl AW2 buffer was added to the QIAamp MinElute column, centrifuged at 8000 rpm for 1 min and placed in a clean 2ml collection tube. Again, the collection tube containing the flow-through was discarded. The QIAamp MinElute column was then centrifuged at 13200 rpm for 3 min to dry the membrane completely before being transferred to a 1.5ml low-binding protein collection tube (Fisher Scientific, UK). The collection tube containing the flow-through was discarded. 40µl of nuclease-free water was added to the centre of the membrane, incubated at room temperature for 5 min, and centrifuged at full speed for 1 min. The DNA collected in low binding tubes was stored at -20°C until further usage.

2.5.3 Determination of DNA quantity and concentration

DNA concentration was analysed using a Qubit dsDNA HS assay kit (Invitrogen, Paisley, UK) following manufacture's instructions and measured on a Qubit® 2.0 Fluorometer. To assess DNA quality and concentration more specifically, the DNA of the PCR product was run on a Agilent 2200 TapeStation (Agilent, Craven Arms, UK), which automates sample quality control including loading, separation, and imaging. This service was performed by the Genome Centre, Barts and The London School of Medicine and Dentistry, UK.

2.5.4 Mitochondrial DNA (mtDNA) polymerase chain reaction (PCR)

DNA extracted from frozen FAP samples was amplified using two sets of genome-spanning (16,569 bp) mtDNA primers: MTL1 and FRAG1. Primer pairs MTL1-forward + MTL1-reverse were designed to generate a 9065 bp PCR product. Primer pairs FRAG1-forward + FRAG1-reverse generate a 11170 bp PCR product. The PCR reaction mixture was made up as following: 1µl of 100mM of forward and reverse specific primer (see Appendix Table 9.1). 2.5µl of 10X LA PCR buffer (Takara, Saint-Germain-en-Laye, France), 4µl of 2.5mM dNTPs (Applied Biosystems, Warrington, UK), 0.25µl of 5 U/ml AmpliTaq Gold (Applied Biosystems, UK), and 11.25µl of nuclease-free water (Qiagen, UK). 20µl of each master mix was pipetted into a 96 well plate (VWR, Lutterworth, UK). To each reaction, 5µl of extracted DNA was added and the plate sealed with an adhesive PCR film (Fisher Scientific, UK). All PCR reactions were prepared in a UV hood to avoid contamination. For each sample, the PCR mixture was set up in duplicates. Each PCR reaction was run on a G-Storm thermocycler (Fisher Scientific, UK) subjected to the following conditions: 5 min at 94°C, then cycled 30 times through 98°C for 15 sec, 68°C for 10 sec (slow ramp from 68°C to 60°C at 0.2°C per second), 60°C for 15 sec, 68°C for 11 min and after this round of cycles, incubated for 10 min at 72°C and thereafter at 10°C. PCR products were ran through a 1% agarose gel was run to confirm successful amplification.

2.5.5 Gel electrophoresis of PCR product

1% agarose (Bioline, London, UK) gels were prepared in a tris-acetate-EDTA (TAE) solution (Sigma-Aldrich, UK). The mixture was microwaved for 2 min until the agarose was melted. This was then cooled down under running water before adding Gel Red fluorescent nucleic acid dye (Cambridge Biosciences, Cambridge, UK). The gel was poured and allowed to set with combs placed within the gel to form wells. Once set, the gel was loaded into the electrophoresis tank and submerged in TAE solution. HyperLadder 100bp (Bioline, UK) was added to one comb for each row of wells to provide molecular weight markers. For the rest of the wells, a mix of 1.5µl loading dye (Bioline, UK) with 5µl DNA (PCR product) was added to each well. The

samples were run for 40 min at 135V, visualised using a UV transilluminator (Amersham Imager 600, GE Healthcare, Amersham, UK) and photographed.

2.5.6 Library preparation and sequencing of the mitochondrial DNA

Amplified mtDNA was run on an Agilent 2200 TapeStation to verify the size distribution and concentration of each PCR amplicon, and each sample was adjusted to 0.2ng/µl. Library preparation was performed using the Nextera XT DNA Library Prep kit (Illumina, Cambridge, UK). In brief, the input DNA was first fragmented and then tagged with an adapter sequence. 10µl of amplicon tagment mix and 5µl of tagment DNA buffer was added to 5µl of input DNA and heated for 5 min at 55˚C. 5µl of neutralising tagment buffer was added to each well once the reaction cooled down to 10˚C, centrifuged at 280 x g for 1 min, and incubated at room temperature for 5 min. Next, 5µl of each Index 1 adapter and 5µl of each Index 2 adapter was added together with 15µl of the Nextera PCR master mix, and again centrifuged at 280 x g for 1 min. Tagmented DNA was then amplified (72˚C for 3 min, 95˚C for 30 sec, 12 cycles of 95˚C for 1 sec, 55˚C for 30 sec, and 72˚C for 30 sec, then 5 min at 72˚C) and centrifuged at 280 x g for 1 min. Next, a limited-cycle PCR clean-up step was performed using AMPure XP beads that purified the library DNA and also removed short library fragments. 30µl of AMPure XP beads were added to 50µl of the PCR product, shaked at 1800 rpm for 2 min, and then placed on a magnetic stand (Life Technologies, UK) until the liquid was clear and the supernatant removed from each well. The library DNA was then washed twice with 80% ethanol and air-dried on the magnetic stand for 15 min. 52.5µl of resuspension buffer was then added to each well, shaked at 1800 rpm for 2 min, and incubated at room temperature for 2 min. The supernatant was then transferred to a clean plate. Then, beads were used to normalise the quantity of each library ensuring more equal library presentation. 4.4ml of library normalisation additives 1 (LNA1) was mixed with 800µl library normalisation beads 1 (LNB1). 45µl of combined LNA1/LNB1 was added to each well containing the libraries, and the mixture shaked for 30 min at 1800 rpm. Libraries were then placed on a magnetic stand and washed twice in 45µl LNW1 before adding 30µl of 0.1M NaOH to each well. Next, 30µl of LNS1 was added to each well, shaked for 5 min at 1800 rpm, again placed on a magnetic stand until the

liquid was clear, and the supernatant then transferred to a new plate. Then, equal volumes of bead-based normalised library were pooled and diluted. 5µl of each library was transferred to a new PCR 8-tube strip, and the contents of the PCR 8-tube strip were then combined in a new Eppendorf tube. Libraries were then sequenced on a MiSeq Bench-top Sequencer to generate 75 bp paired-end reads (Illumina, UK) at the Genome Centre, Barts and The London School of Medicine and Dentistry, UK.

2.5.7 Analysis of mtDNA sequencing

MtDNA sequencing data was analysed by Marc Williams (Barts Cancer Institute, London, UK). The quality of the raw sequencing reads (fastq files) was assessed using fastQC software (v0.11.3), where each base in each paired-end read is given a quality score, known as a PHRED score. A phred score is assigned to each nucleotide base call by the sequencing machine. If this score is above 20, the probability of an incorrect base call is 1 in 100 and the base call accuracy 99%. Samples with a score > 20 were accepted as good quality. All samples passed this quality control. Then, from the fastq files, bam files were produced using the Burrows-Wheeler Aligner (BWA) software (bwa mem v0.7.5), and aligned using the hg19 human genome as the reference, as bam files assign the reads to a location in the genome. Using the BamQC software (bamqc v0.5.6), the quality of the alignment can be scored. A score > 30 is an indicator for good alignment; at least 70% of all reads per sample had a score > 30. The output alignment files were then sorted according to the genomic coordinates of the mitochondrial genome. Coverage statistics were calculated using the Genome Analysis Toolkit (GATK) (software.broadinstitute.org/gatk/) to calculate the number of reads that have aligned at each position in the mitochondrial genome. To identify somatic variants, the deepSNV algorithm (Gerstung *et al*. 2012) was used. Stromal colon tissue was used as a normal control sample (obtained from the same sequencing run and with the same targeted panel) to identify somatic mutations in the test case that were not present in the control case. In this way, germline polymorphisms were excluded from the analysis. The algorithm produced two output files, one for each replicate that includes the number of mutations at a specific position in the genome, the variant and its variant allele frequency (VAF). Only if a mutation is detected in both

replicates it is considered a true mutation. The number of mutations per patients and the mutation range could then be counted to assess mutational burden.

2.6 Murine intestinal organoids

2.6.1 Crypt extraction

The intestinal tract of wild type (WT), WT ROSA$^{mT/mG}$, and *Apc*$^{1322/+}$ mice was removed and the small intestine divided into proximal (SB1), middle (SB2), and distal (SB3) parts. The intestines were washed in PBS and opened longitudinally using a scalpel and a gut preparation apparatus (Rudling *et al*. 2006). The villi were scraped off the intestines using a glass slide by firmly, repeatedly drawing the edge of the slide along the entire length of the intestines. The intestines were then cut into small pieces and washed with cold PBS. For *Apc*$^{1322/+}$ mice, polyps were dissected with a scalpel, and washed with ice cold PBS (Figure 2.6).

2.6.2 Culture of murine intestinal WT crypts

Murine intestinal fragments were isolated and cultured as previously described (Sato *et al*. 2011). In brief, tissue pieces were washed in ice cold PBS, allowed to settle and the supernatant was removed. Tissue pieces were then resuspended in 25ml of 2.5mM EDTA/PBS and rotated for 30 min at 4°C. After removing the supernatant, tissue was resuspended in 10ml basic culture media (100µg/ml penicillin/streptomycin, 2mM Glutamax (both from Life Technologies, UK), 10mM HEPES (Sigma-Aldrich, UK), 1× N2-Supplement (Fisher Scientific, UK), 1× B27-Supplement (Fisher Scientific, UK), 1mM N-acetylcysteine (Sigma-Aldrich, UK), and 0.25µg/ml Fungizone (Life Technologies, UK) in advanced Dulbecco's modified Eagle medium/F12 (Life Technologies, UK)) (Table 2.3). The entire volume was pipetted up and down, and the supernatant collected in a new 50ml Falcon tube. At this point, the crypts were being dislodged from the pieces and were floating in the supernatant. This step was repeated 3-4 more times, each time adding the supernatant to the 50ml Falcon tube. The solution was centrifuged for 5 min at 1200 rpm at 4°C

and the supernatant poured off carefully. The pellet was resuspended in 10ml basic culture media, passed through a 70µm cell strainer (VWR, UK) to remove residual villous material and centrifuged at 300 x g for 3 min. The pellet was resuspended in $^{2}/_{3}$ Matrigel (SLS, Nottingham, UK) and $^{1}/_{3}$ basic culture media, and 40µl was plated out in each well of a 24-well plate (Corning, UK). To each well, organoid media was added (500µl of basic culture media, 50ng/ml Epidermal Growth Factor (EGF) (Life Technologies, UK), 100ng/ml Noggin (PeproTech, London, UK) and 100µl/ml R-spondin1 (R and D systems, Abingdon, UK)) (Table 2.3). The organoid media was changed every 2 days (Figure 2.6).

Basic culture media	
Reagent	*Final concentration*
Advanced Dulbecco's modified Eagle medium/F12	
Penicillin/streptomycin	100µg/ml
Glutamax	2mM
Hepes	10mM
N2-Supplement	1X
B27-Supplement	1X
N-acetylcysteine	1mM
Fungizone	0.25µg/ml
Organoid media	
Basic culture media	
Epidermal growth factor	50ng/ml
Murine noggin	100ng/ml
R-Spondin	100µl/ml

Table 2.3: Basic culture and organoid media.

2.6.3 Culture of mouse intestinal *Apc*$^{1322/+}$ adenomas

Polyps from *Apc*$^{1322/+}$ mice were washed 5 times in ice cold PBS. After removing the supernatant of the last wash, the tissue fragments were incubated in 2mmol/L EDTA

cold chelation buffer (5.6mmol/L Na_2HPO_4, 8.0mmol/L KH_2PO_4, 96.2mmol/L NaCl, 1.6mmol/L KCl, 43.4mmol/L sucrose, 54.9mmol/L D-sorbitol, 0.5mmol/L DL-dithiothreitol) (all from Sigma-Aldrich, UK) for 1 h on ice. After removal of the chelation buffer, tissue fragments were vigorously resuspended in chelation buffer. The tissue fragments were allowed to settle and the supernatant was removed. This procedure was repeated 3-5 times. Tissue fragments were then incubated in digestion buffer (advanced Dulbecco's modified Eagle medium supplemented with 2.5% fetal bovine serum (FBS), 2.5% penicillin/streptomycin, 125ug/ml Dispase type II (all Life Technologies, UK), and 75U/ml Collagenase type IX (Sigma-Aldrich, UK)) for 30 min at 37°C. The supernatant was then enriched for crypts by centrifugation (300 x g for 5 min) and resuspended in 10ml basic culture media. This fraction was passed through a 70µm cell strainer to remove residual villous material. Isolated crypts were centrifuged at 300 x g for 3 min and washed in cold PBS. This fraction consisted of essentially pure crypts. The pellet was resuspended in $^2/_3$ Matrigel and $^1/_3$ basic culture media, and 40µl was plated out per well in a 24-well plate (Corning, UK). The Matrigel was polymerised for 15 min at 37°C, and 500µl basic culture media was overlaid containing 50ng/ml EGF. The medium was changed every 2 days (Figure 2.6).

2.6.4 Passaging and embedding of organoids

After intestinal crypts had grown into spheroid structures, usually after 5-7 days, they were passaged by adding 500µl cold PBS to melt the Matrigel, spin down at 800 rpm for 3 min, and subsequently re-plated in fresh Matrigel. To collect material for embedding, Matrigel was melted with cold PBS and then multiple wells were combined. The cells were fixed in 500µl 4% paraformaldehyde (PFA) for 30 min at room temperature, centrifuged at 5000 rpm for 5 min and resuspended in 200µl 2% Agarose (in PBS). The cell pellet was then processed and embedded using standard protocols.

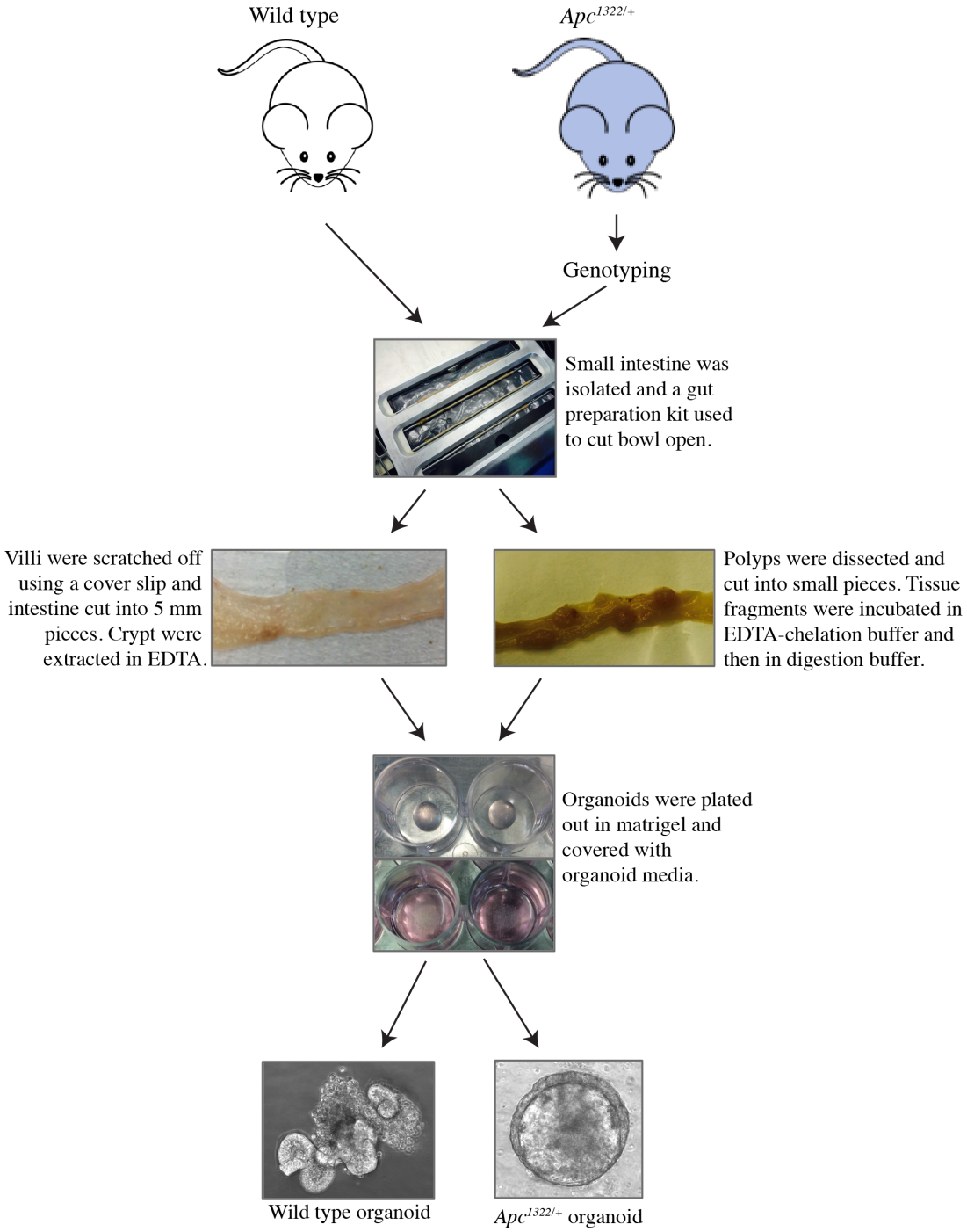

Figure 2.6: Extraction and culturing of murine organoids.

2.7 Co-culture of WT and *Apc*$^{1322/+}$ murine organoids

Apc$^{1322/+}$ organoids were placed directly next to WT organoids in a 12 –well plate (Corning, UK) and controlled with WT with WT and *Apc*$^{1322/+}$ with *Apc*$^{1322/+}$ organoids only for 48 h and 72 h. 1ml of organoid media was overlaid. Each experiment was set up in triplicate. Organoids were collected separately after 48 h and 72 h. RNA was immediately extracted and stored at -80°C until further use. To assess the concentration and quality of the extracted RNA, 1µl of each sample was run on a RNA Nano Bioanalyser chip (Agilent Technologies, UK). RIN values > 8 were chosen for mRNA sequencing (Figure 2.7) (see section 2.10.3).

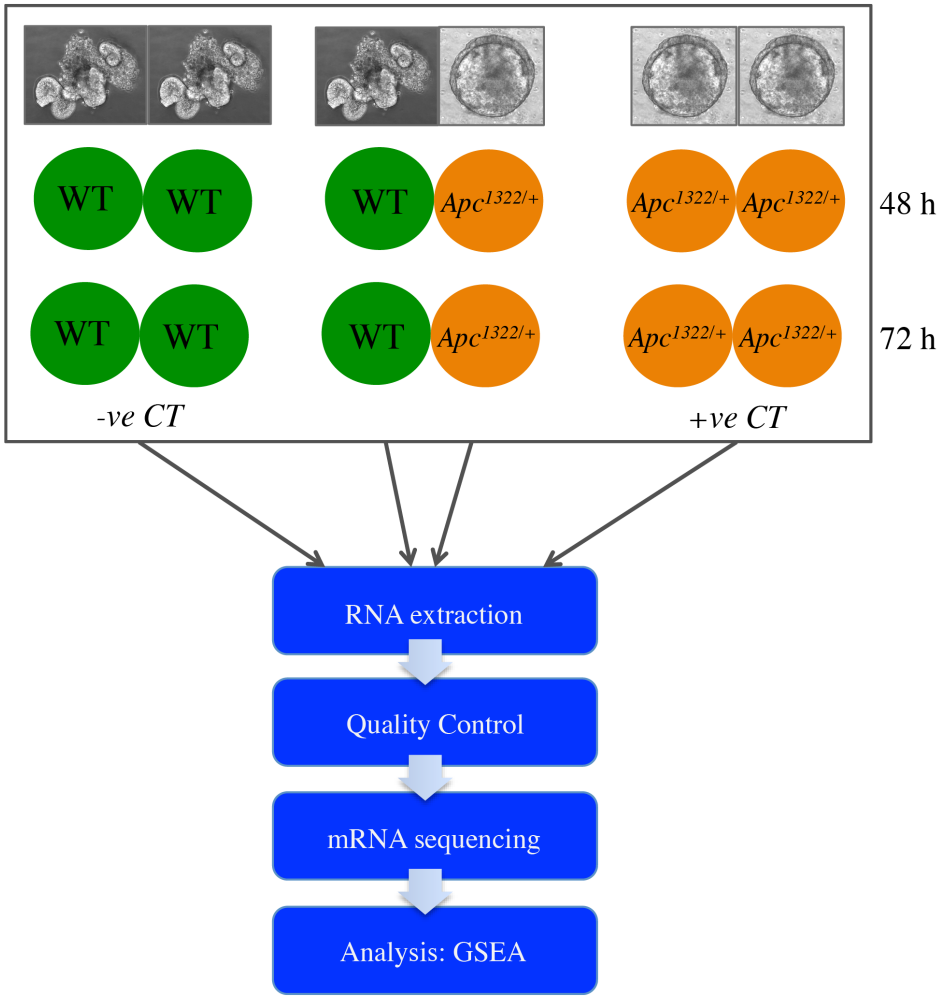

Figure 2.7: Co-culturing of WT and *Apc*$^{1322/+}$ organoids and mRNA sequencing workflow.
WT and *Apc*$^{1322/+}$ organoids were co-cultured in close proximity to each other for 48 h and 72 h, and controlled with WT with WT (-ve CT) and *Apc*$^{1322/}$ with *Apc*$^{1322/+}$ organoids (+ve CT) only. Experiment was set up in triplicates and RNA extracted from all conditions followed by a quality control step before sequencing of the mRNA was performed. Gene expression profiles were analysed with the gene set enrichment analysis software (GSEA).

2.8 Transwell co-culture of WT and *Apc*$^{1322/+}$ organoids

WT organoids were placed in the top compartment of a transwell insert (CytoOne, Fisher Scientific, UK) and *Apc*$^{1322/+}$ organoids were placed on the bottom of a 24-well plate (Figure 2.8A). Experiment was controlled with WT with WT and *Apc*$^{1322/+}$ with *Apc*$^{1322/+}$ organoids only. 500µl organoid media was overlaid. Each experiment was set up in triplicate. Organoids were collected separately after 72 h. RNA was immediately extracted and stored at -80°C until further use. Quantity and quality of the RNA was assessed on the RNA Nano Bioanalyser chip (Agilent Technologies, UK). RIN values > 8 were chosen for mRNA sequencing (see section 2.10.3).

2.9 Transwell co-culture of WT and *Apc*$^{1322/+}$ organoids with murine fibroblasts

2.9.1 Isolation of intestinal murine fibroblasts

The intestinal tract was dissected from a WT mouse and the small intestine opened longitudinally using a scalpel. The intestine was then cut into 5mm pieces and placed in Hank's Balanced Salt Solution (HBSS) (Life Technologies, UK). The tissue was then washed 5 times in HBSS until all detritus was removed.

The epithelium was then removed by incubation in 25ml of 1mM EDTA (Life Technologies, UK) in HBSS at 37°C with constant shaking for 15 min. The fluid was carefully poured off and refilled with 25ml of 1mM EDTA. This step was repeated for a total of 5 washes or until no more cells could be removed. The tissue was then placed in 50ml RPMI media containing 10% FBS, 1% Pen/Strep, 1.5mg/ml Dispase (all Life Technologies, UK), and 1mg/ml Collagenase (Sigma-Aldrich, UK), and shaked at 250 rpm for 30 min until the tissue began to look stringy. The tissue was then pelleted at 1200 rpm for 5 min and the supernatant carefully discarded. The pellet was then resuspended in 10ml RPMI media containing 10% FBS and 1% Pen/Strep and plated out into a 75mm TC-treated flask (Corning, UK) and incubated at 37°C and 5% CO_2. After 3 h, non-adherent cells were washed off and replaced with 12ml of fresh media (PRMI/10% FBS/1% Pen/Strep). Fibroblasts were then

slowly adjusted to basic culture media for co-culture with WT and *Apc*$^{1322/+}$ organoids: after 2 days, 6ml of fresh media and 6ml of basic culture media was added, and after 4 days 12ml of only basic culture media was added to the fibroblasts.

2.9.2 Organoid and fibroblast co-culture

Extracted murine fibroblasts were transferred to the bottom of a 24-well plate (Corning, UK) and overlaid with organoid media. After 5 h, giving the fibroblasts time to adhere, transwell inserts with *Apc*$^{1322/+}$ organoids were placed on top of the fibroblasts and incubated with 500µl organoid media. After 72 h, the *Apc*$^{1322/+}$ organoids were collected. RNA was immediately extracted and stored at -80°C. Then, transwell inserts containing WT organoids were exposed to the same fibroblasts for 72 h that were previously exposed to *Apc*$^{1322/+}$ organoids, and overlaid with fresh organoid media (Figure 2.8B). After 72 h, WT organoids were collected and RNA was immediately extracted. Each experiment was set up in triplicate. Extracted RNA of WT and *Apc*$^{1322/+}$ organoids was run on a RNA Nano Bioanalyser chip (Agilent Technologies, UK). RIN values > 8 were chosen for mRNA sequencing (see section 2.10.3).

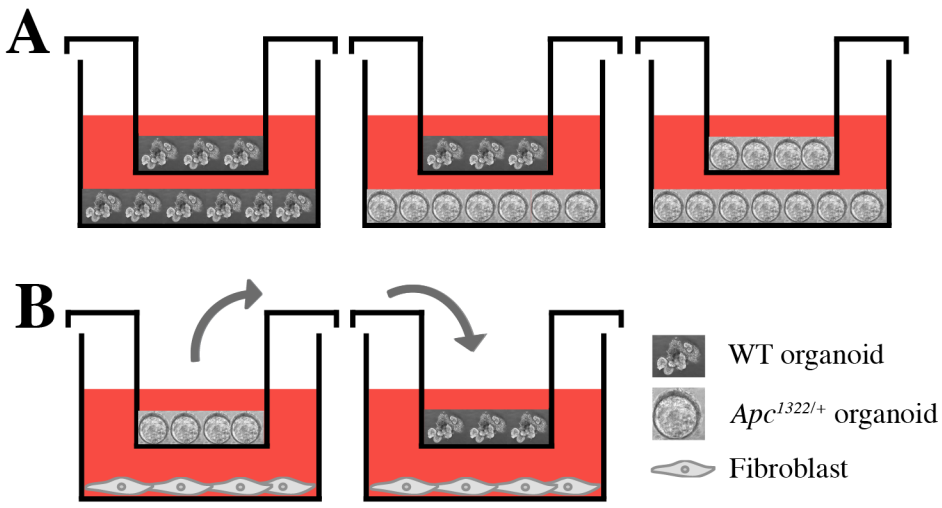

Figure 2.8: Transwell experiment of WT and *Apc*$^{1322/+}$ organoids with and without fibroblasts.
A) WT organoids were placed in a transwell on top of *Apc*$^{1322/+}$ organoids for 72 h and controlled with WT with WT and *Apc*$^{1322/+}$ with *Apc*$^{1322/+}$ organoids only. Experiment was set up in triplicates. B) *Apc*$^{1322/+}$ organoids were grown on top of murine WT fibroblasts for 72 h. The transwell with the *Apc*$^{1322/+}$ organoids was then taken off and replaced with WT organoids for 72 h. Here, the effect of fibroblasts – previously exposed to mutants – on WT organoids was studied.

2.10 RNA related methods

2.10.1 Total RNA extraction

RNA was extracted from organoids using a RNeasy micro Kit (Qiagen, UK) as per the manufacturer's instructions. In brief, organoids were harvested in PBS, spin down at 5000 rpm for 5 min and the supernatant discarded before 350µl of RLT buffer and β-mercaptoethanol (10µl in 1ml RLT buffer) (Sigma-Alridch, UK) was added and vortexed for 30 sec. Then, 350µl of 70% ethanol was added to the lysate, mixed well by pipetting and then immediately transferred to a RNeasy MinElute spin column in a 2ml collection tube (supplied with kit). The lysate was centrifuged at 8000 rpm for 15 sec and the flow-through discarded. Next, 350µl RW1 buffer was added to the RNeasy MinElute spin column, centrifuged at 8000 rpm for 15 sec and the flow-through discarded. The RNeasy MinElute spin column was placed in a new 2ml collection tube and 500µl RPE buffer added to the spin column, centrifuged at 8000 rpm for 15 sec and the flow-through discarded. Then, 500µl of 80% ethanol was added to the spin column, centrifuged at 8000 rpm for 2 min before placing the RNeasy MinElute spin column in a clean 2ml collection tube and spin for 5 min at full speed to dry the membrane. The collection tube containing the flow-through was discarded. Finally, the RNeasy MinElute spin column was placed in a new 1.5ml collection tube (provided by the kit). To elute the RNA, 12µl of RNase-free water was added directly to the centre of the spin column membrane and centrifuged at full speed for 1 min. Extracted RNA was kept at -80°C until further usage.

2.10.2 Determination of RNA quality and quantity

RNA concentration was analysed using a Qubit RNA assay kit (Invitrogen, UK) following manufacture's instructions. To assess RNA quality, extracted RNA was run on the RNA Nano Bioanalyser chip (Agilent Technologies, UK), which measures the RNA Integrity Number (RIN) between 0-10 to demonstrate how intact the sampled RNA is. All samples passed quality and samples with a RIN value of > 8.0 were chosen for sequencing.

2.10.3 Library preparation and sequencing of mRNA

Extracted RNA samples from WT and *Apc*$^{1322/+}$ organoids that passed quality control were normalised to 100ng/µl. Library preparation was performed using the NEBNext® Ultra™ Directional RNA Library Prep Kit (Illumina, UK). In brief, mRNA was isolated and fragmented from total RNA. NEBNext Oligo $d(T)_{25}$ beads were resuspended in 50µl of RNA binding buffer and added to 50µl of total RNA. The mixture was placed on a thermal cycler for 5 min at 65˚C and held at 4˚C. Beads were then resuspended and incubated at room temperature for 5 min, before being placed on a magnetic stand for 2 min until the liquid was clear. The supernatant was removed and the beads washed twice with 200µl of wash buffer. Then, 50µl of Tris buffer was added to each tube and placed on a thermal cycler for 2 min at 80˚C and held at 25˚C. 50µl of RNA binding buffer was then added to each sample and incubated for 5 min at room temperature to allow the mRNA to re-bind the beads. Beads were then washed again in 200µl of wash buffer and incubated for 2 min at room temperature. 15.5µl of the first strand synthesis reaction buffer and random primer mix was added to elute the mRNA from the beads. The mixture was then incubated at 94˚C for 15 min, and immediately after placed on a magnetic rack. Purified mRNA was collected by transferring 13.5µl of the supernatant to a clean nuclease-free tube and placed on ice.

First strand cDNA synthesis was performed by adding 0.5µl murine RNase inhibitor, 5µl Actinomycin D, and 1µl ProtoScript II reverse transcriptase to the purified mRNA, and incubated in a thermal cycler (10 min at 25˚C, 15 min at 42˚C, and 15 min at 70˚C).

Second strand cDNA synthesis was performed by adding 8µl of second strand synthesis reaction buffer, 4µl of second strand synthesis enzyme mix, and 48µl of nuclease-free water to the first strand reaction. The mixture was then incubated for 1 h at 16˚C.

Double stranded cDNA was then purified with 144µl (1.8X) Agencourt AMPure XP beads, incubated for 5 min at room temperature, and placed on a magnetic stand. Once the liquid was clear, the supernatant was removed and the beads washed in 200µl of 80% ethanol. Next, cDNA was eluted from the beads into 60µl 0.1X Tris-EDTA (pH 8.0) buffer. 55.5µl of the supernatant was transferred into a clean nuclease-free tube.

End prep of cDNA library was then performed by adding 6.5µl end repair reaction buffer and 3µl end repair enzyme mix to the purified double stranded cDNA and incubated in a thermal cycler (30 min at 20˚C and 30 min at 65˚C). 15µl of ligase master mix, 1µl of diluted adaptor and 2.5µl nuclease-free water was added to the end prep reaction to ligate adapters, and incubated for 15 min at 20˚C.

Next, the ligation reaction was purified with 45µl (1.0X) of AMPure XP beads, then incubated for 5 min at room temperature, and washed twice in 200µl 80% ethanol. cDNA was eluted in 52µl 0.1X Tris-EDTA (pH 8.0) buffer, and incubated at room temperature for 2 min. The purification step using 20µl AMPure XP beads was repeated and DNA eluted in 19µl 0.1X Tris-EDTA (pH 8.0) buffer. 17µl of the supernatant was then transferred into a clean tube.

A PCR was then performed to enrich the adapter ligated DNA. 3µl of USER enzyme, 5µl of the universal primer mix and 25µl of the PCR master mix was added to the cDNA and placed in a thermal cycler (37˚C for 15 min, 98˚C for 30 sec, 15 cycles at 98˚C for 10 sec and 65˚C for 75 sec, and 65˚C for 5 min). The PCR reaction was then purified again using 45µl (0.9X) AMPure XP beads, incubated for 5 min at room temperature, and washed twice in 200µl 80% ethanol. cDNA was eluted into 23µl 0.1X Tris-EDTA (pH 8.0) buffer, vortexed, and incubated for 2 min at room temperature. Mixture was placed in a magnetic stand until the liquid was clear, and 20µl of the supernatant was transferred into a clean tube.

The library quality was then assessed on a D1000 TapeStation (Agilent Technologies, UK) and the concentration measured using a Qubit dsDNA HS assay kit (Invitrogen, UK). Sequencing was performed on a NextSeq 500 High Output Flow Cell generating approximately 15 Million 75 bp paired-end reads per sample (Illumina, UK) at the Genome Centre, Barts and The London School of Medicine and Dentistry, UK. Sequencing reads from organoid samples were submitted to BaseSpace Illumina (https://basespace.illumina.com/s/OvBOgSa2z4Xa.).

2.10.4 Transcriptome analysis

Differential gene expression analysis was performed by Christian Owusu (Sanger Institute Cambridge, UK). The quality of the fastq files was assessed using fastQC software (v.0.11.4). All samples passed this quality control. Then, for each sample,

fastq files representing forward and reverse reads were aligned to the mouse reference using the splice-aware aligner, Tophat2 (v.2.1.0) (Kim *et al*. 2013). Briefly, the mouse reference genome (mm10) was downloaded from the Ensembl Genomes FTP server in fasta format and indexed prior to mapping using the bowtie2-build command. Reads were then mapped with Tophat2, which in turn makes use of the Bowtie2 aligner (v.2.1.0) (Langmead *et al*. 2012). Reads that could be unambiguously assigned to exons were counted with HTSeq-count (v 0.6.1) (Anders *et al*. 2015), using default parameters. Differential gene expression analysis was performed using DESeq2 v1.6.2 (Love *et al*. 2014) available from Bioconductor (Gentleman *et al*. 2004) and implemented in R v3.1.2. DESeq2 corrects for variation in library size among samples using a scaling factor calculated by dividing the counts of a gene in a particular sample by the geometric mean count of the gene across all samples. Counts are modelled using the negative binomial distribution, which is able to capture the overdispersion seen within biological replicates (Love *et al*. 2014). The false discovery rate (FDR) was used to correct for multiple testing and only genes showing $\log_2$ fold changes of ≥ 1 and adjusted p-values ≤ 0.05 were considered biologically significant. In order to identify genes, DESeq2 results were cross-referenced with the genes in the KEGG database (Kanehisa *et al*. 2000). Gene clustering was done using the R package MBCluster.seq (Si *et al*. 2014).

2.10.5 Gene Set Enrichment Analysis

Expression profiles were analysed using the Gene Set Enrichment Analysis (GSEA) software v.2.2.1 (Broad Institute, http://software.broadinstitute.org/gsea/index.jsp) (Subramanian *et al*. 2005) to detect up- and/or downregulated pathways. GSEA is a method of analysing and interpreting RNA sequencing data using biological knowledge and enables detection of gene sets enriched in genes that are significantly associated with a phenotype of interest.

After choosing a pre-defined collection of gene sets as input, GSEA then provides a score to each gene set's association with a phenotype. These predefined biological set of genes are published information about biochemical pathways. Here, the predefined gene set that was used in the analysis was the curated c2.cp.kegg.v5.1.symbols.gmt gene set, using the GSEA Pre-ranked tool.

Using the GSEA pre-ranked analysis, the analysis is run against the ranked list of genes and then determines whether a significant number of genes from predefined biological sets occur towards the top or bottom of ranked list. Such enrichment is computed using the Kolmogorov-Smirnov (KS) statistic. This statistic compares the anticipated random distribution of a set of genes and their actual distribution among a genome-wide list of genes ranked based on their association with the phenotype. The KS statistic is then normalised for gene set size and its significance is adjusted to take into account multiple hypotheses testing.

The primary output of GSEA is an enrichment score (ES), which reflects the degree to which a gene set is overrepresented at the top or bottom of this ranked list of genes, depending on the correlation with the phenotype. The ES is the maximum deviation from zero encountered in walking the list. A positive ES indicates gene set enrichment at the top of the ranked list; a negative ES indicates gene set enrichment at the bottom of the ranked list. By normalising the enrichment score, GSEA accounts for differences in gene set size and in correlations between gene sets and the expression dataset; therefore, the normalised enrichment scores (NES) can be used to compare analysis results across gene sets.

Parameters used for the analysis were as follows: 1000 permutations were used to calculate the p-value. All basic and advanced fields were set to default, except for "Enrichment statistics", which was set to "classic", and graphs for the top set of each phenotype was set to 200.

2.10.6 Ingenuity pathway analysis

The list of differentially expressed genes from the mRNA sequencing experiment was then analysed using the Ingenuity Pathway Analysis software (IPA) (Qiagen, Germany; http://www.ingenuity.com) to identify the main biological processes associated to the experimental system. IPA identifies significant networks, functions and canonical pathways associated with the differentially expressed genes for each comparison analysed in relation to larger biological or chemical systems. Importantly, the causal analytics are based on the Ingenuity Knowledge Base, which is a uniquely structured repository of biological and chemical findings curated from various sources including the literature and is continuously updated (Jimenez-Marin

et al. 2009, Kramer *et al*. 2014). IPA maps the differentially expressed genes onto proteins in its database and then organises the proteins into networks based on the number of members observed in the data set of significantly altered proteins, which then allows to detect new targets and candidate genes. The Ingenuity Knowledge Base currently contains approximately 5 million individual findings describing the relationships between molecules and/or diseases or biological functions (Kramer *et al*. 2014).

2.10.7 Quantitative reverse transcriptase polymerase chain reaction (qRT-PCR) of WT and *Apc*$^{1322/+}$ organoids

2.10.7.1 Complementary DNA synthesis

Extracted RNA was normalised to 100ng/µl. The first strand cDNA was synthesised using the QuantiTect Reverse Transcription kit (Qiagen; UK) with integrated removal of genomic DNA contamination following manufacture's instructions. In brief, the genomic DNA elimination reaction was prepared on ice by adding 1µl gDNA Wipeout Buffer to 100ng template RNA and topped up with RNase-free water to reach a final volume of 7µl per sample. This reaction was then incubated for 2 min at 42°C and then immediately placed on ice. Next, the reverse-transcription master mix was prepared containing all components required for first strand cDNA synthesis. The template RNA (entire genomic DNA elimination reaction) of each sample was added to 0.5µl Quantiscript Reverse Transcriptase, 2µl Quantiscript RT Buffer, and 0.5µl RT Primer Mix to reach a final volume of 10µl. The mixture was then incubated for 30 min at 42°C followed by an incubation for 3 min at 95°C to inactivate Quantiscript Reverse Transcriptase. 40µl of RNase-free water was then added to the cDNA and stored at -20°C until further usage.

2.10.7.2 qRT-PCR reaction preparation

Prepared cDNA was thawed on ice, gently vortexed and centrifuged. Each reaction was prepared in duplicate, in a 20µl total reaction volume containing 10µl of 1X ABsolute Blue SYBR Green ROX Mix (Fisher Scientific, UK), 1µl of 100mM gene specific forward and reverse primer (Appendix Table 9.3), 1µl cDNA template, and

8µl nuclease-free water (Qiagen, UK) in a 96 MicroAmp, fast optical reaction plate (Applied Biosystems, UK). Reactions were run on an Applied Biosystems StepOnePlus Real Time PCR system (Amersham, UK) with thermal cycling conditions suggested by the manufacturer (Table 2.4).

	Temperature	Time	Number of cycles
Enzyme activation	95°C	15 min	1 cycle
Denaturation	95°C	15 sec	
Annealing	60°C	30 sec	40 cycles
Extension	72°C	30 sec	

Table 2.4: qRT-PCR thermal cycling conditions.

2.10.7.3 qRT-PCR gene expression analysis

Genes of interest (see Appendix Table 9.3) were normalised using the housekeeping gene GAPDH (Glyceraldehyde 3-phosphate dehydrogenase; reference sequence: forward: ttgtggaagggctcatgacc, reverse: tcttctgggtggcagtgatg) between samples in each set to calculate the relative expression of genes of interest. The ΔΔCT method (Schmittgen *et al*. 2008) was used to assess the relative expression level of each gene as follows:

1. ΔCT was calculated by subtracting the average gene CT value from the average housekeeping CT value.
2. ΔCT values from each sample were subtracted from the reference sample to get the ΔΔCT value: $\Delta\Delta CT = \Delta CT^{WT\ exposed} - \Delta CT^{WT}$. The relative gene expression values $2^{(-\log fold\ values)}$ were calculated using the following equation: $-2^{-\Delta\Delta CT}$.
3. The results were analysed in Prism 6.0 using a t-test with Welch correction on fold changes relative to the control sample.

2.11 *In situ* hybridisation (ISH)

ISH for Lgr5 expression was performed on 5µm FFPE sections using a RNAscope 2.0 High Definition assay according to the manufacturer's protocol (Advanced Cell

Diagnostics, Abingdon, UK). Briefly, sections were baked at 60°C for 1 h, followed by de-paraffinisation and incubation with Pretreat 1 buffer for 10 min at room temperature. Slides were boiled in Pretreat 2 buffer for 15 min, followed by incubation with Pretreat 3 buffer for 30 min at 40°C. Slides were incubated with the relevant probes for 2 h at 40°C, followed by successive incubations with Amp1 to 6 reagents. Staining was visualised with DAB-A and DAB-B (brown staining) for 10 min, and then lightly counterstained with Gill's haematoxylin (Sigma-Aldrich, UK). RNAscope probes used were Lgr5 (NM_003667.2, region 560– 1589, # 311021), POLR2A (positive control probe, NM_000937.4, region 2514–3433, # 310451) and dapB (negative control probe, EF191515, region 414–862, # 310043).

Photographs of individual organoids were taken using a brightfield microscope and the number of positive stained Lgr5 probes per cell per organoid manually counted in each group in Photoshop CS6.

2.12 Cytospin

Normal charged glass slides were coated with 40µl poly-l-lysine (Sigma-Aldrich, UK) and left to dry in an incubator at 37°C for 20 min. Organoids were collected, spin down for 3 min at 800 rpm, the supernatant discarded and resuspended in 100µl ice cold PBS. The coated slides were then removed from the incubator and added on to a stainless steel Cytoclip slide clip together with filter paper and a Cytofunnel sample chamber. Organoids were then added into the little groove and centrifuged in a Shandon CytoSpin III Cytocentrifuge for 3 min at 500 rpm. After centrifugation, the slides were carefully taken out of the sample holder. A circle was then drawn around the organoids using a pap pen (Sigma-Aldrich, UK) before they were fixed in 4% PFA followed by immunofluorescence staining.

2.12.1 Immunofluorescence

Immunofluorescence was performed on cytospin material of organoids. Organoids were fixed for 10 min in 4% PFA and permeabilised in PBS/0.5% Triton X (PBST) (Sigma-Aldrich, UK) for 30 min. Sections were then blocked with Protein-Free block (Dako, UK) for 10 min. Anti-Ki67 (Abcam, Cambridge, UK; dilution 1:100)

was diluted in PBST and 5% Donkey serum for 45 min and then washed 3 x 5 min in PBST. Organoids were then incubated in Alexa Fluor 488 donkey anti-rabbit secondary antibody (Life Technologies, UK) (1:800 dilution in PBST and 5% donkey serum) for 45 min and washed 3 x 5 min in PBST. Then, DAPI (Sigma-Aldrich, UK) was diluted 1:2000 in PBST and added for 5 min following a 3 x 5 min washing step in PBST. Lastly, mounting medium (Vectorshield for fluorescence; Vector labs, UK) was applied to cover slip the sections. Immediately after, slides were stored in a box to prevent light exposure and kept dry at 4°C until being analysed with confocal microscopy.

2.12.2 Confocal microscopy and image analysis

Fluorescent stained slides were scanned in with a confocal microscope (LSM 710 Zeiss, Germany) using the 20x objective. WT ROSA$^{mT/mG}$ (membrane-Tomato/membrane-Green) organoids express strong membrane-targeted tdTomato (mT), a red fluorescent protein (https://www.jax.org/strain/007576). DAPI, tdTomato and Ki67^{+} cells were scanned in in separate channels and a z-stack was produced. Representative organoid images were analysed in Image J 1.48v (https://imagej.nih.gov/ij/). The percentage of Ki67^{+} cells/area was measured. In brief, the area of the organoid was assessed in the DAPI image by manually drawing around the organoid and the same area was kept for the Ki67^{+} stained image. The tdTomato image was used to identify WT ROSA$^{mT/mG}$ organoids when grown in presence of *Apc*$^{1322/+}$organoids. A threshold was then applied to measure the percentage of Ki67^{+} cells/area, which was kept the same for each image (Figure 2.9).

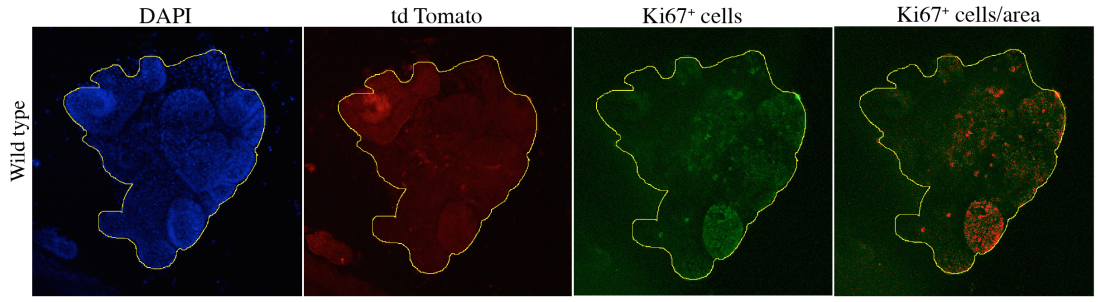

Figure 2.9: Assessing Ki67^{+} cells in WT ROSA$^{mT/mG}$ organoids.
Three channels were scanned in using the confocal microscope: DAPI, tdTomato and green fluorescent Ki67^{+} cells. Area of organoid was assessed on the DAPI image. A threshold was applied to the Ki67 image to measure the percentage of positive stained cells per area.

2.13 Statistical analysis

GraphPad Prism® 6 programme and R 3.3.0 were used for all statistical analyses. All statistical analyses are explained in further detail in the relevant section. Data was considered statistically significant when the *P* value was less than 0.05. All statistical tests were two-sided. Error bars represent standard error of the mean unless otherwise stated.

2.13.1 Statistical test for the assessment of immunohistochemical analyses of Ki67, γH2AX, nuclear β-catenin, intraepithelial lymphocytes (CD8), α-SMA, and phenotypic characteristics

First, a Shapiro-Wilk normality test was performed in Prism 6 to test for normal distribution of the data. For each marker, the data did not pass the normality test. Thus, the non-parametric Kruskal-Wallis test was used. An unpaired t-test with a two-tailed Mann-Whitney test was performed to assess which of the ranks were significantly different (see section 3.2.1, 3.2.3, 3.2.4, 3.2.5).

2.13.2 Statistical test for the assessment of immunohistochemical analyses of the stromal markers CD4, CD8, CD68, and α-SMA

A Pearson's χ^2 test was performed (see section 3.2.2).

2.13.3 Statistical test for the assessment enzyme histochemical analysis of cytochrome *c* oxidase and the measurement of mean cell number and circumference per crypt

A Kruskal-Wallis test was performed and an unpaired t-test with a two-tailed Mann-Whitney test (section 3.2.6).

2.13.4 Statistical test for the quantification of stem cell dynamics *in vivo*

The relative change in clone size per section in terms of number of cells per crypt was plotted in R 3.3.0 using the density function and skewness was calculated (section 4.2.1).

2.13.5 Statistical test for the quantification of cell proliferation in murine organoids

A one-way ANOVA was performed and an unpaired t-test with a two-tailed Mann-Whitney test (section 6.4.6).

2.13.6 Statistical test for the quantification of Lgr5 expression in murine organoids

Data passed Shapiro-Wilk normality test. A one-way ANOVA followed by a Bonferroni's multiple comparisons test was performed. A Pearson's χ^2 test was performed on the stacked plot (section 6.4.7). Pairwise comparisons were done using an unpaired t-test with Welch correction.

3 Chapter III: Clonal Interactions

3.1 Introduction

Colonic crypts are clonal units, each cell is derived from a common stem cell and according to the somatic evolution of cancer theory, cancers are derived from clonal lesions, such as monocryptal adenomas (Humphries *et al*. 2008, Novelli *et al*. 1996). Therefore, at the root of CRC development lies the normal crypt stem cell (Brittan *et al*. 2002). Neoplastic changes occur when a crypt stem cell acquires sufficient mutations or genetic defects to confer a selective growth advantage over the other stem cells and by clonal conversion results in a mutant and perhaps premalignant phenotype. As the mutant crypt divides by fission, a *monoclonal* tumour forms (Nowell 1976). This theory has formed the bedrock of our knowledge of tumourigenesis in most tissues. However, clonal analysis of murine and human familial intestinal adenomas has shown that tumours can develop from more than one founder mutant crypt, leading to a *polyclonal* tumour (Gausachs *et al*. 2017, Merritt *et al*. 1997, Novelli *et al*. 2003, Novelli *et al*. 1996, Thirlwell *et al*. 2010, Thliveris *et al*. 2005, Thliveris *et al*. 2013). Using a mathematical model, it was predicted that recruitment occurs in short-range interactions between clones, and polyclonal tumours could be best explained by the transformation of a single neighbour within 144μm from its initial progenitor (Thliveris *et al*. 2013) (see introduction 1.15).

However, no data exists on the nature of these clonal interactions, the field effect this may cause and indeed there is no explanation on the role of the stroma in this process. The research that has been done to understand these interactions between mutated and normal clones suggests that when a crypt undergoes neoplastic changes it alters its local environment and begins to affect the stroma and neighbouring crypts (Bjerknes 1996, Bjerknes *et al*. 1999). Here, it is hypothesised that an initiated crypt exerts mutational or neoplastic pressure on surrounding neighbouring crypts, that results in the formation of two independently derived crypts that combine to form a polyclonal tumour. Further, multiple initiated crypts can interact to generate a dysplastic field effect. Evolution is based on natural selection (Merlo *et al*. 2006), therefore competition or cooperation between

independent crypts develops where a 'winner' crypt (or clone) proceeds to become the dominant lineage within an adenoma and therefore becomes the monoclonal origin of cancer.

There is therefore an urgent need to understand if and how different clones interact, as it will determine risk of malignancy in adenomas. Thus, the aim of this chapter is to demonstrate clonal interactions between dysplastic and non-dysplastic epithelium driving expansion. Determining unique clones within the colon is difficult without large amounts of next generation sequencing of crypts. Further, adenomas are removed when detected making temporal analysis in the human colon difficult. Therefore, a phenotypic distinction of clones was used: the dysplastic crypts of the adenoma and surrounding non-dysplastic crypts. It is known through other sequencing studies that these are genetically distinct (Cancer Genome Atlas Network 2012). Therefore, the field effect of adenomatous crypts on their non-dysplastic neighbouring will be studied as a proxy of a clonal interaction.

To characterise this field effect, immunohistochemistry (IHC) was used to illustrate cellular behaviour in FAP and sporadic patient samples. Adenomatous and surrounding non-adenomatous crypts were analysed using markers for cell proliferation (Ki67) and DNA damage (γH2AX) and analysing the effect of distance on these markers in crypts away from an adenoma.

Ki67, a nuclear protein expressed in all proliferating cells, was looked at because it is commonly used as a biomarker to estimate the proportion of dividing cells to aid tumour grading (Sobecki *et al*. 2017). High levels of Ki67 in carcinomas have been associated with poor prognosis (Li *et al*. 2015). Thus, a greater percentage of positive Ki67 cells was hypothesised to be present in adenomas and surrounding non-adenomatous crypts compared to normal crypts distant to the adenoma.

The histone protein H2AX, a marker for DNA damage, was also chosen for this analysis since it is responsible for recruiting cell cycle checkpoint and DNA repair factors to sites of double strand breaks (DSBs). The human *H2AX* gene is located on chromosome 11 at position 11q23 – a region that is frequently associated with mutations or deletions in a large number of human cancers. DSBs are serious lesions that can initiate genomic instability (Bonner *et al*. 2008). Thus, it is of interest to investigate the status of DNA damage in dysplastic and surrounding non-dysplastic crypts. Again, a greater percentage of positive γH2AX was hypothesised in adenomatous and non-adenomatous crypts compared to normal crypts far away

from the adenoma.

To further investigate the behaviour of adenomatous crypts on surrounding non-adenomatous crypts, nuclear β-catenin was chosen as an additional marker, since there is strong evidence of an optimal level of WNT signalling critical for adenoma development (Albuquerque *et al*. 2002). In normal epithelium, β-catenin is mainly expressed in the membrane, whereas in adenocarcinomas cytoplasmic β-catenin is translocated into the nucleus regulating tumour growth, a process associated with poor prognosis (Dai *et al*. 2012, Wong *et al*. 2004). Therefore, IHC for nuclear β-catenin was also performed in adenomatous and surrounding non-adenomatous crypts as a modulator of Wnt signalling, hypothesising a greater percentage of nuclear β-catenin staining in adenomatous crypts and surrounding non-adenomatous crypts compared to non-dysplastic crypts distant to the adenoma, and that this effect is again decreasing with increasing distance away from the adenoma.

Very little is known on tumour-stroma interactions at the very early stages of tumour initiation and its progression. Understanding these interactions might help understanding how their progression is regulated. Therefore, the composition of the stroma was investigated by assessing the percentage of helper T-cells (CD4), cytotoxic T-cells (CD8), macrophages (CD68) and α-smooth muscle actin (α-SMA) in the stroma of adenomas and their neighbouring non-dysplastic stroma, as immune cells are important in anti-tumour immunity. α-SMA is a marker for fibroblasts, responsible for tissue remodelling and homeostasis. The aim here was to examine how signals emanating from the adenoma are affecting the stroma of nearby non-adenomatous crypts.

For all immune markers and fibroblasts, it was hypothesised to detect a higher percentage of staining in the stroma surrounding dysplastic crypts, as well as non-dysplastic crypts surrounding the adenoma compared to non-dysplastic crypts far away from the adenoma, and that this effect is decreasing with increasing distance away from the adenoma.

Furthermore, an increased susceptibility to mutations in non-dysplastic crypts neighbouring adenomas compared to distant crypts was hypothesised. The mutation burden of mtDNA mutations in adenomatous and neighbouring non-dysplastic crypts was investigated using CCO-deficiency as a marker for mutagenesis. It was hypothesised that adenomas harbour more CCO-deficient crypts than surrounding

non-dysplastic crypts in the zones and that this effect is decreasing with increasing distance away from the adenomatous zone.

To further demonstrate this mutagenic field effect genetically, the nearest non-dysplastic crypts to an adenoma were laser capture microdissected from FAP patients, sequentially dissected at an increasing distance from the adenoma, and next generation sequencing (NGS) of the mitochondrial genome performed. As stated earlier, mtDNA mutations are a good indicator for mutagenic pressure (see section 1.6). Although genomic mutations provide a basis for the cellular phenotype that is selected for clonal expansion, they are rare in non-dysplastic tissue given the efficient DNA repair mechanisms (Walther *et al*. 2016). Therefore, it was proposed that adenomatous crypts have a greater mtDNA mutation burden and a greater diversity of mutations than normal crypts due to an increased mutation rate induced by dysplasia. The aim here was to compare the mutation burden of dysplastic and surrounding non-dysplastic epithelia and to demonstrate that mutagenic pressure is generated through a field effect of one clone onto another.

These data will provide a comprehensive analysis of the field effect emanating from adenomas.

3.2 Results: Demonstrating clonal interactions

Data presented in this chapter were primarily generated by myself, but collaboration with two BSc students Ashwin Sivaharan from Imperial College London and Yara Fadaili from Queen Mary University of London contributed to this work. Bioinformatic processing presented in sub-heading 3.2.7 was performed with the help of Marc Williams at Barts Cancer Institute, Queen Mary University of London.

3.2.1 Greater cell proliferation, DNA damage and Wnt-signalling found in non-dysplastic crypts surrounding an adenoma

To characterise the field effect of adenomatous crypts on non-dysplastic crypts of increasing distance away from adenomas, analysis of cell proliferation (Ki67), DNA damage (γH2AX), and Wnt-signalling (nuclear β-catenin) was performed using immunohistochemistry (see section 2.2.3). Sections of FAP and sporadic patients were stained with the appropriate antibody and slides were digitally scanned in (3D Histotech, Hungary). Adenomas were then identified with the help of pathologist Dr Marnix Jansen (University College Hospital, London) and the surrounding non-dysplastic crypts divided into zones based on physical distance from the tumour. Crypts < 50μm away from the adenoma were categorised as zone 1, crypts 50-150μm away from the adenoma as zone 2 and crypts 150-250μm as zone 3 (see section 2.3.1). Physical distances of the zones surrounding the adenoma were based on a mathematical model that suggested interactions should occur within 144μm of an initiated progenitor (Thliveris *et al*. 2013). Table 3.1 gives an overview of the number of adenomas counted for each of the markers. Positive (brown) and negative unstained cells within an adenoma and their surrounding non-dysplastic crypts (zone 1 – 3) were counted manually in the Pannoramic Viewer software and the proportion of positive stained cells calculated (see section 2.3.2). This was controlled with counts of positive and negative stained cells of non-dysplastic crypts as far away as possible from each adenoma of FAP and sporadic patients, and are referred to as distant crypts. To assess overall significance, a Kruskal-Wallis (KW) test was used, and for pairwise comparisons a Mann Whitney test was performed, both in Prism 6 (see section 2.13.1).

	Ki67	γH2AX	β-catenin
N (patients)	10	10	9
N (samples)	13	13	9
N (FAP adenomas)	28	26	17
N (sporadic adenomas)	22	26	10

Table 3.1: Number of adenomas counted in samples stained for epithelial markers.
For example, for Ki67, 13 samples (FFPE blocks) from 10 patients were used and of those samples 50 adenomas were counted, of which were 28 FAP adenomas and 22 sporadic adenomas.

Ki67 expression has been shown to be associated with progression to CRC (Barone *et al*. 2010, Li *et al*. 2015). Therefore, the percentage of $Ki67^+$ staining was investigated in adenomas and neighbouring non-adenomatous crypts.

A significant increase in the percentage of $Ki67^+$ cells per adenomatous crypt compared to distant crypts was expected and also observed in both FAP and sporadic adenoma patients. There were significantly more $Ki67^+$ cells in non-dysplastic crypts from all three zones compared to distant crypts in patients with FAP (Kruskal-Wallis test, $p = 0.028$) (Figure 3.1A, C) and patients with sporadic adenomas ($p = 0.028$) (Figure 3.1B, D). For FAP patients, there were significantly more proliferating cells in the adenoma compared to distant crypts ($p = 0.003$). Interestingly, no significant difference in cell proliferation was found between the adenomas and their surrounding zones. However, distant non-dysplastic crypts were significantly lower compared to zone 1 ($p = 0.002$), zone 2 ($p = 0.014$) and zone 3 ($p = 0.002$).

Similar results were obtained from sporadic adenoma patients. No significant difference was found between adenomas and their surrounding zones, but the percentage of $Ki67^+$ cells within sporadic adenoma crypts was significantly higher compared to distant crypts ($p = 0.001$). Cell proliferation in non-dysplastic crypts in zones 2 and 3 was also significantly higher compared to distant crypts (zone 2: $p = 0.021$; zone 3: $p = 0.006$).

Together these data suggest there is a strong local proliferative field effect on non-dysplastic crypts emanating from the adenoma.

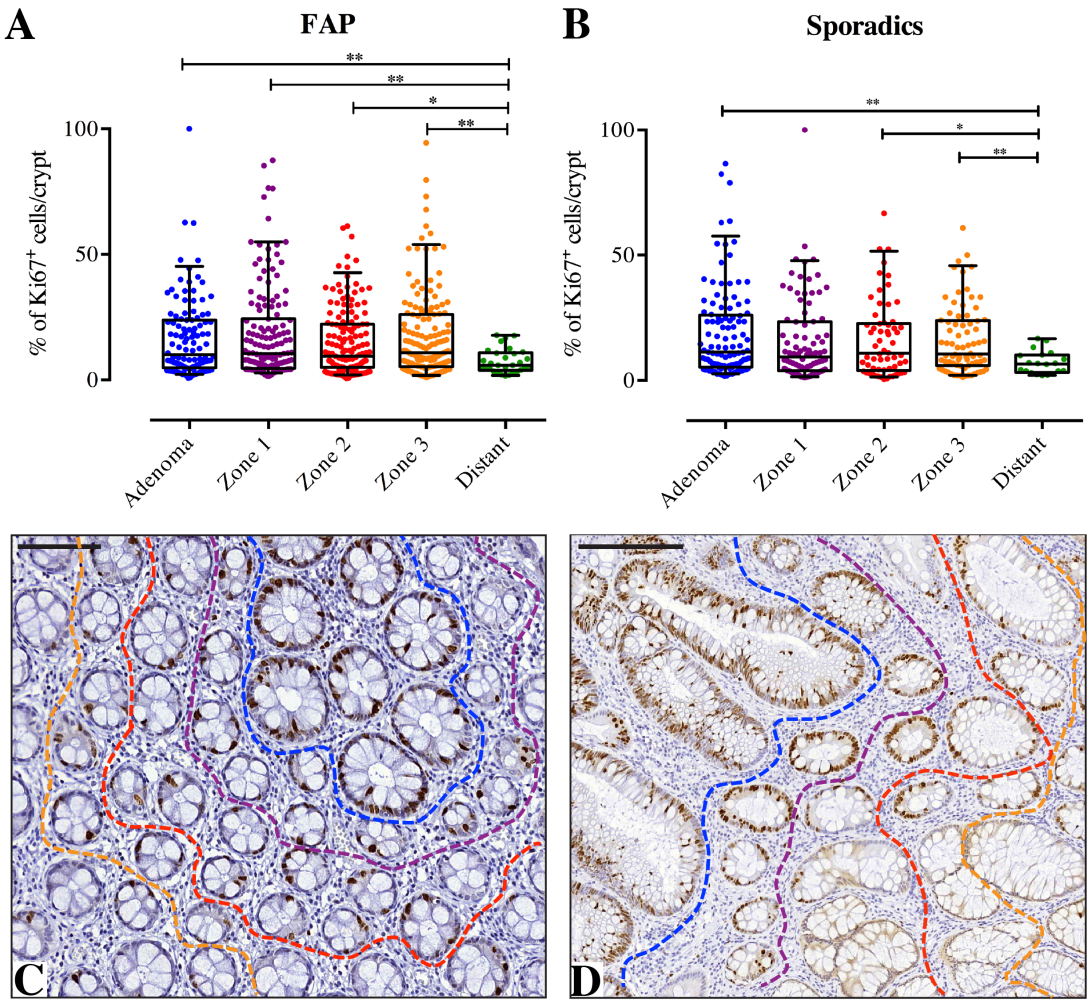

Figure 3.1: Cell proliferation in adenomas and surrounding non-adenomatous crypts.
Effect of dysplastic crypts on their surrounding non-dysplastic crypts in terms of cell proliferation (Ki67 marker) for FAP (A) and sporadic adenomas (B). The percentage of positive stained Ki67 cells/crypt in adenomas (blue) and surrounding non-dysplastic crypts in zone 1 (purple), zone 2 (red), zone 3 (orange) and non-dysplastic distant crypts (green) for FAP patients ($p = 0.028$) and sporadic patient samples ($p = 0.028$). The box plot indicates the mean, upper and lower quartile. Staining for Ki67 is shown from a FAP adenoma (C; scale bar: 100µm) and from a sporadic adenoma (D; scale bar sporadics: 200µm). The dashed blue line outlines crypts within the dysplastic zone, the dashed purple line non-dysplastic crypts in zone 1, the dashed red line non-dysplastic crypts in zone 2, and the dashed orange line non-dysplastic crypts in zone 3.

DNA damage ($\gamma H2AX^+$ cells) is a common sign for cancer progression and was thus investigated in adenomatous and neighbouring non-adenomatous crypts. DNA damage within crypts within adenomas was significantly higher to $\gamma H2AX^+$ cells counted in the zones and in distant crypts for FAP patients (Kruskal-Wallis test; $p < 0.0001$) (Figure 3.2A, C) and for sporadic adenoma patients (Kruskal-Wallis test; $p < 0.0001$) (Figure 3.2B, D).

In FAP patients, the percentage of $\gamma H2AX^+$ cells within adenomatous crypts was significantly higher compared to non-dysplastic crypts in zones 1 ($p < 0.0001$), 2 ($p < 0.0001$) and 3 ($p < 0.0001$). There were no significant differences between crypts in each non-dysplastic zone. Interestingly, $\gamma H2AX^+$ cells in distant crypts were significantly lower to the $\gamma H2AX^+$ cell count in the adenoma ($p < 0.0001$), but not significantly lower to non-dysplastic crypts in zone 1 ($p = 0.144$), in zone 2 ($p = 0.229$), zone 3 ($p = 0.17$) (Figure 3.2A).

Similarly, for sporadic adenoma patients, DNA damage was significantly higher in adenomatous crypts compared to non-dysplastic crypts in zone 1 ($p < 0.0001$), zone 2 ($p < 0.0001$), and zone 3 ($p < 0.0001$), and also to distant crypts ($p < 0.0001$). Non-dysplastic crypts in each zone were not significantly different to each other and also not to distant crypts (Figure 3.2B).

This suggests that DNA damaged crypts exert a field effect on surrounding non-adenomatous crypts.

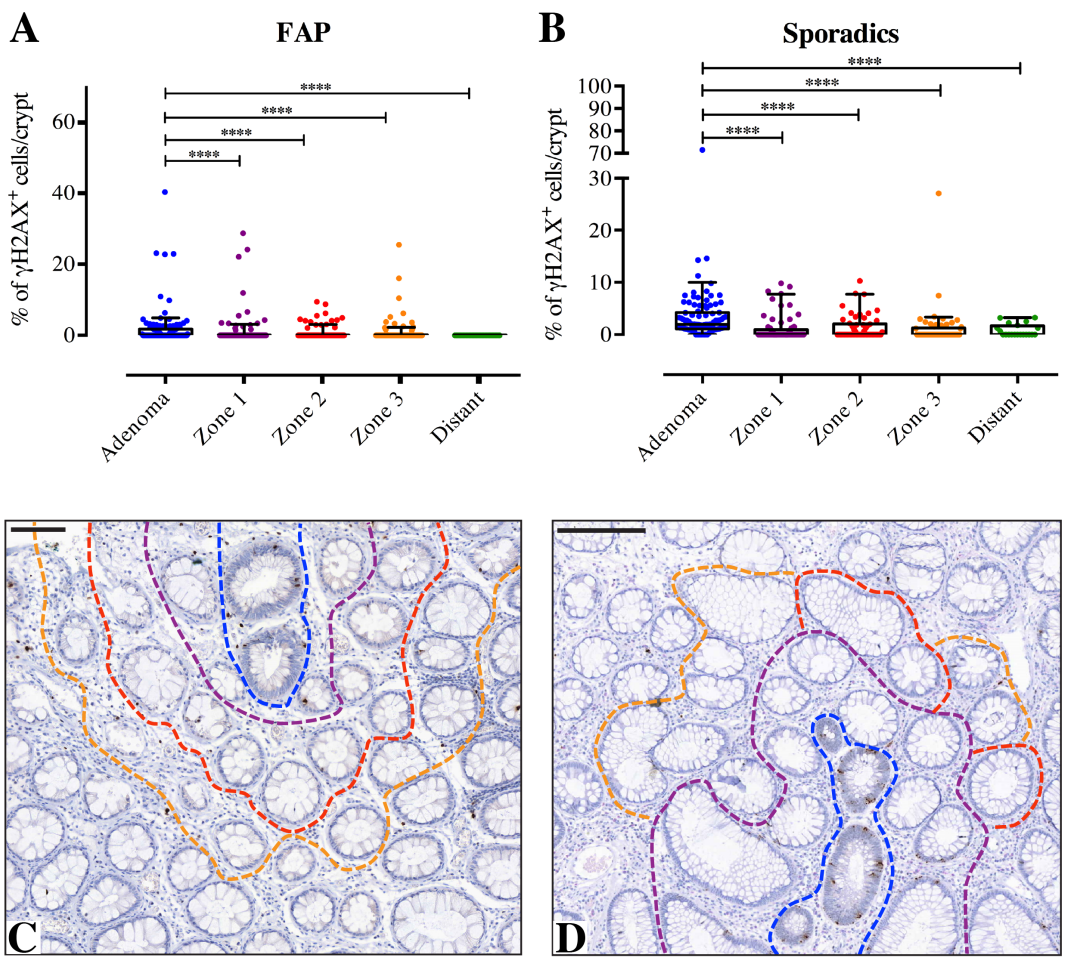

Figure 3.2: DNA damage in adenomas and surrounding non-adenomatous crypts.
Effect of dysplastic crypts on their surrounding non-dysplastic crypts in terms of DNA damage (γH2AX marker) for FAP (A) and sporadic adenomas (B). The percentage of positive stained γH2AX cells/crypt in the adenoma (blue) and surrounding non-dysplastic crypts in zone 1 (purple), zone 2 (red), zone 3 (orange) and non-dysplastic distant crypts (green) for FAP patients (Kruskal-Wallis: $p < 0.0001$) and sporadic patient samples (Kruskal-Wallis: $p < 0.0001$). The box plot indicates the mean, upper and lower quartile. Staining for γH2AX is shown from a FAP adenoma (C; scale bar: 100μm) and for a sporadic adenoma (D; scale bar sporadics: 200μm). The dashed blue line outlines crypts within the dysplastic zone, the dashed purple line non-dysplastic crypts in zone 1, the dashed red line non-dysplastic crypts in zone 2, and the dashed orange line non-dysplastic crypts in zone 3.

To further investigate whether dysplastic crypts have a field effect on their neighbouring non-dysplastic crypts, sections were stained for nuclear β-catenin, a marker for Wnt signalling, which is one of the most critical pathways in cancer progression (Clevers 2006). The percentage of nuclear β-catenin$^+$ cells within crypts within adenomas was significantly higher to nuclear β-catenin$^+$ cells counted in the zones and in distant crypts in FAP patients (Kruskal-Wallis test; $p < 0.0001$) (Figure 3.3A) and in sporadic patients (Kruskal-Wallis test; $p < 0.0001$) (Figure 3.3B).

Specifically for FAP patients, significant differences were found between the adenoma and zone 1 ($p = 0.002$), zone 2 ($p = 0.0003$) and zone 3 ($p < 0.0001$) and the distant crypts ($p < 0.0001$). A decreasing percentage of nuclear β-catenin can be seen as proximity to the adenoma decreases, with no nuclear β-catenin seen in distant crypts. Distant crypts displayed significantly less nuclear β-catenin than non-dysplastic crypts in all zones ($p < 0.0001$). No significant differences were found between non-dysplastic crypts in the zones.

In sporadic adenoma patients, significant differences in nuclear β-catenin were found between the adenoma and zone 1 ($p = 0.015$), zone 3 ($p = 0.032$) and the distant crypts ($p = 0.008$), but not to zone 2 ($p = 0.055$), although this was close to being considered significant. Non-dysplastic crypts in the control group were significantly lower than non-dysplastic crypts in zone 1 ($p = 0.008$), zone 2 ($p = 0.047$) and zone 3 ($p = 0.047$). No significant differences were found among the non-dysplastic crypts in the zones.

This suggests that increased nuclear β-catenin expression is associated with a field effect emanating from the dysplastic zone.

Overall, the results show that adenomatous crypts have a higher rate of cell proliferation, DNA damage and nuclear β-catenin compared to surrounding non-dysplastic and distant crypts. Taken together, this demonstrates that clonal interactions occur in close proximity between dysplastic and surrounding non-dysplastic crypts and further suggests, that the adenoma exerts a pro-tumourigenic effect. The percentage of cell proliferation, DNA damage and nuclear β-catenin within crypts increases the closer a non-dysplastic crypt is to an adenoma, indicating that adenomas are having a significant effect on neighbouring crypts. Thus, adenomas create a field effect.

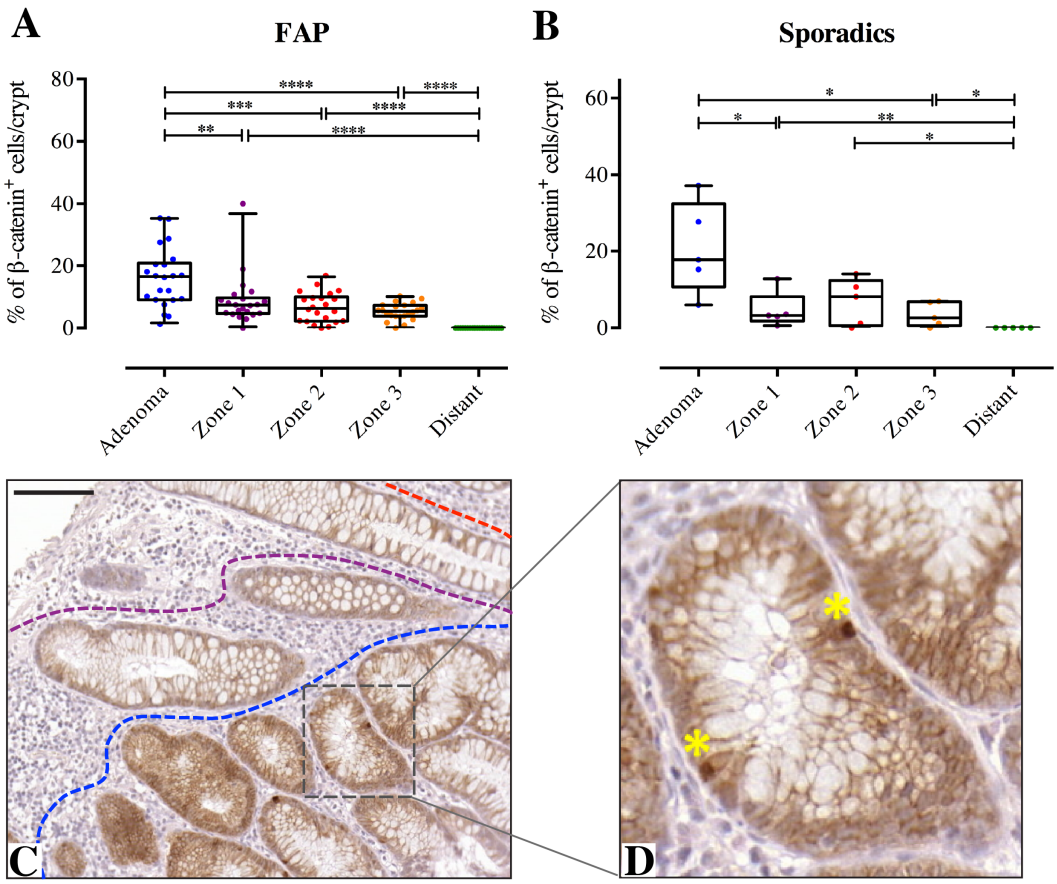

Figure 3.3: Nuclear β-catenin in adenomas and surrounding non-adenomatous crypts.
Effect of dysplastic crypts on their surrounding non-dysplastic crypts in terms of Wnt-signalling (β-catenin marker) for FAP (A) and sporadic patients (B). The percentage of positively stained nuclear β-catenin cells/crypt in adenomas (blue) and surrounding non-dysplastic crypts in zone 1 (purple), zone 2 (red), zone 3 (orange) and non-dysplastic distant crypts (green) in FAP patients ($p < 0.0001$) and sporadic patients ($p < 0.0001$). The box plot indicates the mean, upper and lower quartile. C) Staining for nuclear β-catenin is shown for a sporadic patient (scale bar: 100µm). The dashed blue line outlines crypts within the dysplastic zone, the dashed purple line non-dysplastic crypts in zone 1, and the dashed red line the non-dysplastic crypt in zone 2. D) Asterisk in the adenomatous crypt shows positive stained nuclear β-catenin cells.

3.2.2 Stromal alterations in the mucosa surrounding adenomas

The field effect was also investigated within the stroma using a semi-quantitative scoring system. Because crypts are physically separated by lamina propria, any potential field effect may be amplified through stromal cells. The aim here is to investigate whether non-dysplastic crypts surrounding the adenoma have a higher proportion of stromal cells than non-dysplastic crypts that are not in close proximity to the adenoma.

IHC was performed using antibodies against CD4 (helper T-cells), CD8 (cytotoxic T-cells), CD68 (macrophages), and α-smooth muscle actin (α-SMA, fibroblasts and smooth muscle cells) (Table 3.2). Adenomas were identified on serial H&E sections, and the adenoma and surrounding non-dysplastic crypts divided into zones as described in section 2.3.1. A semi-quantitative scoring method was used to quantify the proportion of positively stained cells in the dysplastic and non-dysplastic zone (see section 2.3.3). The proportion was assessed according to the scoring system as shown in Table 2.2. Stromal cells surrounding distant non-dysplastic crypts were used as control. A stacked bar plot visualised the percentage of positive stained cells in the stroma in each zone for each marker tested for FAP (Figure 3.4) and sporadic patients (Figure 3.5). Semi-quantitative scoring of inflammatory infiltration and fibroblasts of the adenoma, the three surrounding zones, and the distant stroma is given in Table 3.3 for FAP patients and in Table 3.4 for sporadic patients.

	CD4	CD8	CD68	α-SMA
N (patients)	7	9	6	6
N (samples)	11	12	8	10
N (FAP adenomas)	23	34	28	30
N (sporadic adenomas)	25	20	15	21

Table 3.2: Number of adenomas counted in samples stained for stromal markers.
For example, for CD4, 11 samples (FFPE blocks) from 7 patients were used and of those samples 23 were FAP adenomas and 25 sporadic adenomas.

Increased concentrations of helper T-cells have been associated with the progression to cancer (Chirica *et al*. 2015). Therefore, the concentration of CD4 cells was investigated in the stroma surrounding adenomas and its neighbouring non-adenomatous crypts.

For FAP patients, a statistically significant decrease of $CD4^+$ cells in the stroma over distance was observed overall (χ^2 test: $p < 0.0001$) (Figure 3.4A), indicating that a greater percentage of $CD4^+$ cells was found surrounding adenomas, that decreases with distance. More specifically, a significant decrease between dysplastic crypts and zone 1 ($p < 0.0001$), from zone 1 to zone 2 ($p < 0.0001$), from zone 2 to zone 3 ($p < 0.0001$) and from zone 3 to the control group ($p = 0.0024$) was found suggesting an immune gradient towards adenomas.

A similar trend was observed for sporadic adenoma samples. Positively stained cells for CD4 were found in significantly greater concentration in the stroma surrounding the dysplastic zone and this is gradually decreasing with increasing distance away from dysplasia (χ^2 test: $p < 0.0001$) (Figure 3.5A).

This suggests that the adenoma alters the surrounding microenvironment, and also indicates it emanates a pro-inflammatory field effect.

Cytotoxic T cells (CD8) have also been associated with the progression to cancer (Deschoolmeester *et al*. 2010, Liu *et al*. 2016), and were thus investigated in the stroma surrounding the adenoma and its non-dysplastic crypts.

Results for CD8 show a very similar effect in FAP patients as compared to CD4. Cytotoxic T cells are significantly higher in the stroma surrounding the adenoma than in their surrounding non-dysplastic zones with overall significance (χ^2 test: $p < 0.0001$) (Figure 3.4B). Again, $CD8^+$ cells are significantly higher in the adenoma than in zone 1 ($p < 0.0001$) and are significantly higher in zone 1 than in zone 2 ($p = 0.0135$). The same trend is observed when analysing the expression of cytotoxic T cells in sporadic adenoma patients. $CD8^+$ cells were significantly higher expressed in the stroma surrounding the adenoma and this effect is decreasing over distance (χ^2 test: $p < 0.0001$) (Figure 3.5B).

These results suggest that the adenoma exerts a pro-inflammatory response in the dysplastic and surrounding non-dysplastic region, potentially promoting clonal interactions.

Studies on macrophage infiltration have also shown its progression to cancer. Differences in the concentration in the tumour stroma and matching normal mucosa were detected (McLean *et al*. 2011). Thus, it was of interest to investigate macrophage concentration in the stroma surrounding the adenoma and in its surrounding non-adenomatous stroma.

Macrophages (CD68) were significantly increased in the stroma surrounding the adenoma compared to their neighbouring non-dysplastic zones for FAP patients (χ^2 test: $p < 0.0001$) (Figure 3.4C). The results show a pattern of gradual increase of score 1 (0 – 25% of positive stained cells) with it being lowest surrounding the adenomatous region and highest in the distant normal stroma (Dysplasia < Zone1 < Zone2 < Zone3 < Normal). This pattern is reversed with a gradual decrease of score 3 (75 - 100% of positive stained cells) with it being highest surrounding the adenomatous region and lowest in the normal control region (Dysplasia > Zone1 > Zone2 > Zone3 > Normal). A statistical significant decrease between dysplastic crypts and zone 1 ($p < 0.0001$), from zone 1 to zone 2 ($p = 0.0373$), from zone 2 to zone 3 ($p < 0.0001$) and from zone 3 to the control group ($p < 0.0001$) was observed.

A similar trend was observed for sporadic adenoma samples. Positive stained cells for CD68 were found in significantly greater concentration in the stroma surrounding the dysplastic zone and this is gradually decreasing with increasing distance away from dysplasia (χ^2 test: $p < 0.0001$) (Figure 3.5C).

The here observed increased concentration of macrophage infiltration in the stroma of adenomas and its surrounding non-adenomatous crypts supports the hypothesis that the adenoma exerts a field effect leading to a pro-tumourigenic environment.

Increased fibroblast concentrations in tumours have been associated with progression to cancer (Hinz *et al*. 2001, Mo *et al*. 2016), therefore the concentration of α-SMA$^+$ cells in the adenoma and surrounding non-adenomatous crypts was investigated.

Similar to the immune cell markers, a statistically significant decrease of α-SMA$^+$ cells in the stroma over distance away from the adenoma was observed overall for FAP patients (χ^2 test: $p < 0.0001$) (Figure 3.4D), indicating that a higher proportion α-SMA$^+$ cells was found surrounding the adenoma, but less positive stained cells gradually declining over distance away from the adenoma. α-SMA$^+$

cells are significantly higher in the stroma surrounding the adenoma compared to stromal cells in zone 1, significantly higher in zone 1 to zone 2, as well as significantly higher in zone 2 to zone 3 and in zone 3 to the control group (for all: $p < 0.0001$).

Similarly to FAP patients, a significantly greater α-SMA expression surrounding the adenoma compared to non-dysplastic and distant crypts (χ^2 test: $p < 0.0001$) (Figure 3.5D) was observed in the stroma of sporadic adenoma patients.

This suggests that the adenoma exerts a pro-tumourigenic field promoting the progression of adjacent cells.

Taken together, the obtained results suggest that the stroma surrounding the adenoma plays an essential role in tumour development and is actively involved in generating a field effect emanating from the adenoma leading to a pro-tumourigenic environment.

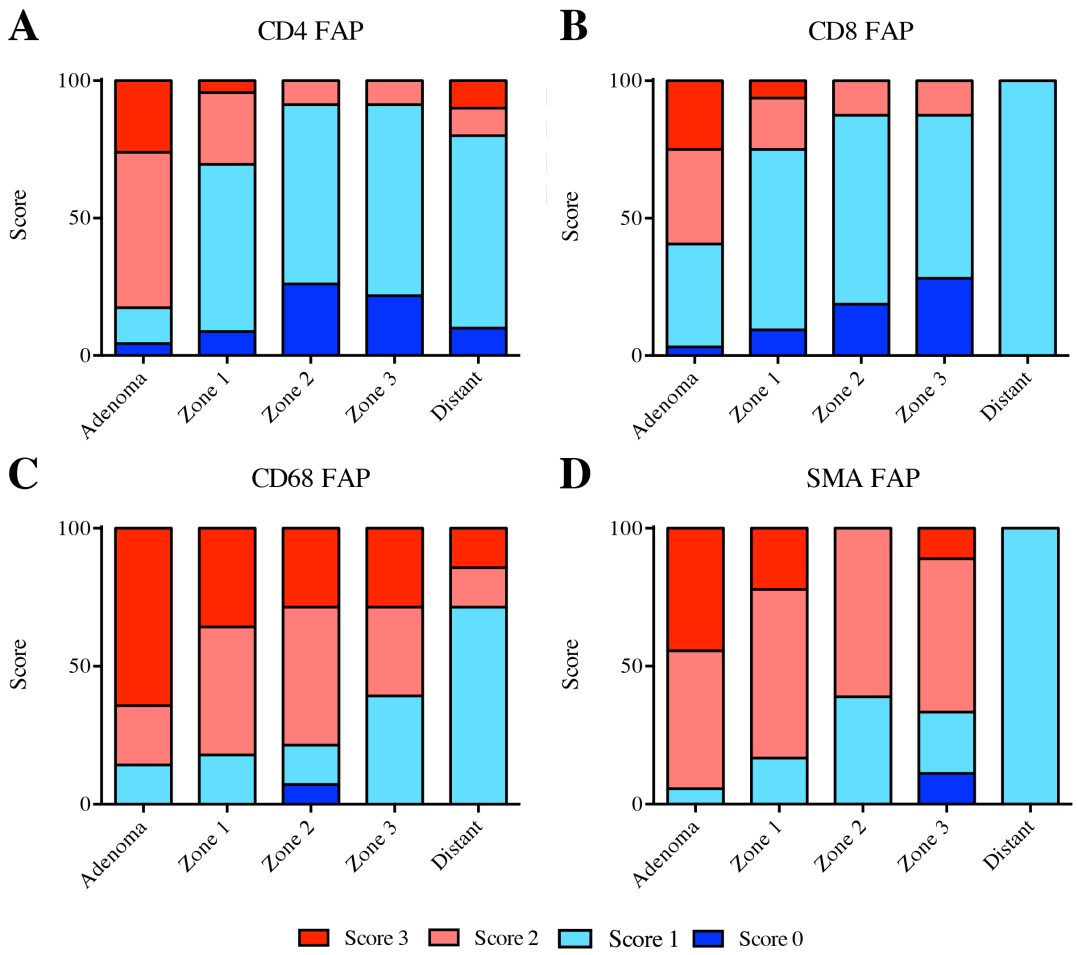

Figure 3.4: Proportion of stromal cells in dysplastic and surrounding non-dysplastic crypts of FAP patients.

Stacked bar plot depicting the proportion of the intensity of stromal markers in adenomas and their surrounding non-dysplastic crypts that were positive for CD4, CD8, CD68, and α-SMA. Red bars show the proportion of positive stained cells in the stroma that were given score 3 (75 – 100%), salmon coloured bars the proportion of positive stained cells that were given score 2 (25 – 75%), turquoise coloured bars the proportion of positive stained cells that were given score 1 (0 – 25%), and samples that showed no staining were given score 0 (blue coloured bars). A statistically significant decrease of the number of CD4, CD8, CD68 and α-SMA positive stained cells as a function of distance was observed (χ^2 test: $p < 0.0001$).

	Adenoma	Zone 1	Zone 2	Zone 3	Distant
CD4 (n = 23)					
Score 0	1 (4.4)	2 (8.7)	6 (26.1)	5 (21.7)	1 (10)
Score 1	3 (13)	14 (60.9)	15 (65.2)	16 (69.6)	7 (70)
Score 2	13 (56.5)	6 (26.1)	2 (8.7)	2 (8.7)	1 (10)
Score 3	6 (26.1)	1 (4.3)	0 (0)	0 (0)	1 (10)
CD8 (n = 32)					
Score 0	1 (3.1)	3 (9.4)	6 (18.8)	9 (28.1)	0 (0)
Score 1	12 (37.5)	21 (65.6)	22 (68.8)	19 (59.4)	10 (100)
Score 2	11 (34.4)	6 (18.8)	4 (12.4)	4 (12.5)	0 (0)
Score 3	8 (25)	2 (6.2)	0 (0)	0 (0)	0 (0)
CD68 (n = 28)					
Score 0	0 (0)	0 (0)	2 (7.1)	0 (0)	0 (0)
Score 1	4 (14.3)	5 (17.9)	4 (14.3)	11 (39.3)	5 (71.4)
Score 2	6 (21.4)	13 (46.4)	14 (50)	9 (32.1)	1 (14.3)
Score 3	18 (64.3)	10 (35.7)	8 (28.6)	8 (28.6)	1 (14.3)
α-SMA (n =33)					
Score 0	0 (0)	0 (0)	0 (0)	2 (6.1)	0 (0)
Score 1	4 (12.1)	9 (27.3)	15 (45.5)	10 (30.3)	10 (100)
Score 2	17 (51.5)	20 (60.6)	18 (54.5)	19 (57.6)	0 (0)
Score 3	12 (36.4)	4 (12.1)	0 (0)	2 (6.1)	0 (0)

Table 3.3: Semi-quantitative scoring of inflammatory infiltration and fibroblasts in colonic adenomas of FAP patients.

Semi-quantitative scoring of inflammatory infiltration and fibroblasts of the adenoma and the three different zones around the adenoma region, controlled with distant normal stroma, based on four levels of infiltration and fibroblast presence. Score 0 = no stained cells (0%); score 1 = low number of stained cells (0 – 25%), score 2 = medium number of stained cells (25 – 75%), score 3 = high number of stained cells (75 – 100%). Values are given as numbers (percentage).

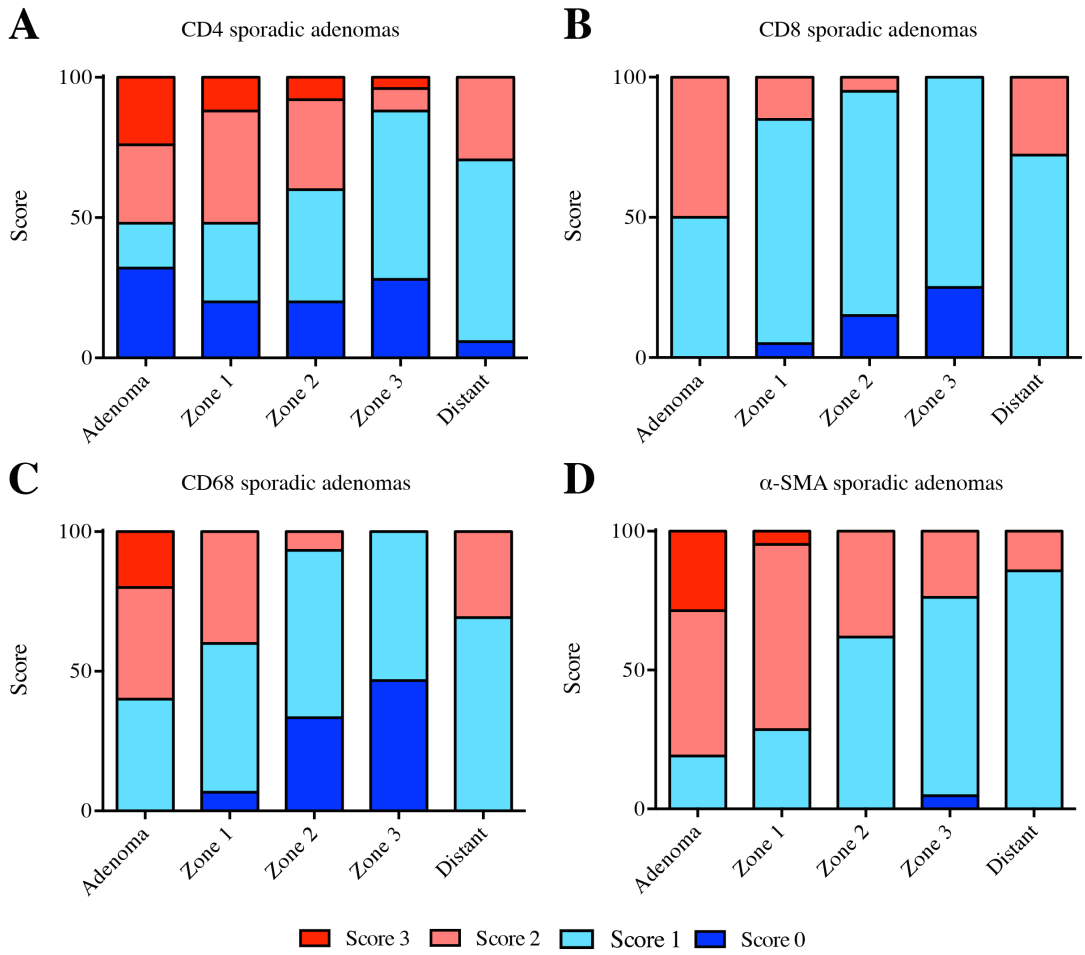

Figure 3.5: Proportion of stromal cells in dysplastic and surrounding non-dysplastic crypts in sporadic adenomas.

Stacked bar plot depicting the proportion of the intensity of stromal markers in adenomas and their surrounding non-dysplastic crypts that were positive for CD4, CD8, CD68, and α-SMA markers. As per Figure 1.4 Red bars show a score of 3 (75 – 100%), salmon bars a score of 2 (25 – 75%), turquoise bars a score of 1 (0 – 25%), and samples that showed no staining were given score 0 (blue coloured bars). A statistical significant decrease of CD4 (χ^2 test: $p < 0.0001$), CD8 ($p < 0.0001$), CD68 ($p < 0.0001$) and α-SMA ($p < 0.0001$) positive stained cells over distance away from the adenomatous zone in the stroma was observed.

	Adenoma	Zone 1	Zone 2	Zone 3	Distant
CD4 (n = 25)					
Score 0	8 (32)	5 (20)	5 (20)	7 (28)	1 (5.6)
Score 1	4 (16)	7 (28)	10 (40)	15 (60)	12 (66.7)
Score 2	7 (28)	10 (40)	8 (32)	2 (8)	5 (27.7)
Score 3	6 (24)	3 (12)	2 (8)	1 (4)	0 (0)
CD8 (n = 20)					
Score 0	0 (0)	1 (5)	3 (15)	5 (25)	0 (0)
Score 1	10 (50)	16 (80)	16 (80)	15 (75)	13 (72.5)
Score 2	10 (50)	3 (15)	1 (5)	0 (0)	5 (27.5)
Score 3	0 (0)	0 (0)	0 (0)	0 (0)	0 (0)
CD68 (n =15)					
Score 0	0 (0)	1 (6.7)	5 (33.3)	7 (46.7)	0 (0)
Score 1	6 (40)	8 (53.3)	9 (60)	8 (53.3)	10 (71.4)
Score 2	6 (40)	6 (40)	1 (6.7)	0 (0)	4 (28.6)
Score 3	3 (20)	0 (0)	0 (0)	0 (0)	0 (0)
α-SMA (n = 21)					
Score 0	0 (0)	0 (0)	0 (0)	1 (4.8)	0 (0)
Score 1	4 (19)	6 (28.6)	13 (61.9)	15 (71.4)	18 (85.7)
Score 2	11 (52.4)	14 (66.7)	8 (38.1)	5 (23.8)	3 (14.3)
Score 3	6 (28.6)	1 (4.7)	0 (0)	0 (0)	0 (0)

Table 3.4: Semi-quantitative scoring of inflammatory infiltration and fibroblasts in colonic adenomas of sporadic adenomas.

Semi-quantitative scoring of inflammatory infiltration and fibroblasts of the adenoma and the three different zones around the adenoma region, controlled with distant normal stroma, based on four levels of infiltration and fibroblast presence. Score 0 = no stained cells (0%); score 1 = low number of stained cells (0 – 25%), score 2 = medium number of stained cells (25 – 75%), score 3 = high number of stained cells (75 – 100%). Values are given as numbers (percentage).

3.2.3 Intraepithelial CD8$^+$ cell numbers increase with increasing distance from adenomas

Cytotoxic T cells are not only present in the stroma, but also in the gastrointestinal epithelium of a crypt (Mowat *et al*. 2014). These intraepithelial lymphocytes (IELs) are crucial in maintaining intestinal homeostasis (Renuka *et al*. 2017) on the one hand, but have been associated with progression to cancer on the other hand (Cheroutre *et al*. 2011). Therefore, the role of IELs in adenomas and surrounding non-dysplastic crypts was investigated.

IELs are predominantly CD8$^+$ and can be visualised using the same CD8 antibody as per Figure 3.4 and Figure 3.5. 34 FAP sections and 7 sporadic adenoma sections from a total of 9 patients were manually counted in each crypt within adenomas, each surrounding zone and in distant non-dysplastic crypts. The proportion of positive stained IELs as a proportion of the total number of epithelial cell nuclei was calculated to assess whether the levels of IELs are increased in crypts surrounding dysplasia.

In FAP adenomas (Figure 3.6A), significantly more CD8$^+$ IELs were observed in crypts further away from the adenoma. Indeed adenomatous crypts displayed the lowest concentration of CD8$^+$ IELs. An increase in IEL numbers in surrounding non-dysplastic crypts in all three zones and distant crypts was observed (Kruskal-Wallis: $p < 0.0001$). Further, this appeared to increase as a gradient proportional to increasing distance. Thus, the number of IELs in the adenomatous zone was significantly lower compared to zone 1 ($p < 0.0001$), to zone 2 ($p < 0.0001$), to zone 3 ($p < 0.0001$), and to the distant crypts ($p < 0.0001$). Moreover, distant crypts were significantly higher to zone 1 ($p = 0.004$), to zone 2 ($p = 0.012$) and to zone 3 ($p = 0.005$). No significant differences were found between non-dysplastic crypts in the zones.

In sporadic adenoma samples (Figure 3.6B, C), a similar gradient was observed with a lower percentage of IELs in the adenomatous crypts and an increasing number in crypts with increasing distance away from the adenoma, however this was not significant (Kruskal-Wallis: $p = 0.1625$). Pairwise comparison has shown that adenomatous crypts are significantly lower to non-dysplastic crypts in the control group ($p = 0.012$). No significant differences were found between non-dysplastic crypts in the zones.

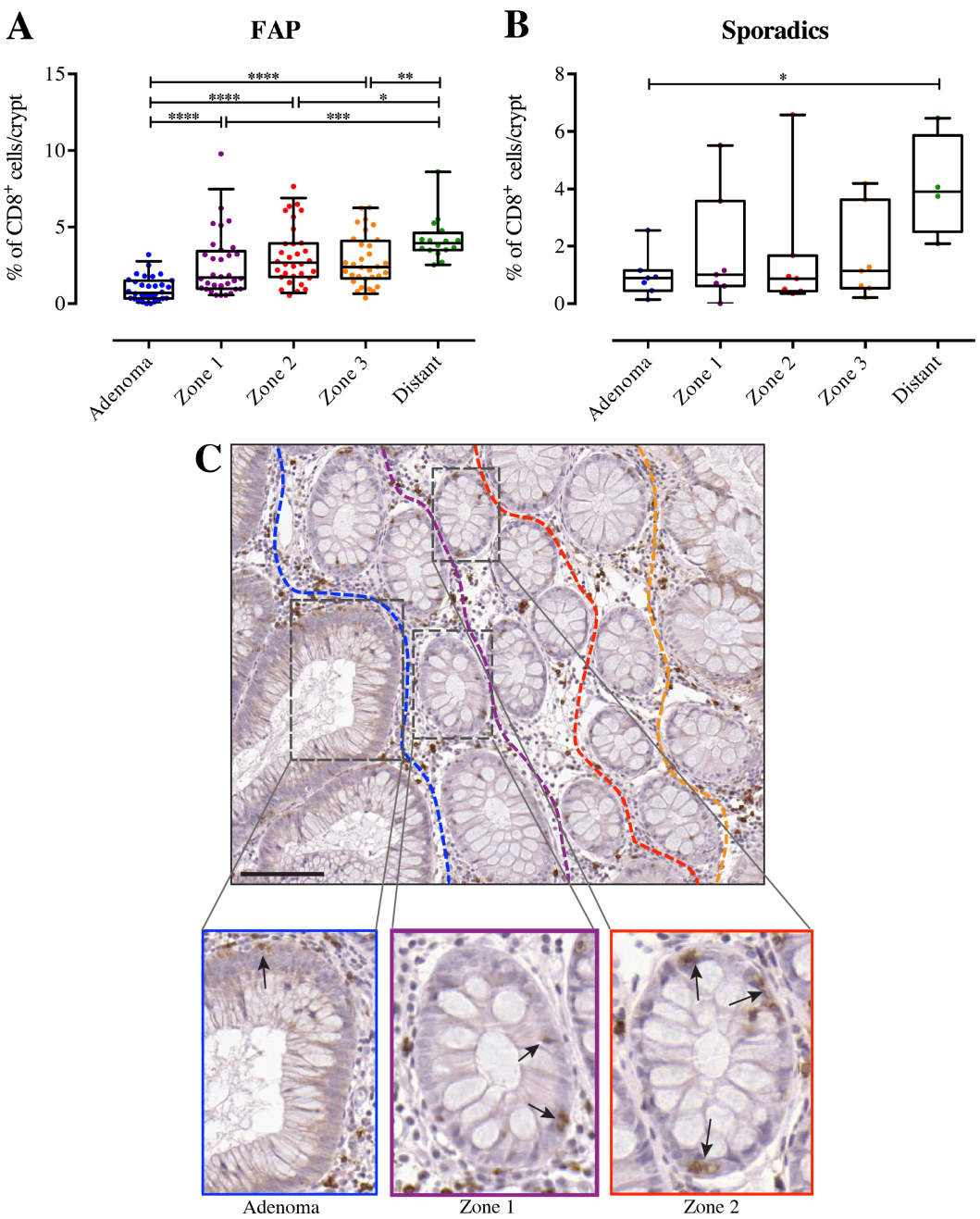

Figure 3.6: Intraepithelial lymphocytes are increased in non-dysplastic crypts surrounding an adenoma.

A) Beeswarm plot visualising the percentage of positive stained IELs/crypt in the adenoma (blue) and surrounding non-dysplastic crypts in zone 1 (purple), zone 2 (red), zone 3 (orange) and non-dysplastic distant crypts (green) for FAP patients ($p < 0.0001$) and B) sporadic patients ($p = 0.16$). The box plot indicates the mean, upper and lower quartile. C) Staining for IELs is shown for a sporadic patient (scale bar: 100µm). The dashed blue line outlines crypts within the dysplastic zone, the dashed purple line non-dysplastic crypts in zone 1, the dashed red line non-dysplastic crypts in zone 2, and the dashed orange line non-dysplastic crypts in zone 3. High power images show positive IELs within the epithelial lining of a crypt from an adenoma and from non-dysplastic crypts located in zone 1 and zone2. Arrows indicate IELs.

The difference between FAP and sporadic cases could be explained by the size of the adenomas. Sporadic adenomas were on the whole far bigger and may generate a larger field effect.

These results show a decrease of IELs in adenomatous crypts and a significant increase in non-dysplastic crypts as the distance increases away from the dysplastic area. This could indicate that IELs have lost their function and can no longer protect intestinal homeostasis.

3.2.4 Higher density of subepithelial α-SMA$^+$ cells adjacent to adenomas

Fibroblasts (α-SMA$^+$ cells) are found in the stroma but are also located surrounding the crypt as a fenestrated sheath (subepithelial myofibroblasts). Myofibroblasts provide structural support and its disruption has been associated with tumour progression (Yen *et al*. 2010).

To characterise how these cells are affected by the presence of an adenoma, the density of α-SMA$^+$ cells in tissue sections was measured using the DensitoQuant application in Pannoramic Viewer (see section 2.3.4). The mean density of negative and positive pixels was plotted for the adenomatous region, each surrounding zone and the distant crypts for both, FAP and sporadic tissue sections.

For FAP patients, there is a gradient of the α-SMA$^+$ cell density with a lower number of subepithelial myofibroblasts surrounding the adenoma compared to its surrounding zones, and an increase in α-SMA$^+$ cells in the surrounding normal zone, whilst the α-SMA$^+$ density count decreases again in distant crypts (Kruskal-Wallis test; $p < 0.0001$) (Figure 3.7A). The mean α-SMA$^+$ density between the dysplastic region and all three zones shows an increase with statistical significance ($p < 0.0001$). Pairwise comparison has shown that distant crypts are significantly lower to non-dysplastic crypts in zone 1 ($p = 0.01$), zone 2 ($p = 0.0007$), and zone 3 ($p = 0.0002$). No significant differences were found between non-dysplastic crypts in the zones. Interestingly, the mean density of α-SMA$^+$ cells in the dysplastic region and normal control region show no significance difference ($p = 0.374$).

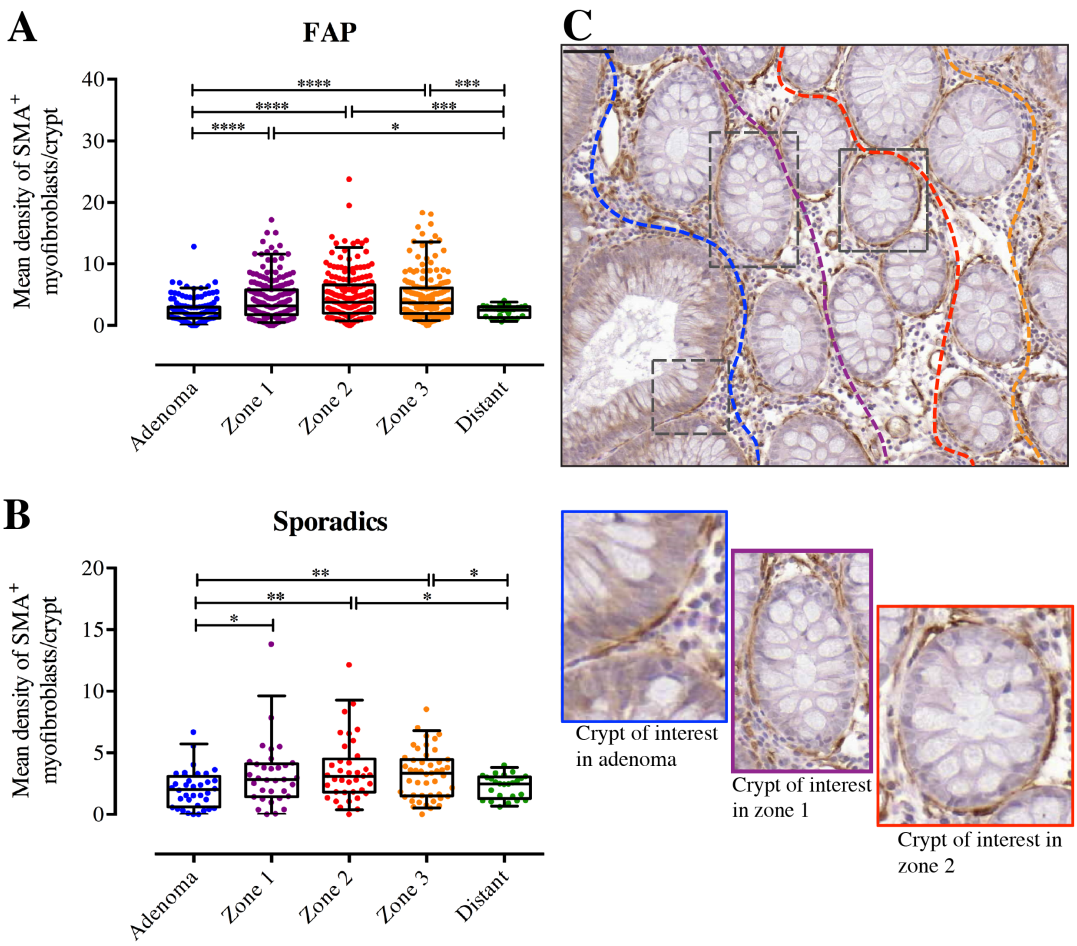

Figure 3.7: Density of myofibroblasts in dysplastic and surrounding non-dysplastic crypts.
Effect of dysplastic crypts on their surrounding non-dysplastic crypts shown for myofibroblasts (α-SMA marker). A) Beeswarm plot visualising the density of myofibroblasts surrounding the adenoma (blue) and neighbouring non-dysplastic crypts in zone 1 (purple), zone 2 (red), zone 3 (orange) and non-dysplastic distant crypts (green) for FAP patients (Kruskal-Wallis: $p < 0.0001$) and B) sporadic patients (Kruskal-Wallis: $p = 0.0078$). The box plot indicates the mean, upper and lower quartile. C) Staining for α-SMA is shown for a sporadic patient (scale bar: 50µm). The dashed blue line outlines crypts within the dysplastic zone, the dashed purple line non-dysplastic crypts in zone 1, the dashed red line non-dysplastic crypts in zone 2, and the dashed orange line non-dysplastic crypts in zone 3. Zoomed in images show density of myofibroblasts surrounding an adenomatous crypt and a non-dysplastic crypt in zone 1 and zone 2.

Similarly, for sporadic adenoma patients (Figure 3.7B, C), the α-SMA$^+$ cell density is higher in the zones compared to the adenoma, whilst the α-SMA$^+$ density count decreases again in distant crypts (Kruskal-Wallis test; $p = 0.0078$). There are significantly less myofibroblasts surrounding the adenoma compared to zone 1 ($p = 0.0266$), to zone 2 ($p = 0.0041$), and to zone 3 ($p = 0.0031$), but not to non-dysplastic distant crypts ($p = 0.305$). However, myofibroblasts surrounding non-dysplastic crypts in zone 2 ($p = 0.04$) and zone 3 ($p = 0.029$) are significantly denser compared to distant crypts, but not to zone 1 ($p = 0.155$). There are no significant differences between non-dysplastic crypts in the zones.

Taken together, this shows that the density of myofibroblasts decreased the closer to an adenoma. This suggests that adenomatous crypts have lost its structure with progression to cancer, and further indicating a field effect emanating from the adenoma.

3.2.5 Adenomatous crypts are significantly larger and have more nuclei compared to their surrounding non-dysplastic crypts

Phenotypic characteristics of crypt size and nuclei density were measured for both FAP (n = 30 adenomas and surrounding zones) and sporadic patient samples (n = 21 adenomas and surrounding zones).

The crypt size was manually measured in Pannoramic Viewer by contouring the area of each crypt in each zone (see section 2.3.5). Adenomatous crypts are significantly larger than non-dysplastic crypts for both FAP (Kruskal-Wallis: $p < 0.0001$) (Figure 3.8A) and sporadic patients ($p = 0.002$) (Figure 3.8C). Pairwise comparison has shown that adenomatous crypts are significantly larger compared to non-dysplastic crypts in zone 1 ($p < 0.0001$), zone 2 ($p < 0.0001$), and zone 3 ($p < 0.0001$), as well as to non-dysplastic crypts away from the dysplastic zone ($p < 0.0001$) for FAP patients. Moreover, non-dysplastic crypts in zone 1 are significantly larger than in zone 3 ($p = 0.042$). However, there is no statistical significance between zone 1 and zone 2 ($p = 0.767$), as well as zone 2 to zone 3 ($p = 0.057$). Non-dysplastic crypts were not significantly different in size to distant non-dysplastic crypts. This suggests that adenomatous crypts are significantly larger compared to

their surrounding non-dysplastic crypts and distant crypts, and moreover, independently of where non-dysplastic crypts are located, they do not become significantly larger when being in close proximity to an adenoma.

Interestingly, pairwise comparison for sporadic patients has revealed no significant difference between the adenomatous crypts and non-dysplastic crypts in zone 1, however adenomatous crypts were significantly larger in size compared to non-dysplastic crypts in zone 2 ($p = 0.0379$) and zone 3 ($p = 0.0099$). Non-dysplastic crypts in zone 1 were significantly larger than crypts in zone 3 ($p = 0.0348$). Distant crypts were significantly larger compared to crypts in zone 2 ($p = 0.0026$) and zone 3 ($p < 0.0001$). This might indicate that non-dysplastic crypts in zone 1 could be in the process of transformation, and additionally given that the adenoma is significantly larger as well, crypts in zone 2 and 3 might suffer from spatial constraints.

The nuclear density of crypts in the dysplastic and surrounding non-dysplastic zones and non-dysplastic distant control regions was assessed using the DensitoQuant tool in the Pannoramic Viewer software for both, FAP (Figure 3.8B) and sporadic patients (Figure 3.8D). The mean nuclear density of adenomatous crypts is significantly higher compared to the surrounding non-dysplastic zones, as well as to the distant non-dysplastic crypts for both FAP (Kruskal-Wallis: $p < 0.0001$) and sporadic patients ($p < 0.0001$), indicating that more nuclei are present in the adenoma, and that the number of nuclei decreases with increasing distance away from the dysplastic zone. For both, FAP and sporadic patient samples, there is a greater density of nuclei in the dysplastic zone compared to zone 1 ($p < 0.001$), zone 2 ($p < 0.001$), zone 3 ($p < 0.001$), as well as the non-dysplastic distant crypts ($p < 0.0001$). However there is no significant difference between the non-dysplastic zones and between the non-dysplastic zones and the control group indicating a clear phenotypic difference in nuclei density between adenomatous and non-dysplastic crypts, but also suggesting that nuclei density is not changing in non-dysplastic crypts surrounding the adenoma.

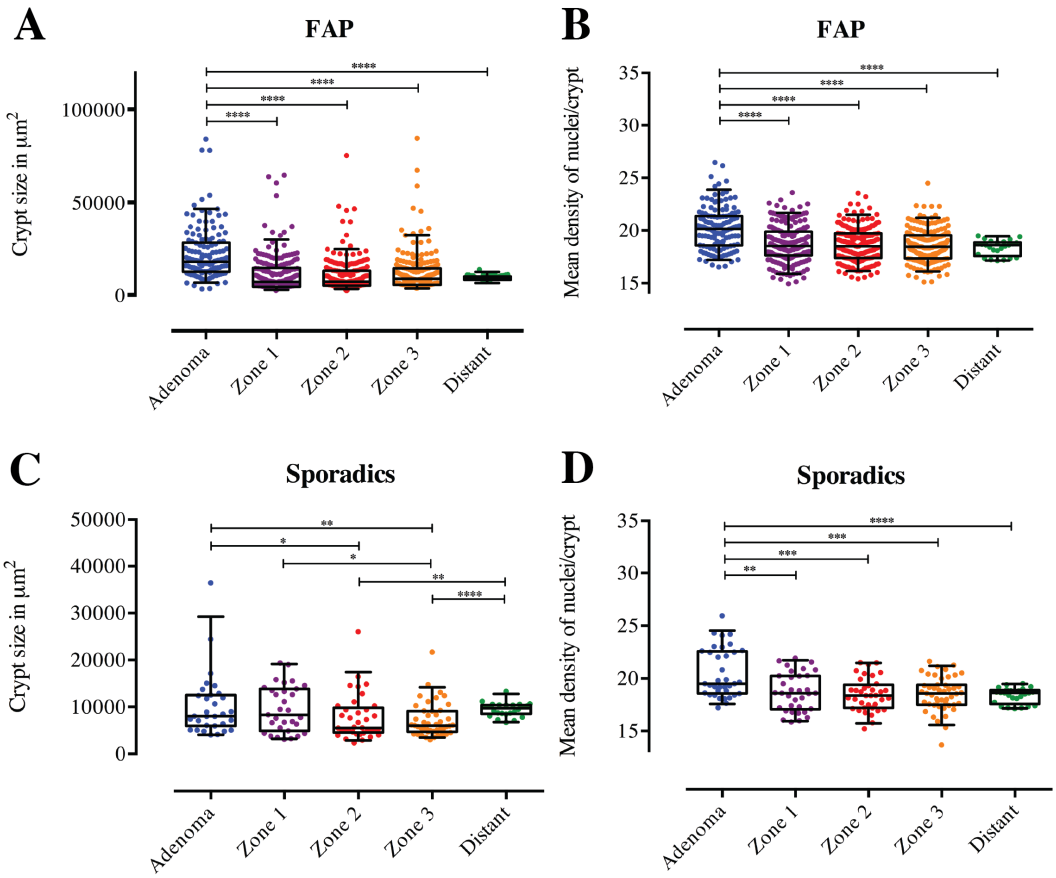

Figure 3.8: Phenotypic characteristics of crypt size and nuclei density.
A) Crypts (area in µm^2) are significantly larger in the dysplastic zone compared to the surrounding non-dysplastic zones, as well as the distant non-dysplastic crypts for FAP (Kruskal-Wallis: $p < 0.0001$) and C) sporadic samples (Kruskal-Wallis: $p = 0.002$). B) The mean density of adenomatous nuclei is significantly higher compared to the surrounding non-dysplastic zones, as well as the distant non-dysplastic crypts for both FAP (Kruskal-Wallis: $p < 0.0001$) and D) sporadic samples (Kruskal-Wallis: $p = 0.0003$).

3.2.6 Higher concentration of mutant crypts surrounding adenomas

It was hypothesised that polyclonal tumours are generated by a field effect. To this effect it would be reasonable to predict that crypts that immediately surround an adenoma show more mutations than those further away. To investigate whether adenomas induce a higher mutation burden in surrounding non-dysplastic crypts, the percentage of CCO-deficient crypts was assessed and used as a proxy for mutagenesis. Frozen FAP sections were stained for CCO activity, adenomas identified, and mutated blue vs. non-mutated brown crypts counted within the adenoma, its surrounding normal crypts (zone 1 – 3), and in distant non-dysplastic crypts (Table 3.5).

	FAP	AFAP	Total
N (patients)	3	1	**4**
N (samples)	20	3	**23**
N (total)	35	3	**38**

Table 3.5: Number of adenomas counted in samples stained for cytochrome *c* oxidase.
For example, 20 frozen samples from 3 patients were used and of those samples, 35 adenomas and their surrounding non-dysplastic crypts were assessed.

The percentage of CCO-deficient crypts was significantly higher in adenomas compared to non-dysplastic crypts in the zones and the distant crypts (Kruskal-Wallis; $p = 0.009$). Pairwise comparison showed that there is a significantly greater number of CCO-deficient crypts in the adenoma compared to zone 2 ($p = 0.019$) and zone 3 ($p = 0.006$) (Figure 3.9), suggesting that dysplastic, mutated crypts have an effect on their surrounding non-mutated crypts and that the surrounding normal crypts exhibit more neutral, non-pathological mtDNA mutations. No significant differences were found between the zones, but the percentage of CCO-deficient crypts was significantly higher in zone 1 compared to distant crypts ($p = 0.023$). Non-dysplastic crypts in zone 2 and zone 3 were not significantly different to distant normal crypts.

Taken together, this shows a higher concentration of mutant crypts in adenomas, as well as in non-dysplastic crypts surrounding the adenoma, and this effect decreases over increasing distance with lower mutation burden in distant normal crypts. This could potentially be explained by clonal expansion.

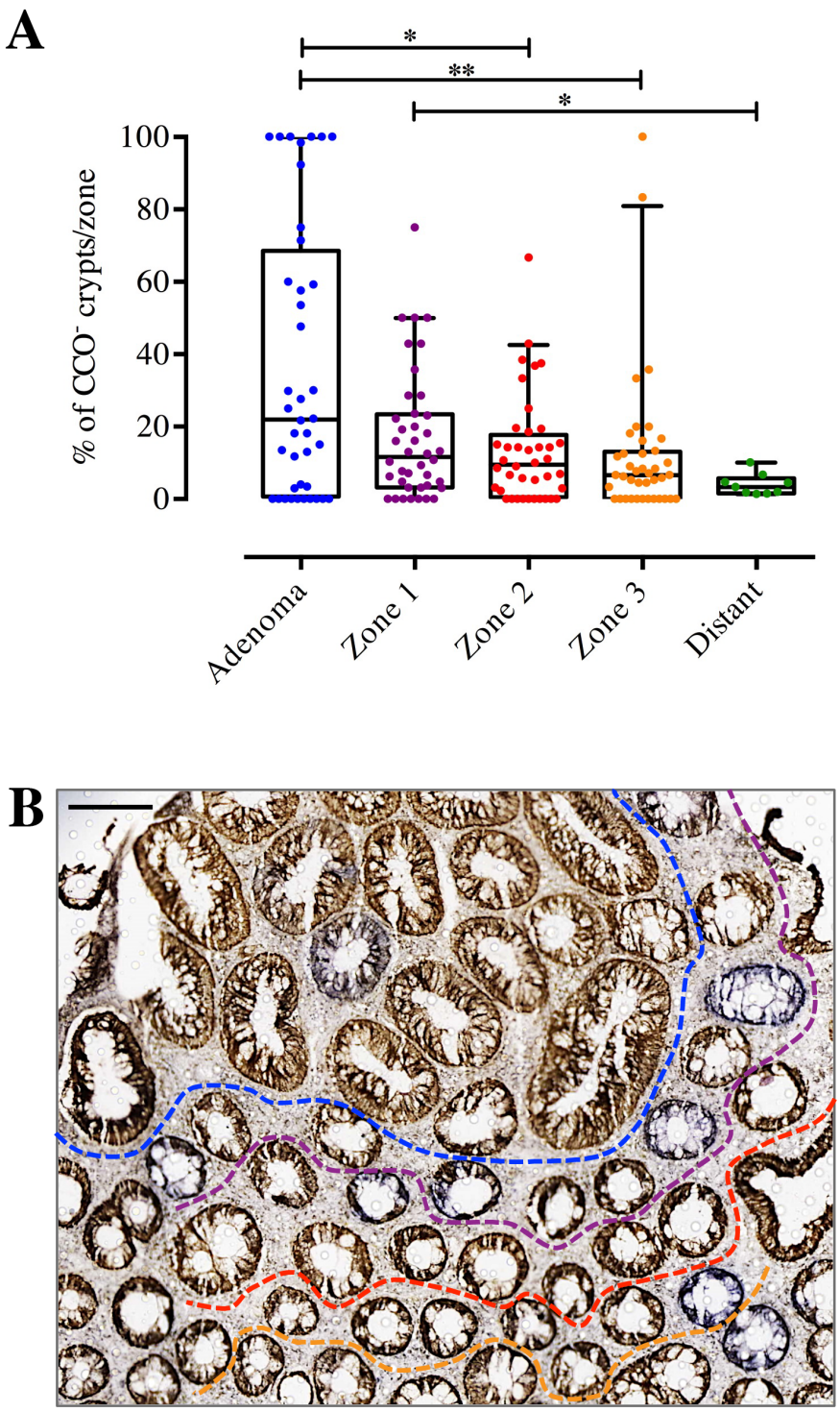

Figure 3.9: Effect of mutational burden from dysplastic crypts on non-dysplastic neighbouring crypts using the neutral marker cytochrome *c* oxidase (CCO).

A) Beeswarm plot visualising the number of CCO-deficient crypts surrounding the adenoma (blue) and neighbouring non-dysplastic crypts in zone 1 (purple), zone 2 (red), zone 3 (orange) and non-dysplastic distant crypts (green) for FAP patients (Kruskal-Wallis: p = 0.009) The box plot indicates the mean, upper and lower quartile. B) Staining for CCO is shown: CCO-deficient crypts are stained in blue, CCO-positive crypts in brown. The dashed blue line indicates dysplastic crypts, the dashed purple line non-dysplastic crypts in zone 1, the dashed red line non-dysplastic crypts in zone 2, and the dashed orange coloured line non-dysplastic crypts in zone 3. Scale bar = 200μm.

3.2.7 Mutation burden in surrounding non-dysplastic crypts

To further investigate mtDNA mutation burden in crypts surrounding adenomas, a next generation sequencing approach was employed where crypts from each zone were microdissected and the mutation burden quantified to demonstrate a mutagenic field effect. H&E slides of frozen sections were digitally scanned and used to identify adenomas (Figure 3.10A). Zone distances of normal crypts were measured as before: zone 1 was considered to include all crypts less than 50μm away from the dysplastic area, zone 2 50-150μm and zone 3 150-250μm (Figure 3.10B). Frozen sections of the same samples were then cut serially on membrane slides and sections were then stained with dual CCO/SDH enzyme histochemistry (see section 2.2.2). Identified adenomas on H&E slides were then located on CCO/SDH stained membrane slides (Figure 3.10C), individual crypts of the adenoma and each zone were labelled in different colours (Figure 3.10D), and laser capture microdissected (Figure 3.10E). Stroma and distant non-dysplastic crypts were also laser captured and used as controls.

In total, 10 adenomas and their surrounding zones were cut from 4 FAP patients, from here onwards referred to as FAP1 to FAP4, and DNA extracted (see section 2.5; Appendix Table 9.2). Both mtDNA amplicons from individual samples were pooled at the start of the library preparation and sequenced together. The entire mitochondrial genome was sequenced at a depth of approximately 1213-3316X with a mean average read depth from the 48 samples calculated to be 2183X.

27 out of 48 samples had poor or no primer coverage and were excluded from further analysis. Due to the large sample drop out, there was only one complete set (crypts from an adenoma, the three zones and matching distant normal crypts) from patient FAP3. Poor average depth and poor primer coverage is likely the result from pooling the amplicons at the start of the library preparation. An example of the mean depth and primer coverage is given in Figure 3.11.

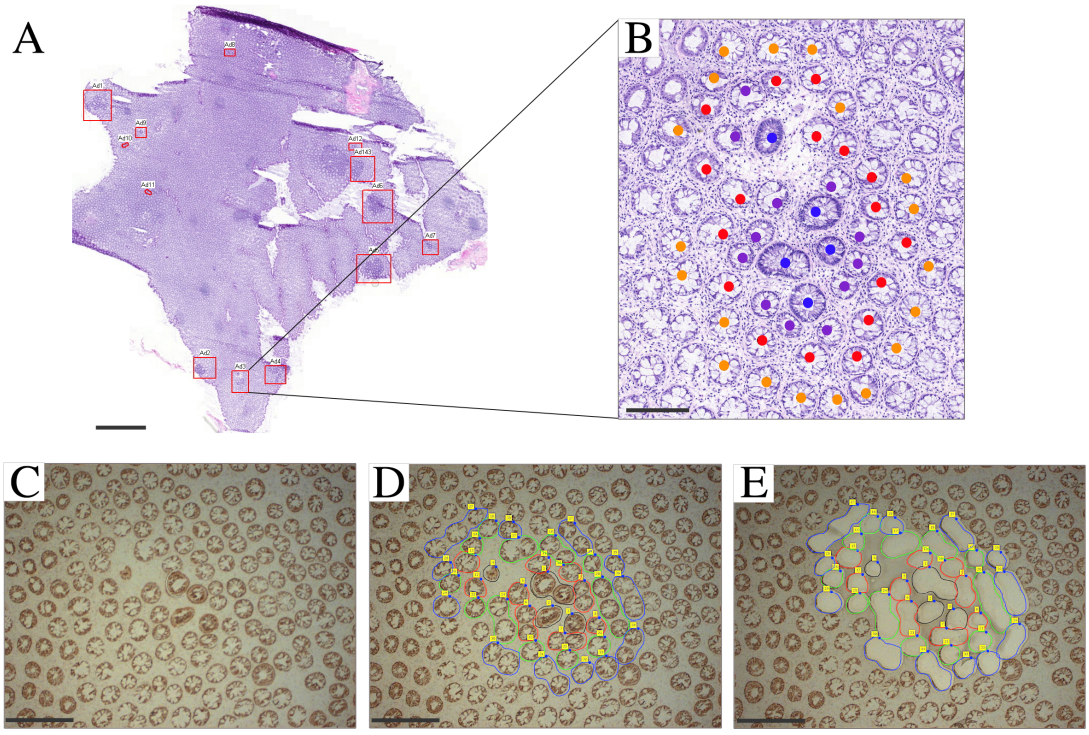

Figure 3.10: Laser capture microdissection of crypts from human colon frozen sections.
A) H&E staining of an entire section of an FAP patient and all identified adenomatous regions (red squares). Scale bar = 2000µm. B) Enlargement of one of the identified adenomas. Blue dots represent all adenomatous crypts, purple dots all non-dysplastic crypts in zone 1, red dots all non-dysplastic crypts in zone 2, and orange dots all non-dysplastic crypts in zone 3. Scale bar = 200µm. C) CCO/SDH staining of the same sample as in B). In D), adenomatous (black labelling) and their surrounding normal crypts (red = zone 1, green = zone 2, blue = zone 3) were labelled. E) Crypts that were laser capture microdissected. Scale bar = 200µm.

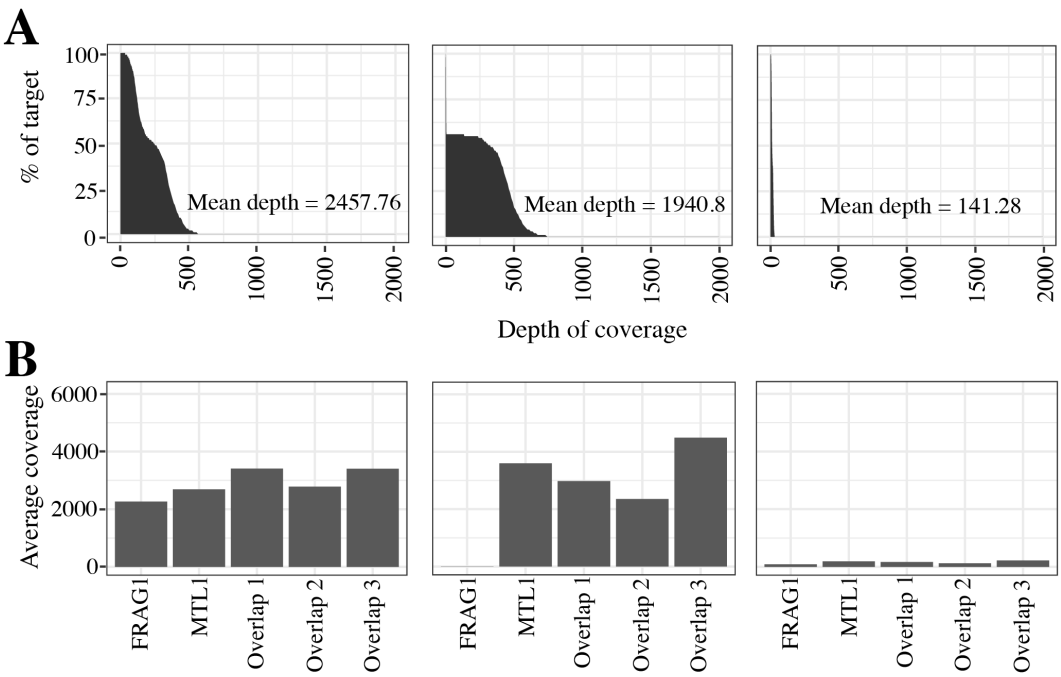

Figure 3.11: Examples of sequencing depth and primer coverage.

A) Average read depth. This graph demonstrates the coverage attained on analysis of patient FAP3 and indicates an average read depth of 2457.72X. B) Average primer coverage. This graph shows the average coverage of the primers FRAG1 and MTL1 and for the overlaps 1 – 3. Overlap 1 -3 refers to the point in the genome when the primers FRAG1 and MTL1, as the mitochondrial genome are circular.

The quality of each PCR replicate was confirmed by checking the similarity of variant allele frequencies (VAFs) between each replicate shown (Figure 3.12A). Small differences between the VAFs of each PCR replicate were observed given the dots do not line up on the straight line. Therefore, the PCR process used to generate amplicons might have introduced errors to the NGS results. This again might have been due to the fact that amplicons of both primers were pooled before library preparation and sequencing. Nevertheless, it is noticeable that although the majority of mutations occur at low level of VAF, 2 mutations of patient FAP3 and 5 mutations of patient FAP4 occur at a frequency of > 10%, indicating large numbers of mitochondria share the same mutations.

The most frequent occurring mutations per zone amongst all patients were investigated. C > T, as well as T > C base changes were observed to occur with high frequency in zone 2 and zone 3, and less often in the adenoma and zone 1. Base changes from C > A were only observed in zone 3, and C > G only in zone 2 (Figure 3.12B). This profile has been previously associated with age related mutations (Milholland *et al*. 2015).

Analysing the frequency of base changes per patient, the most common types of mutation found in all 4 patients were C > T and T > C changes. Additionally, for patient FAP2, base changes of C > G, and for patient FAP3, base changes of C > A were commonly occurring with detectable frequency (Figure 3.12C). An example of a T > C mutation is illustrated in Figure 3.12D.

To assess the mutation burden of the remaining samples, the total number of crypts that were laser capture microdissected in each zone was counted and normalised in order to compare the mutational burden among the zones (Figure 3.13). A table with the raw counts is given in the Appendix Table 9.2.

For patient FAP1, two adenomas and their surrounding zones (Ad1 and Ad2) were sequenced. On average 3 mutations (range: 1 – 4) were detected (Table 3.6). After normalising the count, slightly more mutations were detected in zone 1 compared to the adenoma of Ad1, and fewer mutations were identified in zone 3 compared to the adenoma of Ad2. The mutation burden in the remaining zones could not be analysed as samples dropped out due to poor primer coverage.

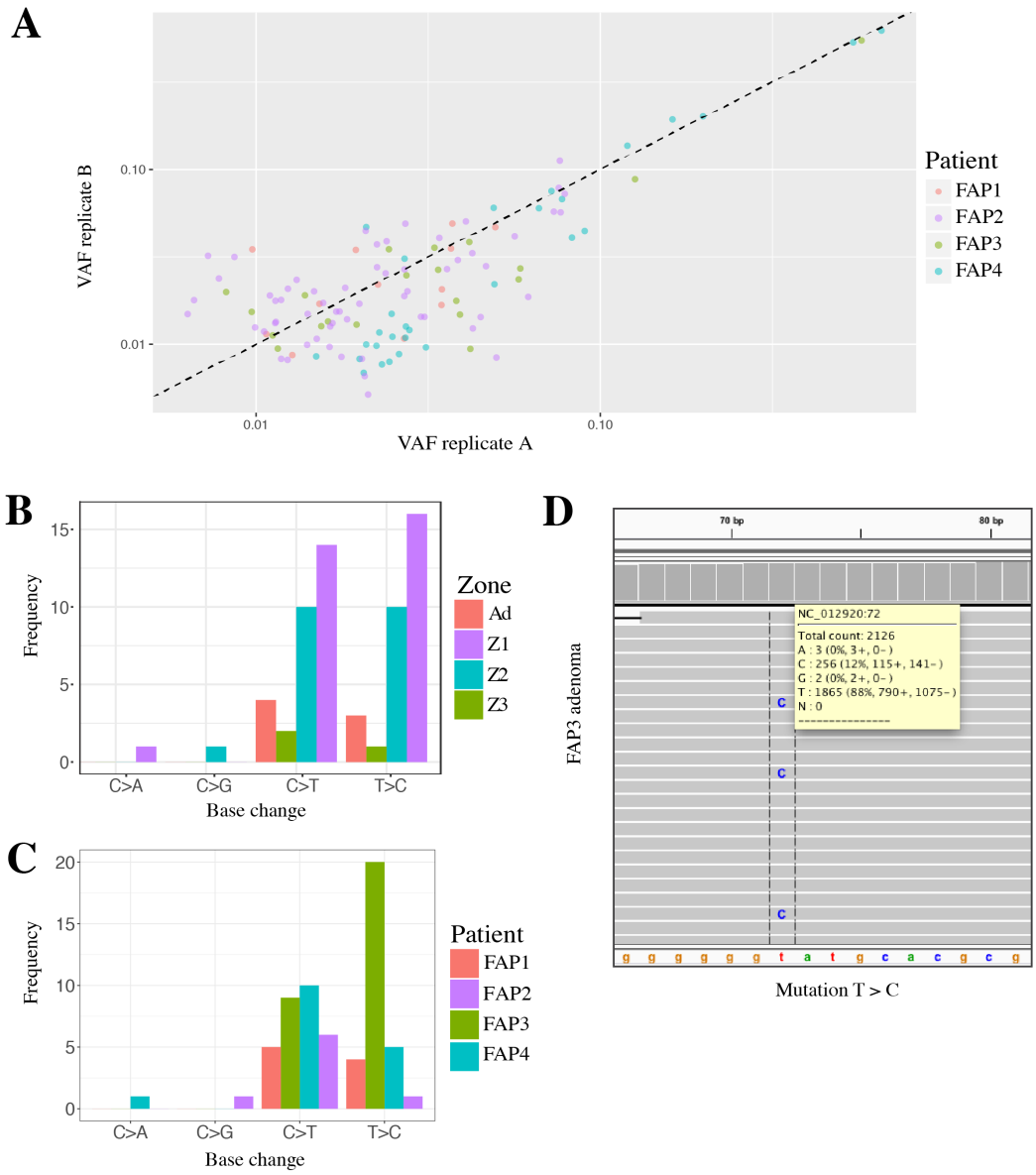

Figure 3.12: Mutation profiles of FAP patients.

A) Logarithmic scale of VAF for duplicates. Replicates are not very well matched along a best fit line indicating that there is some difference between the VAFs of each PCR replicate therefore the PCR process to generate the amplicons in duplicate might have introduced errors to the NGS sequencing. Although the majority of mutations occur at a low level of VAF frequency, some mutations show a level of heteroplasmy of >10% (VAF > 0.1) indicating that some mitochondria share the same mutations. B) Mutation profiles. Graph indicates the frequency of the most common mutations per zone. C) Mutation profiles. Graph indicates the frequency of the most common mutations of FAP patients. D) Illustration of a T > C mutation in the mitochondrial genome of an adenoma of patient FAP3 at position 72 using the Integrative Genomics Viewer (IGV) software.

For patient FAP2, two adenomas and their surrounding zones (Ad1 and Ad2) were assessed and an average of 12 mutations (range: 8 – 17) found. Most mutations were found in zone 2 of Ad1. The number of mutations in zone 1 and zone 3 was also greater compared to the number of mutations in the adenoma and zone 1 of the second adenoma assessed (Ad2).

The average number of mutations for patient FAP3 was 2.86 (range: 1 – 5). The highest number of mutations was found in the adenoma followed by zone 3 and then zone 1. Distant non-dysplastic normal crypts had slightly more mutations compared to zone 2.

For patient FAP4, two adenomas and their surrounding zones (Ad1 and Ad2) were sequenced. An average of 5.8 mutations (range: 2 – 15) was detected (Table 3.6). Interestingly, most mutations were found in zone 3 of both adenomatous regions sequenced.

Taken together, there is a clear association with age, even though there are only 4 patients investigated in this analysis. Patient FAP 2 (67 years old) and patient FAP 4 (39 years old) had on average more mutations than patient FAP 1 (16 years old) and FAP 3 (14 years old).

To conclude, for all four patients, the number of mutations is too low to calculate statistical power. Due to the huge sample drop out and the low number of mutations, no conclusions on the mutational burden could be drawn. Therefore, the hypothesis that non-dysplastic crypts surrounding the adenoma harbour a higher mutation load could not be tested on this data set. Pooling of amplicons before the library preparation should be avoided in order to achieve better primer coverage and sequencing depth. Additionally, it would have been better to dissect on a crypt-by-crypt basis rather than pooling all crypts from each zone together. Ideally, whole-exome sequencing or whole-genome sequencing should be performed to detect greater number of mutations.

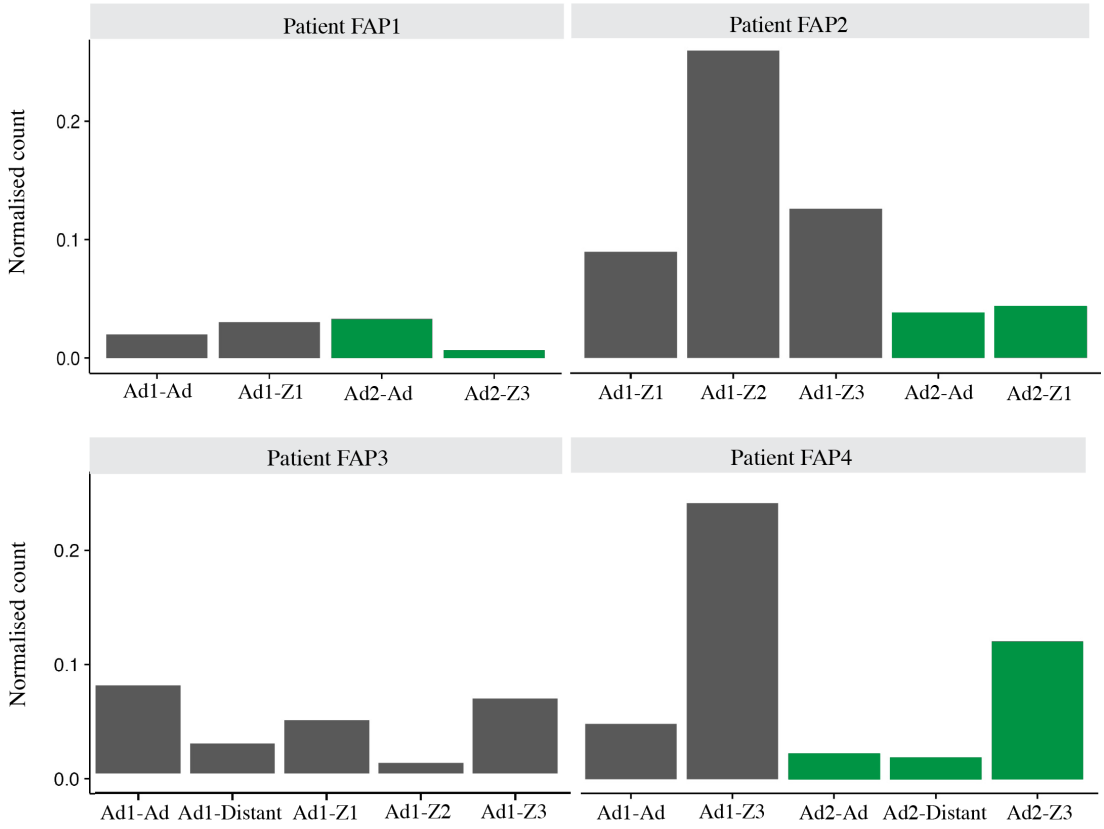

Figure 3.13: Assessing the mutation burden in adenomas and surrounding non-dysplastic crypts using mtDNA mutations.
Number of mtDNA mutations found in each sample sequenced. Bars highlighted in grey belong to one adenoma and its surrounding non-adenomatous crypts; bars highlighted in green belong to another adenoma and its surrounding non-adenomatous crypts.

Patient	Age (years)	Sex	Cancer	Average # mutations	Range
FAP1	16	Female	No	3	1 - 4
FAP2	67	Female	No	12	8 - 17
FAP3	14	Female	No	2.86	1 - 5
FAP4	39	Male	Yes	5.8	2 - 15

Table 3.6: Patient characteristics and average number of mtDNA mutations/patient and range.

3.3 Discussion

In colorectal carcinogenesis, studies on FAP and some sporadic microadenomas have revealed that tumours are polyclonal in origin (see section 1.14). However, the mechanism responsible for causing this polyclonality at the outset of tumour growth is unknown. The aim here was to demonstrate that dysplastic crypts interact with neighbouring non-dysplastic crypts and to characterise the field effect from the dysplastic crypt to the first initiated non-dysplastic crypt (zone 1) to the second (zone 2) and to the third (zone 3), thus driving expansion. Using immunohistochemistry for cell behaviour and cell lineage markers on human FAP and sporadic samples, evidence was found that dysplastic crypts do indeed interact with their surrounding neighbouring non-dysplastic crypts generating a field effect.

3.3.1 Adenomas create a field effect

WNT is one of the most critical pathways involved in the carcinogenesis of many adenocarcinomas and proposed to be an early step in tumourigenesis (Peifer *et al*. 2000). FAP patients carry a germline *APC* mutation, which interacts with β-catenin. This interaction activates the Wnt signalling pathway and results in alterations in cell proliferation (Wang *et al*. 2013). β-catenin is mainly expressed in the membrane of normal cells, whereas in adenocarcinomas cytoplasmic β-catenin is translocated into the nucleus, where it activates downstream signalling pathways regulating tumour growth (Hao *et al*. 1997, Wong *et al*. 2004). Elevated nuclear and cytoplasmic β-catenin expression is a biomarker for metastasis and poor prognosis for the patient (Cheah *et al*. 2002, Wong *et al*. 2004). Therefore, the percentage of nuclear β-catenin was investigated in adenomas and surrounding non-adenomatous crypts to describe the early changes emanating from an adenoma.

In this study, a significant increase in the percentage of nuclear β-catenin cells was found the closer a non-dysplastic crypt is to the adenoma and this effect was decreasing over distance for both, FAP and sporadic patient samples (Figure 3.3). Moreover, positive nuclear β-catenin cells in non-dysplastic crypts in all three zones were significantly higher compared to distant non-dysplastic crypts, providing evidence of a field effect generated by the dysplastic epithelium. The shift from no

nuclear β-catenin staining in non-dysplastic distant crypts to a widespread distribution of nuclear β-catenin staining in the adenoma is in line with previous reports. For example, Wong *et al*. (2004) have reported no nuclear β-catenin accumulation in normal tissues, whereas it was present in 8% of polyps, 92% of adenomas, and 100% of carcinomas (Wong *et al*. 2004). In another study, nuclear accumulation of β-catenin was observed in 48% of the cancer samples (Elzagheid *et al*. 2008). Inomata *et al*. (1996) found a three times higher nuclear β-catenin expression in adenomas of FAP patients compared to their corresponding normal epithelia (Inomata *et al*. 1996). However, this is the first study to show that also non-dysplastic crypts surrounding the adenoma accumulate nuclear β-catenin.

These results demonstrate that increased nuclear β-catenin expression is associated with the field effect emanating from the dysplastic zone. These observations further indicate that β-catenin plays a critical role in the transformation and progression of CRC already in the early stages.

A significant increase in the number of proliferating cells was found the closer a non-dysplastic crypt is to the adenoma and this effect is decreasing over distance for both, FAP and sporadic patient samples (Figure 3.1). Increased cell proliferation suggests that adenomas create a field effect as surrounding non-dysplastic crypts exhibit a higher percentage of positive stained cells compared to the control group (distant non-dysplastic crypts). Interestingly, no significant difference was found between adenomatous crypts and non-dysplastic crypts in the surrounding zones. However, proliferating cells in the non-dysplastic crypts in the three zones were significantly higher compared to distant normal crypts. This demonstrates that mutant crypts have a profound field effect on their neighbours and that the dysplastic epithelium initiates the non-dysplastic epithelium in the development of CRC. It has been shown that Ki67 expression is significantly higher in malignant tissue as compared to normal epithelia and is associated with the development of CRC (Barone *et al*. 2010, Li *et al*. 2015, Oshima *et al*. 2005). Wang *et al*. (2013) specifically assessed Ki67 expression in FAP patients. They found 5% Ki67 expression in non-dysplastic epithelium, 37% in low-grade adenomas, 32% in high-grade adenomas and 41% in invasive carcinomas. Expression of Ki67 was significantly increased in high- and low-grade adenomas combined as compared to

non-dysplastic epithelium. The expression for carcinomas was not significantly different to adenomas but statistically significantly increased as compared to non-dysplastic epithelium (Wang *et al*. 2013). The increase in cell proliferation mirrors the increase in nuclear β-catenin, as this factor drives cell proliferation. Barone *et al*. (2010) also observed a significant increase in Ki67 expression in high- and low-grade dysplasia and carcinomas compared to normal crypts of FAP patients. The results present a progressive and significant increase in cell proliferation along with the progression to cancer (Barone *et al*. 2010). This has also been observed in sporadic colorectal tumours, where the Ki67 expression was greater in carcinomas (38.12 ± 11.01) then in adenomas (30.05 ± 7.6) (Saleh *et al*. 2000).

A limitation of this study pertains specifically to the assessment of Ki67 expression. Due to the fact that there are varying levels of proliferation as one moves up the crypt (most proliferation occurs in the lower third of the crypt), it was difficult to know at which point in the transit amplifying zone the section was at. However, to overcome this limitation, a large number of crypts was counted taking the natural variation into account. Crypts showing no Ki67 staining were excluded, as it implies that the section was not in the proliferative zone. This is all partly due to the fact that the tissue included was from archived blocks; they were not sliced in order for this manner of research, but rather, were obtained for the purpose of diagnostics. This means that most of the tissue did not contain the optimal orientation of the crypts. A more ideal methodology would have been to take serial sections of the tissue obtained, so that the entire proliferative zone was included.

Nevertheless, the results presented here show that adenomatous crypts interact with their surrounding non-dysplastic crypts and initiating a field effect, as Ki67 expression is significantly higher in surrounding non-dysplastic crypts compared to distant normal crypts.

In normal cells, the cellular genomic integrity is monitored by processes, such as cycle checkpoints and DNA repair pathways, that detect and repair DNA double-strand breaks (DSBs) and can stop the cell cycle progression until repair is performed. However, defects in these processes can lead to the accumulation of DNA errors and genomic instability, eventually leading to CRC (Broustas *et al*. 2014). A key component in DNA repair is the histone protein H2AX. In this study, a significant increase in DNA damage was found in adenomatous crypts compared to

neighbouring non-dysplastic crypts for both, FAP and sporadic patients (Figure 3.2). This is consistent with previous investigations, where increased nuclear γH2AX staining was observed in carcinomas compared to low expression in normal epithelium (Beggs *et al*. 2012, Sedelnikova *et al*. 2006). Further, it has been shown that nuclear γH2AX is elevated in some precancerous lesions (Bartkova *et al*. 2006, Lord *et al*. 2012). No significant differences were found between the non-dysplastic crypts in the zones and the distant normal crypts, although non-dysplastic crypts in all three zones have elevated levels of DNA damage. To our knowledge, this is the first study to have investigated the status of DNA damage in surrounding non-dysplastic crypts.

Taken together, this also shows that dysplastic crypts interact with neighbouring non-dysplastic crypts and that adenomas create a field effect.

3.3.2 The tumour microenvironment – the role of the stroma

The adenomatous stroma is a complex medium in which a variety of interactions take place between adenoma and normal cells. Adenomatous cells proliferate and invade the stroma whereas immune cells congregate around the adenomas (Yen *et al*. 2010). Cross-talk between adenomatous cells and immune cells provides the evolving adenoma with sufficient opportunity to acquire mutations and epigenetic alterations that are necessary for cell autonomy (Ferrone *et al*. 2010). Here, the inflammatory cell phenotype within the stromal microenvironment of human adenomas and their surrounding non-adenomatous crypts was defined. The healthy colon has a low-grade mucosal inflammatory activity with T helper and cytotoxic cells, macrophages, and plasma cell infiltrates being present. These stromal cells interact to maintain an appropriate local immune response, as they are constantly challenged by luminal antigens (Wittig *et al*. 2003).

This study has shown that the stroma of adenomas exert a significantly higher number of immune infiltrates (CD4, CD8 and CD68) compared to distant normal stroma, and more importantly that the immune infiltrate of surrounding non-dysplastic crypts is also significantly higher as in distant normal stroma, for both FAP and sporadic adenoma patients (Figure 3.4 and Figure 3.5). Adenomatous polyps are rich in pro-inflammatory T helper and cytotoxic cells, as well as

macrophages and this exerts a significant influence on their surrounding microenvironment. It became clear that a phenotypic change occurs early in the adenoma-carcinoma sequence with expression of inflammatory chemokines and cytokines dysregulated in the transition from normal mucosa to adenomas (Mo *et al*. 2016). McLean *et al*. (2011) have investigated immune infiltrates in adenomas with matching normal mucosa. They also detected a significant increase of T helper cells ($p = 0.004$) and macrophages ($p = 0.0002$) in the adenoma compared to adjacent normal mucosa (McLean *et al*. 2011). In another study, the number of $CD4^+$ T cells infiltrating the tumour stroma was significantly higher compared to those in the neighbouring mucosa, suggesting that the tumour induces modifications of the T cell populations in the surrounding normal stroma (Chirica *et al*. 2015). $CD4^+$ cells might exert a pro-inflammatory response in the dysplastic region, thus promoting clonal interactions through the stroma.

Macrophages mainly engulf and digest cellular debris, but also tumour cells, among others, which can explain the high number of $CD68^+$ cells found surrounding the adenomatous region, but interestingly also adjacent to it. This supports the hypothesis that the adenoma exerts a field effect on the surrounding crypts, leading to the observed increased levels of macrophages.

Deschoolmeester *et al*. (2010) investigated $CD8^+$ cells in cancer invasive margins, inside the tumour and in the surrounding stroma. Most T lymphocytes were found in the invasive margin, but the cytotoxic T lymphocytes were also abundant in the stroma closer to the tumour cells (Deschoolmeester *et al*. 2010). This was confirmed by Liu and colleagues, who showed a significant increase in CD8 infiltration in the adenoma compared to normal mucosa (Liu *et al*. 2016). In CRC, and specifically in MSI CRCs, it has been shown that high numbers of $CD8^+$ cells show a much better clinical outcome compared to their microsatellite stable cancers (Amicarella *et al*. 2017, Baker *et al*. 2009, Deschoolmeester *et al*. 2010, Prall *et al*. 2004). It was reasoned that the number of $CD8^+$ T cells within the tumour could be a good indicator of a systemic immune surveillance mechanisms and that the tumour secretes substances into the stroma, which then can be recognised by the immune system that destroys the tumour (Deschoolmeester *et al*. 2010). However, with progression to colon cancer, T cell infiltration began to decline, indicating that not only the immune response varies between different stages in tumour progression, but

also that due to a varying tumour microenvironment including genetic and epigenetic changes, cancer cells can survive and invade (Liu *et al*. 2016).

Interestingly to note is the difference observed for normal distance crypts in FAP and sporadic patient samples. Generally a higher number of immune infiltrates was found in samples of sporadic patients compared to samples of FAP patients. This could be explained by the different underlying genetic background, indicating that patients with sporadic adenomas have much higher immune infiltrates also in normal non-dysplastic regions.

Surprisingly, the opposite effect was found when analysing intraepithelial lymphocytes (IELs) (Figure 3.6). IELs consist mostly of $CD8^+$ T cells and are found within the epithelial layer of the crypt. IELs are antigen experienced T cells and when spotting antigens, they immediately release cytokines or mediate killing of the infected target cells (Renuka *et al*. 2017). Given their location, they form a critical interface between the core of the body and the outside environment and present the front line of immune defence. Their functions include balancing protective immunity to keep the integrity of the epithelial barrier, but avoiding unnecessary immune response and therefore inflammation. Moreover, IELs are essential for the regulation of intestinal homeostasis, and epithelial cell healing and repair (Cheroutre *et al*. 2011, Sheridan *et al*. 2010). However, they also have pathological responses: cytotoxic $CD8^+$ induced IELs haven been implicated in the initiation and progression of inflammatory bowl disease (IBD) and the promotion of cancer development (Cheroutre *et al*. 2011, Nancey *et al*. 2006, Tajima *et al*. 2008).

In this study, there were significantly less $CD8^+$ cells in the adenoma compared to its surrounding non-dysplastic crypts and also less $CD8^+$ cells in the crypts surrounding the adenoma compared to distant normal crypts for both, FAP and sporadic tissues. The literature has been quite controversial on the infiltration of IELs in dysplastic and non-dysplastic epithelia. Several studies have found a higher $CD8^+$ infiltration in tumour epithelium (Baker *et al*. 2009, Van Acker *et al*. 2016). Menon *et al*. (2004) assessed infiltration of $CD8^+$ cells in the tumour epithelium, stroma and advancing tumour margins of colorectal carcinomas and found a greater infiltration, which related to improved survival, thus concluding that infiltration of $CD8^+$ cells are important prognostic factors in CRC (Menon *et al*. 2004). However, Koch *et al*. (2006) found no difference in the total number of infiltrating $CD8^+$ cells

between CRC and normal mucosa. Interestingly, the percentage of infiltrating $CD8^+$ cells of the total percentage of all T cells ($CD8^+$ and $CD4^+$ cells) was lower in the tumour compared to the normal mucosa. Given they found a significant enrichment of $CD4^+$ cells in tumour samples compared to matching normal mucosa, they reasoned that this explains the decreased proportion of $CD8^+$ cells in the tumour specimens. They explained the increase of $CD4^+$ cells because helper T cells are required in early antigen-specific response to imprint $CD8^+$ cells with the ability to develop into long-living functional memory cells (Koch *et al*. 2006).

However, the induction of cytotoxic T lymphocytes responses takes time, leaving time for the tumour cells to escape the immune system (Deschoolmeester *et al*. 2010). The decrease of IEL $CD8^+$ cells might be explained by immune escape or immune deviation mechanisms or even by regulatory T cells suppressing the host anti-tumour T-cell response (Zou 2006). IEL $CD8^+$ cells may have lost their function and can no longer protect intestinal homeostasis. To our knowledge this is the first study assessing IELs in adenomas and their surrounding non-dysplastic crypt of FAP and sporadic patients. Previous studies only assessed IEL of $CD8^+$ cells in tumour epithelium and tumour margins of CRC and normal mucosa. Furthermore, IELs have been implicated in the repair of intestinal epithelium (Chen *et al*. 2002). A lower concentration of IELs in the adenoma and the surrounding non-dysplastic crypts might indicate lack of repair mechanisms.

The stromal microenvironment is not only comprised of infiltrating immune cells, but also includes fibroblasts and myofibroblasts. In this study, the expression of fibroblasts (α-SMA) was significantly increased in the stroma surrounding adenomas and also significantly increased in the stroma of non-dysplastic crypts surrounding the adenoma compared to distant stroma, for both FAP and sporadic patients (see Figure 3.4D and Figure 3.5D), suggesting that these factors facilitate a pro-tumourigenic environment promoting the progression of adjacent cells. Mo *et al*. (2016) investigated α-SMA expression in aberrant crypt foci (ACF), defined as the earliest morphological identifiable mucosal abnormalities commonly found in the human colon, and normal mucosa. They found an increased number of stromal fibroblasts in ACF compared with normal stroma ($p < 0.0001$) (Mo *et al*. 2016). It has been shown that once activated, fibroblasts alter their cellular phenotype and the expression of α-SMA increases (Hinz *et al*. 2001). A senescent and secretory

phenotype is acquired promoting carcinogenesis by secreting growth factors and inflammatory cytokines (Coppe *et al*. 2010).

The density of myofibroblasts was found to be lower surrounding the epithelia of adenomatous crypts but significantly increased with increasing distance away from the adenoma, with a highest density found in normal distant crypts (Figure 3.7). Myofibroblasts are associated with tumour cells at all stages of tumour development, and thus its disruption affects fundamental cellular processes that are essential for tumour progression (Yen *et al*. 2010). The main functions of myofibroblasts are to provide structural support, to confer protection for crypts, and to mediate signalling. The observation that myofibroblasts are higher in non-dysplastic regions might be due to the fact that adenomatous crypts loose its structure with progression and thus its support from the myofibroblasts. Therefore the density of myofibroblasts is higher in non-dysplastic crypts in zone 3. Moreover, it has also been noted that the anti-inflammatory cytokine interferon- λ (IFN-λ) secreted by T cells plays an important role in density of SMA^+ cells. This is because IFN-λ causes the inhibition of the expression of myofibroblasts and thus actively reduces the density of myofibroblasts (Tanaka *et al*. 2007).

Taken together, these findings suggest that early transformed epithelial cells send signals, which directly influence the stromal microenvironment leading to its reorganisation. By directly analysing adjacent stromal tissue to an adenoma, it was demonstrated that reactive stromal changes accompany the earliest detectable stages of human colonic adenomas. A significant enrichment of the infiltrates of CD4, CD8 and CD68, as well as fibroblasts were observed in the stroma surrounding the adenoma and in adjacent non-dysplastic crypts compared to distant stroma. It further suggests an influx of pro-inflammatory cells and a release of potent cytokines into the adenomatous stromal microenvironment. This supports the hypothesis that the adenoma exerts a field effect on the surrounding crypts, leading to increased levels of immune filtrates. Inflammation is a known driver of crypt fission and therefore clonal expansion (Cheng *et al*. 1986, Salk *et al*. 2009). Clonal expansions are a known cancer risk. Therefore, a potential explanation for the development of polyclonal adenomas could be that increased inflammation surrounding dysplastic tissue increases the likelihood that dysplasia can arise in the normal surroundings.

3.3.3 Mutation burden

A higher mutation burden in non-dysplastic crypts compared to distant crypts was observed based on mtDNA mutations, which suggests that dysplastic, mutated crypts influence their surrounding non-mutated crypts and that the surrounding non-dysplastic crypts exhibit more non-pathological mtDNA mutations. The mutation frequency can also be reflective of the here observed increased proliferation. It has been shown that mutations are increased when proliferation is increased, as proliferating cells are more mutable than quiescent cells, due to the lack of DNA repair mechanisms before DNA replication (Bielas *et al*. 2000). In addition, DNA damage can increase proliferation, thus accelerating this effect (Kiraly *et al*. 2015).

Nevertheless, the result suggests that dysplastic crypts increase the mutagenic pressure in their surrounding non-dysplastic crypts. However, it has to be noted that mtDNA mutations increase naturally with age, and because of this there is an observed increase in the number of CCO-deficient crypts with age. Tissue from patients who were too young would not show any CCO-deficiency, irrespectively of how mutagenic the environment was (this cut-off has been shown to be about 40 years of age (Greaves *et al*. 2006)).

Having established that adenomas generate a field effect, the underlying genetic patterns were analysed by sequencing the mitochondrial genome of adenomatous and neighbouring non-adenomatous crypts. Unfortunately, it was not possible to investigate the mutation burden, since most samples sequenced failed due to poor primer coverage and additionally, of those remaining samples only a low number of mutations was detected. The poor primer coverage can partly be explained by the fact that amplicons were pooled at the start of the library preparation kit. This kit requires 0.2ng/µl of input DNA, but by pooling the amplicons, essentially 0.1ng/µl of DNA of each amplicon was added. The amount of amplified mtDNA was calculated based on the TapeStation results, which verifies the size distribution of each PCR amplicon. The concentration of the amplicon can be determined by measuring the area under the peak. However, with the TapeStation, the limit of detection is already reached for this assay. The concentration was measured on the peak rather than across the whole area, which ideally should have been done. Thus, if there is a slight excess of one primer over the other, only one will get sequenced.

Given that the amount of input mtDNA was low in the beginning, the library preparation should have been done for each primer pair separately and pooled in the end before running them on the sequencer.

Nevertheless, the number and range of mutations detected in all of the four remaining patient samples was too low for any statistics to be performed. For FAP1 and FAP3 the low number and range of mutations observed (FAP1: 3 (1 – 4); FAP3: 2.86 (1 – 5)) can be explained by the fact that these patients were 16 and 14 years, respectively. MtDNA mutations are acquired with age (Greaves *et al*. 2006). Therefore, these patients were potentially too young to detect a meaningful mutation burden in adenomatous and surrounding non-adenomatous crypts. Patients FAP2 and FAP4 were 67 and 39 years of age, respectively, and consequently more mutations should have been observed (FAP2: 12 (8 – 17); FAP4 (5.8 (2 – 15)). However, this is not the case. This might be due to the fact that by sequencing all crypts in each zone together, mutations were diluted out. Each crypt in each of the adenomatous region and neighbouring zones were collected together. Ideally, a few single crypts of each zone should have been laser capture microdissected serially and sequenced individually to achieve higher VAFs. Nevertheless, the question remains whether single crypts will yield a much higher mutation burden to perform statistical analysis.

This leads to the conclusion that using mtDNA to investigate the mutation burden in adenomas and surrounding non-adenomatous crypts is potentially not the correct method. Instead, whole-genome sequencing (WGS) or whole-exome sequencing (WES) could be an alternative method to detect a greater number of mutations. Advantages of using WGS include the detection of more mutations to be able to calculate meaningful statistical outputs and it allows to workout the absolute number of mutations per megabase inferring that each cell has a duplicate genome at this stage in FAP. Disadvantages usually include the high costs, however the Novaseq platform from Illumina is now available with a much higher capacity. Moreover, the starting amount of DNA for WGS used to be 5ng, but with the NEBNext Ultra2 library prep kit from Illumina allowing the amount of input DNA to be as low as 500pg, the amount of DNA is not a limiting factor anymore. In contrast to WGS, with WES fewer regions are sequenced, but deeper sequencing enables to detect low VAFs. A limiting factor of WES is the limited region of examination and that the genes in the region where they are sequenced might be under selection.

3.3.4 Conclusion

In conclusion, these findings suggest that adenomatous crypts within the human colon of FAP and sporadic adenoma patients exert a field effect and thereby initiating increased cell proliferation and DNA damage in surrounding non-adenomatous crypts, and additionally translocating β-catenin from the membrane to the nucleus, as increased levels of nuclear β-catenin were found in the adenoma and adjacent crypts as compared to distant crypt. These changes are associated with the induction of epithelial-stromal interactions that may influence the outcome of these early transformations. Most likely, inflammatory signalling pathways initiated by transformed epithelial cells may activate stromal fibroblasts and recruit immune cells within the stromal microenvironment. A potential mechanism explaining how adenomas generate a field effect is through the involvement of the JNK signalling pathway. Upregulation in genes encoding the JAK/STAT pathway was found, which encoded cytokines in both intra-clonally and inter-clonally mutated fruit flies (Drosophila). When a dominant negative form of the JAK/STAT receptor was expressed, invasive tumours were formed in both cases, suggesting cooperation between these mutations and the JAK/STAT pathway (Wu *et al*. 2010). Potential mechanism underlying the novel field effect and how clones interact will be investigated in greater detail in chapter 5 and 6.

The results here also provide insights into the complex cross-talk between epithelia and stroma that occurs during the earliest stages in the progression to CRC, highlighting the active role of the stroma.

4 Chapter IV: Stem Cell Dynamics

4.1 Introduction

Studying stem cell dynamics in the intestinal crypt is essential for the understanding of tumourigenesis in the human colon, as cancer can be considered as a disease of mutated stem cells originating from the intestinal crypt base (Barker *et al*. 2009, Sangiorgi *et al*. 2008). Quantitative analyses in mouse models have shown that in crypt homeostasis stem cells are continuously in neutral drift competition (clonal expansion and contraction occurs in balance) and on average, each stem cell division results in loss and replacement of an individual stem cell lineage (Kozar *et al*. 2013, Lopez-Garcia *et al*. 2010, Snippert *et al*. 2010).

Since this transgenic approach cannot be applied in humans, Baker *et al*. (2014) have circumvented this problem by using somatic mitochondrial DNA (mtDNA) mutations to trace clonal lineages in order to study stem cell dynamics in human colonic crypts. Somatic mtDNA mutations can result in a loss of cytochrome *c* oxidase (CCO) enzyme activity and when sufficient stem cells have acquired CCO loss, the entire crypt will become CCO-deficient. The rate at which this happens is proportional to the rate of stem cell expansions and contractions within the crypt stem cell niche and are detectable by enzyme histochemistry. Moreover, these mutations increase with age and are under neutral selection, meaning they confer no significant positive or negative selection to the mutant stem cell over neighbouring non-mutant stem cells (Greaves *et al*. 2012). Sequencing of mtDNA has shown that these mutations are clonally derived, thus they are an effective clonal marker for both normal and adenomatous tissue (Fellous *et al*. 2009, Greaves *et al*. 2006, Gutierrez-Gonzalez *et al*. 2009, Taylor *et al*. 2003).

Enzyme histochemistry for CCO activity allows for the observation of crypts that are CCO-proficient (brown, CCO+), crypts that are CCO-deficient (blue, CCO-) and crypts that are partially mutated (a mixture of CCO+ and CCO- cells). These mutations occur at the base of the crypt in the stem cell niche and passed on to their immediate progeny. Importantly, the distance the daughter cell travels up the crypt axis is proportional to the time since it was born in the crypt base, thus enabling

temporal evolutionary dynamics to be inferred from a single time point. When moving upwards the crypt axis, the CCO-deficient cells form a connecting ribbon (Taylor *et al*. 2003). These ribbons can contract when a CCO-deficient cell is replaced by a CCO-proficient cell, thus decreasing the ribbon width, or expand when a CCO-proficient cell is replaced by a CCO-deficient cell, thus increasing the ribbon width. These "wiggles" – the change in CCO-deficient clone size – represent a temporal record of the CCO-deficient stem cell population, which was further confirmed with a mathematical model (Baker *et al*. 2014).

Baker *et al*. (2014) reconstructed the cellular composition of partially mutated adenomatous and normal crypts using adjacent serial sections and BiaQIm imaging software (http://www.deconvolve.net/bialith/BAQIFeatures.htm). The proportion of blue to brown staining was assessed between successive sections. By measuring these deviations in ribbon width between serial *en face* sections, the distribution of the deviation was found to be approximately symmetric around zero for partially mutated normal crypts, non-adenomatous FAP/AFAP crypts, and FAP/AFAP adenomatous crypts, indicating that expansion and contraction of the ribbon width is balanced. This implies that human ISCs evolve according to a neutral drift process. Furthermore, the functional stem cell loss and replacement rate was increased by a factor of approximately 2-fold in adenomas. The loss/replacement rates for non-adenomatous FAP and AFAP were comparable to those of normal tissue, indicating that it is loss of the second APC allele that accelerates the stem cell loss/replacement rate (Baker *et al*. 2014).

In this chapter, the stem cell dynamics of non-dysplastic crypts in zones 1 to 3 surrounding FAP and AFAP adenomas were studied using the same technique as described by Baker *et al*. (2014). It was hypothesised that these crypts should also evolve neutrally and that their stem cell loss/replacement rate is higher than in distant normal crypts.

4.2 Results: Stem cell dynamics

4.2.1 APC mutated crypts alter stem cell dynamics in surrounding non-dysplastic crypts

In order to investigate the stem cell dynamics in the intestinal crypt, frozen sections from three FAP, three AFAP and three healthy patients were stained with CCO/SDH (see section 2.2.2) (Table 4.1). The fraction of CCO-deficiency (blue staining) of crypts in the adenoma (n = 13), of surrounding non-dysplastic crypts in the zones (zone 1: n = 11; zone 2: n = 10; zone 3: n = 8), as well as non-dysplastic distant crypts in FAP (n = 12) and AFAP (n = 10), and crypts from normal patients (n = 11) was measured in successive serial sections throughout the crypt using the Pannoramic Viewer software and aligned to visualise stem cell dynamics using BiaQIm imaging software (see section 2.4.1) (Table 4.2). Data on the deviations in ribbon width in partially mutated crypts for the adenoma, non-dysplastic crypts of FAP and AFAP as well as for normal crypts was provided by Baker *et al*. (2014). Wiggles of the CCO-deficient clone size were quantified by differences in the CCO area between adjacent serial sections and expressed in terms of cell numbers to normalise for crypt size between adenomas and non-dysplastic crypts.

The average number of nuclei per *en face* crypt section as well as the average crypt circumference was measured on H&E sections (Figure 4.1, Table 4.1). There were a significantly greater number of cells in the adenoma compared to the surrounding zones, the non-adenomatous crypts in FAP and AFAP, and the normal crypts (Kruskal-Wallis test; p = 0.0002) (Figure 4.1A). Pairwise comparison has shown that the number of nuclei in adenomatous crypts was significantly higher compared to zone 1 (Mann-Whitney test: p = 0.002), zone 2 (p = 0.002), zone 3 (p = 0.002), but also to non-adenomatous FAP (p = 0.036), AFAP (p = 0.024) and normal crypts (p = 0.024). Interestingly, $APC^{+/+}$ crypts had a significantly lower number of cells on average compared to non-dysplastic crypts in zone 1 (p = 0.0238), to zone 2 (p = 0.0238) and to zone 3 (p = 0.0119). No significant difference in cell number was found between the control groups.

Patient	Age	Sex	Germline mutation	Mean #cells/crypt circumference				
				Adenoma	Zone 1	Zone 2	Zone 3	Non-adenoma
FAP 1	67	F	Unknown	58	31	29	31	34
FAP 2	59	M	Unknown	48	31	31	33	38
FAP 3	39	M	c.896_897del	41	29	31	32	32
AFAP 1	64	F	c.531+3A>C	37	31	32	32	31
AFAP 2	65	F	Unknown	60	25	30	30	31
AFAP 3	61	M	Unknown	41	29	26	35	29
Normal 1	79	M	n/a	n/a	n/a	n/a	n/a	23
Normal 2	60	M	n/a	n/a	n/a	n/a	n/a	24
Normal 3	64	M	n/a	n/a	n/a	n/a	n/a	23

Table 4.1: Table showing age, sex, and number of cells per crypt for each patient.
The number of cells per crypt circumference was counted using an *en-face* H&E-stained section, and these figures were used to convert 'fractional clone size' to 'number of cells in the clone'.

Samples	Adenoma	Zone 1	Zone 2	Zone 3	Normal FAP	Normal AFAP	Normal
FAP 1	8	2	1	5	6		
FAP 2	0	1	0	1	4		
FAP 3	5	7	7	1	2		
AFAP 1		1	2	1		4	
AFAP 2						3	
AFAP 3						3	
Normal 1							4
Normal 2							4
Normal 3							3
Total #crypts/zone	**13**	**11**	**10**	**8**	**12**	**10**	**11**

Table 4.2: Total number of partially mutated crypts measured.

Then, crypt circumference measurements were compared and it was shown that adenomas were on average larger compared to non-dysplastic crypts in the surrounding zones, to non-dysplastic crypts in FAP and AFAP, and to normal crypts (Kruskal-Wallis test; $p = 0.0029$) (Figure 4.1B). Pairwise comparison has shown that the circumference of adenomatous crypts was significantly larger compared to zone 1 (Mann-Whitney test: $p = 0.002$), zone 2 ($p = 0.002$), zone 3 ($p = 0.002$), but also to non-adenomatous FAP ($p = 0.024$), AFAP ($p = 0.024$) and normal crypts ($p = 0.024$). There was no significant difference between the non-dysplastic crypts in the zones and each of the zones to non-dysplastic crypts in FAP and AFAP patients away from the dysplastic zone. However, normal crypts from healthy patients were significantly smaller on average compared to zone 1 ($p = 0.0238$), to zone 2 ($p = 0.0238$), and to zone 3 ($p = 0.0476$). No significant difference was found between the non-adenomatous FAP/AFAP crypts, and normal crypts. The average number of cells per crypt was significantly correlated to the crypt circumference ($R^2 = 0.69$, $p < 0.001$) (Appendix Figure 9.1E). Graphs showing the average number of nuclei per crypt and the crypt circumference for FAP and AFAP only are given in the Appendix Figure 9.1A-D.

The effect of APC mutation on stem cell dynamics was then quantified by examining the temporal evolution in partially mutated crypts. As previously reported (Baker *et al*. 2014), the distribution of deviation was found to be approximately symmetric around zero for partially mutated dysplastic crypts from adenomas (skewness = 0.268). Furthermore, non-dysplastic crypts in all surrounding zones also displayed this symmetric distribution (zone 1 skewness = -0.074, zone 2 skewness = -0.176, and zone 3 skewness = 0.125) (Figure 4.1C). The symmetry around zero indicates that clonal contraction is balanced by equal frequent clonal expansion through time. The flatter and broader distribution in adenomatous crypts and non-dysplastic crypts within the zones as compared to normal indicates more frequent, larger fluctuations in clone size. This implies that clonal evolution of the crypt stem cells follow neutral drift dynamics. Consistent with neutral drift dynamics, examples of clone extinction, where CCO-deficient populations were disconnected from the crypt stem cell base (Figure 4.2A, B), mostly likely due to random loss, and clone fixation, where all cells become CCO-deficient (Figure 4.2C, D), were observed.

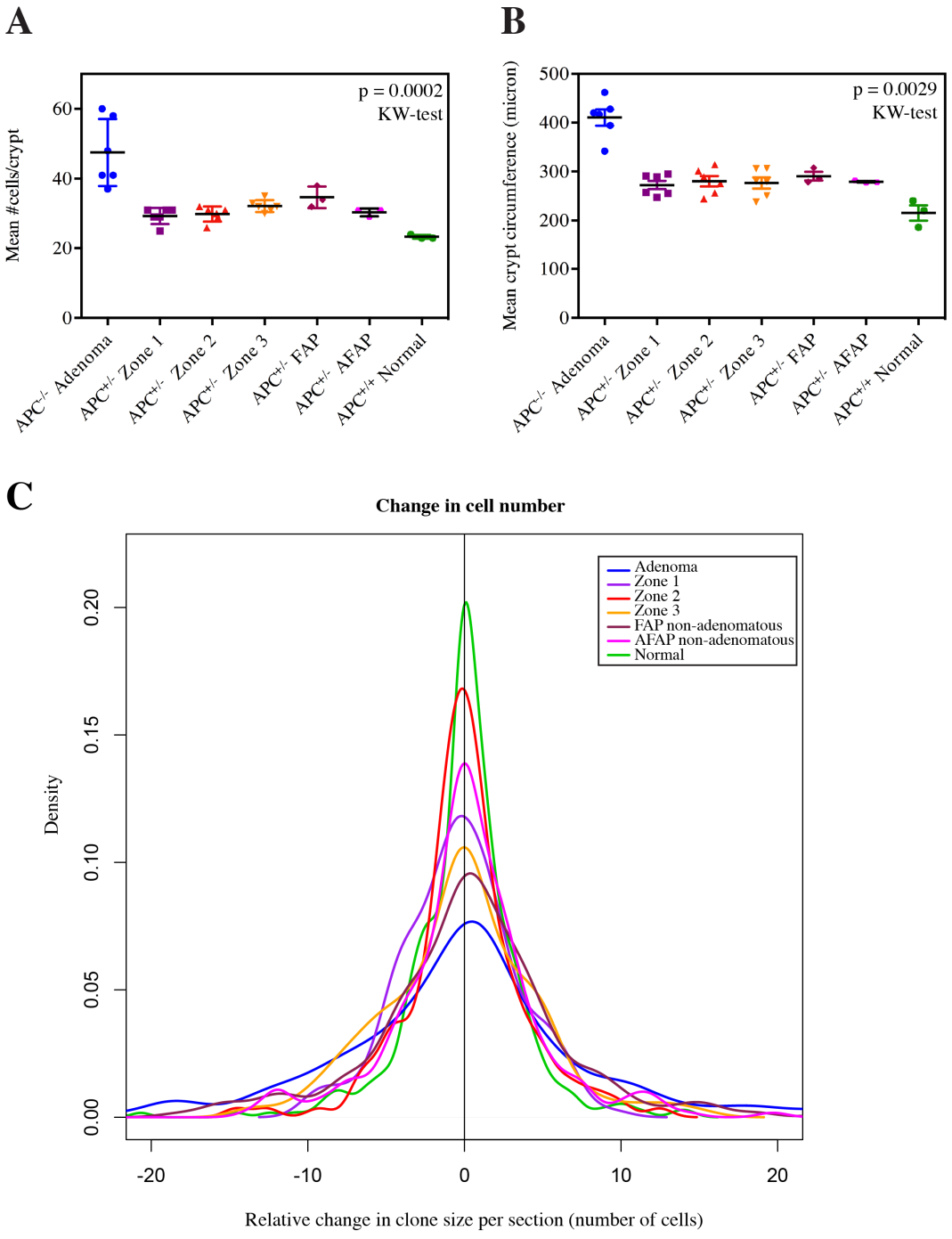

Figure 4.1: Crypt base stem cells follow a neutral drift type process.
Average number of cells per crypt circumference was counted (A) and the crypt circumference (B) measured manually in H&E sections of adenomatous colonic crypts, non-dysplastic crypts in zone 1 – 3, distant non-dysplastic crypts in FAP and AFAP, and non-dysplastic colonic crypts in normal tissue sections. Each point on the graph represents the average number of cells (A) and the average crypt circumference (B) in one patient, which was obtained by analysing at least 20 representative crypts. The line within each count represents the mean. A) Kruskal-Wallis test: p = 0.0002. B) Kruskal-Wallis test: p = 0.0029. C) Density plot showing the change in the relative clone size between sequential sections ("wiggle").

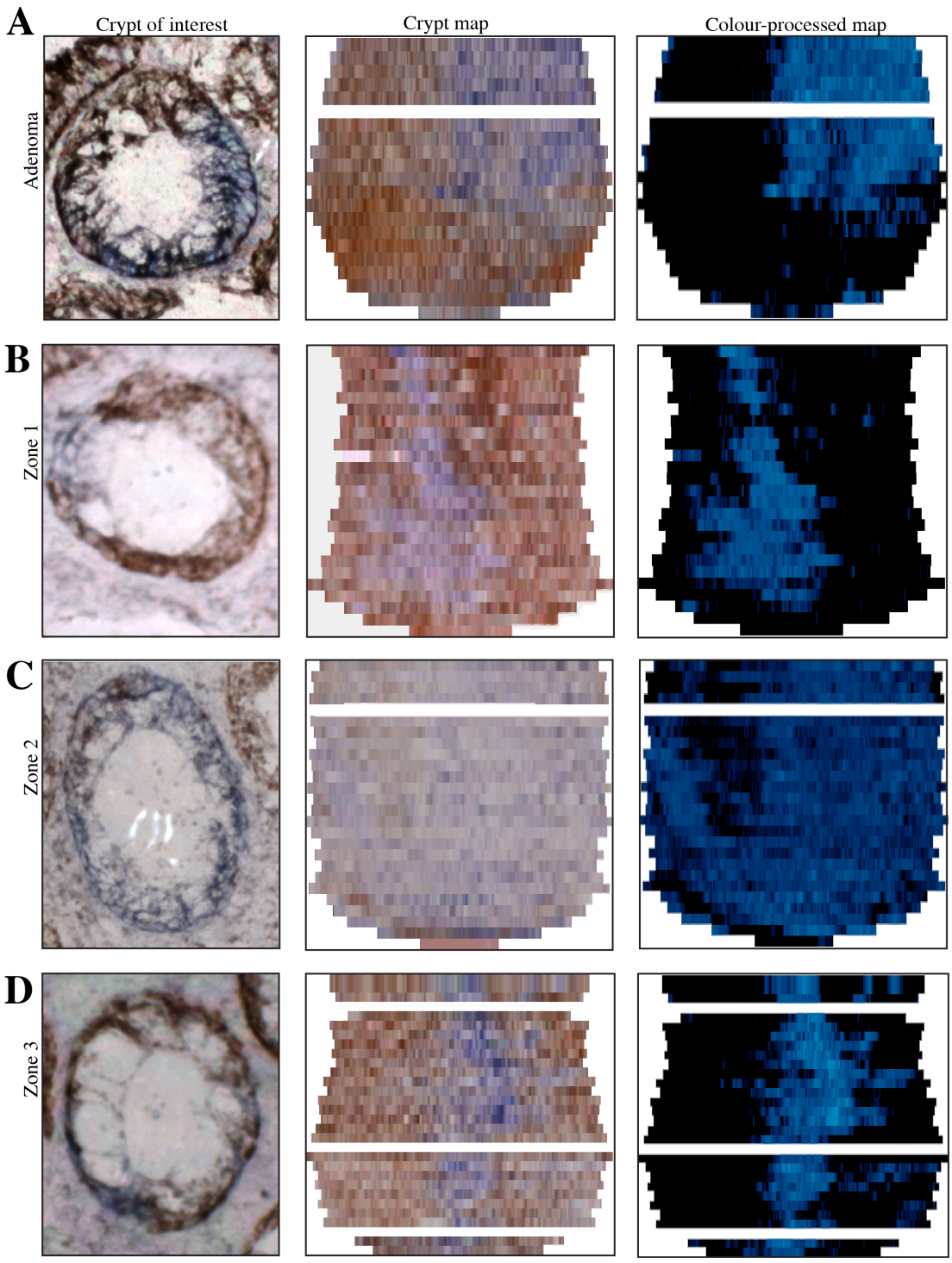

Figure 4.2: Representative examples of crypt maps for the adenoma and zones.
The left column represents an *en face* image of the crypt of interest, the middle column the resulting crypt maps, and the right column represents the colour-processed maps (blue, CCO- cells, black, CCO+ cells). White lines represent missing sections. A) Crypt map of the adenoma representing clone extinction due to random loss. B) Example of a clone in zone 1 that was putatively in the process of becoming extinct, whereas crypt maps of zone 2 (C) and zone 3 (D) showing clones that putatively became fixed.

Analysis of non-dysplastic crypts from FAP and AFAP patients also showed that stem cells evolved neutrally ($APC^{-/+}$ FAP skewness: n = -0.41; $APC^{-/+}$ AFAP skewness: n = 0.76). The deviation in ribbon width in partially mutated normal crypts was also symmetric around zero (skewness = -0.472), indicating stem cells underwent neutral evolution.

To conclude, quantifying the effect of APC mutations on stem cell dynamics in the human colon has revealed that stem cells in adenomatous crypts, as well as in non-adenomatous surrounding the adenoma (crypts in zone 1 to zone 3) and non-adenomatous crypts far away from the adenoma underwent neutral evolution.

Based on studies of neutral drift dynamics in ISCs in mice (Kozar *et al*. 2013, Lopez-Garcia *et al*. 2010, Snippert *et al*. 2010), the temporal evolution of the number of functioning stem cells in the CCO-deficient clones was analysed and hypothesised to follow a one-dimensional random walk and that the temporal evolution in the CCO-deficient ribbon width could be described a as one-dimensional diffusion process. The same model described by Baker *et al*. (2014) was applied here. In brief, if a CCO-deficient clone has a total number of functional stem cells at a specific time, the mean square change in cell number is predicted to vary linearly with a diffusion coefficient defining the functional stem cell loss/replacement rate (Baker *et al*. 2014). The measured diffusion coefficients are listed in Table 4.3. The experimental data (calculated by Trevor Graham) confirmed a linear dependence of the mean-square displacement for the adenoma, for non-dysplastic crypts in all surrounding zones, as well as $APC^{-/+}$ FAP, $APC^{-/+}$ AFAP and normal crypts (Figure 4.3). This confirmed that neutral drift occurs also within the stem cell compartment.

The loss/replacement rate of functional stem cells was then calculated as described by Baker *et al*. (2014) for non-dysplastic crypts in all three surrounding zones. Taking into account the functional stem cell number in proportion to the cells at the crypt base (provided by Baker *et al*. (2014)) and the circumference of the crypts, assuming the ratio remains fixed, the loss/replacement rates for all three zones were comparable to those of $APC^{-/+}$ FAP, $APC^{-/+}$ AFAP and normal crypts. The loss/replacement rate was accelerated in adenomas by a factor of approximately 4, as compared to a factor of approximately 2 measured by Baker *et al*. (2014). This difference is most likely explained by inter-sample variability.

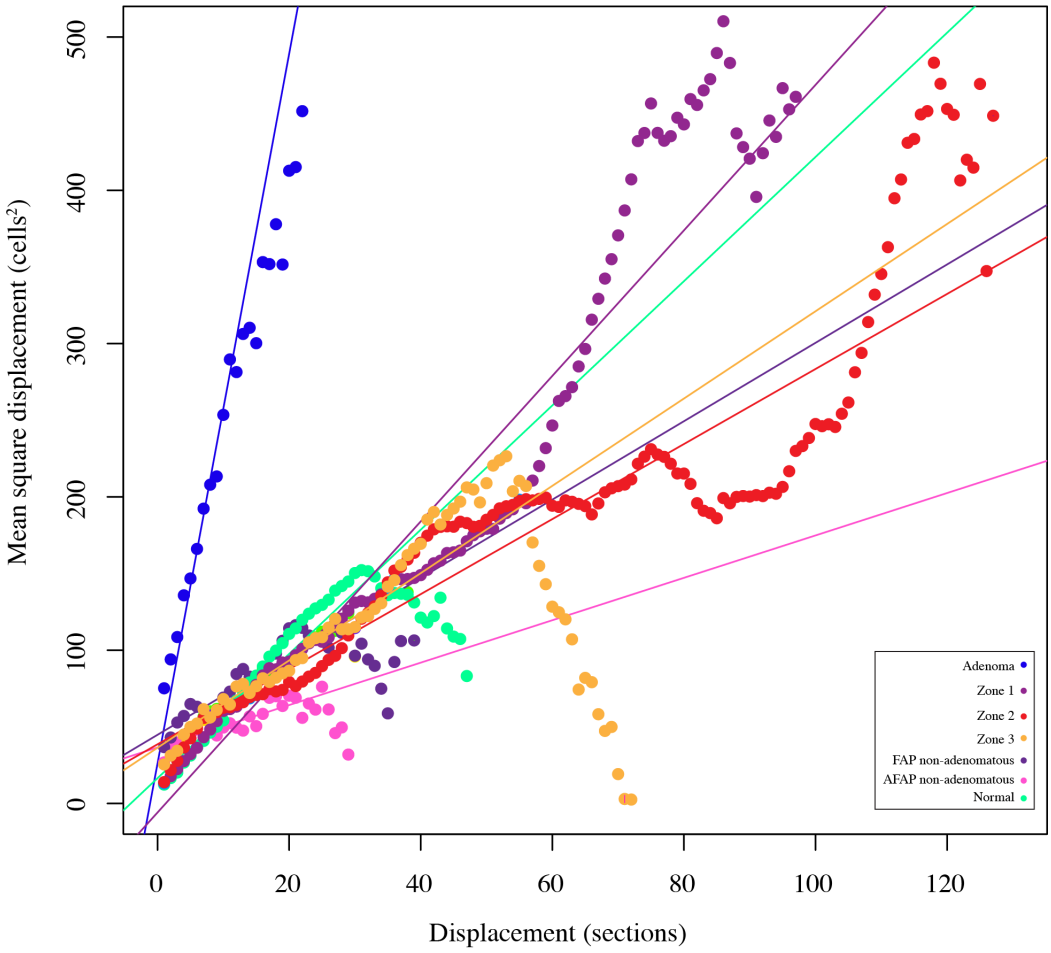

Figure 4.3: Mean squared difference in CCO-deficient ribbons.
The mean squared difference in CCO-deficient ribbon width expressed as a function of distance along the crypt axis.

APC status	Measured diffusion coefficient
Adenoma	23.14
Zone 1	4.75
Zone 2	2.45
Zone 3	2.85
FAP non-adenomatous	2.56
AFAP non-adenomatous	1.38
Normal	4.05

Table 4.3: Measured diffusion coefficient.

4.3 Discussion

Lineage tracing studies in transgenic mice have significantly improved our understanding of stem cell dynamics in intestinal crypts, but the significance remained poorly characterised for the human intestine. Baker *et al*. (2014) have shown that naturally occurring somatic mtDNA mutations together with the unique structure of the intestinal crypt allows tracing the evolutionary record of ISCs and concluded that clonal evolution is a neutral process.

The purpose of this chapter was to show that even the stem cell niche of non-dysplastic crypts in close proximity to an adenoma are governed by neutral drift dynamics, mimicking what has been observed in the murine crypt (Snippert *et al*. 2010). APC mutations not only alter stem cell dynamics in dysplastic crypts, stem cell dynamics have already been altered in non-dysplastic crypts (zone 1 to zone 3) in close proximity to an APC adenoma (Figure 4.1C, Figure 4.3).

The herein described stem cell loss/replacement rate contradicts recent findings. Nicholson *et al*. (2018) applied a different methodology and measured a replacement rate nearly a 100-fold slower, although the number of functional stem cells (mean = 7) was similar to Baker *et al*. (2014), who calculated around 6 functional stem cells in each human colonic crypt. Interestingly, another recent study (Stamp *et al*. 2018) has also measured a slower stem cell loss/replacement rate, supporting the Nicholson study.

Investigating human colonic crypt stem cell dynamics remains challenging as longitudinal studies are not possible and both studies, Baker *et al*. (2014) and Nicholson *et al*. (2018) relied on only one time point. In addition, studies in mice have shown that stem cells position themselves at the centre and at the border of the crypt base exhibiting different self-renewal probabilities, and the ability to exchange between these positions (Ritsma *et al*. 2014). Thus, the described neutral drift dynamics are the result of the total stem cell population. Nicholson *et al*. (2018) argued that given the larger crypt size in humans as compared to mice, such reciprocal exchange could be more complex and could explain the slower loss/replacement rates. This indicates that modelling the colonic stem cell niche is far more complex than we envisaged and more work needs to be done to try to reconcile the differences between these two measurements.

5 Chapter V: Crosstalk between adenomas and normal murine epithelia

5.1 Introduction

Precedent to the growth of a malignant lesion is the acquisition of pro-tumourigenic mutations in a normal cell lineage, which is positively selected for in the microenvironment. As a consequence, the now mutant lineage can grow to produce large patches or fields that predispose to cancer (field cancerization) (see section 1.11.6, 1.15.1) (Curtius *et al*. 2018). During this process, it is assumed that interactions between clones are needed to generate such field. Interactions between transformed and non-transformed epithelial cells are important for understanding tumour initiation and progression (Mo *et al*. 2016).

As described earlier, some early neoplastic lesions are *polyclonal-in-origin* (see section 1.14, 1.15). Even though the mechanisms causing a tumour to be polyclonal are unknown, the paradigm of field cancerization could explain the underlying cause. Potentially through signalling, the initial mutant clone may produce a field, thereby altering the behaviour of surrounding stromal cells, thus creating an environment that can promote mutations in neighbouring cells (Halberg *et al*. 2007). It has been shown that mutated colonic crypts have a profound effect on neighbouring non-dysplastic crypts (Bjerknes *et al*. 1999, Thliveris *et al*. 2005). Gene expression profiles and somatic mutations of the epithelial and stromal compartments of ACF compared to normal mucosa of the same patients demonstrated that the ACF epithelium and stroma displayed distinct patterns from nearby normal mucosa (Mo *et al*. 2016). Interactions have been suggested to aid clone survival and growth of the adenoma (Thliveris *et al*. 2005, Thliveris *et al*. 2013). Mechanical pressure caused by hyper-proliferative cells can also contribute to tumourigenesis (Butcher *et al*. 2009). Mechanical activation emanating from adenomas onto surrounding non-adenomatous epithelium has been shown to initiate the tumourigenic β-catenin pathway in response to hyper-proliferative tumour growth pressure (Fernandez-Sanchez *et al*. 2015). Increased β-catenin expression

together with enlarged crypts led to the formation of early ACF. This indicates that even mechanical stimulation of tumourigenic pathways could occur in normal adjacent crypts, indicating that not only are signalling pathways responsible for tumour induction, and thus enhancing tumour growth, but also physical compression of intestinal crypts (Fernandez-Sanchez *et al*. 2015). This indicates the importance of clonal interactions in the establishment of cancerized fields. Further details regarding the evidence of clonal interactions and its importance in tumourigenesis have been discussed in the introduction in section 1.17.

However, proper description and characterisation of these interactions in the early stages of tumourigenesis has been lacking. Having established in Chapter 3 that clones interact and adenomas create a field effect in surrounding non-dysplastic crypts, the question remains as to the nature of this interaction. To investigate the gene expression effects of an adenoma on normal colonic epithelium, an *in vitro* stem cell-derived three-dimensional organoid culture system was generated.

Organoids are derived from isolated colonic stem cells forming an organ-like tissue. Initially, stem cells form cystic structures with a single central lumen. Over time, the cysts form crypt like budding structures outward, eventually developing into mini-gut organoids containing $Lgr5^+$ ISCs and all cell lineages present in the intestine (Drost *et al*. 2018). They possess the ability to recapitulate some specific function, mimicking partly the physiology and organisation of the intestine: crypt-like structures including stem- and Paneth cells project outwards into the matrigel, while mature enterocytes migrate to the central cyst structure (Li *et al*. 2012, Middendorp *et al*. 2014). Thus, intestinal organoids provide an elegant system to study gene expression changes *in vitro*.

Intestinal homeostasis in organoids is controlled by four major signalling pathways. The Wnt and Notch pathway are both required for stem cell maintenance, where Notch signalling keeps cells in an undifferentiated state (Sato *et al*. 2011), and Wnt signalling additionally drives proliferation at the crypt bottom, and terminal differentiation of Paneth cells (Hao *et al*. 2012, Koo *et al*. 2011). EGF signalling, which maintains the proliferative state and is essential for self-renewal, initiates the RAS/ERK MAP kinase and PI3K/Akt signalling pathways (Davies *et al*. 2014). BMP signalling is involved in epithelial differentiation and negatively regulates the number of ISCs. BMP inhibitors, such as Noggin or Gremlin, induce crypt formation in the villus and increase the number of ISCs, indicating that suppression of BMP is

necessary for self-renewal of ISCs (Davis *et al*. 2015). Pathways were discussed in more detail in the introduction (see section 1.4.1).

Stem cell self-renewal is controlled by defined extrinsic niche factors: Matrigel, R-spondin, EGF, and Noggin. Therefore, to achieve long-term expansion, self-renewal, and stem cell maintenance of epithelial WT organoids, a cocktail of R-spondin, EGF and Noggin was added. R-spondin induces crypt hyperplasia and is essential for the activation of Wnt in intestinal crypts. Therefore, WT organoids require R-spondin for propagation (Koo *et al*. 2012). Noggin is added because it antagonises BMP proteins and induces the expansion of crypt numbers, essential for long-term maintenance of intestinal organoids (Davis *et al*. 2015). Additionally, long-term culture requires EGF signalling to fuel organoid growth. Laminin is enriched at the crypt base *in vivo*, thus Matrigel is used to support organoid growth *in vitro* mimicking the basal lamina. Matrigel is composed of extracellular matrix molecules, including laminin, collagen type IV and growth factors, such as TGF-β and FGF (Sato *et al*. 2013, Sato *et al*. 2011, Sato *et al*. 2009). All of these signals are essential for establishing a WT organoid culture system.

Using organoids as a model system to study the interactions and the effect of adenomas on normal epithelia provides a comprehensive understanding of how these interactions occur in very early stages of tumourigenesis and how their initiation might be regulated.

The first part of this chapter presents the establishment of murine intestinal organoids of WT mice and mice with an *Apc* mutation. In humans, the most frequent APC mutation is at codon 1309, also associated with severe FAP. The APC^{1322T} mouse model is equivalent to the 1309 codon changes in humans. These 1322T mice have severe intestinal polyposis (Lewis *et al*. 2010). The second part focuses in on how $Apc^{1322/+}$ organoids influence WT organoids in a co-culture system. Therefore, gene expression changes were analysed in WT organoids exposed to $Apc^{1322/+}$ organoids at two time points (48 h and 72 h).

5.2 Results: mRNA sequencing of co-cultured *Apc*$^{1322/+}$ and WT organoids

5.2.1 Establishment of murine intestinal organoids

Murine intestinal organoids from WT and WT ROSA$^{mT/mG}$ organoids were successfully grown from single isolated crypts *in vitro* and cultured in a 3D matrix with organoid media following the established protocol by Sato *et al*. (2009) (see section 2.6.2, Figure 2.6). Both, WT and WT ROSA$^{mT/mG}$ organoids developed into initial cyst structures, which then initiated bud formation leading to the formation of numerous crypt-like structures (Figure 5.1A).

Apc$^{1322/+}$ organoids were also successfully cultured in Matrigel. Polyps of *Apc*$^{1322/+}$mice were dissected and tissue fragments incubated in EDTA-chelation buffer. *Apc*$^{1322/+}$ organoids were then plated out in Matrigel and covered with basic culture media containing EGF (see section 2.6.3, Figure 2.6). *Apc*$^{1322/+}$ organoids only require EGF for intestinal organoid growth. APC–deficiency confers R-spondin and Noggin independent growth of organoids (Schwitalla *et al*. 2013). In contrast to WT organoids that form budding structures, *Apc* deficient organoids formed cysts, which began to grow in size over time (Figure 5.1B).

WT ROSA$^{mT/mG}$ organoids were successfully co-cultured with *Apc*$^{1322/+}$ organoids in organoid media. WT mice homozygous for this mT/mG knock in express cell membrane-localised red fluorescence in all tissue and cell types (rosa locus) (https://www.jax.org/strain/007576). WT ROSA$^{mT/mG}$ organoids and *Apc*$^{1322/+}$ organoids can be clearly distinguished using fluorescence microscopy: WT ROSA$^{mT/mG}$ organoids are red fluorescent, while *Apc*$^{1322/+}$ organoids are non-fluorescent (Figure 5.1A, B). Thus, when grown together, both types of organoids can be easily distinguished (Figure 5.1C).

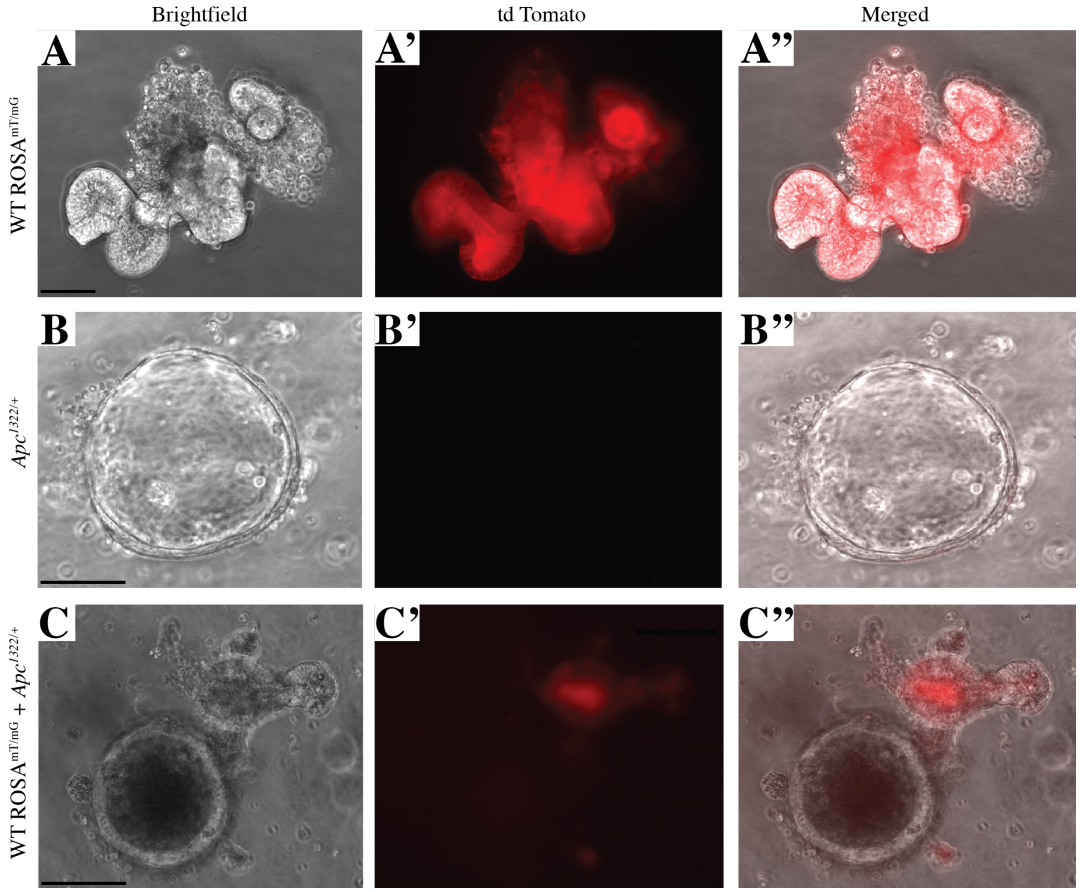

Figure 5.1: Co-culturing of *Apc*$^{1322/+}$ and WT ROSA$^{mT/mG}$ organoids.
A) WT ROSA$^{mT/mG}$ organoids alone, A') Tomato and A'') merged. B) *Apc*$^{1322/+}$ organoids alone, B') Tomato and B'') merged. C) Visualising *Apc*$^{1322/+}$ and WT ROSA$^{mT/mG}$ organoids together in brightfield, C') Tomato, and C'' merged. Scale bar = 100µm.

5.2.2 WT and *Apc*$^{1322/+}$ organoids display distinct expression profiles

In order to investigate the effects of an adenoma on normal murine intestinal epithelium, WT and *Apc*$^{1322/+}$ organoids were co-cultured in organoid media for 48 h and 72 h and controlled with WT and *Apc*$^{1322/+}$ organoids only (see section 2.7, Figure 2.7). RNA was extracted in triplicates from all organoid groups (see section 2.10.1, 2.10.2) and cDNA generated, which was then subjected to mRNA sequencing (see section 2.10.3). After completing the transcriptome analysis (see section 2.10.4), principal component analysis (PCA) was used to evaluate broad transcriptional difference across all samples.

PCA showed variation between WT and *Apc*$^{1322/+}$ organoids for both time points (Figure 5.2). *Apc* deficient organoids (1322) alone and *Apc* deficient organoids exposed to WT (1322.WT) clustered together for both time points. Whilst WT and WT organoids exposed to *Apc*$^{1322/+}$ organoids (WT.1322) clustered closely together for both time points, there was a clear separation between these two groups, with WT.1322 showing slightly more similarity to *Apc* deficient organoids.

These results not only demonstrate that WT organoids are transcriptionally different from *Apc* deficient organoids, but also show that WT organoids are transcriptionally different from WT organoids exposed to *Apc* deficient organoids after 48 h and 72 h.

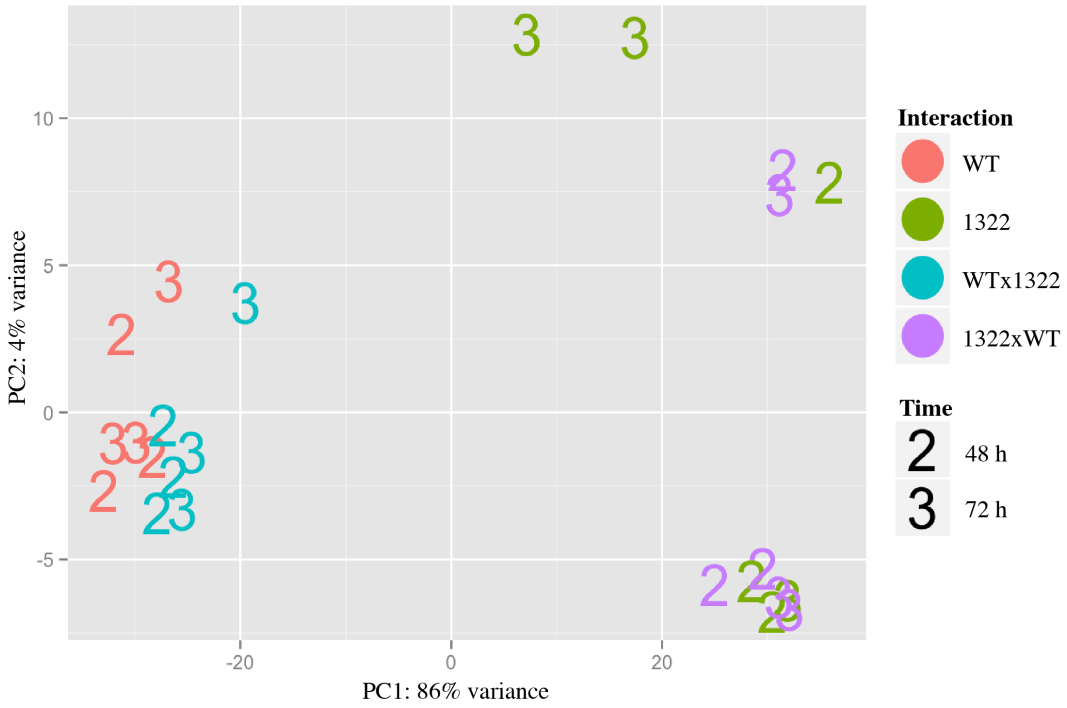

Figure 5.2: Expression profiles of *Apc*$^{1322/+}$ organoids on WT organoids.
Principal Component Analysis (PCA). Conditions are WT only (red), *Apc*$^{1322/+}$ (green), WT grown in presence of *Apc*$^{1322/+}$ (blue) (WT.1322) and *Apc*$^{1322/+}$ grown in presence of WT (purple) (1322.WT) for 48 h and 72 h indicated by the number 2 and 3, respectively. First principal component axis shows 86% variance and nicely separates WT from *Apc*$^{1322/+}$ organoids. PC2 has a variance of 4%.

5.2.3 Specific gene expression patterns in WT organoids exposed to *Apc*$^{1322/+}$ organoids

Differential gene expression analysis was then performed and results were cross-referenced with genes in the KEGG database (see section 2.10.4) to assess the signalling pathways responsible for the distinction in clustering observed in the PCA. The KEGG pathway database is a collection of manually drawn pathway maps representing the knowledge on molecular interactions, reactions and relation networks for metabolism, genetic information processing, environmental information processing, cellular processes, organismal systems, and disease pathways (http://www.genome.jp/kegg/pathway.html). The mRNA expression profile of WT organoids co-cultured with other WT organoids was then compared to the mRNA profile of WT organoids exposed to *Apc*$^{1322/+}$ organoids (WTxWT.1322). Two time points (48 h and 72 h) were examined using gene set enrichment analysis (GSEA) (Subramanian *et al*. 2005) to investigate the effects *Apc* deficient organoids have on WT organoids when grown in close proximity and sharing organoid medium. GSEA associates gene sets with phenotypes; its use is predicated on the choice of a pre-defined collection of sets (here: KEGG; see section 2.10.5) (Subramanian *et al*. 2005).

GSEA identified pathways enriched in WT organoids grown in presence of *Apc*$^{1322/+}$ organoids compared to WT organoids (WTxWT.1322) on the transcription data for both time points. Overall, differential expression analysis identified 10 significantly upregulated pathways (false discovery rate (FDR) < 0.05) after 48 h. Of those, 60% were categorised into genetic information processing, 10% to metabolism, 10% to cellular processes, 10% to diseases (including pathways in cancer) and 10% to environmental information processing after 48 h (Figure 5.3A). Moreover, GSEA identified 15 significantly downregulated pathways. Interestingly, 60% of those belong to metabolic pathways and only 7% were pathways categorised into genetic information processing, 13% to cellular processes, and the remaining 20% belong to disease pathways (Figure 5.3B).

After 72 h, GSEA identified 11 significantly upregulated and 16 significantly downregulated pathways. Strikingly, the distribution looked very different compared to the first time point, with only 28% of significantly upregulated pathways belonging to genetic information processing, as compared to 60% after 48 h. The

number of significantly induced pathways increased in the category diseases and environmental information processing with 27% each. Comparable to 10% detected in the first time point, 9% of the significantly upregulated pathways were metabolic pathways after 72 h, and 9% were found to part of organismal systems, as compared to 0% after 48 h (Figure 5.3C).

A different pattern emerged for the significantly downregulated pathways after 72 h as compared to after 48 h. The number of significantly downregulated pathways decreased to 25% for metabolic pathways, slightly decreased to 12% for cellular processes, but increased to 38% for disease related pathways and increased to 25% for pathways in the category of genetic information processing. Additional 13% of significantly downregulated pathways were categorised into organismal systems (Figure 5.3D).

These results indicate that a number of pathways belonging to different categories were already significantly altered in WT organoids after only 48 h and 72 h of being exposed to *Apc* deficient organoids. This further highlights the fact that exposure for only 48 h is sufficient to cause global regulatory profile changes in WT organoids exposed to $Apc^{1322/+}$ organoids when grown in close proximity to each other.

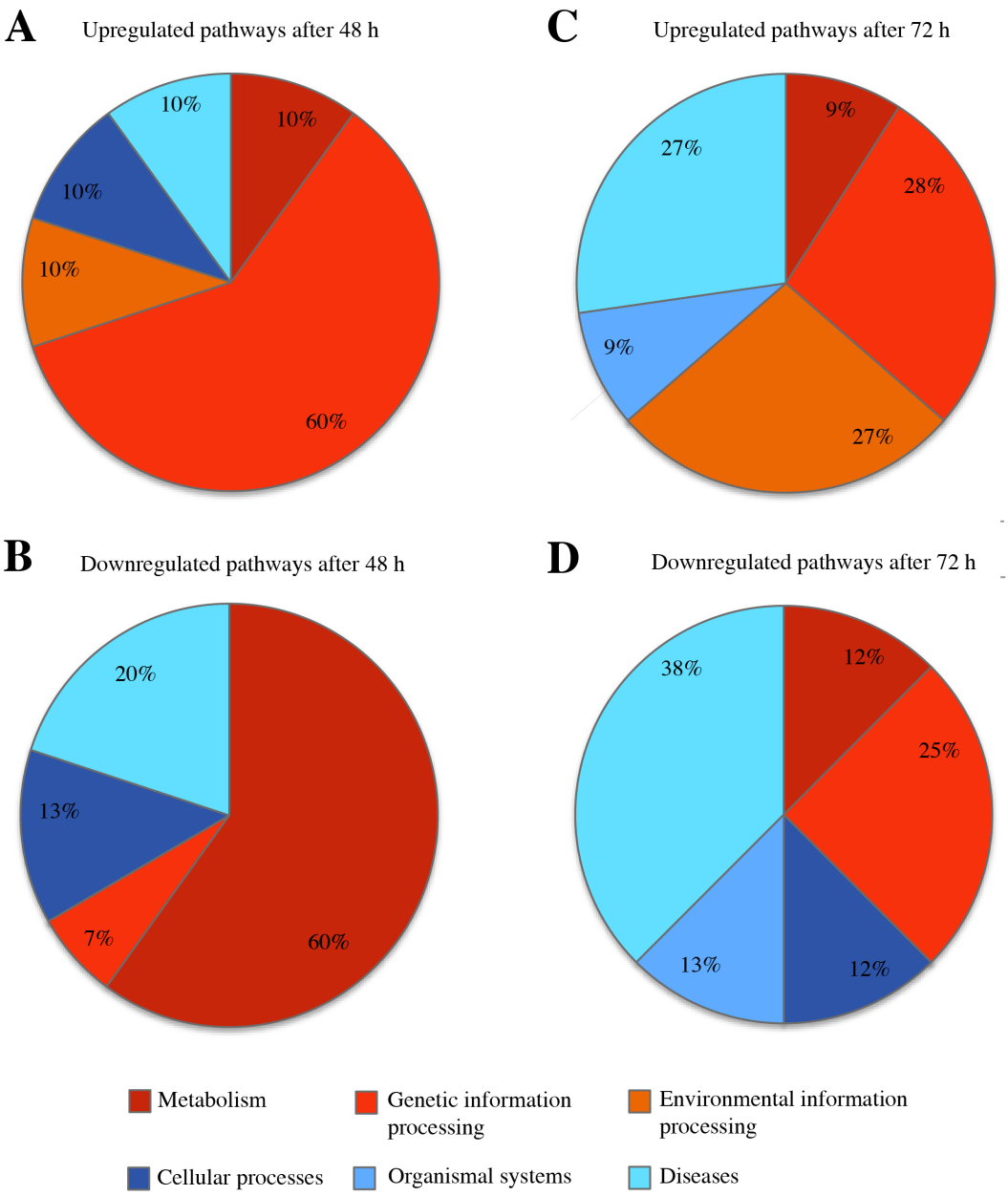

Figure 5.3: Categorisation of enriched pathways.
Pie charts show the percentage of up- and downregulated pathways of mRNA expression profiles of WT organoids grown in presence of *Apc*$^{1322/+}$ organoids compared to WT organoids only (WTxWT.1322) for 48 h and 72 h analysed using GSEA based on the KEGG pathway database.

5.2.4 Exposure to *Apc*$^{1322/+}$ organoids caused induction in DNA replication pathways in WT organoids after 48 h

DNA replication was identified as the most upregulated pathway after 48 h (NES = 3.088, FDR < 0.001) (Table 5.1A, Figure 5.4A), indicating that WT organoids have an increased rate of DNA replication as a consequence of being in close proximity to *Apc*$^{1322/+}$ organoids. In general, WT organoids exposed to *Apc*$^{1322/+}$ organoids demonstrated upregulation of pathways involved in the repair of DNA double strand breaks (DSBs), splicosome (NES = 3.075, FDR < 0.001), homologous recombination (NES = 2.878, FDR < 0.001), base excision repair (NES = 2.716, FDR < 0.001), and in the ribosome pathway (NES = 2.073, FDR = 0.034). Homologous recombination, for example, is involved in repairing DNA DSBs and damaged replication forks (Helleday 2010). Enrichment of homologous recombination suggests increased cell proliferation (Bishop *et al*. 2002).

As part of cellular processes, the cell cycle pathway was significantly upregulated pathway (NES = 2.241, FDR = 0.019). Categorised as environmental information processing, the calcium signalling pathway was significantly upregulated (NES = 2.018, FDR = 0.038), indicating that after only 48 h the calcium signal has already been altered by *Apc* deficient organoids in exposed WT organoids. Intracellular calcium ions (Ca^{2+}) play crucial roles in maintaining the cell's physiology, including gene transcription, cell cycle control, migration and apoptosis. Disruption of intracellular Ca^{2+} homeostasis has been shown to contribute to tumour initiation and progression (Cui *et al*. 2017).

Metabolic pathways accounted for the majority of downregulated pathways 48 h post exposure to *Apc*$^{1322/+}$ organoids. Of those, the most reduced pathway was oxidative phosphorylation (NES = -4.129, FDR < 0.001) (Table 5.1B, Figure 5.4B). Moreover, glutathione metabolism (NES = -2.336, FDR = 0.007), fatty acid metabolism (NES = -2.278, FDR = 0.01) and sphingolipid metabolism (NES = -2.032, FDR = 0.036) were also significantly altered. This indicates that pathways involved in nutritional storage are significantly reduced. Oxidative phosphorylation is a process during which cells use enzymes to oxidize nutrients, thereby releasing energy, which is then used to produce adenosine triphosphate (ATP) (Korzeniewski 2001). The reduction of these metabolic pathways shows a potential metabolic shift towards the Warburg effect (Zheng 2012). Taken together, these results

demonstrated a conclusive change in cell status: proliferation/cell division was potentially increased whilst metabolism was decreased.

In order to study gene expression changes, transcriptional profiles were compared between WT vs. WT organoids grown in presence of *Apc*$^{1322/+}$ organoids (WTxWT.1322). Results can be visualised with a MA plot (statistical significance: FDR < 0.05 and effect size: $\log_2$ fold change ≥ 1), which plots the differences between measurements taken in WT and WT.1322 by transforming the data onto M (log ratio) and A (mean average) scales. MA plots detect significantly altered genes between WT and WT.1322. However, no significant gene expression changes were detected after 48 h (Figure 5.5A, Table 5.2).

Nevertheless, GSEA identified genes that led to the enriched signature in DNA replication, some of which were *Pold2*, *Pold3*, *Pold4*, *Pole*, *Mcm4* and *Mcm6* among others. The expression changes of these genes were verified using quantitative reverse transcriptase-PCR (qRT-PCR). It was shown that *Pold3* (t-test with Welch's correction: $p = 0.047$), *Pold4* ($p = 0.03$) and *Mcm6* ($p = 0.031$) were significantly upregulated in WT organoids exposed to *Apc*$^{1322/+}$ organoids, indicating that these genes significantly contributed to the induction of this pathway (Figure 5.5B). *Pold3* and *Pold4* also significantly contributed to the upregulation of homologous recombination and the base excision repair pathway. However, the genes *Pold3* (0.24-fold, $p > 0.05$), *Pold4* (0.13, $p > 0.05$), and *Mcm6* (0.11, $p > 0.05$) were not significant in the RNA analysis. Thus, these results have to be analysed with caution.

Taken together, this indicates that exposure to *Apc*$^{1322/+}$ organoids for 48 h is not long enough to see global transcriptional changes in gene expression alteration in WT organoids.

A

Upregulated pathway after 48 h	NES	*FDR* value
DNA replication	3.088	<0.001
Splicosome	3.075	<0.001
Homologous recombination	2.878	<0.001
Base excision repair	2.716	<0.001
RNA degradation	2.377	0.009
Cell cycle	2.241	0.019
Pyrimidine metabolism	2.098	0.032
Ribosome	2.073	0.034
Pathways in cancer	2.052	0.034
Calcium signaling pathway	2.018	0.038

B

Downregulated pathway after 48 h	NES	*FDR* value
Parkinsons disease	-4.161	<0.001
Oxidative phosphorylation	-4.129	<0.001
Huntigtons disease	-3.425	<0.001
Proteasome	-3.226	<0.001
Alzheimers disease	-2.914	<0.001
Drug metabolism cytochrome p450	-2.596	<0.001
Lysosome	-2.516	<0.001
Glutathione metabolism	-2.336	0.007
Fatty acid metabolism	-2.278	0.010
Sphingolipid metabolism	-2.032	0.036

Table 5.1: Altered pathways in WT organoids exposed to *Apc*$^{1322/+}$ for 48 h.
GSEA identified multiple enriched pathways based on the KEGG gene set. A) shows the ten most upregulated pathways and B) the ten most downregulated pathways after 48 h. Cut-off *FDR*-value = 0.05. NES, normalised enrichment score; FDR, false discovery rate.

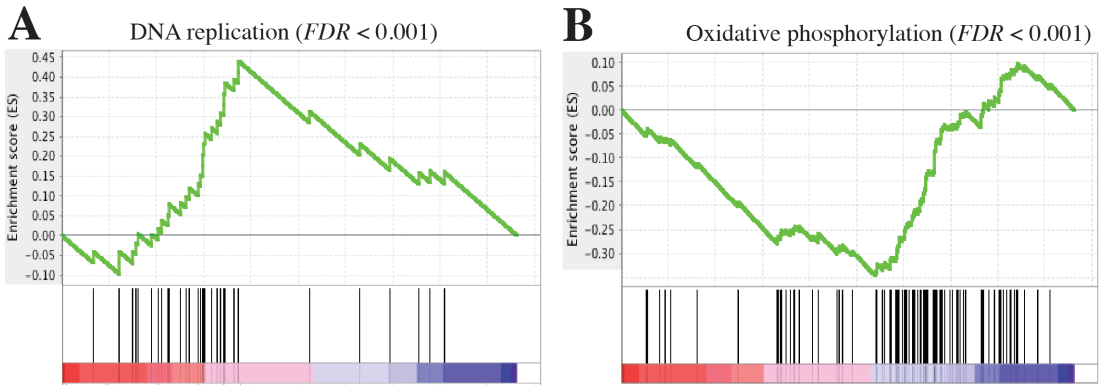

Figure 5.4: GSEA expression profiles for WTxWT.1322 after 48 h.
Representative enrichment plots resulting from the comparison between WT organoids exposed to *Apc*$^{1322/+}$ and WT organoids only using the established gene set KEGG. WT organoids exposed to *Apc*$^{1322/+}$ were positively enriched for DNA replication (A), while negatively enriched for genes in the oxidative phosphorylation pathway (B) after 48 h. Vertical lines indicate the positions of the gene along the comparison for each gene set. FDR, false discovery rate.

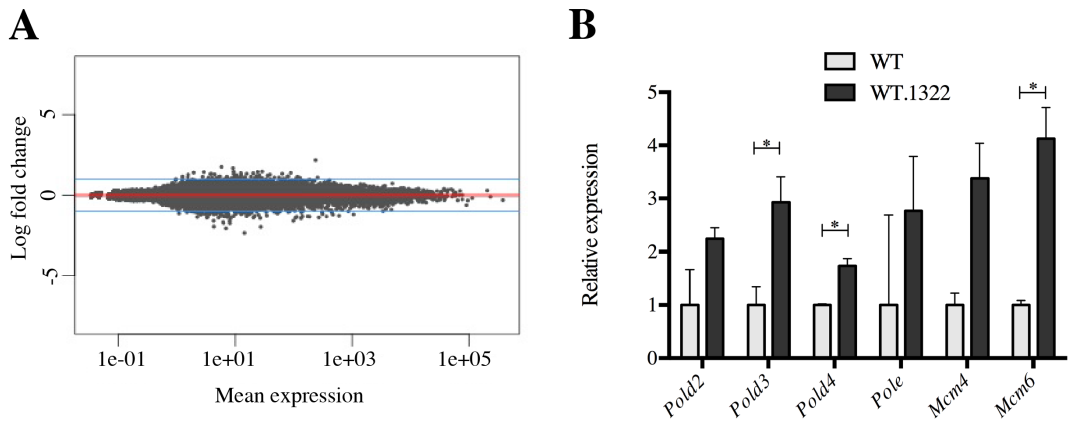

Figure 5.5: Gene expression changes of WT organoids exposed to *Apc*$^{1322/+}$ organoids after 48 h.
A) MA plots indicating the differential expression of genes between WT and WT organoids grown in presence of *Apc*$^{1322/+}$ organoids after 48 h. Grey dots indicate genes that show no statistically significant difference in abundance between WTxWT.1322 organoids (FDR < 0.05). The blue line indicates the $\log_2$ fold change cut-off of 1. B) Gene expression changes measured with qPCR. Genes related to upregulated pathways of DNA replication, homologous recombination and base excision repair. Three genes were significantly upregulated (asterisk = $p < 0.05$) in WT organoids exposed to *Apc*$^{1322/+}$ organoids after 48 h. Error bar represents standard error or mean (SEM). *Pold2*, *Pold3*, *Pold4, DNA polymerase delta subunit 2, 3, 4*, respectively; *Pole*, *DNA polymerase epsilon*; *Mcm4*, *Mcm6*, *mini-chromosome maintenance complex component 4, 6*, respectively.

A

Upregulated genes after 48 h	log2 fold change	p-value
mt-Co3	2.17	0.495
1110032F04Rik	1.75	0.828
D16Ertd472e	1.47	1.000
Gm3468	1.45	0.962
9430065F17Rik	1.45	1.000
Akap6	1.43	1.000
Hecw1	1.39	1.000
Rpl3-ps2	1.38	1.000
Guca1b	1.37	1.000
Smkr-ps	1.36	0.937

B

Downregulated genes after 48 h	log2 fold change	p-value
Gm9396	-2.35	NA
Gckr	-2.07	0.495
Car4	-1.97	0.564
1110028F18Rik	-1.96	0.644
Gm11769	-1.76	0.818
Rps13-ps1	-1.74	NA
Pdilt	-1.66	0.927
Tmem221	-1.6	0.963
Tmem27	-1.59	NA
Rit2	-1.58	0.991

Table 5.2: Gene expression changes of WT organoids exposed to *Apc*$^{1322/+}$ after 48 h.
A) Shows the ten most upregulated and B) the ten most downregulated genes ($\log_2$ fold change) for WTxWT.1322 after 48 h. Statistical significance: $p \leq 0.05$.

5.2.5 *Apc*$^{1322/+}$ organoids activate mismatch repair and ECM receptor interaction pathways in adjacent WT organoids after 72 h

After 72 h, ribosome (NES = 3.347, FDR < 0.001) (Figure 5.6A), mismatch repair (MMR) (NES = 2.225, FDR = 0.01) and homologous recombination (NES = 1.938, FDR = 0.041) pathways were significantly upregulated in WT exposed to mutant organoids (Table 5.3A). Ribosomes play a major role in protein synthesis and the process includes ribosome DNA transcription in the nucleus, rRNA assembly in the neoplasm and ribosome completion in the cytoplasm (Cisterna *et al*. 2010). There is evidence that upregulation of ribosome biogenesis poses an increased risk of CRC onset (Derenzini *et al*. 2017).

The MMR pathway is involved in multiple processes including apoptosis, and the MMR mechanism corrects mutations arising during DNA replication or damage. Lack of MMR-mediated DNA repair can initiate tumourigenesis resulting in a phenotype known as microsatellite instability (MSI) and strikingly loss of APC alone can contribute to MMR-deficient tumourigenesis, as mutations in MMR and APC can enhance MSI and lead to the accumulation of more mutations over time (Li *et al*. 2016).

The calcium signalling pathway was still enriched after 72 h (NES = 2.477, FDR = 0.003), and was comparable to the change observed at the 48h time point, indicating that calcium signals were still altered and homeostasis disrupted.

Interestingly, the ECM receptor interaction pathway (NES = 2.092, FDR = 0.02), also categorised as environmental information processing, was significantly upregulated after 72 h in WT organoids when exposed to *Apc* deficient organoids. The extracellular matrix (ECM) plays an important role in the maintenance of cell tissue and structure, and function (Hayes *et al*. 2016). Specific interactions between cells and the ECM are mediated by transmembrane molecules, and these molecules control gene expression, cell proliferation, differentiation, and migration among other aspects of a cell's life (Teller *et al*. 2001). Expression changes of ECM proteins were shown to have a high impact on tumour development, as ECM structurally supports tumour cells and their cellular functions (Hay 1993, Hayes *et al*. 2016, Stankevicius *et al*. 2016). Thus, upregulation of this pathway hints towards altered cell development and homeostasis.

GSEA revealed significantly downregulated pathways in the category of genetic information processing. The splicosome pathway was the most affected pathway in this category (NES = -3.759, FDR < 0.001) (Figure 5.6B, Table 5.3B), which was interesting, as it was significantly upregulated after 48 h. Other downregulated pathways included proteasome (NES = -3.438, FDR < 0.001), ubiquitin-mediated proteolysis (NES = -2.731, FDR < 0.001) and basal transcription factors (NES = -2.305, FDR = 0.006).

Oxidative phosphorylation was still identified as the most reduced pathway in the metabolic pathway category (NES = -4.5, FDR < 0.001). Oxidative phosphorylation is the major energy provider of a cell, indicating that energy production is reduced after 72 h. However, it might also indicate that by downregulation of the oxidative phosphorylation pathway more ROS were accumulated, which are known to cause mutations (Yadav *et al*. 2015). Defects in oxidative phosphorylation are one of the key reasons for attenuation of apoptosis in cancer cells (Dey *et al*. 2000). Here, the apoptosis pathway was significantly reduced (NES = -2.003, FDR = 0.033) as well, strengthening the above stated hypothesis.

Further, the insulin signalling pathway (NES = -2.464, FDR = 0.002) was significantly downregulated as part of the organismal systems category. Expression changes in components of the insulin growth factor system can contribute to the transformation of normal colonic epithelial cells (Vigneri *et al*. 2015).

Transcriptional profiles were analysed and 54 upregulated and 26 downregulated genes were detected in WT organoids exposed to *Apc* deficient organoids when compared to WT organoids only after 72 h (Figure 5.7A). The 50 most differentially expressed genes are visualised in Figure 5.8. The top ten most up- and downregulated genes are listed in Table 5.4A and B, respectively. Interestingly, *Lamb1* (1.74-fold, p = 0.03) was significantly upregulated as part of the ECM receptor interaction pathway. *Lamb1* interacts with integrins to form a cell adhesion network in the intestinal epithelium (McCole 2014). Induction of *Lamb1* could suggest changes in the basal lamina thereby potentially altering the structure of such cell adhesion network.

Moreover, GSEA identified various genes contributing to the enrichment of MMR, some of which included *Pold2*, *Pold3, Pold4* and *Pole*, as well as *Mhl1* and *Msh6*. *Pold3* (t-test with Welch's correction: p = 0.012) and *Pold4* (p = 0.03) were

significantly induced, indicating these genes might contribute to the upregulation of the MMR pathway (Figure 5.7B).

Bax and *Casp6*, among other genes identified by GSEA, might contribute to the reduction seen in the apoptosis pathway. However, verification via qPCR did not confirm this result (Figure 5.7B). *Bcl2l15* (-1.27fold, p = 0.049) and *Osgin1* (-1.04fold, p = 0.005), both regulators of apoptosis (Sinicrope *et al*. 2008, Yao *et al*. 2008), were also downregulated. This is consistent with the findings from GSEA, as apoptosis was significantly reduced. When downregulated, the oxidative stress induced growth inhibitor 1 (*Osgin1*) does not respond to oxidative stress and cells will continue to grow (Liu *et al*. 2014). *Osgin1* has been shown to be induced by DNA damage (Yao *et al*. 2008), which is in line with the induced MMR pathway.

Taken together, this indicates that exposure of WT organoids to $Apc^{1322/+}$ organoids for 72 h was sufficient to cause significant alteration in gene expression compared to WT organoids only. This further suggests that these alterations in pathways are early events in the transformation. Collectively, these findings suggest that exposure of $Apc^{1322/+}$ organoids to WT organoids for 72 h enforced transcriptional changes that alter critical cellular processes associated with tumour initiation.

A

Upregulated pathway after 72 h	NES	*FDR* value
Neuroactive ligand receptor interaction	3.543	<0.001
Ribosome	3.347	<0.001
Axon guidance	2.552	0.002
Calcium signaling pathway	2.477	0.003
Dilated cardiomyopathy	2.434	0.003
Mismatch repair	2.255	0.010
Purine metabolism	2.144	0.019
Hypertrophic cardiomyopathy	2.096	0.022
ECM receptor interaction	2.092	0.020
Arrhythmogenic right ventricular cardiomyopathy	2.013	0.030

B

Downregulated pathway after 72 h	NES	*FDR* value
Huntigtons disease	-4.625	<0.001
Oxidative phosphorylation	-4.500	<0.001
Parkinsons disease	-3.845	<0.001
Splicosome	-3.759	<0.001
Alzheimers disease	-3.440	<0.001
Proteasome	-3.438	<0.001
Aminoacyl tRNA biosynthesis	-2.801	<0.001
Ubiquitin mediated proteolysis	-2.731	<0.001
Lysosome	-2.529	0.001
Insulin signaling pathway	-2.464	0.002

Table 5.3: Altered pathways in WT organoids exposed to *Apc*$^{1322/+}$ for 72 h.
GSEA identified multiple enriched pathways based on the KEGG gene set. A) shows the ten most upregulated pathways and B) the ten most downregulated pathways after 72 h, respectively. Cut-off *FDR*-value = 0.05. NES, normalised enrichment score; FDR, false discovery rate.

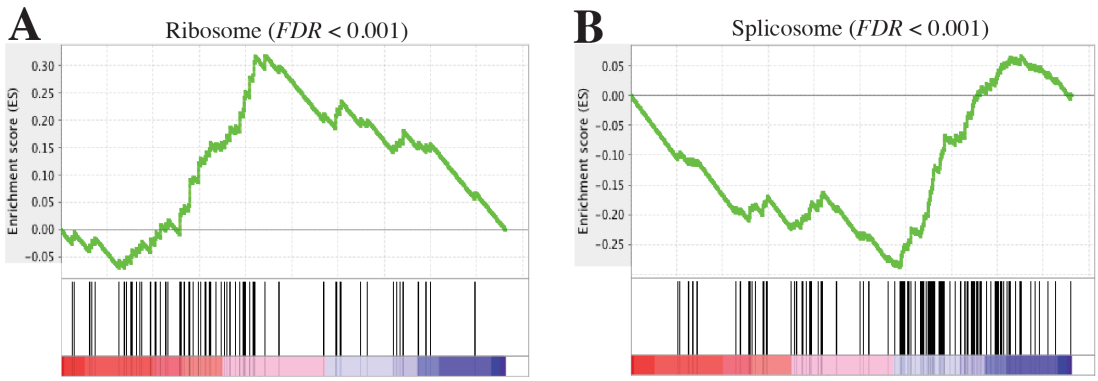

Figure 5.6: GSEA expression profiles for WTxWT.1322 after 72 h.
Representative enrichment plots resulting from the comparison between WT organoids exposed to *Apc*$^{1322/+}$ and WT organoids only using the established gene set KEGG. WT organoids exposed to *Apc*$^{1322/+}$ were positively enriched for ribosome (A), while negatively enriched for genes in the splicosome pathway (B) after 72 h. Vertical lines indicate the positions of the gene along the comparison for each gene set. FDR, false discovery rate.

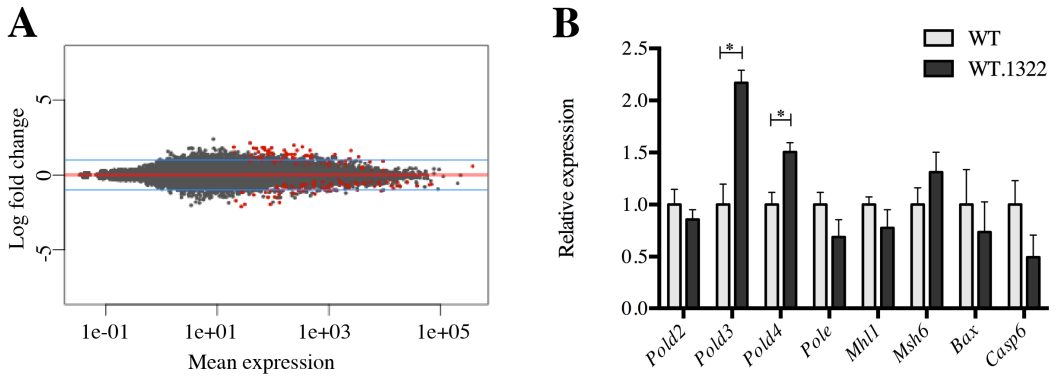

Figure 5.7: Gene expression changes of WT organoids exposed to mutants after 72 h.
A) Over- and underexpressed genes in WT organoids exposed to *Apc*$^{1322/+}$ organoids compared to WT organoids only. MA plots indicating the differential expression of genes between WT and WT organoids grown in presence of *Apc*$^{1322/+}$ organoids after 48 hours. Grey dots indicate genes that show no statistically significant difference in abundance between WTxWT.1322 organoids, whilst red dots indicate significantly differentially expressed genes (FDR < 0.05). The blue line indicates the $\log_2$ fold change cut-off of 1. B) Genes related to the upregulated MMR pathway and downregulated apoptosis pathway. *Pold3* and *Pold4* genes were significantly upregulated ($p < 0.05$) as part of the MMR pathway in WT organoids exposed to *Apc*$^{1322/+}$ organoids after 72 h. Error bar represents standard error or mean (SEM). Significance: $p < 0.05$ (*). *Pold2*, *Pold3*, *Pold4*, *DNA polymerase delta subunit 2, 3, 4*, respectively; *Pole*, *DNA polymerase epsilon*; *Mhl1*, *MutL homolog 1*; *Msh6*, *MutS homolog 6*; *Bax, Bcl-2-associated X*; *Casp6*, *Caspase 6*.

A

Upregulated genes after 72 h	log2 fold change	p-value
Gsap	2.13	0.001
Sema3f	1.98	0.001
Dpysl3	1.88	0.001
Lzts1	1.86	0.014
Mvb12b	1.84	0.005
8430408G22Rik	1.84	0.012
Vill	1.82	0.001
AI481877	1.79	0.017
Casp12	1.76	0.025
Lamb1	1.74	0.030

B

Downregulated genes after 72 h	log2 fold change	p-value
Aqp8	-2.1	0.012
Rpl3-ps2	-1.96	0.014
Gm4294	-1.96	0.015
Fosb	-1.84	0.029
Bdh2	-1.72	0.045
Sgk1	-1.5	0.044
Pros1	-1.49	0.005
Slamf9	-1.47	0.007
Mpz	-1.33	0.010
Hoxa7	-1.31	0.038

Table 5.4: Gene expression changes of WT organoids exposed to *Apc*$^{1322/+}$ after 72 h.
A) Shows the ten most upregulated and B) the ten most downregulated genes ($\log_2$ fold change) for WTxWT.1322 after 72 h. Statistical significance: $p \leq 0.05$.

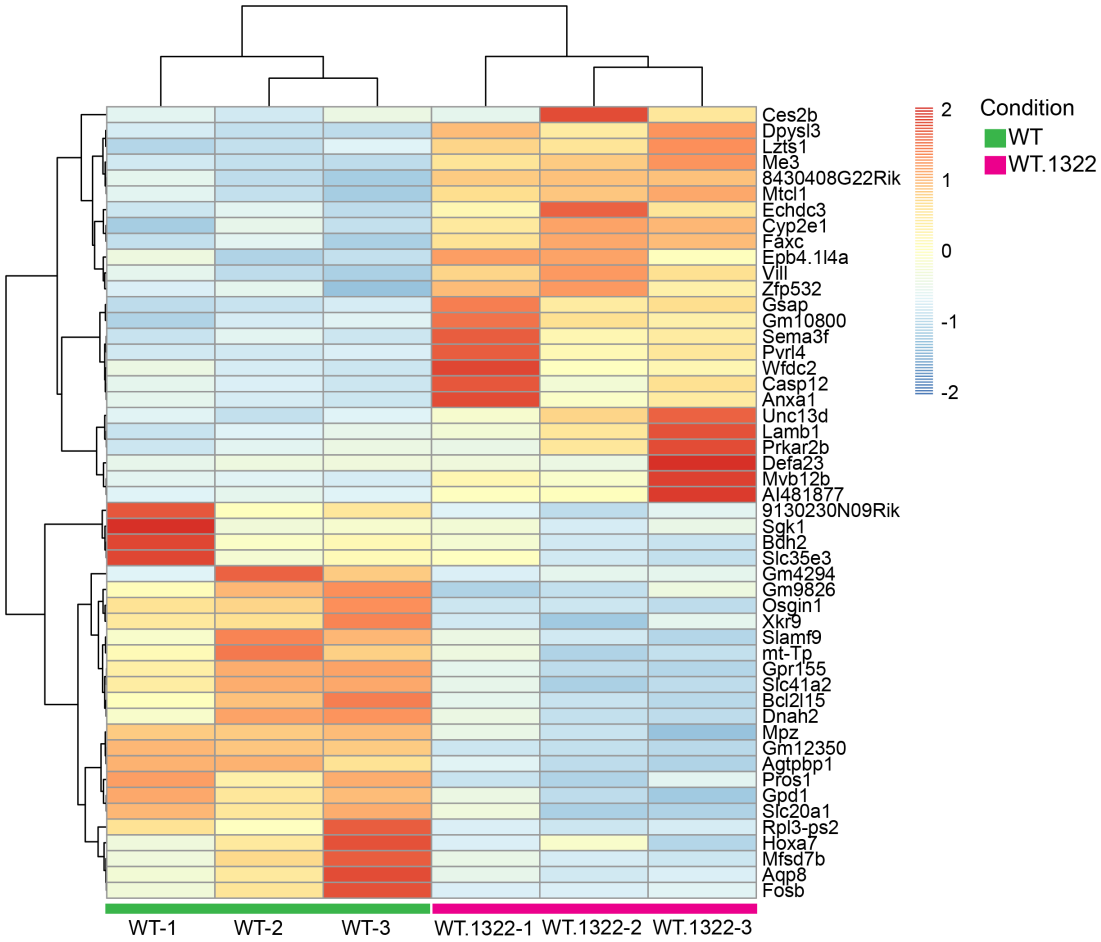

Figure 5.8: Differential gene expression profiles between WT and WT.1322 after 72 h.
Heatmap shows the 25 most significantly upregulated and the 25 most downregulated genes between WT organoids (green) and WT organoids exposed to mutants (pink). Columns for WT organoids and WT organoids exposed to mutants refer to biological replicates WT-1 – WT-3 and WT.1322-1 – WT.1322-3, respectively.

5.3 Discussion

Our understanding of the earliest events associated with neoplastic transformation remains limited. To gain insight into the earliest stages of colon cancer development, interactions between *Apc*$^{1322/+}$ and WT organoids were investigated in a co-culture set up. This experimental design allowed us to investigate how *Apc* deficient organoids influence WT organoids when grown adjacent to each other for 48 h and 72 h. Understanding the nature of these interactions might uncover specific intercellular signalling pathways that could be monitored and targeted for cancer prevention.

The main focus here was to study gene expression patterns in WT organoids grown in presence of *Apc* deficient organoids compared to WT organoids only. An important observation in the current study is that a heterozygous mutation (*Apc*$^{1322/+}$) in organoids grown adjacent to WT organoids can activate distinct transcriptional changes within the WT epithelium after only 48 h and 72 h. Indeed, transcriptionally distinct gene signatures were identified in WT organoids exposed to *Apc*$^{1322/+}$ organoids, as they clustered slightly independently from WT organoids only, indicating that *Apc*$^{1322/+}$ organoids have an effect on WT organoids.

DNA replication was identified as the main upregulated pathway in WT organoids exposed to *Apc* deficient organoids for 48 h. Incidents during DNA replication can cause replicative stress, which is a main feature in the early stages of tumourigenesis (Herlihy *et al*. 2017). DNA replication is tightly controlled in normal cells and genome duplication in dividing cells makes DNA replication an important factor in limiting cancer risk. For instance, disruptions in the catalytic activity of the DNA polymerase subunit δ (POLD) increase genomic instability (Pillaire *et al*. 2010). POLD proteins are thought to replicate the lagging strand and are involved in DNA repair, chromosomal replication and participate in DNA MMR and base excision repair, key processes shown to be defective in CRC (Miquel *et al*. 2007). Upregulation of *Pold3* and *Pold4* in this study could hint towards increased replication or lack of DNA repair.

The MCM protein family is essential for the initiation of genome replication, and specifically *Mcm6* is involved in the initiation of genome replication and elongation, and ensures that chromosomal replication occurs once per cell cycle (Maiorano *et al*. 2006). Here, *Mcm6* was significantly induced, which could indicate

its potential role in these processes. Moreover, homologous recombination was also significantly upregulated. Perturbations in homologous recombination can alter genome stability and initiate LOH (Pires *et al*. 2017). Enrichment of homologous recombination hints towards increased cell proliferation (Bishop *et al*. 2002), which in the future could be confirmed with an organoid formation and proliferation assay.

The main downregulated pathways after 48 h were categorised as metabolic pathways, with oxidative phosphorylation being a key player. Metabolic activities in normal cells rely on oxidative phosphorylation to generate ATP for energy. It is a known fact that in cancer cells, oxidative phosphorylation is reduced while anaerobic glycolysis is increased, a phenomenon known as the Warburg effect (Zheng 2012). In this study, downregulation of oxidative phosphorylation in exposed WT organoids indicated reduced aerobic energy production, which could be analysed by monitoring changes in level of Acetyl-CoA and Lactate. Glycolysis was upregulated, however not yet significantly (NES = 1.458, FDR = 0.33).

Other downregulated metabolic pathways included the fatty acid metabolism and glutathione metabolism pathways, suggesting that pathways involved in nutritional storage were significantly downregulated. The role of fatty acid metabolism in cancer is complex and controversial, as on the one hand, fatty acid metabolism is involved in cancer development and cell growth (Deberardinis *et al*. 2008), but on the other hand, fatty acid metabolism plays a role in the energy supply for cancer cells through beta oxidation and glucose metabolism (Samudio *et al*. 2010). Reduced fatty acid metabolism indicates that cells no longer store neutral lipids and divert the oxidation of fatty acids from energy production to support tumour proliferation (Xu *et al*. 2017). This could be verified with oil red O staining. Glutathione is an antioxidant protecting cells from damage (Wu *et al*. 2004). Thus, glutathione deficiency could lead to increased susceptibility to oxidative stress, which in turn can lead to increased levels of ROS. Excess of ROS formation generates cell damage that can lead to a mutagenic environment in the long term, and thus to the progression to cancer (Traverso *et al*. 2013).

Taken together, this firstly indicates that $Apc^{1322/+}$ organoids had a strong effect on WT organoids after only 48 h and secondly, pathways such as DNA replication and metabolic pathways were affected early on in the progression to tumour development. These results showed a conclusive change in cell status, as proliferation is potentially increased whilst metabolism decreased.

Ribosome biogenesis was significantly upregulated in exposed WT organoids after both time points, which could indicate tumour initiation (Derenzini *et al*. 2017). Since DNA replication was significantly upregulated, it is unsurprising to find ribosome biogenesis upregulated, as it regulates cell cycle progression in proliferating cells (Thomas 2000). Upregulation of the ribosome pathway has been identified in tumours of CRC patients compared to matching normal mucosa (Guo *et al*. 2017). However, our results demonstrate that this change is an early step in tumourigenesis and represents a functional change in field cancerization.

The DNA MMR pathway was significantly upregulated in WT organoids exposed to mutants after 72 h. Alterations in the DNA MMR system have been linked to CRC (Li *et al*. 2016). Impaired MMR gene function leads to the onset of MSI tumours (Kheirelseid *et al*. 2013). Germline mutations in the MMR genes *MSH2*, *MSH6*, or *MLH1* predispose to CRC (Jiricny *et al*. 2003, Truninger *et al*. 2005). GSEA identified a certain number of genes contributing to this induction, which included *Pold2*, *Pold3, Pold4* and *Pole*, as well as *Mhl1* and *Msh6*. These genes play an important role in mediating correct DNA MMR and DNA replication (Jiricny *et al*. 2003, Pal *et al*. 2008). Briefly, MMR starts with the heterodimer MSH6 recognising the mismatched base pairs and followed by the recruitment of MHL1-PMS2 heterodimer complex. PCNA is then loaded and interacts with MHL1-PMS2 to enable PMS2 to exert its endonuclease activity. The exonuclease 1 then mediates excision of the mismatched DNA. Finally, DNA polymerase δ synthesises new DNA to fill the excised bases (Li *et al*. 2016). Upregulation of MMR might indicate a greater degree of mismatched DNA. Overexpression of *Msh6* could suggest difficulties in mismatched base pair recognition. Indeed, *Pold3* and *Pold4* were found to be significantly upregulated in exposed WT organoids, demonstrating that at this step in the pathway significant alterations occur and that new DNA base pairs are potentially not accurately synthesised to fill the excided bases. However, the network of these genes caused the significant upregulation of the MMR pathway rather than individual genes. Nevertheless, changes in DNA MMR expression of WT organoids exposed to $Apc^{1322/+}$ organoids seem to be an early step in carcinogenesis.

Furthermore, the ECM receptor interaction pathway was significantly upregulated after 72 h. The ECM is composed of the basement membrane, containing the specific macromolecules type IV collagens, laminins and proteoglycans, and the interstitial matrix, containing collagens and fibronectins.

Laminins are the most abundant glycoproteins in the basal lamina and are involved in cell differentiation, migration and adhesion (Teller *et al*. 2001). ECM composition, stiffness and condition regulate normal cell behaviour and tissue development, and are important during major developmental processes. Its components are in constant interaction with the epithelia, thereby instigating intracellular activities that are related to a variety of biological functions, such as tissue development and homeostasis (Bonnans *et al*. 2014). These interactions are mediated by specific cell surface receptors called integrins, which are the largest family of receptors mediating cell adhesion to fibronectins, and laminins to collagens (Heino *et al*. 2009). Gene expression of relevant ECM genes was shown to be significantly different between CRC tumour and matched normal samples (Xu *et al*. 2017). ECM remodelling, especially via the degradation of extracellular proteins and the collagen matrix is necessary for tumour expansion, metastasis and epithelial to mesenchymal transition (Kessenbrock *et al*. 2010, Lu *et al*. 2011). The gene expression pattern observed in ECM indicates substantial dysregulation and remodelling of ECM during tumourigenesis (Hayes *et al*. 2016). ECM interactions influence cell shape, function, proliferation, migration and apoptosis. Upregulation of the ECM interaction pathway could therefore indicate alterations of those characteristics occurring very early on in the transformation.

Here, the largest dysregulation was observed in laminin subunit beta-1 (*Lamb1*). It was significantly upregulated in WT organoids exposed to $Apc^{1322/+}$ organoids. However, this upregulation was mostly driven by one sample, as represented in a heatmap, which visualised the gene expression changes in each of the samples (Figure 5.8). Nevertheless, in the remaining biological replicates *Lamb1* was still upregulated. It is worth noting that alterations in *Lamb1* expression have been observed in colon cancer. Specifically, *Lamb1* has been reported in malignant epithelial to mesenchymal transition (Petz *et al*. 2012). Immunohistochemistry for *Lamb1* could be performed in murine intestines of WT and $Apc^{1322/+}$ mice to further verify the induction at the protein level.

As seen after 48 h, oxidative phosphorylation was still significantly downregulated after 72 h. Reduction in oxidative phosphorylation indicates that cells oxidise less nutrients and less energy in form of ATP is produced. Oxidative phosphorylation consists of five complexes in the mitochondria and components of these complexes are encoded by either mtDNA or nuclear DNA. Thus, alterations in

either mtDNA or nuclear DNA could potentially cause oxidative phosphorylation-deficiency. Furthermore, oxidative phosphorylation deficiency has been associated with an increase in ROS (Yadav *et al*. 2015). Excessive ROS production can lead to oxidative damage, which in turn can lead to DNA damage, replication errors and even to genetic abnormalities (Selim *et al*. 2017). This could explain the upregulation seen in the MMR and DNA replication pathway.

Oxidative phosphorylation deficiency has been associated with attenuation of apoptosis (Chandra *et al*. 2011). Thus, one could speculate that downregulation of oxidative phosphorylation influences expression of genes involved in the apoptosis pathway, as this pathway was significantly reduced in WT organoids exposed to $Apc^{1322/+}$ organoids. Especially, *Osgin1*, an oxidative stress response protein regulating apoptosis, was found significantly reduced. *Osgin1* has been shown to induce apoptosis through the induction of cytochrome *c* oxidase release and by its localisation to mitochondria (Yao *et al*. 2008). Thus, reduced expression of this gene could lead to increased cell proliferation, which could eventually result in tumour initiation and progression, as cells no longer respond to oxidative stress.

In summary, these results indicate that WT organoids were significantly affected by mutant $Apc^{1322/+}$ organoids after 72 h, and that exposed WT organoids underwent specific transcriptional changes very early on. DNA replication was induced after 48 h, while DNA MMR was induced after 72 h. This indicates that from its earliest stages, tumour development is associated with DNA replication stress leading to DNA DSBs, which eventually will lead to genomic instability and selective pressure for further mutations.

The initial hypothesis was that clonal interactions drive expansion. Features of such expansion are proliferation, replication, crypt fission and mutations. Gene sets in pathways contributing to proliferation and replication were activated, whilst metabolic pathways were downregulated in WT organoids grown adjacent to $Apc^{1322/+}$ organoids. These results provide insights into the dynamic and complex interplay occurring early in WT organoids after being exposed to $Apc^{1322/+}$ organoids.

6 Chapter VI: Influence of tumour-exposed fibroblasts on WT organoids

6.1 Introduction

In the previous chapter, the effect of mutated epithelium on normal epithelium in close proximity was investigated using murine intestinal organoids to better understand initial events in tumourigenesis. However, the transformation of normal to mutated epithelium is likely to be dependent on the interactions with the surrounding stroma (Parrinello *et al*. 2005). Therefore, this chapter focussed on the influence of tumour-exposed fibroblasts (TEFs) on WT organoids.

The stroma in healthy tissue acts as a barrier against tumourigenesis, but in the presence of tumour cells, crucial changes are initiated that convert the environment into one that supports tumourigenesis (Junttila *et al*. 2013). The stroma constitutes a large fraction of solid tumours and in some carcinomas it makes up more than 80% of the tumour mass. Stromal cells constitute a heterogeneous population of different cell types: the tumour stroma is composed of neoplastic cells, but also non-malignant cells, such as normal stromal cells, infiltrating immune cells, cytokines and chemokines, and specialised fibroblasts, termed cancer-associated fibroblasts (CAFs), all embedded in a network of extracellular matrix proteins (Belov *et al*. 2010, Rupp *et al*. 2015). The stroma is in direct contact with the adenoma and once it becomes activated, an altered phenotype is displayed that produces growth-promoting factors, as well as enhances tumour cell proliferation and migration, thus speeding up tumourigenesis and depicting important drivers of tumourigenesis (Mo *et al*. 2016).

A major contributor to the tumour microenvironment is inflammation (Kortlever *et al*. 2017). Inflammatory reactions within tumours have been associated with better prognosis for CRC patients, although different infiltrating immune cells affect tumour progression differently (Fridman *et al*. 2012). Specifically $CD8^+$ cells have been linked to better clinical outcome, as opposed to immune regulatory T cell populations that promote tumour escape from immune surveillance (Quigley *et al*.

2015). Immune infiltrates are also heterogeneous between tumour types, and are very diverse from patient to patient. Variable numbers of infiltrating immune cells are found in different tumours of the same type, and in different locations within and around a tumour (Fridman *et al*. 2012). Nevertheless, immune cell components are found at higher densities in tumours compared to normal tissues (see Chapter 3).

Fibroblasts, a major cell type in the colonic stroma, are responsible for tissue remodelling and homeostasis by providing scaffolding and regulatory growth factors (Chen *et al*. 2014). Myofibroblasts, found surrounding the colonic crypt, are mainly involved in the synthesis of various collagens and extracellular matrix proteins to provide scaffold (Kalluri 2016). In tumour tissues, activated fibroblasts expressing high levels of α-SMA are referred to CAFs. CAFs are suspected to promote tumour development and progression, since they nourish cancer cells with a vast number of growth factors. Thus, cancer cells are capable of reprogramming normal fibroblasts into CAFs with pro-tumourigenic activity and enhanced cell proliferation, a process that is mediated by cancer cell-derived factors (Mukaida *et al*. 2016). Studies using patient-derived organoids have shown that CAFs increase the frequency of tumour-initiating cells (Calon *et al*. 2015).

As shown in Chapter 3, the stroma that was in direct contact with adenomatous crypts became activated: a greater concentration of immune cells and fibroblasts were found surrounding the adenomatous mucosa. It has previously been shown that altered mucosal phenotypes that exhibit similar cellular makeup also produce growth-promoting factors, therefore promoting tumour progression (De Wever *et al*. 2003, Rasanen *et al*. 2010). Thus, there are various different pathways by which oncogenes can impact on the immune environment, and understanding this interplay will be important to improving immune eradication of tumours.

However, little is known regarding epithelial-stromal interactions in the very early stages of tumourigenesis and the accompanying critical steps leading to tumour progression. Here, we exposed WT murine organoids to $Apc^{1322/+}$ organoids and examined the changes in mRNA expression. Furthermore, $Apc^{1322/+}$ organoids were co-cultured with murine fibroblasts to generate tumour-exposed fibroblasts (TEFs). These TEFs were then exposed to WT organoids in order to investigate the reciprocal interactions between tumour-associated stroma and normal epithelium. Understanding these epithelial-stromal interactions may help to develop a better understanding of tumour initiation and progression.

In the first part of this chapter, the mRNA expression profiles of co-cultured epithelial organoids and fibroblasts are shown. In the second and third part, mRNA expression changes in WT organoids exposed to *Apc*$^{1322/+}$ organoids, and WT organoids co-cultured with TEFs were investigated, respectively, both co-cultured in a transwell setting (as opposed to adjacent to each other as shown in Chapter 5).

6.2 Distinct expression profiles between WT organoids and WT organoids exposed to either *Apc*$^{1322/+}$ organoids or tumour-exposed fibroblasts (TEFs)

In order to study the impact of tumour-exposed fibroblasts (TEFs) on WT organoids, gene expression changes were assessed on WT organoids co-cultured with *Apc*$^{1322/+}$ organoids, and on WT organoids co-cultured with TEFs, generated by co-culture with *Apc*$^{1322/+}$ organoids for 72 h in a transwell set up. These TEFs were then co-cultured with WT organoids for another 72 h (see section 2.8, 2.9; Figure 2.8). The 72 h time point here was chosen based on findings in Chapter 5 that showed maximal gene expression changes at 72 h rather than 48 h. Thus, the sample set was comprised of WT organoids, WT organoids exposed to *Apc*$^{1322/+}$ organoids, and WT organoids exposed to TEFs. RNA was extracted from all organoid groups in triplicate, and quality and quantity measured (see section 2.10.1, 2.10.2). Samples with a RIN value > 8 were chosen for mRNA sequencing (see section 2.10.3). RNA of *Apc*$^{1322/+}$ organoids, *Apc*$^{1322/+}$ organoids exposed to WT organoids and *Apc*$^{1322/+}$ organoids exposed to WT fibroblasts was also subjected to mRNA sequencing. After completing the transcriptome analysis, principal component analysis (PCA) was used to evaluate the broad transcriptional differences across all samples (Figure 6.1).

In general, WT and *Apc*$^{1322/+}$ organoids clustered separately from each other. Unsurprisingly, *Apc*$^{1322/+}$ organoids and *Apc*$^{1322/+}$ organoids exposed to WT organoids clustered together, however *Apc*$^{1322/+}$ organoids exposed to normal fibroblasts clustered separately. More importantly, a clear separation was visible between WT organoids and WT organoids exposed to *Apc*$^{1322/+}$ organoids (WT.1322). Strikingly,

WT organoids co-cultured with TEFs (WT.F.1322) clustered independently from both, WT organoids and those exposed to *Apc*$^{1322/+}$ organoids.

These results demonstrate that WT organoids are transcriptionally different from WT organoids exposed to *Apc*$^{1322/+}$ organoids, but more importantly that by adding a stromal component – tumour-exposed fibroblasts – transcription profiles change drastically: both WT organoids and WT organoids exposed to *Apc* deficient organoids were transcriptionally distinct from WT organoids exposed to TEFs, further highlighting the role of the stroma in early transformation.

This was further supported when comparing gene expression patterns between WT, WT.1322 and WT.F.1322 (Figure 6.2). Differential expression analysis identified the 50 most variable genes between these three conditions highlighting some of the genes driving the observed clustering pattern. Gene expression changes between WT and WT.1322 were similar, however distinct patterns were observed in WT.F.1322. Gene expression changes will be discussed in more detail between WT and WT.1322 organoids in section 6.3.2, and between WT and WT.F.1322 organoids in section 6.4.1.

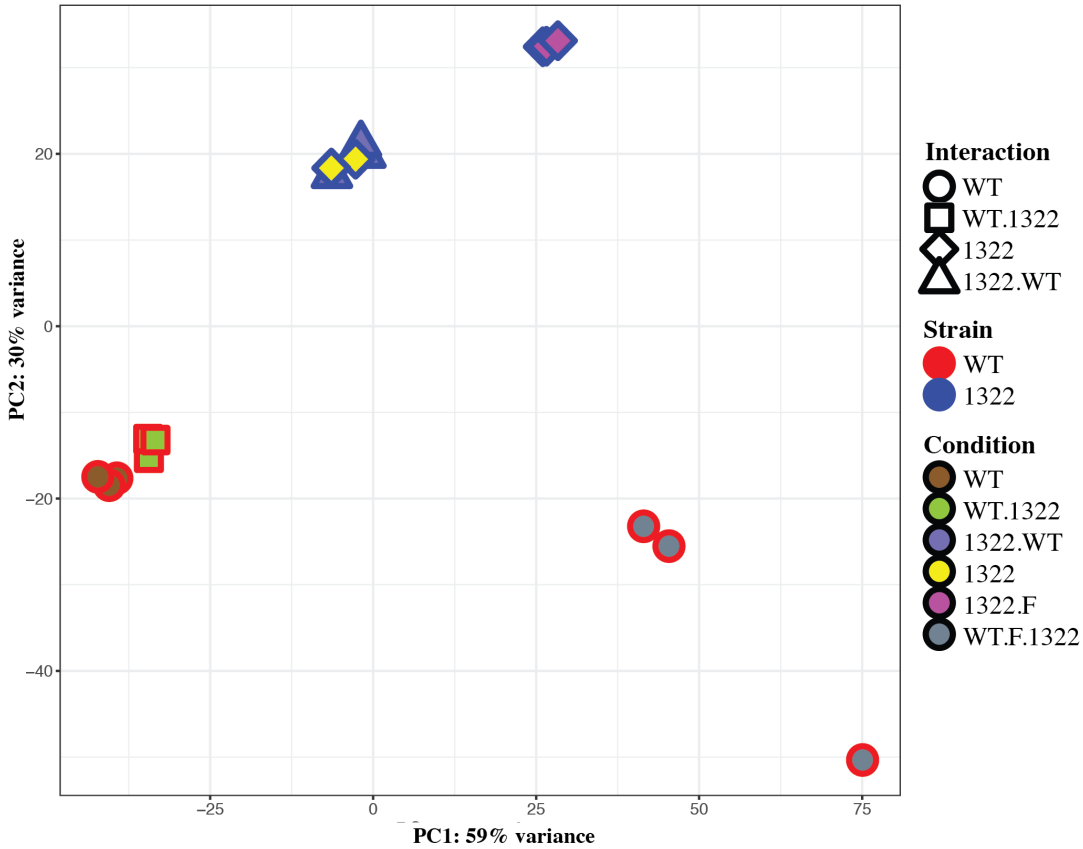

Figure 6.1: Effect of *Apc*$^{1322/+}$ organoids and TEFs on WT organoids.
PCA shows the variation in the RNA sequencing data. *Apc*$^{1322/+}$ organoids (1322; outlines in blue) are separately clustered from WT organoids (outlines in red). WT organoids (brown) cluster separately from mutant (green) organoids. WT and WT.1322 organoids cluster closer together than WT organoids exposed to TEFs (grey). *Apc*$^{1322/+}$ organoids (1322, yellow) and *Apc*$^{1322/+}$ organoids exposed to WT (1322.WT, purple) cluster together, but *Apc*$^{1322/+}$organoids exposed to normal fibroblasts (1322.F, pink), cluster separately.

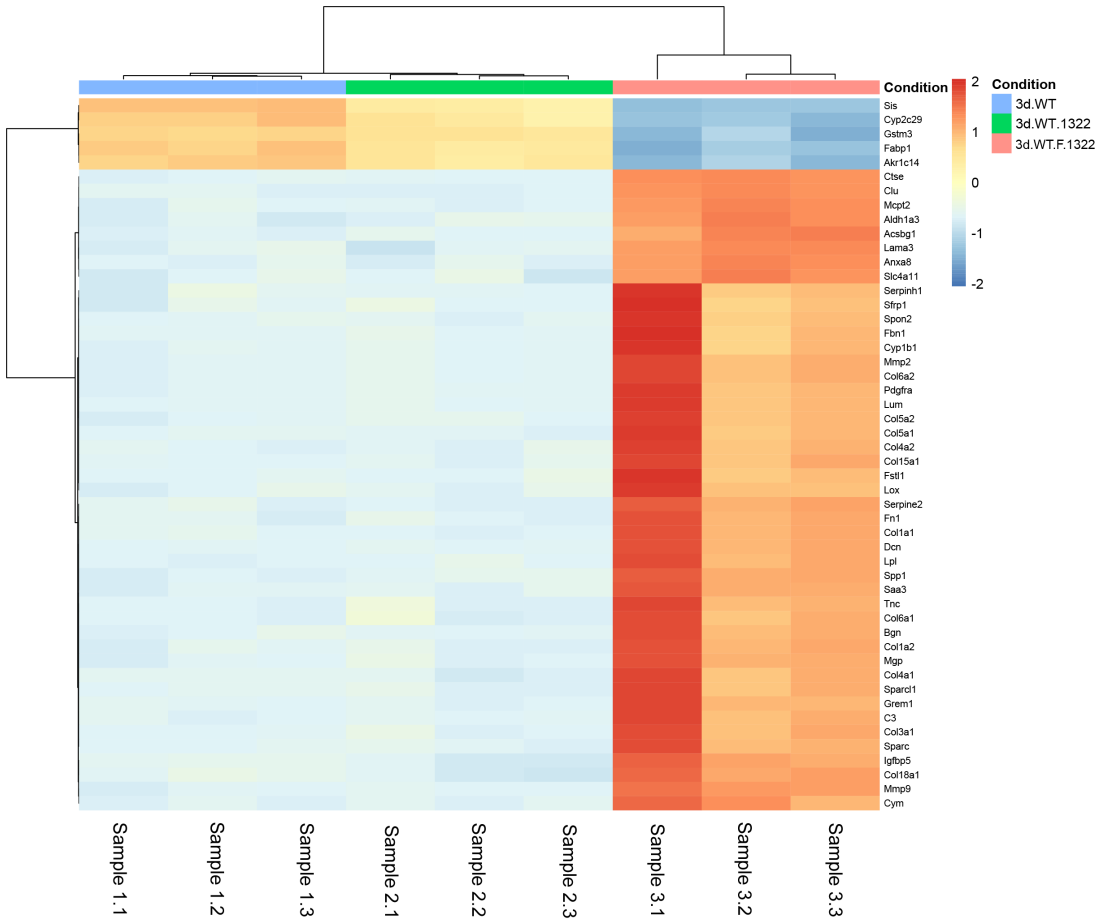

Figure 6.2: Comparison of WT, WT.1322 and WT.F.1322 gene expression patterns.
Heatmap shows the 50 most variable genes between WT (blue), WT.1322 (green) and WT.F.1322 (pink) explaining the separation of the PCA. The largest variation comes from WT organoids exposed to tumour-exposed fibroblasts (WT.F.1322). Each condition was sequenced in biological replicates.

6.3 Co-culture of WT and *Apc*$^{1322/+}$ organoids in a transwell setting

6.3.1 Exposure of WT organoids to *Apc*$^{1322/+}$ organoids activates pathways involved in DNA double strand break repair while metabolic pathways are reduced in WT organoids

Expression profiles were analysed using GSEA to detect altered pathways and results were cross-referenced with genes in the KEGG database (see section 2.10.5) to determine the signalling pathways responsible for the differential clustering observed in PCA. Overall, GSEA identified 6 significantly upregulated pathways (FDR < 0.05) in WT organoids exposed to *Apc*$^{1322/+}$ organoids compared to WT organoids alone only after 72 h, of which were 67% categorised into genetic information processing, 17% into diseases, and 16% into cellular processes (Figure 6.3A). In contrast, GSEA identified 14 downregulated pathways, of which were 50% categorised into metabolic pathways, 15% into cellular processes, 14% into organismal systems, 14% into diseases, and the remaining 7% fall into the category of environmental information processing (Figure 6.3B).

The most upregulated pathway, as part of the genetic information processing category, was the ribosome pathway (NES = 7.18, FDR < 0.001), indicating that this pathway is increased in WT organoids exposed to *Apc*$^{1322/+}$ organoids. Ribosomes are responsible for translating mRNA into proteins and upregulation of the ribosome pathway indicates an altered mRNA translation mechanism that has been shown to be a risk factor for cancer initiation (Nieminen *et al*. 2014).

Furthermore, as part of the cellular processes category, the cell cycle pathway was significantly upregulated (NES = 2.93, FDR < 0.001) (Figure 6.4A), indicating increased cell proliferation.

In general, WT organoids exposed to *Apc*$^{1322/+}$ organoids demonstrated upregulation of pathways involved in the repair of DNA DSBs, DNA replication (NES = 2.856, FDR < 0.001) (Figure 6.4B), splicosome (NES = 2.83, FDR < 0.001), and the DNA MMR pathway (NES = 2.506, FDR = 0.002) (Table 6.1A).

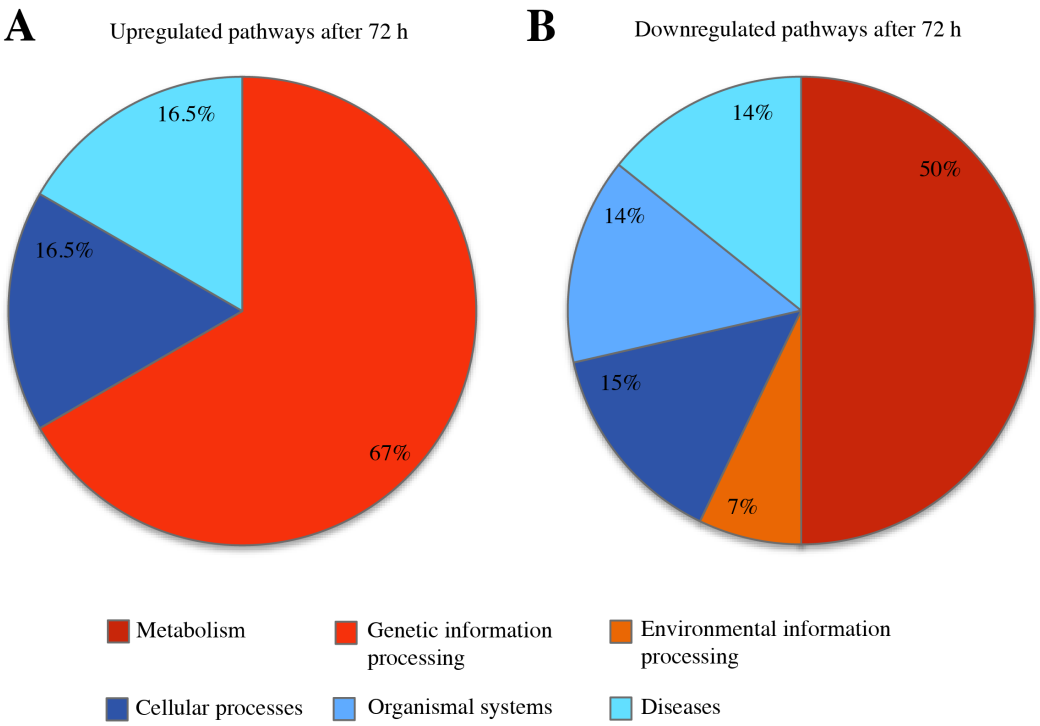

Figure 6.3: Categorisation of enriched pathways for WTxWT.1322.
Pie charts show the percentage of all upregulated (A) and downregulated (B) pathways of WT organoids co-cultured with WT organoids exposed to mutants (WTxWT.1322) for 72 h. Expression profiles were analysed using GSEA based on the KEGG pathway database.

A

Upregulated pathways	NES	*FDR* value
Ribosome	7.180	<0.001
Cell cycle	2.930	<0.001
DNA replication	2.856	<0.001
Splicosome	2.830	<0.001
Systemic lupus erythematosus	2.529	0.002
Mismatch repair	2.506	0.002
Purine metabolism	1.926	0.089
Homologous recombination	1.914	0.084
ECM receptor interaction	1.891	0.083
Nucleotide excision repair	1.793	0.133

B

Downregulated pathways	NES	*FDR* value
Peroxisome	-3.212	<0.001
Endocytosis	-2.961	0.001
Phosphatidylinositol signaling system	-2.778	0.001
ABC transporters	-2.539	0.004
PPAR signaling pathway	-2.440	0.006
Fatty acid metabolism	-2.382	0.007
Glycerophospholipid metabolism	-2.380	0.006
Citrate cycle	-2.280	0.010
Oxidative phosphorylation	-2.239	0.012
Glycerolipid metabolism	-2.238	0.011

Table 6.1: Enriched pathways for WT organoids exposed to *Apc*$^{1322/+}$ organoids for 72 h.
GSEA identified multiple enriched pathways based on the KEGG gene set. A) The ten most upregulated and B) downregulated pathways after 72 h. Cut-off FDR-value < 0.05.

The two most downregulated pathways, peroxisome (NES = -3.212, FDR < 0.001) (Figure 6.4C) and endocytosis (NES = -2.961, FDR = 0.001), were part of the cellular processes category, as identified by GSEA (Table 6.1B). Peroxisomes are involved in metabolic pathways, where they catalyse oxidation reaction, including fatty acid oxidation, the reduction of ROS, as well as enzymes that protect cells from oxidative damage. Thus, peroxisomes are essential for maintaining basic metabolic functions. Reduction of peroxisome activity can lead to disruptions in peroxisome homeostasis, thus initiating pathologies related to CRC (Kim *et al*. 2015, Tripathi *et al*. 2016). It is therefore not surprising that the majority of pathways that were downregulated after 72 h were categorised as metabolic pathways. Of those, the most downregulated one was the phosphatidylinositol signalling system (NES = -2.778, FDR = 0.001). Moreover, fatty acid metabolism (NES = -2.382, FDR = 0.007), glycerophospholipid metabolism (NES = -2.38, FDR = 0.006), citrate cycle (NES = -2.28, FDR = 0.01), oxidative phosphorylation (NES = -2.239, FDR = 0.012), glycerolipid metabolism (NES = -2.238, FDR = 0.011), and the drug metabolism cytochrome P450 pathway (NES = -2.011, FDR = 0.034) were significantly downregulated, indicating that pathways involved in nutritional storage were significantly reduced. It is also not surprising that fatty acid metabolism was downregulated, since peroxisomes are known to breakdown fatty acids (Delille *et al*. 2006).

Categorised as organismal systems, the PPAR signalling pathway (NES = -2.44, FDR = 0.006) (Figure 6.4D) and the insulin signalling pathway (NES = -2.051, FDR = 0.03) were significantly downregulated in WT organoids exposed to $Apc^{1322/+}$ organoids. Peroxisome proliferator-activated receptor (PPAR) signalling plays a role in cell differentiation and has anti-tumourigenic effects (Feige *et al*. 2006). When activated, PPAR induces apoptosis and controls tumour development by preventing proliferation, angiogenesis and reducing tumour microenvironment inflammation (Dai *et al*. 2010). Deficiency in PPAR has been associated with increased tumourigenicity in mouse intestine and colon (McAlpine *et al*. 2006). Thus, its downregulation might indicate loss of its protective functions and potentially induce tumour development. PPAR is also involved in glucose metabolism through improving insulin sensitivity (Dai *et al*. 2010). This could explain the reduction seen for the insulin signalling pathway.

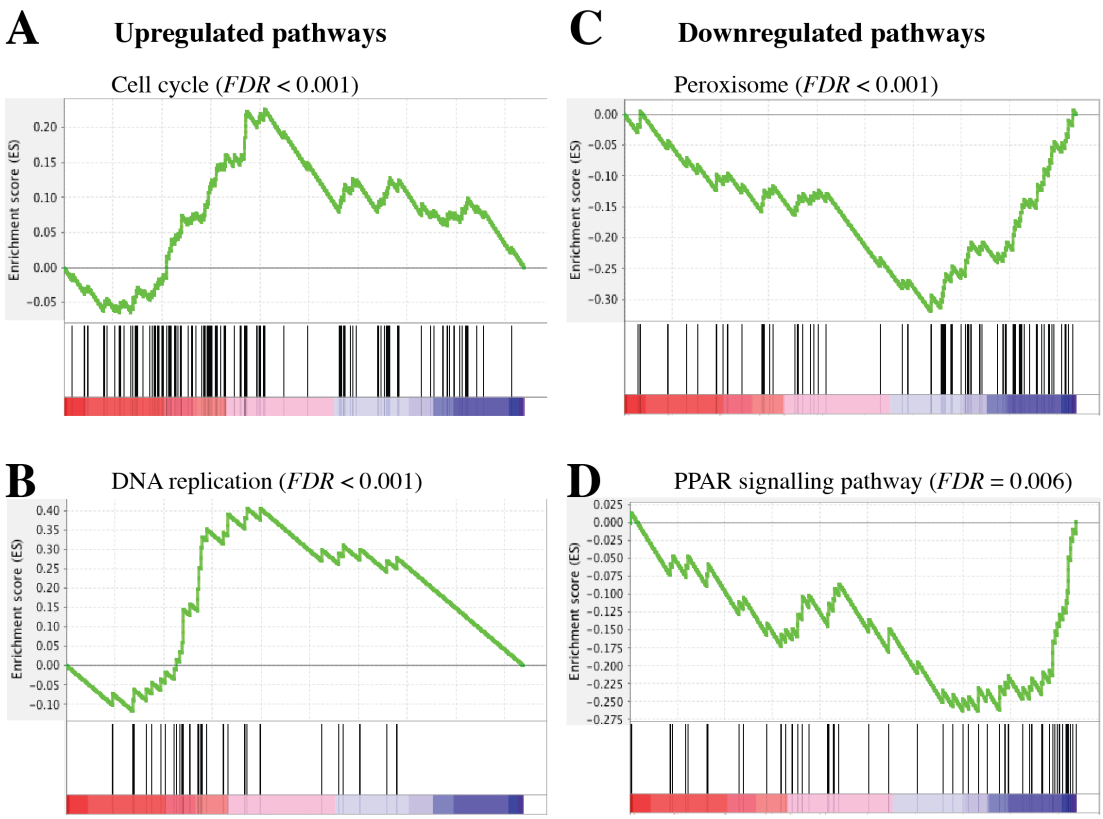

Figure 6.4: GSEA expression profiles for WTxWT.1322 after 72 h.
Representative enrichment plots resulting from the comparison between WT organoids exposed to *Apc*$^{1322/+}$ and WT organoids only using the established gene set KEGG. WT organoids exposed to mutants were positively enriched for cell cycle (A) and DNA replication (B), while the peroxisome pathway (C) and PPAR signalling pathway (D) were downregulated. Vertical lines indicate the positions of the gene along the comparison for each gene set. Cut-off *FDR*-value < 0.05.

Further analysis using ingenuity pathway analysis (IPA) (see section 2.10.6) supported the observation that PPAR was significantly reduced (Figure 6.5). The PPAR subfamily consists of three isoforms, PPAR-α, PPAR-β/δ and PPAR-γ, of which only PPAR-α was significantly reduced (-1.08-fold, $p = 0.002$). Additionally, it was shown that its downregulation led to the reduction in fatty acid oxidation, metabolism and transport, which was consistent with the results provided by GSEA, as the fatty acid metabolism pathway was significantly downregulated (Table 6.1B).

Moreover, IPA identified upregulation of the transmembrane receptor TLR4, as well as the cytokine TNF-α, which could potentially induce a proinflammatory response and an adaptive immune response. However, this could not be verified with qRT-PCR (Figure 6.6).

Furthermore, the ATP-binding cassette (ABC) transporter pathway was downregulated as part of the environmental information processing category. ABC transporters play an important role in the active transport of substances across the membrane (Mercado-Lubo *et al*. 2010). Reduction of the ABC transporter pathway could indicate the impairment of such transport.

Taken together, these results demonstrate that upon exposure of WT organoids to *Apc*$^{1322/+}$ organoids, pathways involved in proliferation and DNA repair are activated, while metabolic pathways are downregulated. Both processes have been shown to occur in the early stages of transformation.

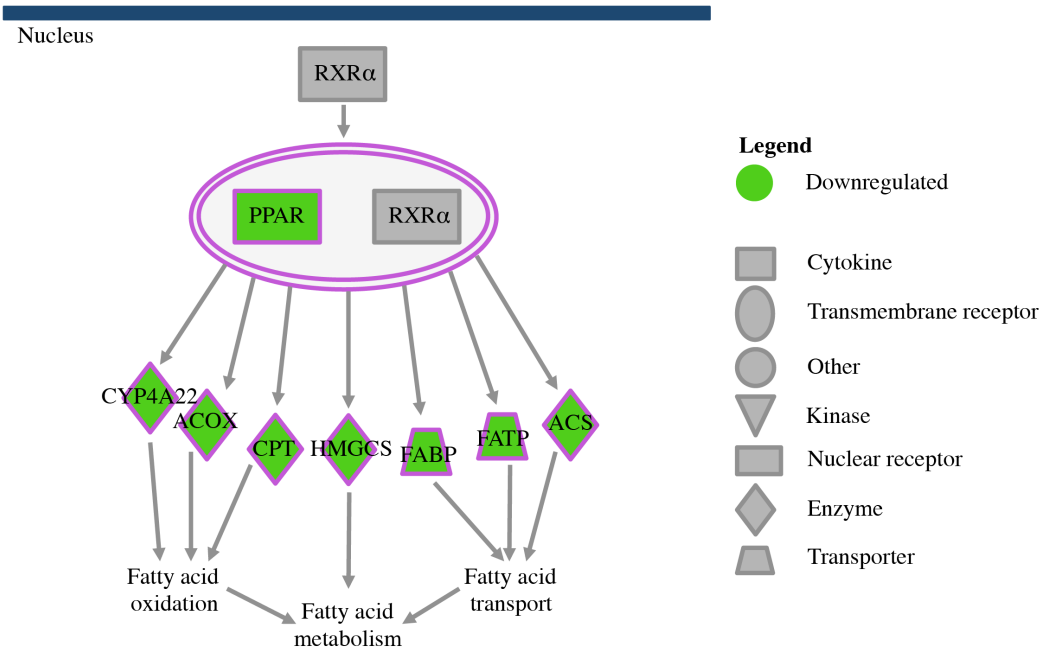

Figure 6.5: PPAR signalling reduced fatty acid metabolism.
Adaptation of the LPS/IL-1 mediated inhibition of the RXR function pathway from IPA. PPAR was reduced, as well as the enzymes and transporters it regulates, leading to reduced expression of fatty acid oxidation, metabolism and transport. Altered genes: PPAR, peroxisome proliferator-activated receptor; CYP4A22, cytochrome P450 family 4 subfamily A member 22; ACOX, Acyl-CoA Oxidase 1; CPT, Carnitine Palmitoyltransferase; HMGCS, 3-Hydroxy-3-Methylglutaryl-CoA Synthase; FABP, fatty acid binding protein; FATP, fatty acid transport protein; ACS, Acyl-CoA Synthetase. Pathway was adapted from IPA.

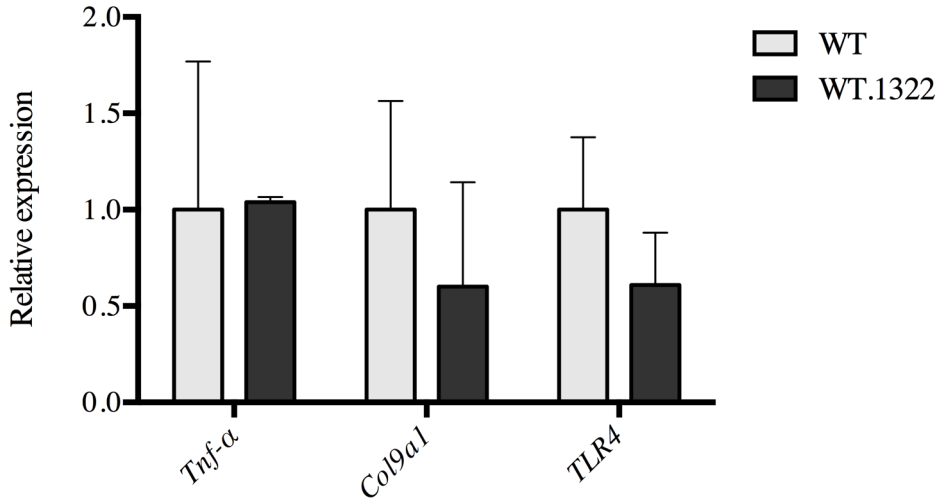

Figure 6.6: Validation of gene expression changes of WTxWT.1322 using qPCR.
Gene expression changes were compared between WT organoids and *Apc*$^{1322/+}$ organoids after 72 h of exposure. Three genes were not significantly altered in transcription. Error bar represents standard error or mean (SEM). *Col9a1*, *Collagen type IX alpha 1 chain*; TLR4, Toll Like Receptor 4; *Tnf-α*, *tumour necrosis factor alpha*.

6.3.2 Transcription patterns in WT organoids exposed to *Apc*$^{1322/+}$

After having established which pathways were significantly altered, the next step was to investigate expression changes at the gene level. Transcriptional profiles were analysed in WT organoids exposed to *Apc*$^{1322/+}$ organoids. 83 upregulated and 204 downregulated genes were detected in exposed WT organoids when compared to WT organoids only ($\log_2$ fold change ≥ 1, $p < 0.05$) (Figure 6.7). The top twenty most altered genes are listed in Table 6.2.

One of the significantly upregulated genes was *Col9a1* (1.81-fold, $p = 0.048$). However, one has to notice that *Col9a1* was strongly upregulated in one of the three biological replicates, thus driving the observed fold change, as depicted in Figure 6.8. Nevertheless, the remaining two samples showed upregulation in *Col9a1*. Col9a1 is a component of the basement membrane, which is part of the ECM providing structural support to epithelial cells. Upregulation of *Col9a1* suggests changes in the architecture of the basement membrane. This was consistent with the finding of the upregulated ECM receptor interaction pathway (see Table 6.1). Upregulation of *Col9a1* was further tested with qPCR, however the observed expression change could not be validated (Figure 6.6).

Another significantly upregulated gene was *Lgr5* (1.55-fold, $p < 0.001$). *Lgr5* is a member for the Wnt signalling pathway. Thus, upregulation of Lgr5 might hint towards perturbations in the Wnt signalling pathway, however the Wnt signalling pathway was not significantly enriched at this stage (FDR = 0.573).

Cyp2d34, a member of the cytochrome P450 oxidative system, was significantly downregulated in WT organoids exposed to *Apc*$^{1322/+}$ organoids (-2.2-fold, $p < 0.001$) (Table 6.2). This indicates a significant role of *Cyp2d34*, as the drug metabolism cytochrome P450 pathway (NES = -2.011, $p = 0.034$) was also significantly reduced in this dataset. Moreover, *Cyp4a22* (-2.14-fold, $p < 0.001$) was downregulated by PPAR leading to fatty acid oxidation, as identified by IPA (Figure 6.5).

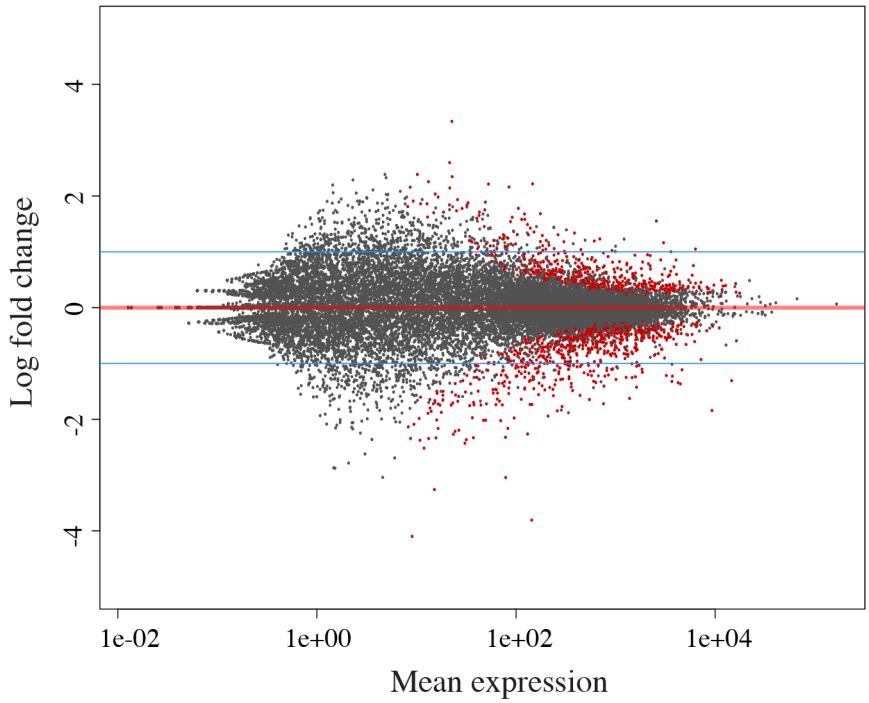

Figure 6.7: Gene expression changes of WT organoids exposed to *Apc*$^{1322/+}$ for 72 h.
MA plots indicating the differential expression of genes between WT and WT organoids grown in presence of *Apc*$^{1322/+}$ organoids after 72 h (WTxWT.1322). Grey dots indicate genes that show no statistically significant difference in abundance between WTxWT.1322 organoids, whilst red dots indicate significantly differentially expressed genes ($p < 0.05$). The blue line indicates the $\log_2$ fold change cut-off of 1. 83 genes were upregulated, while 204 genes were downregulated.

A

Upregulated genes	log2 fold change	p-value
Alb	3.34	<0.001
Ptgds	2.6	0.001
Gm5530	2.39	0.017
Fxyd6	2.35	0.004
Bhlhb9	2.26	0.030
Entpd3	2.22	0.002
Fam171a2	2.21	<0.001
Hpcal4	2.16	0.009
Gm14027	2.16	0.013
Gm17619	2.14	<0.001
Ttc8	2.04	0.044
Faim2	1.98	0.036
Nptxr	1.94	0.032
Spib	1.91	0.016
St6galnac6	1.89	0.015
Pgc	1.88	0.006
Gm15441	1.86	0.015
Fgf14	1.86	0.020
Dmxl2	1.84	0.029
Col9a1	1.81	0.048

B

Downregulated genes	log2 fold change	p-value
Enpp7	-4.1	<0.001
Lct	-3.81	<0.001
Slc28a1	-3.26	<0.001
Cubn	-3.04	<0.001
Acsm5	-2.52	<0.001
Otop3	-2.43	<0.001
Pcp4l1	-2.38	0.003
Slc5a11	-2.36	<0.001
Slc23a1	-2.34	0.002
Gm13963	-2.34	0.007
Slc13a2	-2.33	<0.001
Slc5a8	-2.33	0.011
Bst1	-2.32	<0.001
C87977	-2.27	<0.001
Adh4	-2.26	<0.001
Cyp2d34	-2.22	<0.001
Cd36	-2.2	0.003
Slc2a7	-2.17	<0.001
G6pc	-2.16	<0.001
Slc5a4a	-2.14	0.024

Table 6.2: Gene expression changes.
A) The twenty most upregulated and B) downregulated genes (log2 fold change ≥ 1) are listed for WTxWT.1322 after 72 h. Cut-off p-value ≤ 0.05.

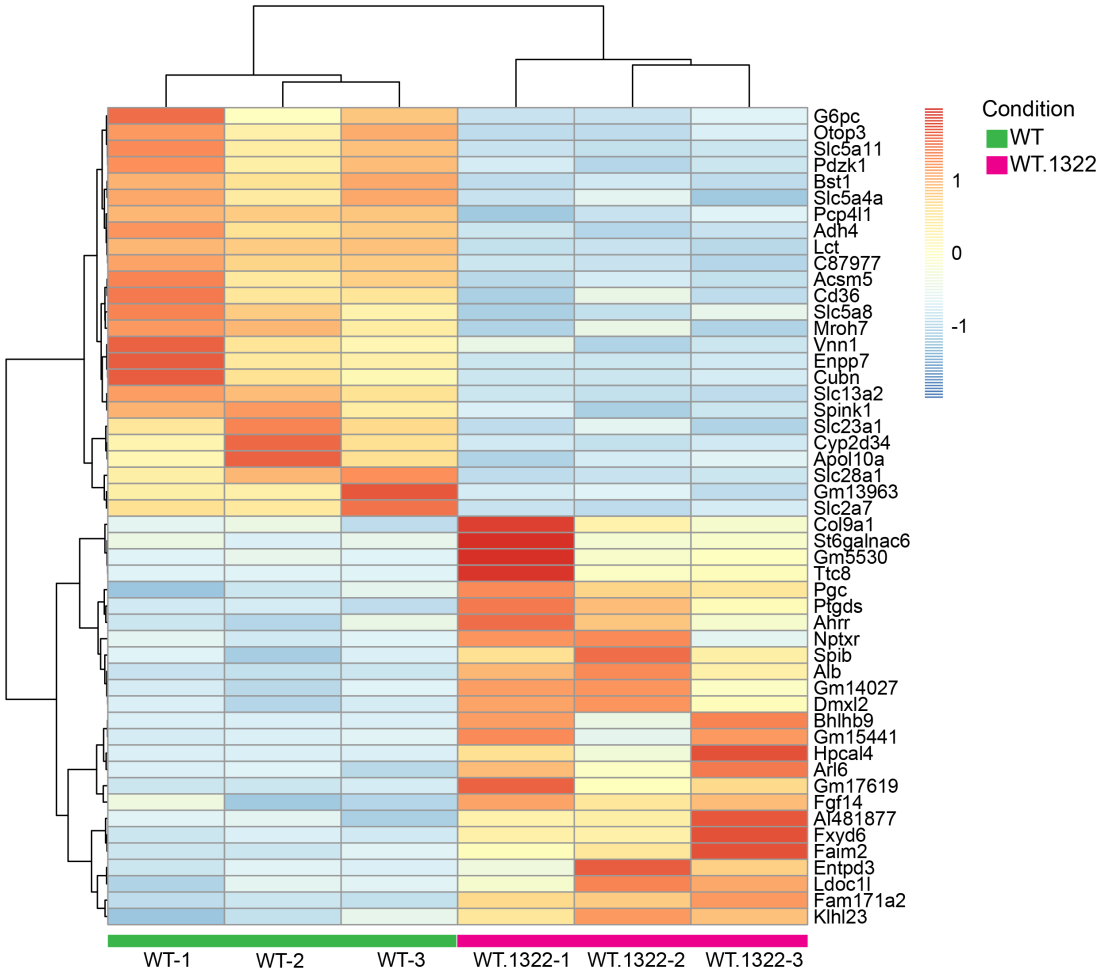

Figure 6.8: Comparison of WT and WT.1322 gene expression patterns.
Heatmap shows the 25 most significantly upregulated and the 25 most downregulated genes between WT organoids (green) and WT organoids exposed to *Apc*$^{1322/+}$ (pink). Columns for WT organoids and WT organoids exposed to *Apc*$^{1322/+}$ organoids refer to biological replicates WT-1 – WT-3 and WT.1322-1 – WT.1322-3, respectively.

6.4 Effect of tumour-exposed fibroblasts on WT organoids

6.4.1 Exposure of WT organoids to tumour-exposed fibroblasts leads to the induction of MAPK and Wnt signalling and to the reduction of metabolic pathways in WT organoids

The effect of tumour-exposed fibroblasts (TEFs) on gene expression in murine WT organoids was investigated. PCA has revealed a great variation between WT organoids and those that were exposed to TEFs (see Figure 6.1). These two groups clustered separately, indicating that WT organoids were transcriptionally different from WT organoids exposed to TEFs. To investigate the underlying pathways responsible for this differential clustering, expression profiles were analysed using GSEA and results were again cross-referenced to the KEGG database.

Overall, GSEA identified 76 significantly upregulated and 48 downregulated pathways (FDR < 0.05) in WT organoids exposed to TEFs compared to WT organoids only after 72 h (Figure 6.9). Of the upregulated pathways 30% were categorised into organismal systems and 30% into diseases (including pathways in cancer). 17% were assigned to environmental information progressing and 12% into cellular processes (Figure 6.9A). Interestingly, only 2% of the upregulated pathways were categorised as genetic information processing, while 16% were downregulated. Moreover, only 9% of metabolic pathways were upregulated, whereas 72% were downregulated. Furthermore, 6% of downregulated pathways were categorised as diseases, 4% as organismal systems, and the remaining 2% fall into the category of cellular processes (Figure 6.9B). The twenty most altered pathways identified by GSEA are listed in Table 6.3, excluding disease pathways that are not relevant to this study.

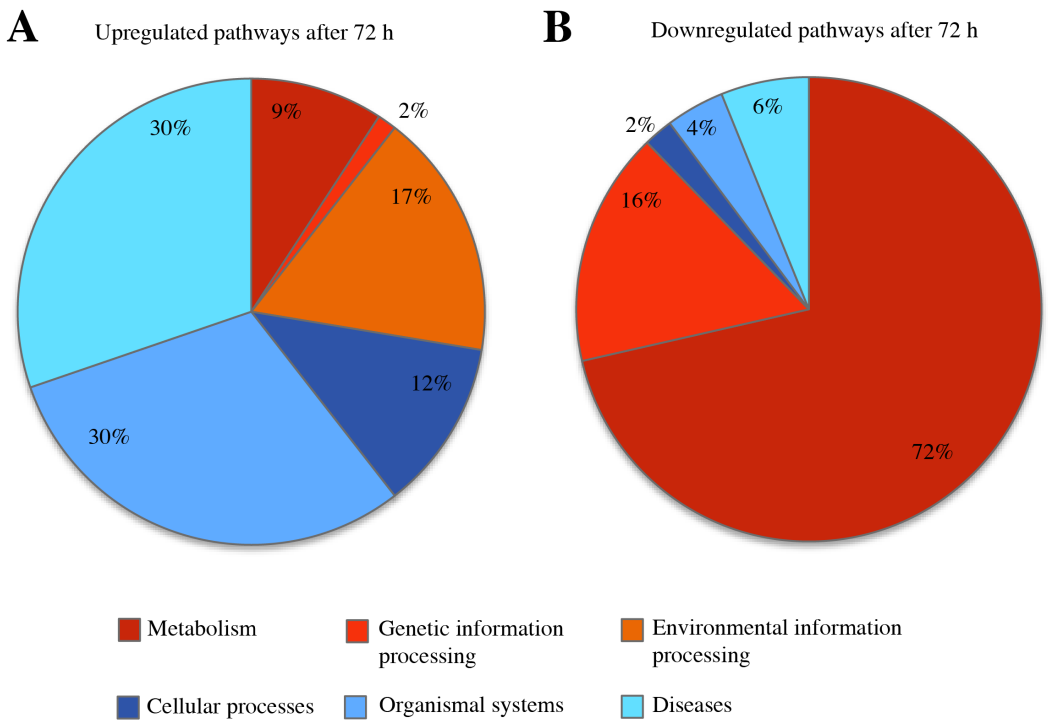

Figure 6.9: Categorisation of enriched pathways for WTxWT.F.1322.
Pie charts show the percentage of all upregulated (A) and downregulated (B) pathways of WT organoids co-cultured with tumour-exposed fibroblasts (WTxWT.F.1322) for 72 h. Expression profiles were analysed using GSEA based on the KEGG pathway database.

The most upregulated pathway was identified as the focal adhesion pathway (NES = 6.082, FDR < 0.001), followed by the regulation of the actin cytoskeleton pathway (NES = 5.552, FDR < 0.001) (Table 6.3A), both were categorised as cellular processes. Focal adhesions are subcellular structures mediating regulatory signals that are transmitted between the ECM and the interacting cell, vital for the maintenance of tissue integrity (Wu 2007). Additionally, categorised as environmental information processing, the ECM receptor interaction pathway (NES = 5.532, FDR < 0.001) (Figure 6.10A), as well as the cell adhesion molecules pathway (NES = 3.354, FDR < 0.001) were significantly upregulated.

Other environmental information processing pathways significantly induced included MAPK signalling (NES = 4.745, FDR < 0.001) (Figure 6.10B), cytokine-cytokine receptor interaction (NES = 4.622, FDR < 0.001), and Wnt signalling (NES = 2.95, FDR < 0.001). Mitogen activated protein kinase (MAPK) signalling is essentially a protein chain in the cell that communicates a signal from the receptor on the membrane surface to the DNA in the nucleus (Selim *et al*. 2017). Alterations of MAPK signalling could induce proliferation and differentiation changes (Martinelli *et al*. 2017). Cytokine interactions are crucial to ensure accurate binding to a specific receptor on the surface of target cells. Thus, upregulation of this pathway could indicate abnormal cell growth.

Wnt signalling is important for maintaining homeostasis in the intestinal epithelium. Dysfunctions of the canonical Wnt signalling pathway could lead to abnormal accumulation of β-catenin, which has been associated with tumour progression. In contrast, one of the noncanonical Wnt pathways interacts with calcium to regulate calcium release in order to control calcium levels (De 2011). Interestingly, the calcium signalling pathway was also significantly upregulated (NES = 2.779, FDR < 0.001). Alterations in calcium levels could influence cell adhesion and migration. The gene sets leading to the enrichments of MAPK and Wnt signalling, as well as genes contributing to the enrichment seen in the cytokine-cytokine interaction pathway will be discussed in subsequent sections.

In summary, the analysis suggests that activation of MAPK and Wnt signalling pathways seems to be an early event in colonic transformation.

A

Upregulated pathways	NES	*FDR* value
Focal adhesion	6.082	<0.001
Regulation of actin cytoskeleton	5.552	<0.001
ECM receptor interaction	5.532	<0.001
MAPK signaling pathway	4.765	<0.001
Cytokine cytokine receptor interaction	4.622	<0.001
Axon guidance	4.293	<0.001
Chemokine signaling pathway	4.222	<0.001
Leucocyte transendothelial migration	3.918	<0.001
Neurotrophin signaling pathway	3.834	<0.001
Endocytosis	3.811	<0.001
Toll like receptor signaling pathway	3.447	<0.001
FCγR mediated phagocytosis	3.446	<0.001
Gap junctions	3.406	<0.001
JAK STAT signaling pathway	3.356	<0.001
Cell adhesion molecules	3.354	<0.001
T-cell receptor signaling pathway	3.226	<0.001
Melanogenesis	2.979	<0.001
Tight junctions	2.954	<0.001
Hedgehog signaling pathway	2.953	<0.001
Wnt signaling pathway	2.949	<0.001

B

Downregulated pathways	NES	*FDR* value
Ribosome	-7.315	<0.001
Oxidative phosphorylation	-6.177	<0.001
Peroxisome	-4.669	<0.001
Citrate cycle	-4.207	<0.001
Valine leucine and isoleucine degradation	-4.118	<0.001
Aminoacyl tRNA biosynthesis	-3.859	<0.001
Drug metabolism cytochrome P450	-3.853	<0.001
Propanoate metabolism	-3.824	<0.001
Fatty acid metabolism	-3.824	<0.001
Pyruvate metabolism	-3.401	<0.001
Splicosome	-3.271	<0.001
Glycolysis gluconeogenesis	-3.126	<0.001
β-alanine metabolism	-2.878	<0.001
Arginine and proline metabolism	-2.773	<0.001
Glyoxylate and dicarboxylate metabolism	-2.747	<0.001
Glutathione metabolism	-2.676	<0.001
PPAR signaling pathway	-2.618	<0.001
Retinol metabolism	-2.617	<0.001
Butanoate metabolism	-2.601	<0.001
Tryptophan metabolism	-2.561	<0.001

Table 6.3: Enriched pathways for WT organoids exposed to TEFs for 72 h.
GSEA identified multiple enriched pathways based on the KEGG gene set. A) shows the twenty most upregulated and B) downregulated pathways after 72 h. Cut-off *FDR*-value < 0.05.

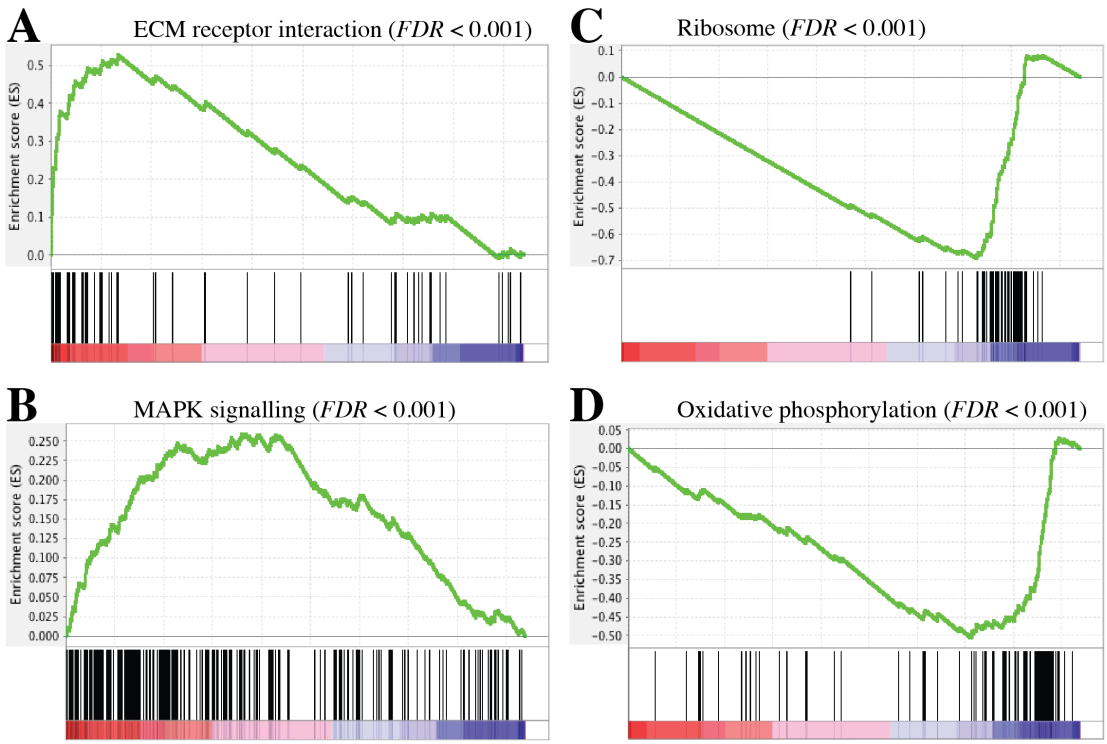

Figure 6.10: GSEA expression profiles for WT organoids exposed to TEFs for 72 h.
Representative enrichment plots resulting from the comparison between WT organoids exposed to TEFs and WT organoids only using the established gene set KEGG. WT organoids exposed to TEFs were positively enriched for ECM receptor interaction signalling (A) and MAPK signalling (B), while the ribosome pathway (C) and oxidative phosphorylation (D) were significantly reduced. Vertical lines indicate the positions of the gene along the comparison for each gene set. Cut-off *FDR*-value = 0.05.

The majority of pathways downregulated in WT organoids exposed to TEFs were metabolic pathways, with oxidative phosphorylation a key player (NES = -6.177, FDR < 0.001) (Figure 6.10D). Other reduced metabolic pathways included fatty acid metabolism (NES = -3.824, FDR < 0.001), pyruvate metabolism (NES = -3.401, FDR < 0.001), and glycolysis (NES = -3.126, FDR < 0.001).

Surprisingly, the ribosome pathway (NES = -7.315, FDR < 0.001) (Figure 6.10C) was significantly reduced in WT organoids exposed to TEFs, indicating reduced protein synthesis.

Moreover, the PPAR signalling pathway (NES = -2.618, FDR < 0.001) was significantly reduced. PPARs are metabolic regulators. Activated PPAR ligands form heterodimers with retinoid X receptor (RXR), which then bind to PPAR response elements, regulating the transcription of target genes involved in proliferation, differentiation and inflammation response. Especially PPAR-α has been shown to regulate peroxisome proliferation and fatty acid oxidation (Park *et al*. 2012). Independent analysis using IPA has confirmed downregulation of the PPAR signalling pathway (Figure 6.11). *Ppar-α* (-4.1-fold, p < 0.001), in particular, reduced peroxisome proliferation, which in turn was also identified with GSEA (NES = -4.67, FDR < 0.001). Furthermore, IPA has revealed that reduced PPAR-α caused a decrease in fatty acid oxidation and led to degradation of fatty acids. Moreover, PPAR-α caused downregulation of CD36, which impeded fatty acid uptake. CD36 is known to import fatty acids inside cells and altered expression of CD36 can lead to metabolic dysfunctions (Pepino *et al*. 2014). In addition, through downregulation of *Cyp4a22* (-3.25-fold, p < 0.001), PPAR led to reduced fatty acid oxidation. Several other *Cyp* genes were significantly downregulated as well (*Cyp2c29*: -8.38fold, p < 0.001; *Cyp3a11*: -8.35, p < 0.001; *Cyp3a25*: -7.76, p < 0.001) (Table 6.4). Through downregulation of fatty acid-binding proteins (FABPs), fatty acid transport proteins (FATPs), as well as acyl-CoA synthetases (ACS), fatty acid transport was reduced, resulting in an overall reduced fatty acid metabolism, which was also identified with GSEA (NES = -3.824, FDR < 0.001). Genes involved in the downregulation of fatty acid metabolism included *alcohol dehydrogenase 4* (*Adh4*) (-9.01, p < 0.001) (Table 6.4), *Adh1* (-6.69, p < 0.001), and *Adh7* (-5.21, p < 0.001), indicating these are key genes for the fatty acid metabolism pathway. Reduction in fatty acid metabolism suggests that fatty acids are no longer synthesised, therefore the energy that is produced is immediately used up.

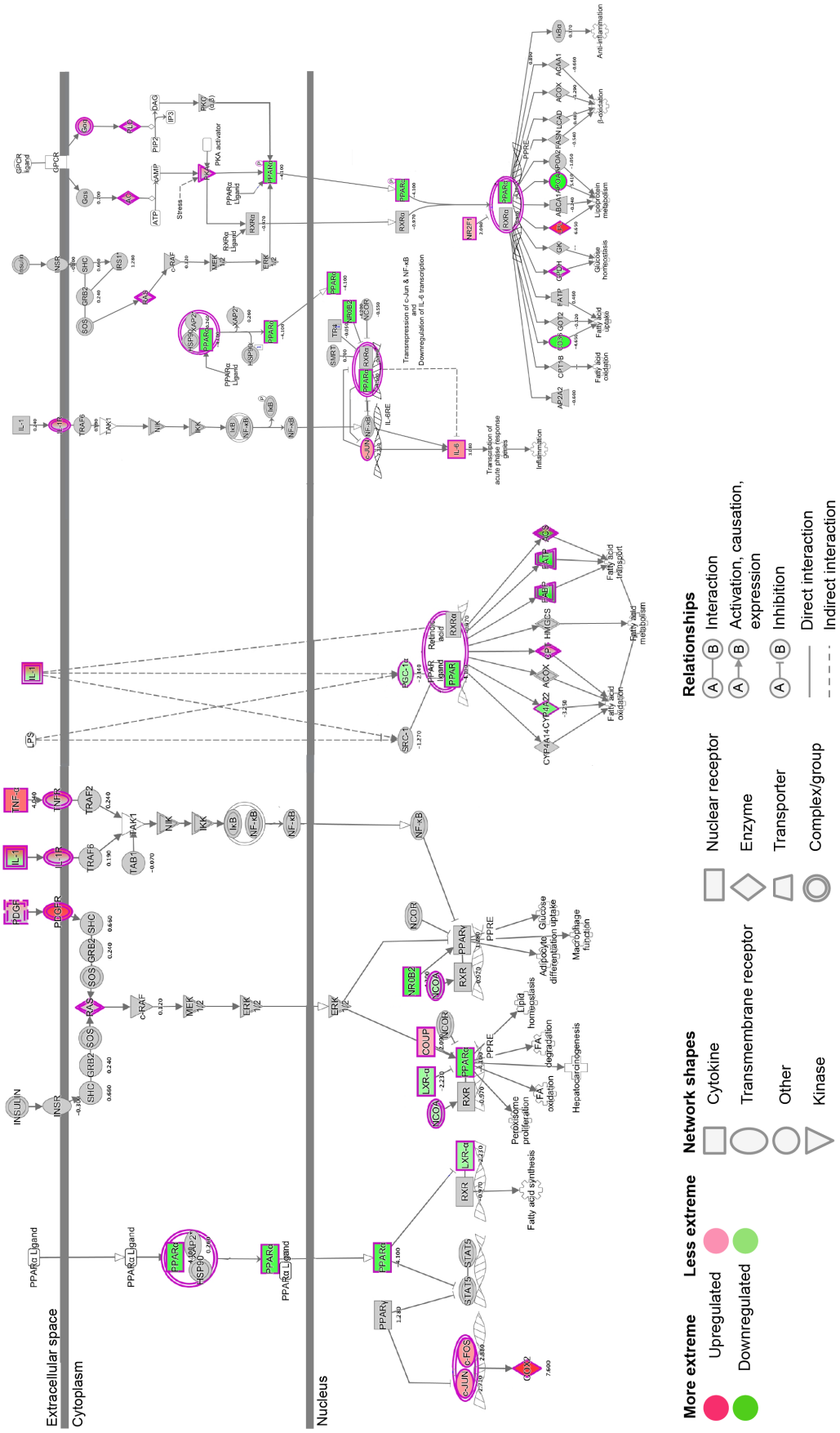

Figure 6.11: PPAR signalling pathway adapted from IPA.

6.4.2 Comparison of altered pathways between WT organoids exposed to *Apc*$^{1322/+}$ and those exposed to TEFs after 72 h

GSEA identified altered pathways for both WT organoids exposed to *Apc*$^{1322/+}$ organoids (WTxWT.1322) and WT organoids exposed to TEFs (WTxWT.F.1322). As stated above, 76 significantly upregulated pathways were identified in WT organoids exposed to TEFs, and 6 in WT organoids exposed to *Apc*$^{1322/+}$. However, none of these upregulated pathways overlapped (Figure 6.12A). In contrast, 48 pathways were significantly downregulated in WT organoids to TEFs, and 14 in WT organoids exposed to *Apc*$^{1322/+}$. 9 reduced pathways overlapped between these two groups (Figure 6.12B), which are listed in Figure 6.12C. It is notable that these pathways were more negatively enriched in WT organoids exposed to TEFs compared to WT organoids exposed to *Apc*$^{1322/+}$. For instance, oxidative phosphorylation and the peroxisome pathway were much reduced in greater extent.

In order to identify the changes in WT organoids caused due to the exposure to TEFs, enriched pathways were compared between these two groups and represented in a heatmap (Figure 6.13), which includes all pathways significantly altered in either WTxWT.1322 or WTxWT.F.1322.

In general, most pathways were enriched to a greater extent in WT organoids exposed to TEFs compared to WT organoids exposed to *Apc*$^{1322/+}$, which is not only true for downregulated pathways. The focal adhesion and ECM receptor interaction pathways were much stronger induced after 72 h (Figure 6.13).

However, some pathways were only significantly downregulated in WT organoids exposed to *Apc*$^{1322/+}$ organoids, but not significantly reduced in WT organoids exposed to TEFs. Examples included the ABC transporter pathway and the glycerophospholipid metabolism. It is important to note that the number of significantly reduced metabolic pathways have increased in WT organoids exposed to TEFs, indicating that the presence of TEFs altered the metabolic behaviour in WT organoids.

Interestingly, some pathways switched from being downregulated in WTxWT.1322 to being upregulated in WTxWT.F.1322. The most significant contrast was observed for the ribosome pathway, which was significantly reduced in WT organoids exposed to *Apc*$^{1322/+}$ organoids, while significantly induced in WT organoids exposed to TEFs. Endocytosis, Wnt signalling, as well as JAK/STAT

signalling were positively enriched in WT organoids exposed to TEFs, but showed reduction when exposed to *Apc*$^{1322/+}$ organoids, indicating that this switch is due to the exposure of TEFs. MMR and DNA replication were significantly downregulated in WT organoids exposed to TEFs, which is in contrast to WT organoids exposed to *Apc*$^{1322/+}$ organoids, as they showed a significant induction of these pathways, indicating the effect of the stroma on WT organoids.

To conclude, TEFs had a much stronger effect on WT organoids, given the number of altered pathways increased substantially in the same amount of time as compared to exposure of *Apc* deficient organoids to WT organoids.

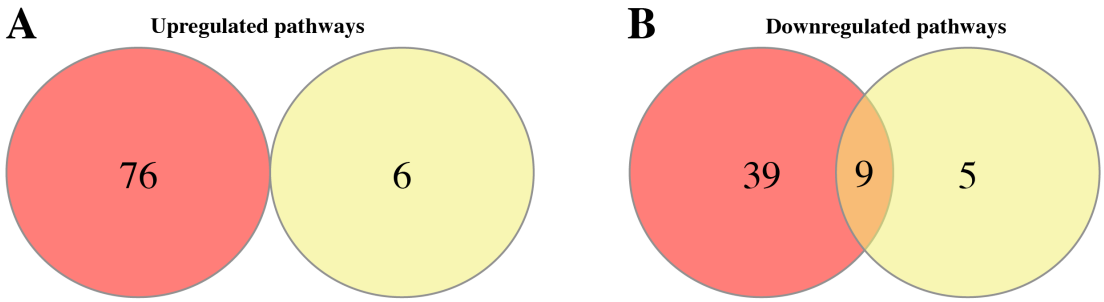

C

	WT organoids exposed to *Apc*$^{1322/+}$		WT organoids exposed to TEFs	
Downregulated pathway	**NES**	**FDR value**	**NES**	**FDR value**
Oxidative phosphorylation	-2.2391748	0.012	-6.1769137	< 0.001
Parkinsons disease	-2.007375	0.033	-6.068629	< 0.001
Alzheimers Disease	-2.2383587	0.010	-4.901239	< 0.001
Peroxisome	-3.2119148	< 0.001	-4.6690183	< 0.001
Citrate cycle	-2.2799911	0.010	-4.207344	< 0.001
Drug metabolism cytochrome P450	-2.0110927	0.034	-3.852578	< 0.001
Fatty acid metabolism	-2.3824382	0.007	-3.8238144	< 0.001
PPAR signalling pathway	-2.4397728	0.006	-2.6182654	< 0.001
Glycerolipid metabolism	-2.2384245	0.011	-2.3758528	< 0.001

Figure 6.12: Overlap of significantly altered pathways.
Venn diagram showing the overlap of significantly altered pathways between WT organoids exposed to both *Apc*$^{1322/+}$ organoids (yellow circle) and TEFs (red circle). A) 76 pathways were significantly upregulated in WT organoids exposed to TEFs, and 6 in WT organoids exposed to *Apc*$^{1322/+}$ organoids. No pathways overlapped. B) 9 pathways were significantly downregulated in both conditions. C) Pathways that overlapped are listed in table C). NES, normalised enrichment score, FDR, false discovery rate.

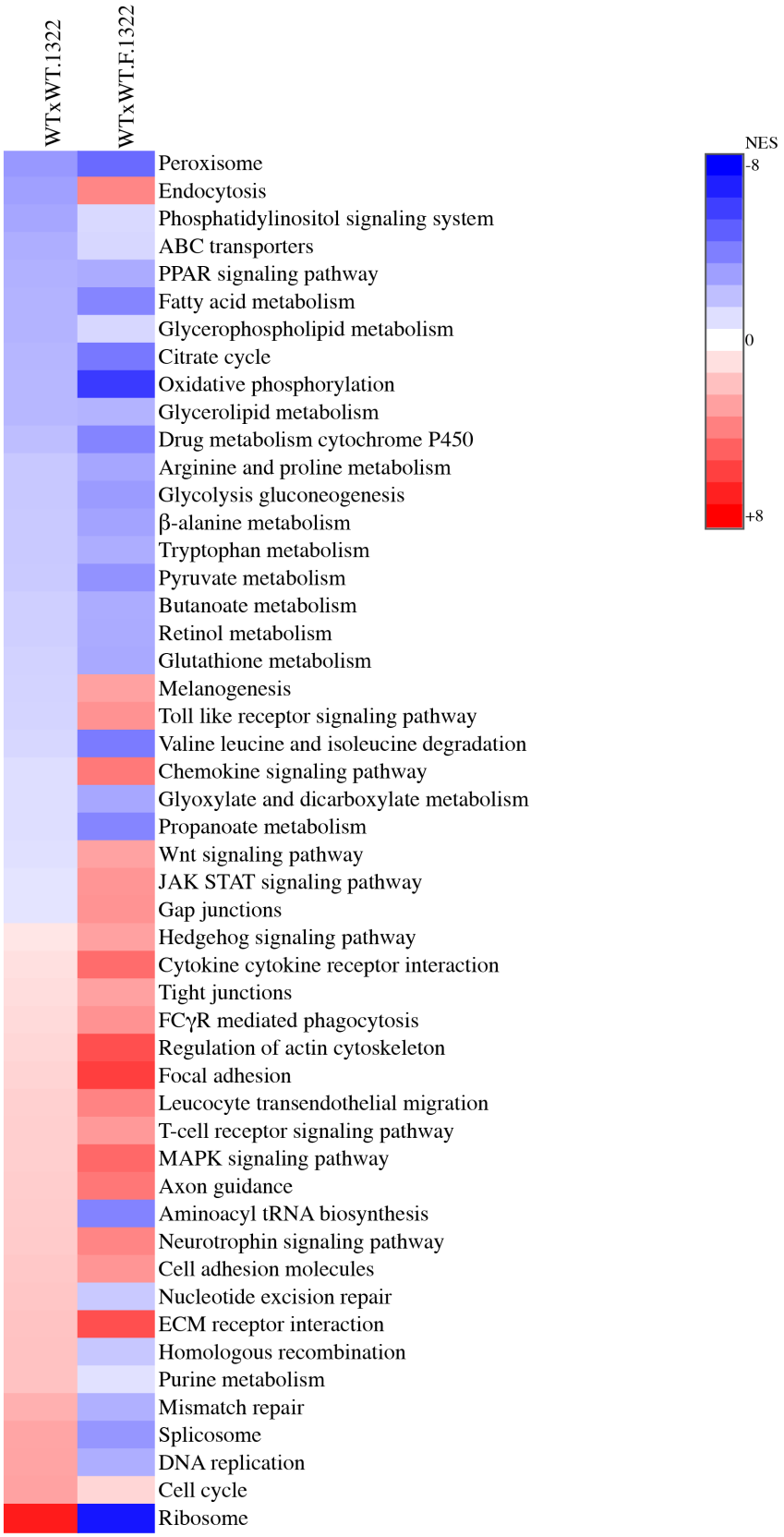

Figure 6.13: Comparison of altered pathways between WT.1322 and WT.F.1322.
Hierarchical clustering of differentially, significantly expressed pathways in WTs exposed to *Apc*$^{1322/+}$ organoids (WTxWT.1322) and WT exposed to TEFs (WTxWT.F.1322) for 72 h based on the normalised enrichment score (NES). Heatmap key: red equals upregulation, blue equals downregulation relative to the mean expression of only WT organoids across all samples.

6.4.3 Overexpression of *Tnf-α* and *Tgf-β* in WT organoids exposed to tumour exposed fibroblasts (TEFs)

Transcriptional profiles were analysed and 2291 upregulated and 1322 downregulated genes were detected in WT organoids exposed to TEFs after 72 h ($\log_2$ fold change ≥ 1, $p < 0.05$) (Figure 6.14). The top twenty most altered genes are listed in Table 6.4. Figure 6.15 shows the gene expression changes in each of the samples sequenced for this comparison.

WT organoids exposed to TEFs demonstrated induction of the cytokine-cytokine receptor interaction pathway (NES = 4.622, FDR < 0.001). Cytokines are released in response to an activating stimulus upon which they induce responses through binding to a specific receptor on the surface of target cells (Landskron *et al*. 2014). Cytokines can be grouped by structure into different families. Here, genes within the TNF and TGF-β family were activated. In particular, *Tnf-α* (4.04-fold, $p < 0.001$) and its receptor *Tnfrsf1b* (2.37-fold, $p < 0.001$) were significantly upregulated, which was further confirmed by IPA (Figure 6.11, Figure 6.17). In addition, *Tnf-α* induction was verified using qRT-PCR in WT organoids exposed to TEFs (4.86-fold, $p = 0.031$) (Figure 6.16). TNF-α is a proinflammatory cytokine secreted by inflammatory cells, such as macrophages, in response to inflammation, and during sustained inflammation the TNF-α level is elevated within colonic mucosa (Coskun *et al*. 2014). Thus, upregulation of *Tnf-α* could hint towards elevated levels of inflammation in WT organoids exposed to TEFs and might indicate increased cell proliferation.

Within the TGF-β family, *Tgf-β* (3.22-fold, $p < 0.001$) and its receptors *Tgfbr1* (1.09-fold, $p < 0.001$) and *Tgfbr2* (1.08-fold, $p < 0.001$) were significantly induced. Downstream of TGF-β, *Smad3* (1.4-fold, $p < 0.001$) was also significantly upregulated. This was further confirmed using IPA (Figure 6.17). Taken together, activation of TGF-β signalling could indicate altered cell growth and survival.

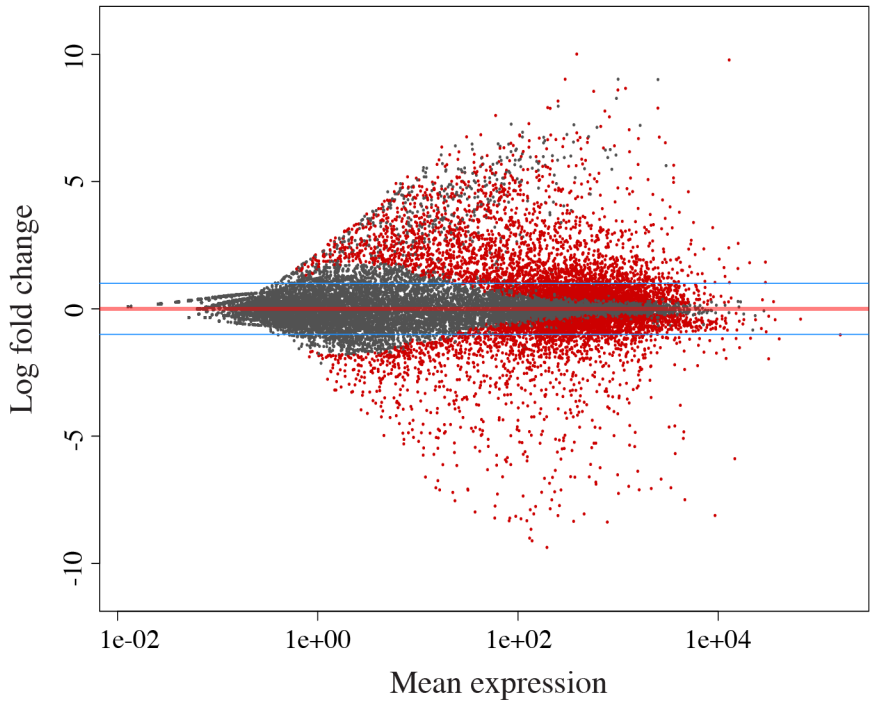

Figure 6.14: Gene expression changes of WT organoids exposed to TEFs for 72 h.
MA plots indicating the differential expression of genes between WT and WT organoids grown in presence tumour-exposed fibroblasts for 72 h (WTxWT.F.1322). Grey dots indicate genes that show no statistically significant difference in abundance between WTxWT.F.1322 organoids, whilst red dots indicate significantly differentially expressed genes (FDR < 0.05). The blue line indicates the $\log_2$ fold change cut-off of 1. 2291 upregulated and 1322 downregulated genes were identified.

A

Upregulated genes	log2 fold change	p-value
Mmp9	10.01	<0.001
Clu	9.78	<0.001
Mcpt2	9.02	<0.001
Ctse	8.66	<0.001
Aldh1a3	8.6	<0.001
Cym	8.55	<0.001
Acsbg1	8.16	<0.001
Prkcdbp	7.91	<0.001
Fn1	7.89	<0.001
Vsig1	7.88	<0.001
Anxa8	7.77	<0.001
Ptgs2	7.6	<0.001
Serpine2	7.54	<0.001
Col6a2	7.28	<0.001
Igfbp5	7.17	<0.001
Col4a1	7.04	<0.001
Sparcl1	6.92	<0.001
Ivl	6.84	<0.001
Ttc9	6.83	<0.001
Angptl2	6.83	<0.001

B

Downregulated genes	log2 fold change	p-value
Reg3a	-9.37	<0.001
Slc5a4b	-9.11	<0.001
Adh4	-9.01	<0.001
Ugt2b5	-8.66	<0.001
Cyp2c29	-8.38	<0.001
Cyp3a11	-8.35	<0.001
Nat8	-8.33	<0.001
Rdh7	-8.32	<0.001
Ugt2b36	-8.25	<0.001
G6pc	-8.22	<0.001
Leap2	-8.22	<0.001
Slc6a4	-8.15	<0.001
Apoc3	-8.12	<0.001
Sis	-8.12	<0.001
Akr1c14	-8.06	<0.001
Lct	-8.05	<0.001
Slc13a2	-7.98	<0.001
Ugt2a3	-7.89	<0.001
2010106E10Rik	-7.85	<0.001
Cyp3a25	-7.76	<0.001

Table 6.4: Gene expression changes.
A) Shows the twenty most upregulated and B) downregulated genes ($\log_2$ fold change) for WTxWT.F.1322 after 72 h. Cut-off p-value < 0.05.

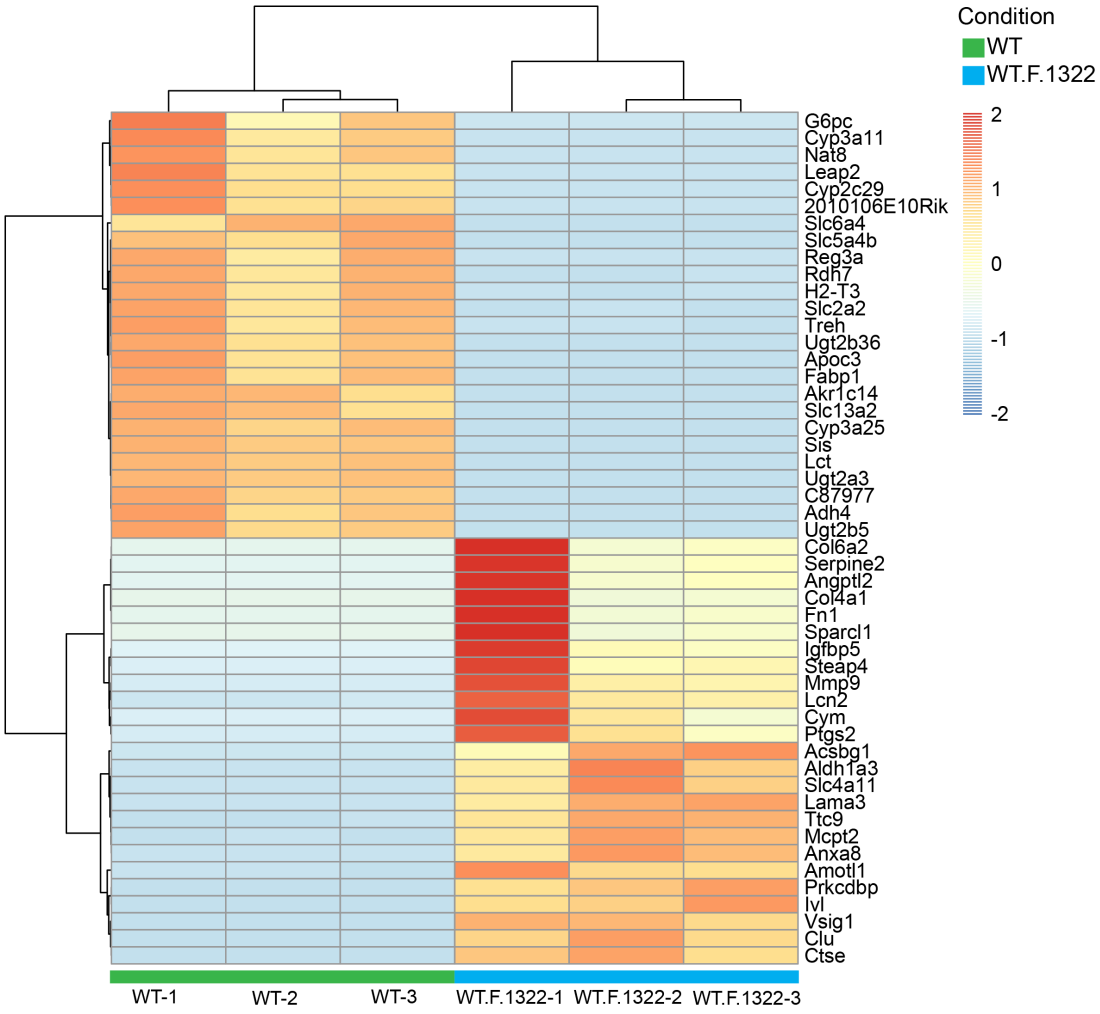

Figure 6.15: Comparison of WT and WT.F.1322 gene expression patterns.
Heatmap shows the 25 most significantly upregulated and the 25 most downregulated genes between WT organoids (green) and WT organoids exposed to TEFs (blue). Columns for WT organoids and WT organoids exposed to TEFs refer to biological replicates WT-1 – WT-3 and WT.F.1322-1 – WT.F.1322-3, respectively.

6.4.4 Exposure of tumour-exposed fibroblasts led to induction of MAPK and Wnt signalling

MAPK signalling was significantly upregulated (NES = 4.745, FDR < 0.001), as identified by GSEA. MAPK is a three-kinase signalling module system consisting of MAPK, MAP2K, and MAP3K. MAPKs can be further subdivided into the growth factor-regulated extracellular signal-related kinases (ERKs) and the stress-activated MAPKs, which can be categorised into c-JUN NH2-terminal kinases (JNKs) (Selim *et al*. 2017). JNK is activated by MKK4, which is in turn activated by MEKK1. Once activated, MAPKs phosphorylate their substrates (Fang *et al*. 2005). Both, MKK4 (0.55-fold, p < 0.001) and MEKK1 (0.41-fold, p = 0.003) were induced in WT organoids exposed to TEFs. ERK is activated by MEK1/2 (Xu *et al*. 1997) and here MEK1 (also known as MAP2K1) was upregulated (0.62-fold, p < 0.001). Once ERK is phosphorylated, it can activate its transcription factors, of which c-JUN (2.7-fold, p < 0.001) and c-FOS (2.88-fold, p < 0.001), as well as AP-1 (2.35-fold, p < 0.001) were significantly upregulated. c-JUN is also a transcription factor of JNK. Induction of c-FOS (3.66-fold, p = 0.003) and c-JUN (2.957-fold, p = 0.033) was verified with qRT-PCR (Figure 6.16). In addition, IPA confirmed upregulation of c-JUN and c-FOS and demonstrated it could lead to increased cell proliferation (Figure 6.17). To conclude, alterations in MAPK activation could result in abnormal proliferation and uncontrolled apoptosis (Selim *et al*. 2017, Shaul *et al*. 2007).

Wnt signalling (NES = 2.95, FDR < 0.001) was significantly upregulated in WT organoids exposed to TEFs after 72 h. The canonical pathway is activated when Wnt binds to Frizzled (FZD) and interacts with LRP. Here, several *Wnt* genes were upregulated, including *Wnt4* (2.71-fold, p = 0.001), *Wnt7a* (4.53-fold, p < 0.001), and *Wnt9a* (2.21-fold, p = 0.002). In addition, *Lrp5* was significantly induced (1.06-fold, p < 0.001). Activation of canonical Wnt signalling causes the accumulation of β-catenin. Here, *Ctnnb1* (β-catenin) was significantly upregulated (1.58-fold, p < 0.001). In addition, the transcription factor *Tfc4* was induced (1.73-fold, p < 0.001), indicating upregulation in Lgr5. Indeed, *Lgr5* was significantly upregulated (1.23-fold, p < 0.001). In addition, Wnt signalling can also be activated by R-spondins, and here R-spondin1 (3.83-fold, p < 0.001) was significantly upregulated.

Analysis with IPA has confirmed the observed Wnt signalling induction. Wnt activated FZD, which led to an increased accumulation of nuclear β-catenin,

indicating increased cell proliferation and cell survival (Figure 6.17). Furthermore, Wnt signalling induced upregulation in cyclo-oxygenase 2 (COX2) (7.6-fold, $p < 0.001$) through Tcf/Lcf signal transduction (Figure 6.17). Lack of COX2 expression is characteristic for normal tissue, but has been shown to be elevated in inflamed tissue and might lead to tumour development due to its anti-apoptotic and proliferating properties (Eisinger *et al*. 2007).

6.4.5 Exposure to TEFs caused overexpression of *MMP9* and collagen genes in WT organoids

The ECM receptor interaction pathway was significantly upregulated (NES = 5.532, FDR < 0.001) in WT organoids exposed to TEFs. The specialised structure of ECM is composed of collagens, laminins and proteoglycans. These components are critical in maintaining the structure of the ECM. MMP activity is responsible for the degradation of the ECM as well as basal membranes, and MMPs are known to control invasion (Akter *et al*. 2015, Kessenbrock *et al*. 2015). MMP9 has been shown to be of particular importance, since it hydrolyses type IV collagen in the basal membrane (Stamenkovic 2003). Here, the matrix metalloproteinases MMP9 (10.01-fold, $p < 0.001$) and MMP7 (2.35-fold, $p < 0.001$) were significantly upregulated, indicating that exposure to TEFs induces structural changes in the ECM. Furthermore, collagens, such as *Col4a1* (7.04-fold, $p < 0.001$) and *Col6a2* (7.28-fold, $p < 0.001$), were significantly induced, indicating alterations in the structural network of the ECM. Upregulation of MMP9 (106.97-fold, $p < 0.0001$), *Col4a1* (114.57-fold, $p < 0.0001$), and *Col6a2* (6.8-fold, $p = 0.031$) was confirmed by qRT-PCR (Figure 6.16).

Other genes contributing to this enrichment observed in the ECM pathway included laminins, such as *Lama2* (3.1-fold, $p < 0.001$), *Lama3* (6.75-fold, $p < 0.001$), and *Lama5* (2.58-fold, $p < 0.001$), as well as *Lamb1* (4.72-fold, $p < 0.001$), *Lamb2* (2.64-fold, $p < 0.001$), and *Lamb3* (2.67-fold, $p < 0.001$).

Taken together, TEF-induced upregulation of tumour-derived MMPs as well as collagens and laminins seem to be an early process in colonic transformation.

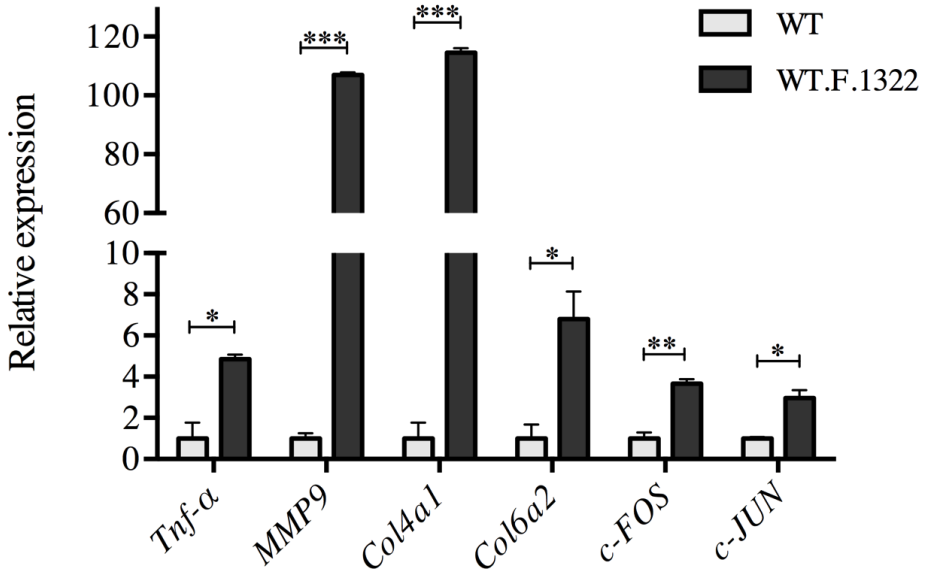

Figure 6.16: Expression validation of WTxWT.F.1322.
Transcriptional validation using qRT-PCR. Genes related to the upregulated MMR pathway and downregulated apoptosis pathway. Error bar represents standard error or mean (SEM). Significance: $p < 0.05$ (*), $p < 0.01$ (**), $p < 0.001$ (***). *Tnf-α*, *Tumour necrosis factor alpha*; *MMP9*, *matrix metalloproteinase 9; Col4a1*, *Collagen type IV alpha 1 chain*; *Col6a2*, *Collagen type VI alpha 2 chain*; *c-FOS*, *FBJ Murine Osteosarcoma Viral Oncogene Homolog*; *c-JUN*, *V-Jun Avian Sarcoma Virus 17 Oncogene Homolog*.

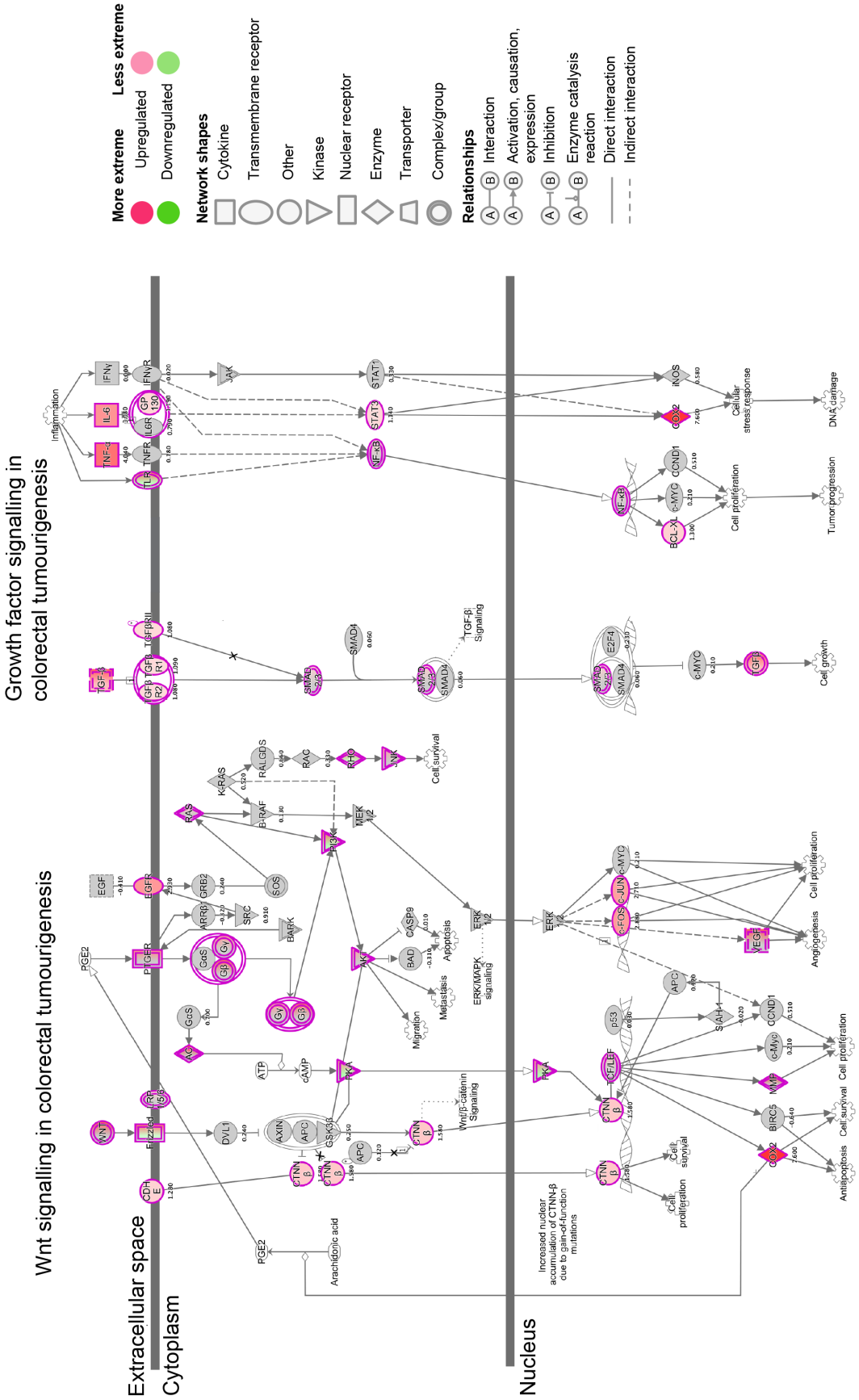

Figure 6.17: Schematic CRC metastasis signalling pathway adapted from IPA.

6.4.6 Exposure of WT organoids to *Apc*$^{1322/+}$ or TEFs does not alter cell proliferation in WT organoids after 72 h

Next, it was hypothesised that WT organoids may show a proliferative response when exposed to either *Apc*$^{1322/+}$ or TEFs. Therefore, WT ROSA$^{mT/mG}$ organoids were grown together with *Apc*$^{1322/+}$ organoids in a mixed set up for 72 h (see section 2.12). Furthermore, WT organoids were exposed to normal murine fibroblasts, as well as TEFs in a transwell set up for 72 h. Organoids were then collected and subjected to cytospinning onto glass slides (see section 2.12), which maintains the 3D structure of organoids. Immunofluorescence staining for Ki67, a cell proliferation marker, was then performed on the organoids for each group (see section 2.12.1), and sections analysed using confocal microscopy (see section 2.12.2). By using WT ROSA$^{mT/mG}$ derived organoids, we ensure that all WT organoids will be labelled fluorescent red whereas the *Apc*$^{1322/+}$ deficient organoids do not have an intrinsic fluorescent marker. Therefore, the direct influence of *Apc*$^{1322/+}$ organoids on WT organoids could be studied.

The percentage of Ki67 expression per area was assessed in Image J (1.48v; https://imagej.nih.gov/ij/) and no significant difference in cell proliferation was detected between the groups (Figure 6.18A). Figure 6.18B illustrates DAPI, td Tomato, and Ki67 staining in WT organoids, WT organoids exposed to *Apc*$^{1322/+}$, to normal fibroblasts, and to TEFs.

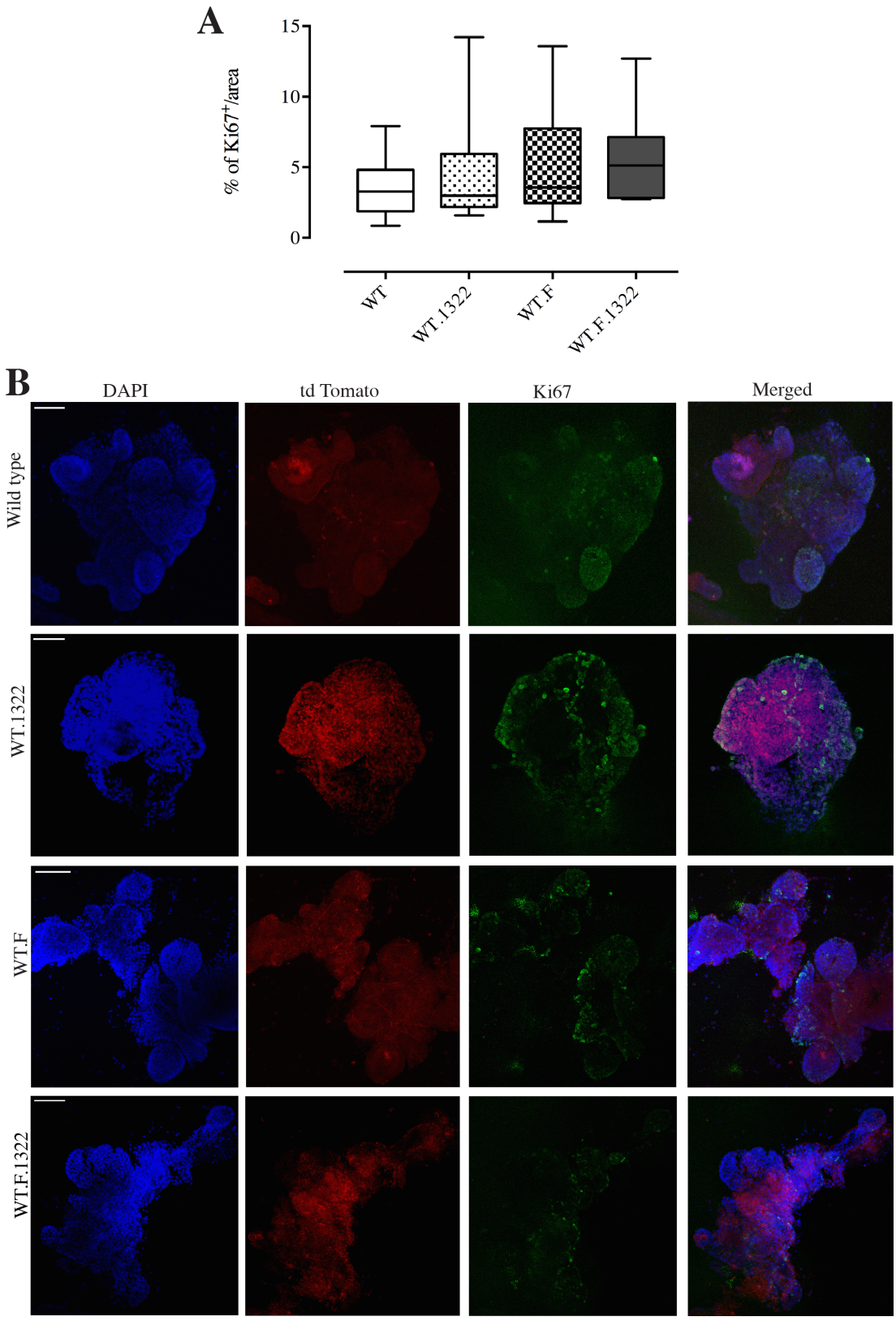

Figure 6.18: Assessing cell proliferation in exposed WT organoids.
A) Shows the percentage of Ki67 staining per area. No significant difference was detected. (B) Illustration of a WT organoid (wild type), a WT organoid exposed to *Apc*$^{1322/+}$ (WT.1322), exposed to normal fibroblasts (WT.F), and exposed to TEFs (WT.F.1322). Left column shows DAPI stain, second left column shows td Tomato expression, second right column shows Ki67 expression, and right column shows merged expression. Scale bar = 100μm.

6.4.7 Greater Lgr5 expression in WT organoids exposed to *Apc*$^{1322/+}$ and tumour exposed fibroblasts (TEFs)

As part of the activated Wnt signalling pathway, *Lgr5* was significantly upregulated (1.23-fold, $p < 0.001$). In order to investigate *Lgr5* expression in WT organoids exposed to *Apc*$^{1322/+}$ organoids in more detail, WT organoids were grown together with *Apc*$^{1322/+}$ organoids (WT.1322). Moreover, the effect of normal fibroblasts (WT.F), as well as of TEFs (WT.F.1322) on Lgr5 expression in WT organoids was also investigated in a transwell set up. After 72 h, organoids from each group were collected, embedded and *in situ* hybridisation (ISH) was performed for Lgr5 expression (see section 2.11). The number of Lgr5$^+$ probes per cell from each group was manually counted and the percentage of positively stained cells calculated. Figure 6.19 illustrates *Lgr5* mRNA expression for each group.

Overall, the number of positive and negative stained probes in each organoid for each group was assessed and the percentage calculated. There was a significantly greater percentage of cells expressing no Lgr5 in WT organoids compared to cells that are Lgr5 positive (t-test with Welch correction: $p < 0.0001$). However, in WT organoids exposed to *Apc* deficient organoids, a significantly greater number of positive stained Lgr5 probes was observed ($p < 0.001$). This was also observed for WT organoids exposed to murine WT fibroblasts ($p < 0.01$), as well as for WT organoids exposed to TEFs ($p < 0.0001$) (Figure 6.20A).

Therefore, a more detailed analysis of the number of Lgr5 probes per cell was performed. Cells were categorised as expressing either 0 Lgr5$^+$ probes, 1 Lgr5$^+$ probe, 2 Lgr5$^+$ probes, or 3+ Lgr5$^+$ probes per cell. Overall, the expression was significantly different among all four groups (χ^2-test: $p < 0.0001$) (Figure 6.20B). Specifically, the percentage of WT organoids expressing no Lgr5 probes was significantly higher compared to WT organoids exposed to *Apc*$^{1322/+}$($p < 0.0001$), to fibroblasts ($p < 0.001$), and to TEFs ($p < 0.0001$) (Figure 6.20C). There was no significant difference detected between all groups expressing 1 Lgr5$^+$ probe per cell (Figure 6.20D). The percentage of cells expressing 2 Lgr5$^+$ probes was significantly lower in WT organoids compared to *Apc*$^{1322/+}$($p < 0.0001$), to fibroblasts ($p < 0.05$), and to TEFs ($p < 0.001$) (Figure 6.20E). Interestingly, the percentage of cells expressing 3+ Lgr5 probes was significantly lower in WT organoids compared to *Apc*$^{1322/+}$($p < 0.01$) and to TEFs ($p < 0.001$), however no difference was observed

between WT organoids and those exposed to fibroblasts. In addition, WT organoids exposed to *Apc*$^{1322/+}$ were significantly lower compared to WT organoids exposed to TEFs ($p < 0.05$) (Figure 6.20F).

Taken together, this indicates that Lgr5 expression is significantly increased in WT organoids exposed to either *Apc* deficient organoids or TEFs.

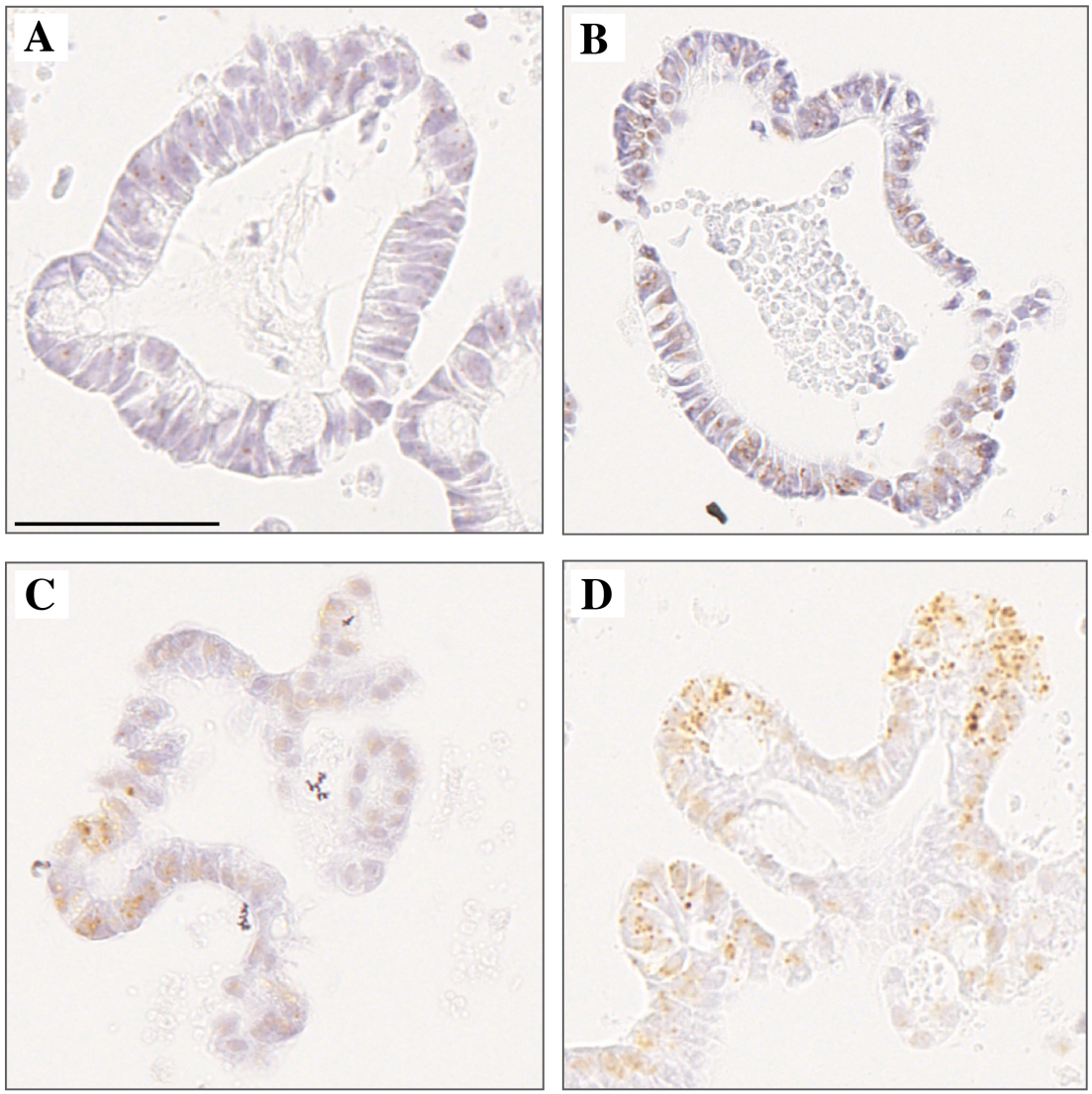

Figure 6.19: Illustration of Lgr5 expression.
A) *In situ* hybridisation of Lgr5 expression in WT, B) in WT organoids exposed to *Apc*$^{1322/+}$, C) in WT organoids exposed to normal fibroblasts and D) in WT organoids exposed to tumour-exposed fibroblasts for 72 h. Scale bar = 50µm.

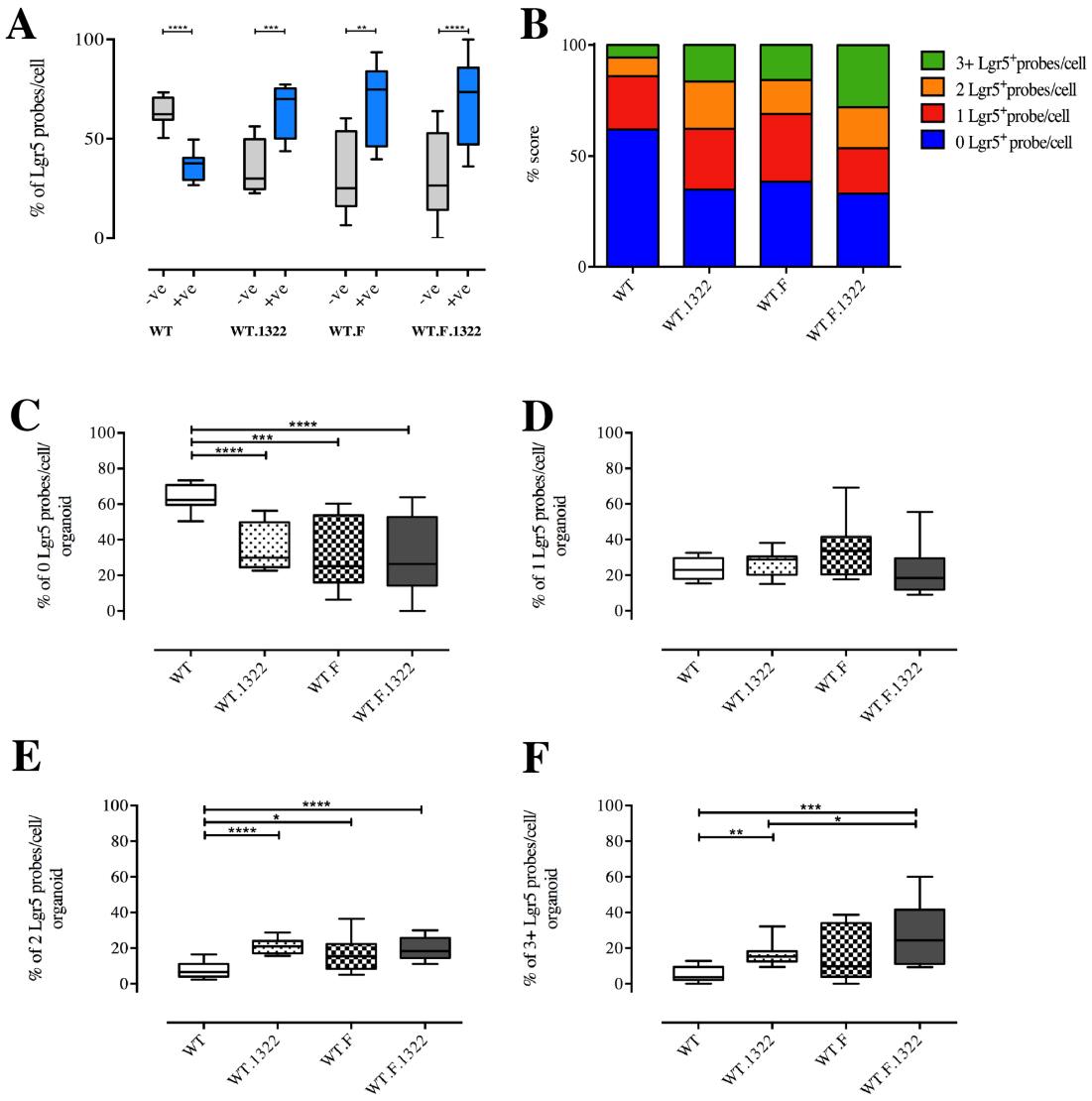

Figure 6.20: Exposure to *Apc*$^{1322/+}$ and TEFs increased the number of Lgr5 probes in WT organoids after 72 h.

A) Percentage of cells expressing Lgr5 (+ve) and cells that do not express Lgr5 (-ve) in WT organoids, WT organoids exposed to *Apc*$^{1322/+}$ (WT.1322), exposed to normal fibroblasts (WT.F), and exposed to TEFs (WT.F.1322). B) Number of Lgr5 probes per cells was measured ranging from 0 probes to 3 or more probes counted per cell. Percentage was then calculated and distribution represented in a stacked bar plot (χ^2: $p < 0.0001$). C) Shows the percentage of 0 Lgr5 probes, D) of 1 Lgr5 probe, E) of 2 Lgr5 probes, and F) of 3+ Lgr5 probes for each group. Pairwise comparisons using a t-test with Welch correction was performed. Significance: $p < 0.05$ (*), $p < 0.01$ (**), $p < 0.001$ (***), $p < 0.0001$ (****).

6.5 Discussion

Progression of mutated colonic epithelial cells to cancer appears to be dependant upon interactions between the initiated epithelium and the surrounding stroma. However, how the stroma of already initiated epithelium influences normal epithelium, and the nature of these interactions are poorly understood. Thus, to gain insight into the earliest stages of colon cancer development, interactions between WT organoids and *Apc*$^{1322/+}$ organoids were investigated in a transwell set up; in addition, the impact of tumour-exposed fibroblasts (TEFs) on WT organoids was also assessed.

As previously shown in Chapter 5, a single *Apc* mutation can activate distinct transcriptional changes within epithelial cells in exposed WT organoids when grown adjacent to each other, as they clustered slightly independently from non-exposed WT organoids, indicating that *Apc*$^{1322/+}$ organoids have an effect on WT organoids already after 72 h. A similar result was obtained here in WT organoids exposed to *Apc*$^{1322/+}$ in a co-culture using transwells. In WT organoids exposed to *Apc*$^{1322/+}$, gene sets for DNA replication, DNA MMR and the ribosome pathway were significantly upregulated, while other pathways, such as oxidative phosphorylation, were significantly downregulated. This was consistent with the findings in Chapter 5, thus showing that the results were reproducible using orthogonal methodology.

Strikingly, WT organoids exposed to TEFs clustered independently from both WT organoids and WT organoids exposed to *Apc*$^{1322/+}$ organoids, indicating an important role of TEFs very early on in neoplastic transformation (Figure 6.1).

Interactions between transformed epithelial cells and their associated stroma is an important determinant of early tumour growth. The stromal microenvironment is composed of ECM components, secreted factors, as well as stromal cells, which include fibroblasts and immune cells (Fridman *et al*. 2012). Previous studies in the colon have shown how a pro-inflammatory stromal environment contributes to pre-malignant changes (Klampfer 2011). Characteristics of such changes included increased cytokine signalling and immune cell infiltration. However, the role of fibroblasts within the stroma is less well defined in the early stages of neoplastic transformation. Understanding interactions between epithelial cells and fibroblasts may ultimately uncover signalling pathways that contribute to early colonic

transformation. Therefore, fibroblasts exposed to *Apc* deficient organoids were generated (TEFs) to mimic the effect of CAFs when grown in close proximity to colonic epithelium.

In order to distinguish whether the identified altered pathways and accompanying gene expression changes were triggered by $Apc^{1322/+}$ organoids or by TEFs, expression profiles from GSEA were compared. In general, pathways altered for epithelial to epithelial interactions were enhanced in WT organoids when exposed to TEFs (Figure 6.15). For instance, the tendency for positive enrichment of the cytokine-cytokine receptor interaction pathway was present in WT organoids exposed to $Apc^{1322/+}$, but was significantly induced in WT organoids exposed to TEFs, indicating that TEFs could potentially accelerate this process.

However, it is unclear whether fibroblasts released cytokines or ligands that caused the observed upregulation, or whether it is an intrinsic effect and cytokine release was stimulated by fibroblasts in these exposed organoids. To establish whether intrinsic or extrinsic effects are responsible for the induction, ELISAs for cytokines of the organoid media from WT organoids, WT organoids exposed to TEFs, and also from WT organoids exposed to $Apc^{1322/+}$, and from $Apc^{1322/+}$ organoids exposed to fibroblasts could be performed in future.

In general, the majority of pathways downregulated in WT organoids exposed to TEFs were metabolic pathways. Altered metabolism is a key factor in neoplastic transformation (Hanahan *et al*. 2011). Alterations in metabolic pathways have been shown to occur at the adenoma stage of carcinogenesis, and a recent study suggested induced MYC expression is responsible for the metabolic reprogramming of CRC (Satoh *et al*. 2017). Findings in this current study would suggest that these metabolic alterations occur even earlier, in fact already in the progression from normal epithelium to adenomas, and that exposure for 72 h of either $Apc^{1322/+}$ or TEFs is sufficient to cause metabolic changes in WT organoids.

In WT organoids exposed to $Apc^{1322/+}$ organoids or TEFs, oxidative phosphorylation was significantly downregulated, indicating that this is not solely driven by TEFs, however, TEFs seem to boost this process. This is further strengthened by the fact that oxidative phosphorylation was significantly downregulated in WT organoids grown adjacent to $Apc^{1322/+}$, as shown in Chapter 5, indicating this is an early event in neoplastic transformation.

Moreover, PPAR signalling, fatty acid metabolism, and cytochrome P450 metabolism were significantly downregulated in WT organoids exposed to both, *Apc*$^{1322/+}$ or TEFs, and again TEFs seem to have accelerated this process.

PPARs are transcription factors mediating metabolic pathways (Souza-Mello 2015). The PPAR subfamily consists of three members, PPAR-α, PPAR-δ and PPAR-γ. PPAR-α is involved in peroxisome proliferation, activation of fatty acid metabolism, and lipid metabolism (Dai *et al*. 2010). It was significantly reduced in WT organoids exposed to both, *Apc*$^{1322/+}$ and TEFs. This is in line with what has previously been demonstrated. PPAR-α expression was significantly reduced in CRC compared to matched-normal tissue (Grau *et al*. 2006, Jackson *et al*. 2003). Thus, one could speculate that reduction in PPAR-α could potentially be an indicator of early signs of neoplastic transformation and growth.

However, it is unclear whether reduced PPAR-α gene expression is reflected at the protein level. IHC or Western blot for PPAR-α could be performed to assess protein expression in WT organoids exposed to *Apc*$^{1322/+}$ organoids or TEFs.

It is known that PPAR-α regulates energy metabolism, including fatty acid oxidation, and one of its major functions is to promote fatty acid utilisation (Varga *et al*. 2011). PPAR-α regulates genes involved in fatty acid uptake, fatty acid activation and transport into the mitochondria (Wang 2010). Indeed, results obtained from IPA analysis would suggest that PPAR-α caused a reduction in fatty acid oxidation and transport that led to further reduction in fatty acid metabolism in WT organoids when exposed to both, *Apc*$^{1322/+}$ or TEFs (Figure 6.11). In addition, reduction of fatty acids in tumour samples compared to matching normal samples has previously been observed (Guo *et al*. 2017), indicating its downregulation occurs early in carcinogenesis.

More specifically, PPAR is negatively regulated by pro-inflammatory cytokines, specifically IFN-γ and TNF-α, indicating that the expression of PPARs is decreased when IFN-γ and TNF-α are present (Varga *et al*. 2011). FABP1 is an important part of PPAR signalling: FABP1 is responsible for the transportation of long chain fatty acids (Wang *et al*. 2015) and plays a role in inflammation through its interaction with PPAR (Gajda *et al*. 2015). In previous studies, FABP1 expression was significantly reduced in colorectal tumours compared to matching normal mucosa (Friedman *et al*. 2016, Lawrie *et al*. 2004) and this decreased expression of

fatty acid storage and PPARs was associated with loss of FABP1 (Wolfrum *et al*. 2001).

FABP1 can activate PPARs resulting in expression of downstream transcription targets, including anti-proliferation and anti-inflammatory genes. Disruption of this interaction via increased TNF-α may lead to inactive PPAR and decreased FABP1 (Wood *et al*. 2017, Xu *et al*. 2017). Thus, the decreased expression of FABP1 could potentially be explained by the observed increase in *Tnf-α* expression in WT organoids exposed to TEFs, which may inhibit PPAR leading to the here observed downregulation of FABP1. This could be verified using immunohistochemistry in future studies.

It has previously been shown that the immune environment of MSI cancers disrupts the PPAR/FABP1 interaction leading to decreased FABP1 expression (Wood *et al*. 2017). Based on FABP1's characteristics including cellular differentiation and anti-proliferation, its loss in CRC would be expected to result in de-differentiated tumours with worse prognosis (Pei *et al*. 2007, Yamazaki *et al*. 1999). Thus, downregulation of PPAR-α could explain the reduction observed for fatty acid metabolism-related gene expression. However, a direct link between PPAR-α and fatty acid metabolism in WT organoids exposed to both, $Apc^{1322/+}$ or TEFs would need to be established.

Through oxidation with glucose metabolism and hypoxia, fatty acid metabolism has been shown to play a role in the energy supply for tumour cells (Samudio *et al*. 2010). These metabolic changes can be inhibited by tumour suppressor genes, which are known to be involved in proliferative and survival signalling (Fritz *et al*. 2010), also potentially explaining the reduction seen in the fatty acid metabolism.

Downregulation found in fatty acid beta oxidisation for ATP production and epithelial cell differentiation suggests that within an inflammatory microenvironment, de-differentiated and rapidly dividing tumour cells divert the oxidation of fatty acids from energy production to support tumour proliferation (Xu *et al*. 2017). Cancer cells then potentially switch from the aerobic mitochondrial oxidative phosphorylation to glycolysis (Warburg Effect) as their primary energy source (Van der Heiden *et al*. 2009). Glycolysis further supplies cancer cells with metabolites, which are essential for cellular proliferation (Gatenby *et al*. 2004).

To conclude, downregulated fatty acid metabolism together with a non-significantly unregulated glycolysis pathway could indicate the first steps towards the Warburg effect in WT organoids when exposed to mutant organoids and/or TEFs.

Looking closer at genes significantly involved in the observed downregulation of fatty acid metabolism revealed three genes that potentially contributed to the differential expression of the fatty acid metabolism pathway: *Adh1*, *Adh4*, and *Adh7* in WT organoids exposed to TEFs, whereby only *Adh4* was significantly reduced in WT organoids exposed to $Apc^{1322/+}$. These genes can therefore be considered to play a key role in the activity of this pathway. Alcohol dehydrogenases (Adhs) are involved in the oxidation of alcohol. Thus, the exact role of the reduced Adhs is not immediately obvious from this data. However, it has been shown that ADH1 was reduced in the progression from adenoma to carcinoma (Carvalho *et al*. 2012). To our knowledge, this is the first study to show that the fatty acid metabolism pathway is already altered in WT organoids solely due to the exposure to either $Apc^{1322/+}$ or TEFs.

The cytochrome P450 metabolism was significantly downregulated in WT organoids exposed to $Apc^{1322/+}$ or TEFs. KEGG pathway analysis of CRC compared to normal tissue has demonstrated downregulation of this pathway (Liang *et al*. 2016), indicating that such reduction occurs even earlier in neoplastic transformation.

Several *Cyp* genes within the cytochrome P450 metabolism pathway were significantly downregulated. *Cyp2d34* was significantly reduced in WT organoids exposed to $Apc^{1322/+}$, whereas *Cyp2c29*, *Cyp3a11*, and *Cyp3a25* were significantly reduced in WT organoids exposed to TEFs. Further analysis using IPA revealed that *Cyp4a22*, a fatty acid ω-hydroxylase (Hardwick *et al*. 2009), was significantly downregulated in WT organoids exposed to $Apc^{1322/+}$ or TEFs. Its downregulation was likely caused by PPAR-α, leading to reduced fatty acid oxidation. It has previously been shown that PPAR interacts with Cyp genes (Hardwick *et al*. 2009). Alterations in members of the CYP4 family can lead to defects in fatty acid metabolism; however, the function of *Cyp4a22* is yet to be determined (Nebert *et al*. 2013).

Unexpectedly, the ribosome pathway was significantly reduced in WT organoids exposed to TEFs, whilst significantly induced in WT organoids exposed to $Apc^{1322/+}$. Ribosomes are essential for protein synthesis, thus protein synthesis could

have been impaired in WT organoids when being exposed to TEFs. Enriched genes of the ribosome pathway have been previously found in adenomas compared to normal colonic mucosa (Lu *et al*. 2006), which is in line with the upregulation found in WT organoids exposed to *Apc*$^{1322/+}$. Upregulated ribosome biogenesis poses an increased CRC risk onset, which is based on the close interconnection between ribosome biogenesis and cell proliferation (Derenzini *et al*. 2017). These results demonstrate that this change is an early step in tumourigenesis and represents a functional change in field cancerization.

Significant induction of the cytokine-cytokine receptor interaction pathway was identified in WT organoids exposed to TEFs, whereas no significant change was detected in WT organoids exposed to *Apc*$^{1322/+}$, suggesting TEFs were driving this upregulation. *Tnf-α* was significantly upregulated as part of this pathway. TNF-α is a proinflammatory cytokine secreted from macrophages as an acute inflammatory response (Cox *et al*. 1992), and during sustained inflammation the TNF-α level is elevated within colonic mucosa (Landskron *et al*. 2014). More importantly, TNF-α has been shown to promote Wnt/β-catenin activity in tumourigenesis (Coskun *et al*. 2014). In the current study, the Wnt signalling pathway was significantly induced in WT organoids exposed to TEFs, but not in WT organoids exposed to *Apc*$^{1322/+}$, indicating that this upregulation is due to the presence of TEFs.

The canonical Wnt pathway is one of the major signalling pathways involved in the establishment of intestinal homeostasis (Clevers 2006). Wnt signalling is fundamental in order to maintain the proliferative compartment of the intestinal crypt. Dysregulation of components in the Wnt signalling pathway, including misexpression of Wnt ligands and secreted inhibitors of this pathway, have been associated with the initiation of colorectal tumourigenesis. The core of this pathway is the protein β-catenin, encoded by *Ctnnb1* (White *et al*. 2012). Although the nature of mutations in the Wnt pathways can be distinct, they all lead to stabilisation of β-catenin in the nucleus. Wnt activating mutations have been shown to be essential for tumour initiation in the colon (Dow *et al*. 2015).

Here, increased induction of the Wnt signalling pathway in WT organoids exposed to TEFs could be explained by the fact that several Wnt ligands (*Wnt4*, *Wnt7a*, and *Wnt9a*) were overexpressed. Wnt ligands are important in maintaining stem-like properties (de Sousa e Melo *et al*. 2016). This suggests the binding of FZD

receptors and LRP families, thereby inhibiting the phosphorylation of β-catenin. Frizzled receptors, such as FZD1 and FZD2, as well as the receptor LRP5 were significantly upregulated in exposed WT organoids. Further inhibition of the destruction complex, composed of the core proteins AXIN, APC, and GSK3β, could allow β-catenin to escape degradation, resulting in accumulation in the cytosol and the translocation to the nucleus, which could explain the upregulation found for *Ctnnb1* in WT organoids exposed to TEFs. In the nucleus, it can be assumed that β-catenin stimulates the transcription factor TCF4, which was significantly induced, to regulate expression of target genes.

In addition, it is also likely that the Wnt signalling pathway was activated by members of the R-spondin protein family. It has been shown that Lgr5, which is both a Wnt signalling component as well as a Wnt target gene, functions as an R-spondin receptor, associates with the FZD/LRP receptor complex, and potentiates Wnt/β-catenin signalling by enhancing Wnt-induced LRP phosphorylation (Carmon *et al*. 2011, de Lau *et al*. 2011). Thus, given the upregulation detected in *Lgr5*, one could assume activation of Wnt signalling was driven in a R-spondin dependent manner (Figure 6.21). *R-spondin1* was significantly induced in WT organoids exposed to TEFs compared to WT organoids only. Overexpression of *R-spondin1* has been shown to increase cell proliferation in the small intestine and colon (Kim *et al*. 2005). Moreover, *R-spondin1* has to be supplied to organoid cultures for crypt growth and survival (Sato *et al*. 2011), thereby indicating its fundamental role in the maintenance of LGR5 stem cells. Thus, one could speculate that *R-spondin1* binds to LGR5 receptors, thereby inhibiting the destruction complex and blocking β-catenin phosphorylation, leading to the observed upregulation of *Ctnnb1*, which in turn could indicate accumulation of β-catenin. In the nucleus, β-catenin potentially bound to the transcription factor TCF4, as increased gene expression of *Ctnnb1* and *Tcf4* was identified in WT organoids exposed to TEFs. Activation of the transcription factor TCF4 has been associated with adenoma formation (Shin *et al*. 2014). However, TCF4 is only activated upon phosphorylation, and phosphorylated TCF4 could increase the transcription of *Lgr5*.

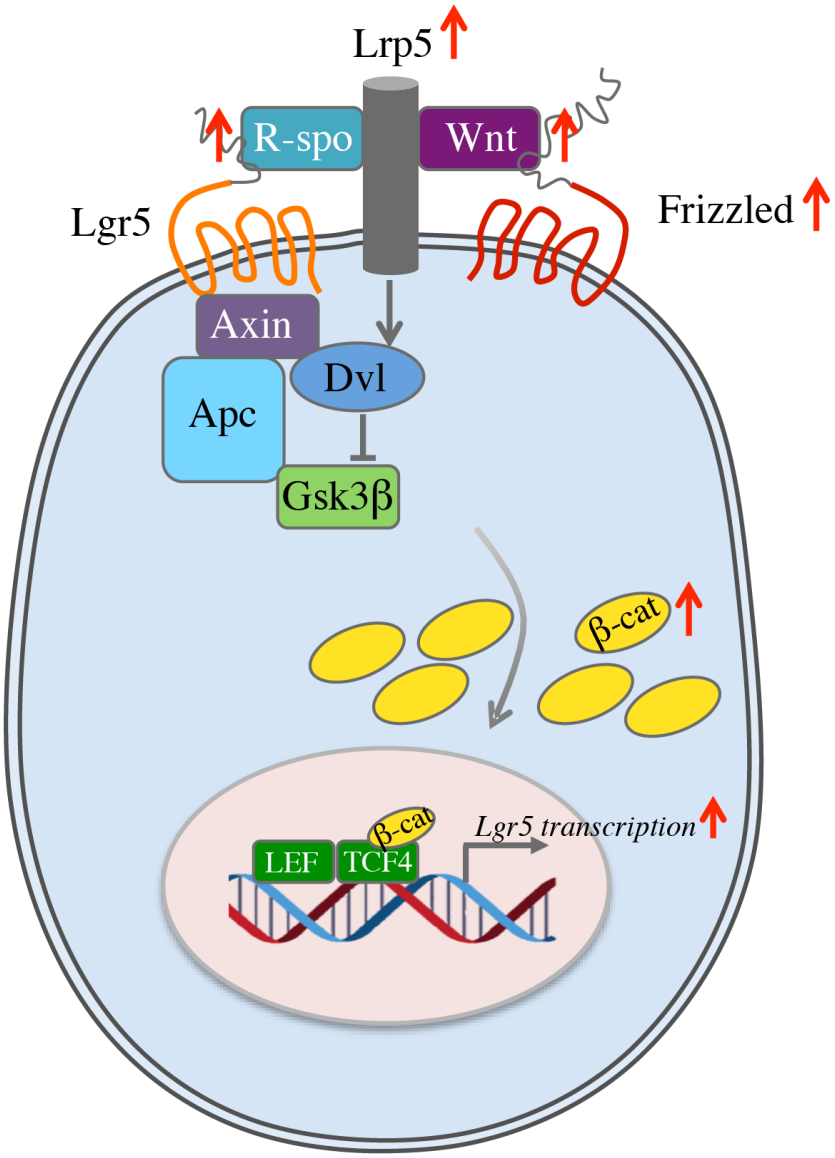

Figure 6.21: Potential mechanism by which Wnt signalling is dysregulated in WT organoids exposed to TEFs.

Overexpression of FZD receptors and WNT ligands can lead to increased activation of the pathway. Upregulated Wnt ligands initiate signalling through R-spondin, Lgr5 receptors and Lrp5 co-receptor, thereby disrupting the destruction complex. Accumulation of β-catenin in the cytoplasm results its translocation into the nucleus, where it binds TCF4, and activates target gene expression of Lgr5. Apc, Adenomatous polyposis coli; Dvl, Disheveled; Gsk3β, glycogen synthase kinase 3; LEF, lymphoid enhancer factor; Lgr5, leucine-rich repeat-containing G-protein coupled receptor 5; Lrp5, lipoprotein receptor-related protein; R-spo, R-spondin; TCF4, T-cell factor 4. Red arrows represent genes that were found significantly upregulated in WT organoids exposed to TEFs.

Future experiments need to establish whether TCF4 is phosphorylated in WT organoids exposed to TEFs and whether *Lgr5* was indeed transcribed. Therefore, IHC or Western blots could be performed for LGR5 to establish protein levels, but also with an anti-phosphorylation antibody to investigate whether TCF4 was activated, as TCF4 can only transcribe *Lgr5* when phosphorylated.

TCF/LEF are two typical binding domains of the LGR5 promoter. However, a recent study has shown that LGR5 expression in normal and neoplastic gastric tissue was regulated by the transcription factor SP-1 (Wilhelm *et al*. 2017). This could present an alternative mechanism explaining the upregulation found for *Lgr5*, as SP-1 was also significantly induced.

Increased levels of *Lgr5* mRNA expression in WT organoids exposed to TEFs compared to WT organoids alone were also shown using *in situ* hybridisation (see Figure 6.20). Upregulation of *Lgr5* in these cells might indicate that these cells have acquired stem-like properties, indicating a change in the stem cell compartment allowing for altered growth and differentiation behaviour. Increased levels of LGR5 expression were detected in CRCs and tumour cells with the highest levels of LGR5 to behave as functional stem cells (Junttila *et al*. 2015, Kemper *et al*. 2012). LGR5 and R-spondins augment Wnt ligand mediated Wnt signalling, which is likely promoting stem cell properties. LGR5 has been shown to reflect on both, the high Wnt activity and the functionality of LGR5 in promoting stem cell functions (Yang *et al*. 2015). There has been evidence that high Wnt expression identifies cells with stem-like properties, and that high Wnt activity defines the cancer stem cell fraction (Prasetyanti *et al*. 2013). In fact, human CRC stem cells can be defined on the basis of high Wnt signalling activity and that these cells are located in the myofibroblast niche (Vermeulen *et al*. 2010).

Further functional experiments need to be done to confirm the properties of these *Lgr5*$^{+}$ cells. In order to determine whether the Lgr5 was indeed transcribed, one could check for protein levels using IHC or Western blots for LGR5. However, LGR5 antibodies for both mouse and humans remain of questionable reliability. Rather, a single cell seeding experiment can be performed: cells positive for *Lgr5* expression from WT organoids exposed to TEFs and WT organoids only are sorted and then seeded into Matrigel. A higher number of fully developed organoids would be expected from *Lgr5*$^{+}$ cells previously exposed to TEFs compared to *Lgr5*$^{+}$cells from WT organoids.

Increased expression of Wnt and β-catenin indicates a positive feedback loop. The more Wnt is expressed, more cells acquiring stem-like behaviour, which could potentially lead to a higher rate of cell proliferation. It was investigated whether WT organoids exposed to TEFs exhibit greater cell proliferation than WT organoids only or WT organoids exposed to normal murine fibroblasts. Organoids in each condition were stained with anti-Ki67. However, no significant change in cell proliferation was shown (Figure 6.18). Instead, great intra-variability within each of the conditions was detected. It has recently been shown that variability of Ki67 expression levels is due to the cell cycle regulation of mRNA and protein in proliferating tissues in human and also in mice (Sobecki *et al*. 2017). Cells that have just exited the cell cycle express lower levels of Ki67. Additionally, Ki67 protein is degraded from mitosis to G1. This must be taking into account when interpreting Ki67 staining in histopathology and its use as a prognostic marker (Sobecki *et al*. 2017). It further explains the observed intra-organoid variability in WT organoids of all conditions tested, since the stage in the cell cycle of the organoids that were assessed for anti-Ki67 staining was unknown. Some organoids could have been in the cell cycle, while others have just left the cell cycle, thus expressing lower levels of Ki67.

To conclude, future work should take into account only organoids that are in the same phase of the cell cycle in order to be able to compare Ki67 expression levels to assess whether cell proliferation is increased in WT organoids exposed to TEFs compared to WT organoids only. Alternatively to Ki67, proliferation could also be measured using EdU/BrdU counts. Therefore, organoids would need to be dissociated and FACS sorted for DAPI and EdU/BrdU. A higher number of proliferating cells would be expected in WT organoids exposed to *Apc*$^{1322/+}$ and TEFs compared to WT organoids.

In addition to Wnt ligands, CAFs and immune cells produce cytokines and signalling molecules, which have been shown to have a direct effect on Wnt signalling. Hepatocyte Growth Factor (HGF), Osteopontin (OPN) and stromal-derived factor 1α (SDF1α) for instance are all secreted by myofibroblasts and are known factors to enhance activity of Wnt signalling in CRC (Vermeulen *et al*. 2010). Therefore, one could assume that TEFs secreted Wnt ligands, and other factors that led to the here observed upregulation of Wnt signalling in WT organoids exposed to TEFs. In order to investigate which Wnt ligands were secreted by TEFs, a Western blot on the organoid media of WT organoids and TEFs as compared to media from

WT organoids only could be performed. A higher expression level of Wnt ligands would be expected in the media of WT organoids exposed to TEFs compared to WT organoids only. Increased Wnt activity through cytokine secretion has been shown to result in increased proliferation and tumourigenicity in stem cells (de Sousa e Melo *et al*. 2016).

In addition to LGR5, cyclo-oxygenase-2 (COX2), a key enzyme of prostaglandin synthesis, is also a known target gene of Wnt signalling (Luo *et al*. 2009) and has been associated with Wnt pathway activation (Bitarte *et al*. 2011). In this study, *Cox2* was significantly upregulated in WT organoids exposed to TEFs. Accumulation of β-catenin has been shown to upregulate *Cox2* (Araki *et al*. 2003). Thus, it can be assumed that, given the upregulation detected in *Ctnnb1* and *Tcf4*, β-catenin was stabilised and activated TCF4, resulting in upregulation of *Cox2*. Whilst most normal tissues lack COX2 expression, its levels increase under mitogens and cytokines resulting in the accumulation of prostanoids in inflamed tissue (Eisinger *et al*. 2007), which is in line with the increased expression of *Tnf-α*. Elevated COX2 levels may have anti-apoptotic effects and may lead to tumour development and expansion (Galamb *et al*. 2010). COX2 has been described to be involved in early stages of colorectal carcinogenesis. Overexpression was observed in 50% of benign polyps compared to normal tissue (Eberhart *et al*. 1994), but also in the mucosa of active ulcerative colitis patients (Hokari *et al*. 2011). Furthermore, COX2 is negatively regulated by APC and loss of APC function and subsequent dysregulation of COX2 expression promotes tumourigenesis (Eisinger *et al*. 2007), indicating that WT organoids exposed to TEFs already had an effect on *Cox2* expression.

Collectively, this data represents a complex and diverse mechanism by which the Wnt signalling pathway and colonic stem cells can be regulated: increased *Lgr5* expression could be explained by R-spondin–mediated enhancement of Wnt/β-catenin signalling.

Upregulation of two MMPs, *Mmp7* and *Mmp9*, has been identified as part of the ECM receptor interaction pathway. In general, MMPs pave the way for tumour growth, invasion and metastasis through the degradation of the ECM (Herszenyi *et al*. 2012, Kessenbrock *et al*. 2015). In addition, MMPs have modulating functions in immunity and inflammation during tumourigenesis through the activation of growth factors, cytokines and other membrane proteins (Bauvois 2012, Nissinen *et al*. 2014).

MMP7 plays an important role in degrading ECM proteins, such as type IV collagen and laminins (Overall *et al*. 2002). Interestingly, MMP7 has previously been shown to be regulated by Wnt signalling through the binding of β-catenin and the transcription factors TCF/LEF (Gustavson *et al*. 2004). Furthermore, binding of TCF/LEF to the activator protein-1 (AP-1) sites has been shown to activate transcription of MMP7 in CRC (Crawford *et al*. 2001). Therefore, the observed induction of Wnt signalling in WT organoids exposed to TEFs could potentially explain the upregulation detected in *Mmp7*. Increased expression of MMP7 has been shown to promote tumour progression (Bai *et al*. 2015) and has been linked to poor survival in CRC patients (Klupp *et al*. 2016).

MMP9 is mainly responsible for the degradation of the ECM and plays a critical role in tumour progression and inflammation (Lee *et al*. 2008). Upregulation of MMP9 has been observed in CRC patient samples compared with healthy mucosa (Chu *et al*. 2012, Kostova *et al*. 2014), but has also been observed in precursor lesions, suggesting upregulation of MMP9 is an early event in tumourigenesis and can be used as a biomarker for early diagnosis of CRC (Herszenyi *et al*. 2008, Lorenc *et al*. 2017).

MMPs also play an important role in shaping the stem cell niche during development, but this process can be altered during tumourigenesis (Kessenbrock *et al*. 2015, Melzer *et al*. 2017). The stem cell niche consists of a microenvironment of adjacent cells and the ECM (Scadden 2006). Due to their ability to cleave, degrade and rearrange ECM molecules, MMPs can regulate the stem cell niche. For example, in human epidermal stem cells, MMP2 and MMP14 are inhibited to maintain long-term survival (Muffler *et al*. 2008). Thus, upregulation of MMP9 in WT organoids exposed to TEFs can alter signalling pathways and might lead to the destruction of niche related structures, promoting stem cell expansion resulting in tumour initiation.

Increased levels of MMP9 in WT organoids exposed to TEFs could suggest structural and functional changes of the ECM. MMP9 expression is regulated at the transcriptional level (Fanjul-Fernández *et al*. 2010), and thus upregulation of MMP9 could be the result of increased transcription. Once different transcription factors are phosphorylated, they can bind the promoters of *MMP9* genes. Activation of transcription factors can be mediated by MAPK and SMAD proteins, which in turn can be activated by TNF-α and TGF-β, respectively (Fanjul-Fernández *et al*. 2010). One of the key transcription factors in the regulation of MMP9 is AP-1 (Overall *et*

al. 2002). In fact, it has been shown for MMP1 that cytokines enhance its activation through MAPK signalling by increasing the levels of the different AP-1 proteins: c-JUN and c-FOS (Wang *et al*. 2005). This leads to the assumption that the observed upregulation of *Tnf-α* could activate MAPK signalling, which in turn activates AP-1, c-JUN, and c-FOS through phosphorylation, leading to increased MMP9 transcription, as these three transcription factors were also significantly upregulated in WT organoids exposed to TEFs (Figure 6.22).

A study on bladder cancer cell lines has shown TNF-α regulated MMP9 expression through AP-1 and SP-1 and that ERK1/2 mediated TNF-α induced MMP9 expression by coordinating the regulation of the binding activity of the transcription factors (Lee *et al*. 2008). In fact, SP-1, a known transcription factor known to regulate MMP9 expression (Murthy *et al*. 2012), was significantly induced in WT organoids exposed to TEFs, indicating that increased induction of SP-1 could enhance MMP9 transcription in WT organoids exposed to TEFs.

Furthermore, upregulation of MMP9 could be mediated by TNF-α through JNK signalling, the non-classical MAPK pathway. It has been shown that the JNK pathway is involved in the regulation of TNF-α-induced gene expression by phosphorylation of transcription factors, mainly c-JUN and ATF-2 (Cohen *et al*. 2006). As significant upregulation of *Tnf-α* and its receptor TNFR was identified, it is likely that increased *Tnf-α* expression could result in upregulation of MMP9 through JNK signalling (Figure 6.22).

Thus, *Tnf-α* could accelerate this event through activation of MAPKs, explaining the observed MMP9 upregulation that could lead to collagen breakdown and thus to structural changes in the ECM, eventually resulting in tumour initiation and progression. It further indicates that activation of MAPK appears to be an early event in neoplastic transformation in WT organoids exposed to TEFs. MAPK plays an important role in regulation of proliferation and transcription and its upregulation has previously been shown in adenomatous colonic crypts when compared to normal tissue, further suggesting its role in the early stages of colonic transformation (Lechner *et al*. 2003).

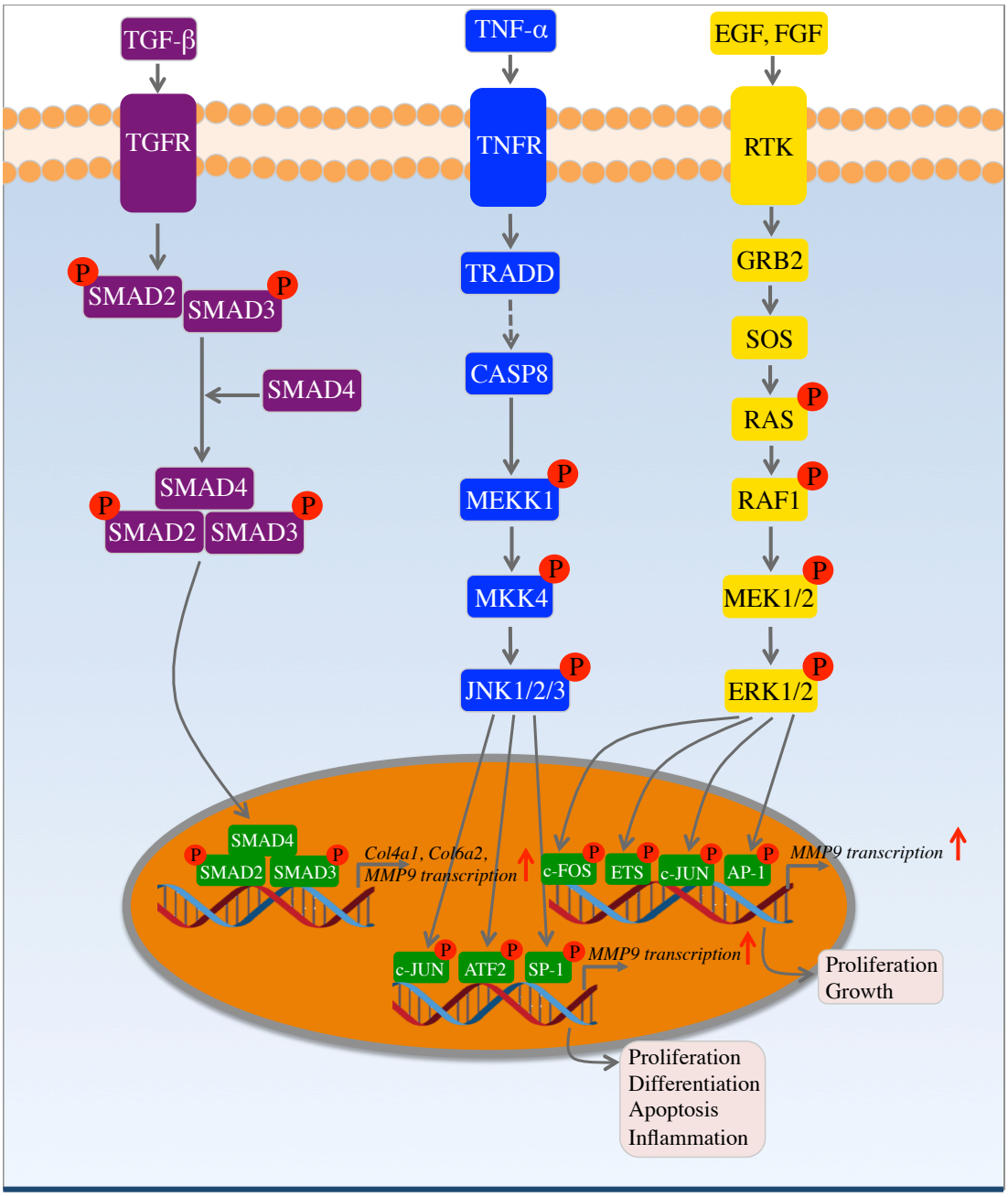

Figure 6.22: Potential mechanism explaining MMP9 activity.

As mentioned above, MMP9 is also regulated by SMADs, which can enhance TGF-β mediated gene expression (Kuo *et al*. 2009). TGF-β plays a role in proliferation, differentiation and migration (Pickup *et al*. 2013). Furthermore, TGF-β signalling can induce expression of ECM proteins, and has been linked to transcription of collagen genes (Di Sabatino *et al*. 2009, Verrecchia *et al*. 2002). Here, *Col4a1* and *Col6a2* were significantly induced as part of the ECM receptor interaction pathway. Collagen type IV is the major component of the ECM and involved in cell adhesion, migration, differentiation, and growth (Ikeda *et al*. 2006). It has previously been shown that TGF-β signalling has a stimulating effect on type IV collagen gene transcription and protein synthesis (Zdunek *et al*. 2001).

Collagen type VI is mainly involved in the regulation of epithelial cell behaviour (Groulx *et al*. 2011). Upregulation of collagen genes could also indicate changes in the composition of the ECM and additionally, that such structural changes occur early on in neoplastic transformation.

Thus, another potential mechanism explaining upregulation of MMP9, as well as the collagen genes, mainly *Col4a1* and *Col6a2*, could be mediated by TGF-β signalling through a SMAD-dependent manner, since TGF-β signalling was also found significantly induced. Induced TGF-β could bind to its TGF-β receptor. Differential phosphorylation of SMAD2 and SMAD3 by TGF-β receptor activation together with SMAD4 could promote their translation into the nucleus leading to a complex that activates SMAD-dependent transcription to induce gene expression, potentially in *Col4a1*, *Col6a2*, and MMP9 (Figure 6.22).

It has been shown that MMP13 gene expression was induced by TGF-β through the activation of SMAD3 together with MAPK signalling (Leivonen *et al*. 2002). This indicates that MMP9 might not be regulated by only one pathway, but rather multiple pathways can control MMP9 transcriptional regulation.

However, future work needs to be done in order to determine whether the elevated MMP9 mRNA was indeed transcribed, as so far, only an upregulation at mRNA level has been observed. To check for protein levels, IHC or Western blots for MMP9 can be performed. Assuming MMP9 was transcribed, the question remains which transcription factor was responsible for MMP9 transcription. Again, IHC or Western blots could be performed with anti-phosphorylation antibodies to investigate which transcription factor was activated, as only phosphorylated transcription factors could potentially transcribe MMP9. Depending on which

transcription factor is activated, it indicates whether MMP9 is transcribed through the classical MAPK-ERK signalling pathway, or through the JNK pathway. siRNA knockdown of activated transcription factors would show whether MMP9 is still transcribed, thus indicating that this could be the pathway responsible for the observed upregulation of MMP9 in WT organoids exposed to TEFs. To check for MMP9 activity, immunofluorescence staining for COL4 and cleaved collagen could be performed. The detection of cleaved collagen indicates degradation and thus MMP9 activity.

Furthermore, several collagen genes, including *Col4a1* and *Col6a2*, were found significantly upregulated. As with MMP9, at this stage these collagen genes were upregulated, but further work needs to be done to determine whether these genes were transcribed. Again, this could be performed using IHC or Western blots to establish protein levels. Assuming the upregulation of these genes is mediated through TGF-β signalling, immunohistochemistry for all SMAD transcription factors using anti-phosphorylation antibodies could be performed to check for activity. Assuming further that SMAD transcription factors were indeed activated, knockdown of each individual SMAD should be performed to see if collagen genes as well as MMP9 are still transcribed. This would indicate whether TGF-β signalling is the responsible pathway.

Since upregulation of MMP9 and collagen genes indicate compositional changes in the ECM, proteomic techniques could be performed to investigate the composition of ECM proteins in WT organoids when exposed to TEFs (Byron *et al*. 2013). Moreover, mass spectrometry could be employed to gain information about absolute abundance of ECM proteins (Goddard *et al*. 2016).

This chapter has highlighted the expression profiles of WT organoids when being exposed to $Apc^{1322/+}$ organoids or TEFs. To ideally distinguish whether the observed changes in WT organoids were due to the TEFs or only due to the presence of fibroblasts, future experiments should include the control of WT organoids being exposed to normal fibroblasts.

To conclude, these experiments have shown that exposure to TEFs have led to significant changes in WT organoids after only 72 h representing early signs of tumour initiation.

7 Chapter VII: Conclusion

It is generally accepted that tumours are *monoclonal-in-origin*, but recent studies have shown that tumours can have a polyclonal origin; they are derived from multiple independently transformed cells (Merritt *et al*. 1997, Novelli *et al*. 2003, Novelli *et al*. 1996, Thirlwell *et al*. 2010, Thliveris *et al*. 2005). However, the mechanism that generates polyclonal tumours is unknown, as is the importance of polyclonality in driving tumour progression. Prior to this project, short-range interactions between multiple initiated clones have been suggested to lead to the formation of polyclonal tumours in the colon. This thesis aimed at better describing these clonal interactions between colorectal adenomas and their surrounding non-dysplastic crypts, to determine the role of the stroma in this process and to provide an insight into the gene expression changes that occur in normal epithelium in close proximity to adenomas.

Consequently, there were three main aims of the project: firstly to demonstrate that clonal interactions between dysplastic and non-dysplastic colonic epithelium drive clonal expansion, secondly to investigate the stem cell dynamics between dysplastic and non-dysplastic colonic epithelium, and thirdly to investigate the underlying mechanisms responsible for the formation of polyclonal tumours. This chapter will summarise the findings of this project with respect to these aims.

To address the first aim (Chapter 3), IHC was used to illustrate cellular behaviour in the FAP colon and in patients with sporadic adenomas. Adenomatous and surrounding non-adenomatous crypts were analysed using markers for cell proliferation (Ki67), DNA damage (γH2AX) and Wnt signalling status (nuclear β-catenin). Tumour-stroma interactions were also investigated by assessing the percentage of helper T-cells (CD4), cytotoxic T-cells (CD8), macrophages (CD68) and α-SMA in the stroma of adenomas and their neighbouring non-dysplastic stroma, examining how signals emanating from the adenoma are affecting the stroma of nearby non-adenomatous crypts. Furthermore, the mutation burden of mtDNA mutations in adenomatous and neighbouring non-dysplastic crypts was investigated using CCO-deficiency as a marker for mutagenesis. The effect of distance from the

adenoma on these markers was analysed.

Results have shown increased cell proliferation (Ki67), DNA damage (γH2AX) and Wnt signalling (nuclear β-catenin) in non-dysplastic crypts close to an adenoma, and these effects decreased over distance for both FAP and sporadic adenoma patient samples. This demonstrates that increased expression for these markers is associated with the field effect emanating from the dysplastic zone. These observations further indicate that these markers play an important role in the early transformation and progression of CRC.

This field effect was further associated with an increase in T cell, macrophage and fibroblast infiltrate in the non-dysplastic stroma surrounding an adenoma for both FAP and sporadic adenoma patients. This supports previous work suggesting that a phenotypic change occurs early in the adenoma-carcinoma sequence with expression of inflammatory chemokines and cytokines dysregulated in the transition from normal mucosa to adenomas (Mo *et al*. 2016). Immune cells might exert a pro-inflammatory response in the dysplastic region, thus promoting clonal interactions through the stroma. Adenomatous polyps were found to be rich in pro-inflammatory T helper and cytotoxic cells, as well as macrophages, and this exerts a significant influence on their surrounding microenvironment. As inflammation is a known driver of crypt fission and therefore clonal expansion (Salk *et al*. 2009), a potential explanation for the development of polyclonal adenomas could be that increased inflammation surrounding dysplastic tissue increases the likelihood that dysplasia can arise in the normal surroundings. These results further highlight the complexity of the cross-talk between epithelia and stroma occurring during the earliest stages in the progression to CRC, supporting an active role of the stroma.

Furthermore, using mtDNA mutations as a proxy for mutation pressure on crypts, it was shown that crypts neighbouring an adenoma contained a higher mutation burden. Therefore, evidence was found that dysplastic crypts increase the mutagenic pressure in their surrounding non-dysplastic crypts, thus interacting with their surrounding neighbouring non-dysplastic crypts to generate a field effect.

Investigation of stem cell dynamics between dysplastic and non-dysplastic colonic epithelium revealed that the proximity of a crypt to an adenoma also affects stem cell dynamics: using somatic mtDNA mutations to trace clonal lineages, it was found that human intestinal stem cell evolution in adenomas and surrounding normal

crypts followed neutral drift dynamics and that the stem cell loss/replacement rate is accelerated in adenomas (Chapter 4).

Having established that clones interact and adenomas create a field effect in surrounding non-dysplastic crypts, proper description and characterisation of these interactions in the early stages of tumourigenesis is required. Therefore, to address the third aim, gene expression effects of an adenoma on normal colonic epithelium were investigated using an organoid culture system to get a better understanding of how these interactions occur in the very early stages of colorectal tumourigenesis and how their initiation might be regulated (Chapter 5 & 6).

In order to investigate the effects of an adenoma on normal murine intestinal epithelium, WT and $Apc^{1322/+}$ organoids were co-cultured in organoid media for 48 h and 72 h and controlled with WT and $Apc^{1322/+}$ organoids only (Chapter 5). Analysis was performed using gene set enrichment analysis (GSEA) (Subramanian *et al*. 2005). The main focus here was to study gene expression patterns in WT organoids grown in presence of *Apc* deficient organoids compared to WT organoids only. Results obtained showed distinct expression profiles for WT organoids and WT organoids exposed to $Apc^{1322/+}$ organoids for both time points. Gene expression analysis revealed that exposure to $Apc^{1322/+}$ organoids for only 48 h caused significant induction of the DNA replication pathway in WT organoids, as well as many other pathways, including those involved in the repair of DNA DSBs, spliceosome, homologous recombination. Perturbations in these pathways have been shown to alter genome stability (Pillaire *et al*. 2010) and could hint towards increased replication and cell proliferation (Bishop *et al*. 2002, Miquel *et al*. 2007), although this needs to be confirmed with further experiments.

Many metabolic pathways were downregulated in WT organoids exposed to $Apc^{1322/+}$ organoids after 48 h and 72 h, indicating that pathways involved in nutritional storage are significantly suppressed. Oxidative phosphorylation was identified as one of the most reduced pathways in WT organoids exposed to *Apc* deficient organoids. Normal cells rely on oxidative phosphorylation to generate ATP for energy, however, in cancer cells oxidative phosphorylation is reduced, while anaerobic glycolysis is increased, a phenomenon known as the Warburg effect (Zheng 2012). At the time points measured in this study, glycolysis was upregulated, however not significantly. Downregulation of oxidative phosphorylation can also suggest that more ROS are being accumulated, which is known to initiate mutations

in CRC (Yadav *et al*. 2015). Excess of ROS production has been shown to lead to oxidative damage, which in turn can activate DNA damage, replication errors and even lead to genetic abnormalities (Selim *et al*. 2017). This could explain the upregulation seen in the MMR and DNA replication pathway.

Exposure of $Apc^{1322/+}$ organoids for 72 h led to the activation of the ECM receptor interaction pathways in WT organoids. The ECM is important for maintaining cell tissue and structure, and function (Hayes *et al*. 2016). ECM expression changes have great impact on tumour development, as ECM structurally supports tumour cells and their cellular functions (Stankevicius *et al*. 2016). Therefore, upregulation of this pathway seems to promote an environment permissive to tumourigenesis.

Whilst exposure to $Apc^{1322/+}$ organoids was not long enough to detect significantly altered genes in WT organoids after 48 h, exposure for 72 h revealed that *Lamb1* was significantly upregulated, which forms a cell adhesion network in the intestinal epithelium together with integrins (McCole 2014) and changes in *Lamb1* expression have previously been observed in CRC (Petz *et al*. 2012). Thus, upregulation of *Lamb1* could hint towards changes in the basal lamina thereby potentially altering the structure of the cell adhesion network.

In addition, genes contributing to the observed enrichment of the MMR pathway were identified, among which *Pold2*, *Pold3, Pold4* and *Pole*, as well as *Mhl1* and *Msh6* were significantly induced. These genes play an important role in mediating correct DNA MMR and DNA replication (Jiricny *et al*. 2003, Pal *et al*. 2008). Perturbations in the DNA MMR pathway have been linked to CRC (Li *et al*. 2016) and impaired MMR gene function can lead to MSI (Kheirelseid *et al*. 2013). These alterations in WT organoids exposed to *Apc* deficient organoids may represent the very early events in the progression towards CRC.

Taken together, gene sets in pathways contributing to proliferation and replication were activated, whilst metabolic pathways were downregulated in WT organoids grown adjacent to $Apc^{1322/+}$ organoids. This indicates that clones interact and drive expansion, as features of such clonal expansion include proliferation and replication. Furthermore, exposure of *Apc* deficient organoids caused significant changes in WT organoids after only 72h, indicating that mutated epithelium has a rapid effect on normal epithelium in close proximity.

However, the transformation from normal to mutated epithelium is likely

dependent on interactions with the surrounding stroma as well. The stroma in normal tissue maintains homeostasis and acts as a barrier against tumourigenesis, but in the presence of tumour cells it can turn into a tumour-promoting environment (Valkenburg *et al*. 2018). This has also been shown in Chapter 3: the stroma surrounding adenomatous and non-adenomatous crypts showed a greater concentration of immune cells and fibroblasts.

Therefore, the effect of tumour-exposed fibroblasts (TEFs) on WT organoids was investigated (Chapter 6). More specifically, $Apc^{1322/+}$ organoids were co-cultured with murine fibroblasts to generate tumour-exposed fibroblasts (TEFs). These TEFs were then exposed to WT organoids aiming to investigate the reciprocal interactions between mutated epithelium and its associated stroma on normal epithelium. Here, mRNA expression changes in WT organoids exposed to $Apc^{1322/+}$ organoids, and WT organoids co-cultured with TEFs were investigated in a transwell setting for only 72 h, as opposed to adjacent to each other as shown in Chapter 5.

Interestingly, a distinct expression profile between WT organoids and WT organoids exposed to TEFs was found. They clustered independently from both, WT organoids and those exposed to $Apc^{1322/+}$ organoids, indicating that by adding a stromal component to the system, WT organoids and WT organoids exposed to *Apc* deficient organoids were transcriptionally distinct from WT organoids exposed to TEFs, highlighting the role of the stroma in early transformation. Similar results were obtained in WT organoids exposed to $Apc^{1322/+}$ organoids in a co-culture using transwells, which was consistent with the findings in Chapter 5, thus demonstrating that with a different method the results were reproducible.

In order to distinguish whether the identified altered pathways and accompanying gene expression changes were triggered by $Apc^{1322/+}$ organoids or by TEFs, the expression profiles from GSEA were compared. In general, TEFs had a much stronger effect on WT organoids compared to WT organoids exposed to $Apc^{1322/+}$ organoids. The number of significantly altered pathways changed drastically in WT organoids exposed to TEFs given both conditions had the same exposure time. More specifically, it has been shown that WT organoids exposed to $Apc^{1322/+}$ organoids or TEFs exhibited a reduced expression of metabolic pathways, however TEFs seem to have accelerated this process. Especially, PPAR-α was significantly reduced, which led to a reduction of fatty acid metabolism, indicating to be an early step in neoplastic transformation. Previously, reduction in these pathways has been

described in CRC compared to matched normal tissue samples (Grau *et al*. 2006, Guo *et al*. 2017, Jackson *et al*. 2003).

Moreover, PPAR is negatively regulated by pro-inflammatory cytokines, such as TNF-α, indicating that the expression of PPARs is decreased when TNF-α is present (Varga *et al*. 2011). FABP1, responsible for the transportation of long chain fatty acids (Wang *et al*. 2015), can activate PPARs resulting in expression of downstream transcription targets, including anti-proliferation and anti-inflammatory genes. Disruption of this interaction via increased TNF-α may lead to inactive PPAR and decreased FABP1 (Wood *et al*. 2017, Xu *et al*. 2017). Thus, the observed decreased expression of FABP1 could potentially be explained by the increase in *Tnf-α* expression in WT organoids exposed to TEFs, which may inhibit PPAR leading to the observed downregulation of FABP1. Further studies are needed to confirm this relationship.

The cytokine-cytokine receptor interaction pathway was significantly upregulated, with *Tnf-α* being a major player. Upregulation of *Tnf-α* can promote Wnt signalling (Coskun *et al*. 2014) and indeed this pathway was significantly induced in WT organoids exposed to TEFs, but not in WT organoids exposed to $Apc^{1322/+}$, indicating that this upregulation is due to the presence of TEFs.

Two scenarios could explain the upregulation observed for the Wnt signalling pathway: (1) Wnt signalling was driven by overexpressed Wnt ligands, and (2) Wnt signalling was driven in a R-spondin dependent manner binding *Lgr5*. Lgr5 is both a Wnt signalling component as well as a Wnt target gene, and functions as an R-spondin receptor, associating with the Frizzled/LRP receptor complex and potentiating Wnt/β- catenin signalling by enhancing Wnt-induced LRP phosphorylation (Carmon *et al*. 2011, de Lau *et al*. 2011). Thus, given the upregulation detected in *Lgr5*, one could assume activation of Wnt signalling was driven in a R-spondin dependent manner, as *R-spondin1* was significantly induced in WT organoids exposed to TEFs compared to WT organoids only.

Both scenarios would explain the upregulation seen for *Ctnnb1*, indicating accumulation of β-catenin. In addition, upregulation of *Lgr5* might indicate that these cells have acquired stem-like properties, but further experiments are needed to investigate the exact role of these $Lgr5^{+}$ cells.

Increased *Tnf-α* expression could have also activated MAPK and/or JNK signalling, which led to an increased expression of MMP9. This could potentially

result in collagen breakdown and structural changes in the ECM, leading to tumour initiation and progression, and is likely to be an early event in neoplastic progression. Moreover, the upregulation detected in MMP9 and collagen genes (*Col4a1* and *Col6a2*) could have also been mediated by TGF-β signalling in a SMAD-dependent manner.

These studies have shed light on epithelial-stromal interactions in the very early stages of colorectal tumourigenesis and the accompanying critical steps leading to tumour progression. Analysis of these epithelial-stromal interactions may help to develop a better understanding of the mechanisms governing tumour initiation and progression.

To summarise, this project has demonstrated clonal interactions between dysplastic and non-dysplastic epithelium driving clonal expansion: adenomas create a field effect, dysplastic crypts exert mutagenic pressure, and crypt-to-crypt crosstalk between adenomatous and stromal cells takes place leading to a pro-tumourigenic environment. Furthermore, the effect of mutated epithelium on normal epithelium in close proximity was investigated using murine intestinal organoids to better understand initial events in colorectal tumourigenesis.

This work has made a significant contribution to the way in which we understand the initial events in tumourigenesis within the human colon.

8 Chapter VIII: References

Adegboyega, P. A., Mifflin, R. C., DiMari, J. F., Saada, J. I. and Powell, D. W. (2002). "Immunohistochemical study of myofibroblasts in normal colonic mucosa, hyperplastic polyps, and adenomatous colorectal polyps." *Arch Pathol Lab Med* **126**(7): 829-836.

Akter, H., Park, M., Kwon, O. S., Song, E. J., Park, W. S. and Kang, M. J. (2015). "Activation of matrix metalloproteinase-9 (MMP-9) by neurotensin promotes cell invasion and migration through ERK pathway in gastric cancer." *Tumour Biol* **36**(8): 6053-6062.

Albuquerque, C., Breukel, C., van der Luijt, R., Fidalgo, P., Lage, P., Slors, F. J., Leitao, C. N., Fodde, R. and Smits, R. (2002). "The 'just-right' signaling model: APC somatic mutations are selected based on a specific level of activation of the beta-catenin signaling cascade." *Hum Mol Genet* **11**(13): 1549-1560.

Amaro, A., Chiara, S. and Pfeffer, U. (2016). "Molecular evolution of colorectal cancer: from multistep carcinogenesis to the big bang." *Cancer Metastasis Rev* **35**(1): 63-74.

Amicarella, F., Muraro, M. G., Hirt, C., Cremonesi, E., Padovan, E., Mele, V., Governa, V., Han, J., Huber, X., Droeser, R. A., Zuber, M., Adamina, M., Bolli, M., Rosso, R., Lugli, A., Zlobec, I., Terracciano, L., Tornillo, L., Zajac, P., Eppenberger-Castori, S., Trapani, F., Oertli, D. and Iezzi, G. (2017). "Dual role of tumour-infiltrating T helper 17 cells in human colorectal cancer." *Gut* **66**(4): 692-704.

Anders, S., Pyl, P. T. and Huber, W. (2015). "HTSeq—a Python framework to work with high-throughput sequencing data." *Bioinformatics* **31**(2): 166-169.

Anderson, E. C., Hessman, C., Levin, T. G., Monroe, M. M. and Wong, M. H. (2011). "The Role of Colorectal Cancer Stem Cells in Metastatic Disease and Therapeutic Response." *Cancers* **3**(1): 319-339.

Angell, H. and Galon, J. (2013). "From the immune contexture to the Immunoscore: the role of prognostic and predictive immune markers in cancer." *Curr Opin Immunol* **25**(2): 261-267.

Aoki, K., Aoki, M., Sugai, M., Harada, N., Miyoshi, H., Tsukamoto, T., Mizoshita, T., Tatematsu, M., Seno, H., Chiba, T., Oshima, M., Hsieh, C. L. and Taketo, M. M. (2007). "Chromosomal instability by beta-catenin/TCF transcription in APC or beta-catenin mutant cells." *Oncogene* **26**(24): 3511-3520.

Aoki, R., Shoshkes-Carmel, M., Gao, N., Shin, S., May, C. L., Golson, M. L., Zahm, A. M., Ray, M., Wiser, C. L., Wright, C. V. and Kaestner, K. H. (2016). "Foxl1-expressing mesenchymal cells constitute the intestinal stem cell niche." *Cell Mol Gastroenterol Hepatol* **2**(2): 175-188.

Araki, Y., Okamura, S., Hussain, S. P., Nagashima, M., He, P., Shiseki, M., Miura, K. and Harris, C. C. (2003). "Regulation of cyclooxygenase-2 expression by the Wnt and ras pathways." *Cancer Res* **63**(3): 728-734.

Auclair, B. A., Benoit, Y. D., Rivard, N., Mishina, Y. and Perreault, N. (2007). "Bone morphogenetic protein signaling is essential for terminal differentiation of the intestinal secretory cell lineage." *Gastroenterology* **133**(3): 887-896.

Azzoni, C., Bottarelli, L., Cecchini, S., Silini, E. M., Bordi, C. and Sarli, L. (2011). "Sporadic colorectal carcinomas with low-level microsatellite instability: a distinct

subgroup with specific clinicopathological and molecular features." *Int J Colorectal Dis* **26**(4): 445-453.
Badawi, M. A., Abouelfadl, D. M., El-Sharkawy, S. L., El-Aal, W. E. and Abbas, N. F. (2015). "Tumor-Associated Macrophage (TAM) and Angiogenesis in Human Colon Carcinoma." *Open Access Maced J Med Sci* **3**(2): 209-214.
Bai, Y. P., Shang, K., Chen, H., Ding, F., Wang, Z., Liang, C., Xu, Y., Sun, M. H. and Li, Y. Y. (2015). "FGF-1/-3/FGFR4 signaling in cancer-associated fibroblasts promotes tumor progression in colon cancer through Erk and MMP-7." *Cancer Sci* **106**(10): 1278-1287.
Baker, A. M., Cereser, B., Melton, S., Fletcher, A. G., Rodriguez-Justo, M., Tadrous, P. J., Humphries, A., Elia, G., McDonald, S. A., Wright, N. A., Simons, B. D., Jansen, M. and Graham, T. A. (2014). "Quantification of crypt and stem cell evolution in the normal and neoplastic human colon." *Cell Rep* **8**(4): 940-947.
Baker, A. M., Graham, T. A. and Wright, N. A. (2013). "Pre-tumour clones, periodic selection and clonal interference in the origin and progression of gastrointestinal cancer: potential for biomarker development." *J Pathol* **229**(4): 502-514.
Baker, K., Foulkes, W. D. and Jass, J. R. (2009). "MSI-H colorectal cancers preferentially retain and expand intraepithelial lymphocytes rather than peripherally derived CD8+ T cells." *Cancer Immunol Immunother* **58**(1): 135-144.
Banziger, C., Soldini, D., Schutt, C., Zipperlen, P., Hausmann, G. and Basler, K. (2006). "Wntless, a conserved membrane protein dedicated to the secretion of Wnt proteins from signaling cells." *Cell* **125**(3): 509-522.
Barker, N. (2014). "Adult intestinal stem cells: critical drivers of epithelial homeostasis and regeneration." *Nat Rev Mol Cell Biol* **15**(1): 19-33.
Barker, N., Ridgway, R. A., van Es, J. H., van de Wetering, M., Begthel, H., van den Born, M., Danenberg, E., Clarke, A. R., Sansom, O. J. and Clevers, H. (2009). "Crypt stem cells as the cells-of-origin of intestinal cancer." *Nature* **457**(7229): 608-611.
Barker, N., van de Wetering, M. and Clevers, H. (2008). "The intestinal stem cell." *Genes Dev* **22**(14): 1856-1864.
Barker, N., van Es, J. H., Kuipers, J., Kujala, P., van den Born, M., Cozijnsen, M., Haegebarth, A., Korving, J., Begthel, H., Peters, P. J. and Clevers, H. (2007). "Identification of stem cells in small intestine and colon by marker gene Lgr5." *Nature* **449**(7165): 1003-1007.
Barone, M., Scavo, M. P., Papagni, S., Piscitelli, D., Guido, R., Di Lena, M., Comelli, M. C. and Di Leo, A. (2010). "ER β expression in normal, adenomatous and carcinomatous tissues of patients with familial adenomatous polyposis." *Scandinavian Journal of Gastroenterology* **45**(11): 1320-1328.
Bartkova, J., Rezaei, N., Liontos, M., Karakaidos, P., Kletsas, D., Issaeva, N., Vassiliou, L. V., Kolettas, E., Niforou, K., Zoumpourlis, V. C., Takaoka, M., Nakagawa, H., Tort, F., Fugger, K., Johansson, F., Sehested, M., Andersen, C. L., Dyrskjot, L., Ornтoft, T., Lukas, J., Kittas, C., Helleday, T., Halazonetis, T. D., Bartek, J. and Gorgoulis, V. G. (2006). "Oncogene-induced senescence is part of the tumorigenesis barrier imposed by DNA damage checkpoints." *Nature* **444**(7119): 633-637.
Batlle, E., Henderson, J. T., Beghtel, H., Born, M. M. v. a. n. d. e. n., Sancho, E., Huls, G., Meeldijk, J., Robertson, J., Wetering, M. v. a. n. d. e., Pawson, T. and Clevers, H. (2002). "Beta-catenin and TCF mediate cell positioning in the intestinal epithelium by controlling the expression of EphB/ephrinB." *Cell* **111**.

Bauvois, B. (2012). "New facets of matrix metalloproteinases MMP-2 and MMP-9 as cell surface transducers: outside-in signaling and relationship to tumor progression." *Biochim Biophys Acta* **1825**(1): 29-36.
Beggs, A. D., Domingo, E., McGregor, M., Presz, M., Johnstone, E., Midgley, R., Kerr, D., Oukrif, D., Novelli, M., Abulafi, M., Hodgson, S. V., Fadhil, W., Ilyas, M. and Tomlinson, I. P. M. (2012). "Loss of expression of the double strand break repair protein ATM is associated with worse prognosis in colorectal cancer and loss of Ku70 expression is associated with CIN." *Oncotarget* **3**(11): 1348-1355.
Belov, L., Zhou, J. and Christopherson, R. I. (2010). "Cell surface markers in colorectal cancer prognosis." *Int J Mol Sci* **12**(1): 78-113.
Berdiel-Acer, M., Cuadras, D., Diaz-Maroto, N. G., Sanjuan, X., Serrano, T., Berenguer, A., Moreno, V., Goncalves-Ribeiro, S., Salazar, R., Villanueva, A. and Mollevi, D. G. (2014). "A monotonic and prognostic genomic signature from fibroblasts for colorectal cancer initiation, progression, and metastasis." *Mol Cancer Res* **12**(9): 1254-1266.
Bielas, J. H. and Heddle, J. A. (2000). "Proliferation is necessary for both repair and mutation in transgenic mouse cells." *Proceedings of the National Academy of Sciences* **97**(21): 11391.
Bishop, A. J. R. and Schiestl, R. H. (2002). "Homologous Recombination and Its Role in Carcinogenesis." *Journal of Biomedicine and Biotechnology* **2**(2): 75-85.
Bitarte, N., Bandres, E., Boni, V., Zarate, R., Rodriguez, J., Gonzalez-Huarriz, M., Lopez, I., Javier Sola, J., Alonso, M. M., Fortes, P. and Garcia-Foncillas, J. (2011). "MicroRNA-451 is involved in the self-renewal, tumorigenicity, and chemoresistance of colorectal cancer stem cells." *Stem Cells* **29**(11): 1661-1671.
Bjerknes, M. (1996). "Expansion of mutant stem cell populations in the human colon." *J Theor Biol* **178**(4): 381-385.
Bjerknes, M. and Cheng, H. (1981). "The stem-cell zone of the small intestinal epithelium. III. Evidence from columnar, enteroendocrine, and mucous cells in the adult mouse." *Am J Anat* **160**(1): 77-91.
Bjerknes, M. and Cheng, H. (1999). "Clonal analysis of mouse intestinal epithelial progenitors." *Gastroenterology* **116**(1): 7-14.
Bjerknes, M. and Cheng, H. (1999). "Colossal crypts bordering colon adenomas in Apc(Min) mice express full-length Apc." *Am J Pathol* **154**(6): 1831-1834.
Blaj, C., Schmidt, E. M., Lamprecht, S., Hermeking, H., Jung, A., Kirchner, T. and Horst, D. (2017). "Oncogenic Effects of High MAPK Activity in Colorectal Cancer Mark Progenitor Cells and Persist Irrespective of RAS Mutations." *Cancer Res* **77**(7): 1763-1774.
Blanpain, C. and Simons, B. D. (2013). "Unravelling stem cell dynamics by lineage tracing." *Nat Rev Mol Cell Biol* **14**(8): 489-502.
Bonilla, X., Parmentier, L., King, B., Bezrukov, F., Kaya, G., Zoete, V., Seplyarskiy, V. B., Sharpe, H. J., McKee, T., Letourneau, A., Ribaux, P. G., Popadin, K., Basset-Seguin, N., Ben Chaabene, R., Santoni, F. A., Andrianova, M. A., Guipponi, M., Garieri, M., Verdan, C., Grosdemange, K., Sumara, O., Eilers, M., Aifantis, I., Michielin, O., de Sauvage, F. J., Antonarakis, S. E. and Nikolaev, S. I. (2016). "Genomic analysis identifies new drivers and progression pathways in skin basal cell carcinoma." *Nat Genet* **48**(4): 398-406.
Bonnans, C., Chou, J. and Werb, Z. (2014). "Remodelling the extracellular matrix in development and disease." *Nat Rev Mol Cell Biol* **15**(12): 786-801.

Bonner, W. M., Redon, C. E., Dickey, J. S., Nakamura, A. J., Sedelnikova, O. A., Solier, S. and Pommier, Y. (2008). " γ H2AX and cancer." *Nature reviews. Cancer* **8**(12): 957-967.
Bozic, I., Antal, T., Ohtsuki, H., Carter, H., Kim, D., Chen, S., Karchin, R., Kinzler, K. W., Vogelstein, B. and Nowak, M. A. (2010). "Accumulation of driver and passenger mutations during tumor progression." *Proc Natl Acad Sci U S A* **107**(43): 18545-18550.
Braakhuis, B. J., Tabor, M. P., Kummer, J. A., Leemans, C. R. and Brakenhoff, R. H. (2003). "A genetic explanation of Slaughter's concept of field cancerization: evidence and clinical implications." *Cancer Res* **63**(8): 1727-1730.
Brabletz, T., Jung, A., Reu, S., Porzner, M., Hlubek, F., Kunz-Schughart, L. A., Knuechel, R. and Kirchner, T. (2001). "Variable β -catenin expression in colorectal cancers indicates tumor progression driven by the tumor environment." *Proceedings of the National Academy of Sciences of the United States of America* **98**(18): 10356-10361.
Brenner, H., Chang-Claude, J., Jansen, L., Knebel, P., Stock, C. and Hoffmeister, M. (2014). "Reduced risk of colorectal cancer up to 10 years after screening, surveillance, or diagnostic colonoscopy." *Gastroenterology* **146**(3): 709-717.
Brittan, M. and Wright, N. A. (2002). "Gastrointestinal stem cells." *J Pathol* **197**(4): 492-509.
Broustas, C. G. and Lieberman, H. B. (2014). "DNA Damage Response Genes and the Development of Cancer Metastasis." *Radiation research* **181**(2): 111-130.
Bruens, L., Ellenbroek, S. I. J., van Rheenen, J. and Snippert, H. J. (2017). "In Vivo Imaging Reveals Existence of Crypt Fission and Fusion in Adult Mouse Intestine." *Gastroenterology* **153**(3): 674-677.e673.
Buchert, M., Athineos, D., Abud, H. E., Burke, Z. D., Faux, M. C., Samuel, M. S., Jarnicki, A. G., Winbanks, C. E., Newton, I. P., Meniel, V. S., Suzuki, H., Stacker, S. A., Nathke, I. S., Tosh, D., Huelsken, J., Clarke, A. R., Heath, J. K., Sansom, O. J. and Ernst, M. (2010). "Genetic dissection of differential signaling threshold requirements for the Wnt/beta-catenin pathway in vivo." *PLoS Genet* **6**(1): e1000816.
Buczacki, S. J., Zecchini, H. I., Nicholson, A. M., Russell, R., Vermeulen, L., Kemp, R. and Winton, D. J. (2013). "Intestinal label-retaining cells are secretory precursors expressing Lgr5." *Nature* **495**(7439): 65-69.
Buller, N. V., Rosekrans, S. L., Westerlund, J. and van den Brink, G. R. (2012). "Hedgehog signaling and maintenance of homeostasis in the intestinal epithelium." *Physiology (Bethesda)* **27**(3): 148-155.
Butcher, D. T., Alliston, T. and Weaver, V. M. (2009). "A tense situation: forcing tumour progression." *Nat Rev Cancer* **9**(2): 108-122.
Byron, A., Humphries, J. D. and Humphries, M. J. (2013). "Defining the extracellular matrix using proteomics." *International Journal of Experimental Pathology* **94**(2): 75-92.
Calon, A., Lonardo, E., Berenguer-Llergo, A., Espinet, E., Hernando-Momblona, X., Iglesias, M., Sevillano, M., Palomo-Ponce, S., Tauriello, D. V. F., Byrom, D., Cortina, C., Morral, C., Barcelo, C., Tosi, S., Riera, A., Attolini, C. S.-O., Rossell, D., Sancho, E. and Batlle, E. (2015). "Stromal gene expression defines poor-prognosis subtypes in colorectal cancer." *Nat Genet* **47**(4): 320-329.
Carethers, J. M. and Jung, B. H. (2015). "Genetics and Genetic Biomarkers in Sporadic Colorectal Cancer." *Gastroenterology* **149**(5): 1177-1190.e1173.

Carlone, D. L. and Breault, D. T. (2012). "Tales from the crypt: the expanding role of slow cycling intestinal stem cells." *Cell stem cell* **10**(1): 2-4.
Carmon, K. S., Gong, X., Lin, Q., Thomas, A. and Liu, Q. (2011). "R-spondins function as ligands of the orphan receptors LGR4 and LGR5 to regulate Wnt/beta-catenin signaling." *Proc Natl Acad Sci U S A* **108**(28): 11452-11457.
Carmon, K. S., Gong, X., Yi, J., Wu, L., Thomas, A., Moore, C. M., Masuho, I., Timson, D. J., Martemyanov, K. A. and Liu, Q. J. (2017). "LGR5 receptor promotes cell–cell adhesion in stem cells and colon cancer cells via the IQGAP1–Rac1 pathway." *The Journal of Biological Chemistry* **292**(36): 14989-15001.
Carvalho, B., Sillars-Hardebol, A. H., Postma, C., Mongera, S., Terhaar Sive Droste, J., Obulkasim, A., van de Wiel, M., van Criekinge, W., Ylstra, B., Fijneman, R. J. and Meijer, G. A. (2012). "Colorectal adenoma to carcinoma progression is accompanied by changes in gene expression associated with ageing, chromosomal instability, and fatty acid metabolism." *Cell Oncol (Dordr)* **35**(1): 53-63.
Cavnar, M. J., Turcotte, S., Katz, S. C., Kuk, D., Gonen, M., Shia, J., Allen, P. J., Balachandran, V. P., D'Angelica, M. I., Kingham, T. P., Jarnagin, W. R. and DeMatteo, R. P. (2017). "Tumor-Associated Macrophage Infiltration in Colorectal Cancer Liver Metastases is Associated With Better Outcome." *Ann Surg Oncol* **24**(7): 1835-1842.
Centelles, J. J. (2012). "General aspects of colorectal cancer." *ISRN Oncol* **2012**: 139268.
Cerami, E., Gao, J., Dogrusoz, U., Gross, B. E., Sumer, S. O., Aksoy, B. A., Jacobsen, A., Byrne, C. J., Heuer, M. L., Larsson, E., Antipin, Y., Reva, B., Goldberg, A. P., Sander, C. and Schultz, N. (2012). "The cBio cancer genomics portal: an open platform for exploring multidimensional cancer genomics data." *Cancer Discov* **2**(5): 401-404.
Chandra, D. and Singh, K. K. (2011). "Genetic insights into OXPHOS defect and its role in cancer." *Biochim Biophys Acta* **1807**(6): 620-625.
Cheah, P. Y., Choo, P. H., Yao, J., Eu, K. W. and Seow-Choen, F. (2002). "A survival-stratification model of human colorectal carcinomas with beta-catenin and p27kip1." *Cancer* **95**(12): 2479-2486.
Chen, S. X., Xu, X. E., Wang, X. Q., Cui, S. J., Xu, L. L., Jiang, Y. H., Zhang, Y., Yan, H. B., Zhang, Q., Qiao, J., Yang, P. Y. and Liu, F. (2014). "Identification of colonic fibroblast secretomes reveals secretory factors regulating colon cancer cell proliferation." *J Proteomics* **110**: 155-171.
Chen, Y., Chou, K., Fuchs, E., Havran, W. L. and Boismenu, R. (2002). "Protection of the intestinal mucosa by intraepithelial gamma delta T cells." *Proc Natl Acad Sci U S A* **99**(22): 14338-14343.
Chen, Y. C. E., Mapp, S., Blumenthal, A., Burgess, M. L., Mazzieri, R., Mattarollo, S. R., Mollee, P., Gill, D. and Saunders, N. A. (2017). "The duality of macrophage function in chronic lymphocytic leukaemia." *Biochim Biophys Acta* **1868**(1): 176-182.
Cheng, H., Bjerknes, M., Amar, J. and Gardiner, G. (1986). "Crypt production in normal and diseased human colonic epithelium." *Anat Rec* **216**(1): 44-48.
Cheng, H. and Leblond, C. P. (1974). "Origin, differentiation and renewal of the four main epithelial cell types in the mouse small intestine. ." *Am J Anat* **141**(4): 537-561.
Cheroutre, H., Lambolez, F. and Mucida, D. (2011). "The light and dark sides of intestinal intraepithelial lymphocytes." *Nature reviews. Immunology* **11**(7): 445-456.
Chinnery, P. F., Thorburn, D. R., Samuels, D. C., White, S. L., Dahl, H. M., Turnbull, D. M., Lightowlers, R. N. and Howell, N. (2000). "The inheritance of

mitochondrial DNA heteroplasmy: random drift, selection or both?" *Trends Genet* **16**(11): 500-505.
Chirica, M., Le Bourhis, L., Lehmann-Che, J., Chardiny, V., Bouhidel, F., Foulboeuf, L., Gornet, J. M., Lourenco, N., Dulphy, N., Toubert, A. and Allez, M. (2015). "Phenotypic analysis of T cells infiltrating colon cancers: Correlations with oncogenetic status." *Oncoimmunology* **4**(8): e1016698.
Christie, M., Jorissen, R. N., Mouradov, D., Sakthianandeswaren, A., Li, S., Day, F., Tsui, C., Lipton, L., Desai, J., Jones, I. T., McLaughlin, S., Ward, R. L., Hawkins, N. J., Ruszkiewicz, A. R., Moore, J., Burgess, A. W., Busam, D., Zhao, Q., Strausberg, R. L., Simpson, A. J., Tomlinson, I. P., Gibbs, P. and Sieber, O. M. (2013). "Different APC genotypes in proximal and distal sporadic colorectal cancers suggest distinct WNT/beta-catenin signalling thresholds for tumourigenesis." *Oncogene* **32**(39): 4675-4682.
Chu, D., Zhao, Z., Zhou, Y., Li, Y., Li, J., Zheng, J., Zhao, Q. and Wang, W. (2012). "Matrix metalloproteinase-9 is associated with relapse and prognosis of patients with colorectal cancer." *Ann Surg Oncol* **19**(1): 318-325.
Chu, M. W., Siegmund, K. D., Eckstam, C. L., Kim, J. Y., Yang, A. S., Kanel, G. C., Tavare, S. and Shibata, D. (2007). "Lack of increases in methylation at three CpG-rich genomic loci in non-mitotic adult tissues during aging." *BMC Med Genet* **8**: 50.
Cisterna, B. and Biggiogera, M. (2010). "Ribosome biogenesis: from structure to dynamics." *Int Rev Cell Mol Biol* **284**: 67-111.
Citarda, F., Tomaselli, G., Capocaccia, R., Barcherini, S., Crespi, M. and Group, T. I. M. S. (2001). "Efficacy in standard clinical practice of colonoscopic polypectomy in reducing colorectal cancer incidence." *Gut* **48**(6): 812.
Cleary, A. S., Leonard, T. L., Gestl, S. A. and Gunther, E. J. (2014). "Tumour cell heterogeneity maintained by cooperating subclones in Wnt-driven mammary cancers." *Nature* **508**(7494): 113-117.
Clevers, H. (2006). "Wnt/beta-catenin signaling in development and disease." *Cell* **127**(3): 469-480.
Clevers, H. (2013). "The Intestinal Crypt, A Prototype Stem Cell Compartment." *Cell* **154**(2): 274-284.
Clevers, H., Loh, K. M. and Nusse, R. (2014). "Stem cell signaling. An integral program for tissue renewal and regeneration: Wnt signaling and stem cell control." *Science* **346**(6205): 1248012.
Clevers, H. and Nusse, R. (2012). "Wnt/beta-catenin signaling and disease." *Cell* **149**(6): 1192-1205.
Cohen, M., Meisser, A., Haenggeli, L. and Bischof, P. (2006). "Involvement of MAPK pathway in TNF-alpha-induced MMP-9 expression in human trophoblastic cells." *Mol Hum Reprod* **12**(4): 225-232.
Coppe, J. P., Desprez, P. Y., Krtolica, A. and Campisi, J. (2010). "The senescence-associated secretory phenotype: the dark side of tumor suppression." *Annu Rev Pathol* **5**: 99-118.
Cortina, C., Turon, G., Stork, D., Hernando-Momblona, X., Sevillano, M., Aguilera, M., Tosi, S., Merlos-Suarez, A., Stephan-Otto Attolini, C., Sancho, E. and Batlle, E. (2017). "A genome editing approach to study cancer stem cells in human tumors." *EMBO Mol Med* **9**(7): 869-879.
Coskun, M., Olsen, A. K., Bzorek, M., Holck, S., Engel, U. H., Nielsen, O. H. and Troelsen, J. T. (2014). "Involvement of CDX2 in the cross talk between TNF-alpha and Wnt signaling pathway in the colon cancer cell line Caco-2." *Carcinogenesis* **35**(5): 1185-1192.

Cox, G. W., Melillo, G., Chattopadhyay, U., Mullet, D., Fertel, R. H. and Varesio, L. (1992). "Tumor necrosis factor-alpha-dependent production of reactive nitrogen intermediates mediates IFN-gamma plus IL-2-induced murine macrophage tumoricidal activity." *J Immunol* **149**(10): 3290-3296.
Crawford, H. C., Fingleton, B., Gustavson, M. D., Kurpios, N., Wagenaar, R. A., Hassell, J. A. and Matrisian, L. M. (2001). "The PEA3 subfamily of Ets transcription factors synergizes with beta-catenin-LEF-1 to activate matrilysin transcription in intestinal tumors." *Mol Cell Biol* **21**(4): 1370-1383.
Crosnier, C., Stamataki, D. and Lewis, J. (2006). "Organizing cell renewal in the intestine: stem cells, signals and combinatorial control." *Nat Rev Genet* **7**(5): 349-359.
Cross, W., Kovac, M., Mustonen, V., Temko, D., Davis, H., Baker, A. M., Biswas, S., Arnold, R., Chegwidden, L., Gatenbee, C., Anderson, A. R., Koelzer, V. H., Martinez, P., Jiang, X., Domingo, E., Woodcock, D. J., Feng, Y., Kovacova, M., Maughan, T., Jansen, M., Rodriguez-Justo, M., Ashraf, S., Guy, R., Cunningham, C., East, J. E., Wedge, D. C., Wang, L. M., Palles, C., Heinimann, K., Sottoriva, A., Leedham, S. J., Graham, T. A. and Tomlinson, I. P. M. (2018). "The evolutionary landscape of colorectal tumorigenesis." *Nat Ecol Evol* **2**(10): 1661-1672.
Cui, C., Merritt, R., Fu, L. and Pan, Z. (2017). "Targeting calcium signaling in cancer therapy." *Acta Pharmaceutica Sinica. B* **7**(1): 3-17.
Curtius, K., Wright, N. A. and Graham, T. A. (2018). "An evolutionary perspective on field cancerization." *Nat Rev Cancer* **18**(1): 19-32.
Dai, X., Wang, L., Zhang, L., Han, Y., Yang, G. and Li, L. (2012). "The expression and mutation of beta-catenin in colorectal traditional serrated adenomas." *Indian J Pathol Microbiol* **55**(3): 288-293.
Dai, Y. and Wang, W.-H. (2010). "Peroxisome proliferator-activated receptor γ and colorectal cancer." *World Journal of Gastrointestinal Oncology* **2**(3): 159-164.
Dalerba, P., Kalisky, T., Sahoo, D., Rajendran, P. S., Rothenberg, M. E., Leyrat, A. A., Sim, S., Okamoto, J., Johnston, D. M., Qian, D., Zabala, M., Bueno, J., Neff, N. F., Wang, J., Shelton, A. A., Visser, B., Hisamori, S., Shimono, Y., van de Wetering, M., Clevers, H., Clarke, M. F. and Quake, S. R. (2011). "Single-cell dissection of transcriptional heterogeneity in human colon tumors." *Nat Biotechnol* **29**(12): 1120-1127.
Daniels, D. L. and Weis, W. I. (2005). "Beta-catenin directly displaces Groucho/TLE repressors from Tcf/Lef in Wnt-mediated transcription activation." *Nat Struct Mol Biol* **12**(4): 364-371.
Davies, E. J., Marsh Durban, V., Meniel, V., Williams, G. T. and Clarke, A. R. (2014). "PTEN loss and KRAS activation leads to the formation of serrated adenomas and metastatic carcinoma in the mouse intestine." *J Pathol* **233**(1): 27-38.
Davis, H., Irshad, S., Bansal, M., Rafferty, H., Boitsova, T., Bardella, C., Jaeger, E., Lewis, A., Freeman-Mills, L., Giner, F. C., Rodenas-Cuadrado, P., Mallappa, S., Clark, S., Thomas, H., Jeffery, R., Poulsom, R., Rodriguez-Justo, M., Novelli, M., Chetty, R., Silver, A., Sansom, O. J., Greten, F. R., Wang, L. M., East, J. E., Tomlinson, I. and Leedham, S. J. (2015). "Aberrant epithelial GREM1 expression initiates colonic tumorigenesis from cells outside the stem cell niche." *Nat Med* **21**(1): 62-70.
De, A. (2011). "Wnt/Ca2+ signaling pathway: a brief overview." *Acta Biochimica et Biophysica Sinica* **43**(10): 745-756.
de Lau, W., Barker, N., Low, T. Y., Koo, B. K., Li, V. S., Teunissen, H., Kujala, P., Haegebarth, A., Peters, P. J., van de Wetering, M., Stange, D. E., van Es, J. E.,

Guardavaccaro, D., Schasfoort, R. B., Mohri, Y., Nishimori, K., Mohammed, S., Heck, A. J. and Clevers, H. (2011). "Lgr5 homologues associate with Wnt receptors and mediate R-spondin signalling." *Nature* **476**(7360): 293-297.
de Sousa e Melo, F., Kurtova, A. V., Harnoss, J. M., Kljavin, N., Hoeck, J. D., Hung, J., Anderson, J. E., Storm, E. E., Modrusan, Z., Koeppen, H., Dijkgraaf, G. J., Piskol, R. and de Sauvage, F. J. (2017). "A distinct role for Lgr5+ stem cells in primary and metastatic colon cancer." *Nature* **543**(7647): 676-680.
de Sousa e Melo, F. and Vermeulen, L. (2016). "Wnt Signaling in Cancer Stem Cell Biology." *Cancers* **8**(7): 60.
De Wever, O. and Mareel, M. (2003). "Role of tissue stroma in cancer cell invasion." *J Pathol* **200**(4): 429-447.
Deberardinis, R. J., Sayed, N., Ditsworth, D. and Thompson, C. B. (2008). "Brick by brick: metabolism and tumor cell growth." *Curr Opin Genet Dev* **18**(1): 54-61.
Delille, H. K., Bonekamp, N. A. and Schrader, M. (2006). "Peroxisomes and Disease - An Overview." *International Journal of Biomedical Science : IJBS* **2**(4): 308-314.
Derenzini, M., Montanaro, L. and Trere, D. (2017). "Ribosome biogenesis and cancer." *Acta Histochem* **119**(3): 190-197.
Deschoolmeester, V., Baay, M., Van Marck, E., Weyler, J., Vermeulen, P., Lardon, F. and Vermorken, J. B. (2010). "Tumor infiltrating lymphocytes: an intriguing player in the survival of colorectal cancer patients." *BMC Immunol* **11**: 19.
Dey, R. and Moraes, C. T. (2000). "Lack of oxidative phosphorylation and low mitochondrial membrane potential decrease susceptibility to apoptosis and do not modulate the protective effect of Bcl-x(L) in osteosarcoma cells." *J Biol Chem* **275**(10): 7087-7094.
Di Sabatino, A., Jackson, C. L., Pickard, K. M., Buckley, M., Rovedatti, L., Leakey, N. A., Picariello, L., Cazzola, P., Monteleone, G., Tonelli, F., Corazza, G. R., MacDonald, T. T. and Pender, S. L. (2009). "Transforming growth factor beta signalling and matrix metalloproteinases in the mucosa overlying Crohn's disease strictures." *Gut* **58**(6): 777-789.
Dow, L. E., O'Rourke, K. P., Simon, J., Tschaharganeh, D. F., van Es, J. H., Clevers, H. and Lowe, S. W. (2015). "Apc Restoration Promotes Cellular Differentiation and Reestablishes Crypt Homeostasis in Colorectal Cancer." *Cell* **161**(7): 1539-1552.
Driehuis, E. and Clevers, H. (2017). "WNT signalling events near the cell membrane and their pharmacological targeting for the treatment of cancer." *Br J Pharmacol* **174**(24): 4547-4563.
Driessens, G., Beck, B., Caauwe, A., Simons, B. D. and Blanpain, C. (2012). "Defining the mode of tumour growth by clonal analysis." *Nature* **488**(7412): 527-530.
Drost, J. and Clevers, H. (2018). "Organoids in cancer research." *Nature Reviews Cancer* **18**(7): 407-418.
Durand, A., Donahue, B., Peignon, G., Letourneur, F., Cagnard, N., Slomianny, C., Perret, C., Shroyer, N. F. and Romagnolo, B. (2012). "Functional intestinal stem cells after Paneth cell ablation induced by the loss of transcription factor Math1 (Atoh1)." *Proc Natl Acad Sci U S A* **109**(23): 8965-8970.
Eberhart, C. E., Coffey, R. J., Radhika, A., Giardiello, F. M., Ferrenbach, S. and DuBois, R. N. (1994). "Up-regulation of cyclooxygenase 2 gene expression in human colorectal adenomas and adenocarcinomas." *Gastroenterology* **107**(4): 1183-1188.

Eisinger, A. L., Prescott, S. M., Jones, D. A. and Stafforini, D. M. (2007). "The role of cyclooxygenase-2 and prostaglandins in colon cancer." *Prostaglandins Other Lipid Mediat* **82**(1-4): 147-154.
Elinav, E., Nowarski, R., Thaiss, C. A., Hu, B., Jin, C. and Flavell, R. A. (2013). "Inflammation-induced cancer: crosstalk between tumours, immune cells and microorganisms." *Nat Rev Cancer* **13**(11): 759-771.
Elson, J. L., Samuels, D. C., Turnbull, D. M. and Chinnery, P. F. (2001). "Random intracellular drift explains the clonal expansion of mitochondrial DNA mutations with age." *Am J Hum Genet* **68**(3): 802-806.
Elzagheid, A., Buhmeida, A., Korkeila, E., Collan, Y., Syrjanen, K. and Pyrhonen, S. (2008). "Nuclear beta-catenin expression as a prognostic factor in advanced colorectal carcinoma." *World J Gastroenterol* **14**(24): 3866-3871.
Esplin, E. D. and Snyder, M. P. (2014). "Genomic era diagnosis and management of hereditary and sporadic colon cancer." *World J Clin Oncol* **5**(5): 1036-1047.
Eto, T., Miyake, K., Nosho, K., Ohmuraya, M., Imamura, Y., Arima, K., Kanno, S., Fu, L., Kiyozumi, Y., Izumi, D., Sugihara, H., Hiyoshi, Y., Miyamoto, Y., Sawayama, H., Iwatsuki, M., Baba, Y., Yoshida, N., Furukawa, T., Araki, K., Baba, H. and Ishimoto, T. (2018). "Impact of loss ‐ of ‐ function mutations at the RNF43 locus on colorectal cancer development and progression." *The Journal of Pathology* **0**(ja).
Fang, J. Y. and Richardson, B. C. (2005). "The MAPK signalling pathways and colorectal cancer." *The Lancet Oncology* **6**(5): 322-327.
Fanjul-Fernández, M., Folgueras, A. R., Cabrera, S. and López-Otín, C. (2010). "Matrix metalloproteinases: Evolution, gene regulation and functional analysis in mouse models." *Biochimica et Biophysica Acta (BBA) - Molecular Cell Research* **1803**(1): 3-19.
Farin, H. F., Jordens, I., Mosa, M. H., Basak, O., Korving, J., Tauriello, D. V., de Punder, K., Angers, S., Peters, P. J., Maurice, M. M. and Clevers, H. (2016). "Visualization of a short-range Wnt gradient in the intestinal stem-cell niche." *Nature* **530**(7590): 340-343.
Farin, H. F., Van Es, J. H. and Clevers, H. (2012). "Redundant sources of Wnt regulate intestinal stem cells and promote formation of Paneth cells." *Gastroenterology* **143**(6): 1518-1529.e1517.
Fearon, E. R. (2011). "Molecular genetics of colorectal cancer." *Annu Rev Pathol* **6**: 479-507.
Fearon, E. R. and Vogelstein, B. (1990). "A genetic model for colorectal tumorigenesis." *Cell* **61**(5): 759-767.
Feige, J. N., Gelman, L., Michalik, L., Desvergne, B. and Wahli, W. (2006). "From molecular action to physiological outputs: peroxisome proliferator-activated receptors are nuclear receptors at the crossroads of key cellular functions." *Prog Lipid Res* **45**(2): 120-159.
Fellous, T. G., McDonald, S. A., Burkert, J., Humphries, A., Islam, S., De-Alwis, N. M., Gutierrez-Gonzalez, L., Tadrous, P. J., Elia, G., Kocher, H. M., Bhattacharya, S., Mears, L., El-Bahrawy, M., Turnbull, D. M., Taylor, R. W., Greaves, L. C., Chinnery, P. F., Day, C. P., Wright, N. A. and Alison, M. R. (2009). "A methodological approach to tracing cell lineage in human epithelial tissues." *Stem Cells* **27**(6): 1410-1420.
Ferlay, J., Soerjomataram, I., Dikshit, R., Eser, S., Mathers, C., Rebelo, M., Parkin, D. M., Forman, D. and Bray, F. (2015). "Cancer incidence and mortality worldwide:

sources, methods and major patterns in GLOBOCAN 2012." *Int J Cancer* **136**(5): E359-386.
Fernandez-Sanchez, M. E., Barbier, S., Whitehead, J., Bealle, G., Michel, A., Latorre-Ossa, H., Rey, C., Fouassier, L., Claperon, A., Brulle, L., Girard, E., Servant, N., Rio-Frio, T., Marie, H., Lesieur, S., Housset, C., Gennisson, J. L., Tanter, M., Menager, C., Fre, S., Robine, S. and Farge, E. (2015). "Mechanical induction of the tumorigenic beta-catenin pathway by tumour growth pressure." *Nature* **523**(7558): 92-95.
Ferrone, C. and Dranoff, G. (2010). "Dual roles for immunity in gastrointestinal cancers." *J Clin Oncol* **28**(26): 4045-4051.
Fevr, T., Robine, S., Louvard, D. and Huelsken, J. (2007). "Wnt/beta-catenin is essential for intestinal homeostasis and maintenance of intestinal stem cells." *Mol Cell Biol* **27**(21): 7551-7559.
Fodde, R. and Brabletz, T. (2007). "Wnt/beta-catenin signaling in cancer stemness and malignant behavior." *Curr Opin Cell Biol* **19**(2): 150-158.
Franklin, R. A., Liao, W., Sarkar, A., Kim, M. V., Bivona, M. R., Liu, K., Pamer, E. G. and Li, M. O. (2014). "The cellular and molecular origin of tumor-associated macrophages." *Science* **344**(6186): 921-925.
Fridman, W. H., Pages, F., Sautes-Fridman, C. and Galon, J. (2012). "The immune contexture in human tumours: impact on clinical outcome." *Nat Rev Cancer* **12**(4): 298-306.
Friedman, K., Brodsky, A. S., Lu, S., Wood, S., Gill, A. J., Lombardo, K., Yang, D. and Resnick, M. B. (2016). "Medullary carcinoma of the colon: a distinct morphology reveals a distinctive immunoregulatory microenvironment." *Mod Pathol* **29**(5): 528-541.
Fritz, V. and Fajas, L. (2010). "Metabolism and proliferation share common regulatory pathways in cancer cells." *Oncogene* **29**(31): 4369-4377.
Fuller, C. E., Davies, R. P., Williams, G. T. and Williams, E. D. (1990). "Crypt restricted heterogeneity of goblet cell mucus glycoprotein in histologically normal human colonic mucosa: a potential marker of somatic mutation." *Br J Cancer* **61**(3): 382-384.
Funada, Y., Noguchi, T., Kikuchi, R., Takeno, S., Uchida, Y. and Gabbert, H. E. (2003). "Prognostic significance of CD8+ T cell and macrophage peritumoral infiltration in colorectal cancer." *Oncol Rep* **10**(2): 309-313.
Gaisa, N. T., Graham, T. A., McDonald, S. A., Poulsom, R., Heidenreich, A., Jakse, G., Knuechel, R. and Wright, N. A. (2011). "Clonal architecture of human prostatic epithelium in benign and malignant conditions." *J Pathol* **225**(2): 172-180.
Gajda, A. M. and Storch, J. (2015). "Enterocyte fatty acid-binding proteins (FABPs): different functions of liver and intestinal FABPs in the intestine." *Prostaglandins Leukot Essent Fatty Acids* **93**: 9-16.
Galamb, O., Spisák, S., Sipos, F., Tóth, K., Solymosi, N., Wichmann, B., Krenács, T., Valcz, G., Tulassay, Z. and Molnár, B. (2010). "Reversal of gene expression changes in the colorectal normal-adenoma pathway by NS398 selective COX2 inhibitor." *British Journal of Cancer* **102**(4): 765-773.
Galandiuk, S., Rodriguez-Justo, M., Jeffery, R., Nicholson, A. M., Cheng, Y., Oukrif, D., Elia, G., Leedham, S. J., McDonald, S. A., Wright, N. A. and Graham, T. A. (2012). "Field cancerization in the intestinal epithelium of patients with Crohn's ileocolitis." *Gastroenterology* **142**(4): 855-864 e858.
Galon, J., Costes, A., Sanchez-Cabo, F., Kirilovsky, A., Mlecnik, B., Lagorce-Pages, C., Tosolini, M., Camus, M., Berger, A., Wind, P., Zinzindohoue, F., Bruneval, P.,

Cugnenc, P. H., Trajanoski, Z., Fridman, W. H. and Pages, F. (2006). "Type, density, and location of immune cells within human colorectal tumors predict clinical outcome." *Science* **313**(5795): 1960-1964.
Garcia, S. B., Park, H. S., Novelli, M. and Wright, N. A. (1999). "Field cancerization, clonality, and epithelial stem cells: the spread of mutated clones in epithelial sheets." *J Pathol* **187**(1): 61-81.
Gatenby, R. A. and Gillies, R. J. (2004). "Why do cancers have high aerobic glycolysis?" *Nat Rev Cancer* **4**(11): 891-899.
Gatenby, R. A. and Gillies, R. J. (2008). "A microenvironmental model of carcinogenesis." *Nat Rev Cancer* **8**(1): 56-61.
Gausachs, M., Borras, E., Chang, K., Gonzalez, S., Azuara, D., Delgado Amador, A., Lopez-Doriga, A., San Lucas, F. A., Sanjuan, X., Paules, M. J., Taggart, M. W., Davies, G. E., Ehli, E. A., Fowler, J., Moreno, V., Pineda, M., You, Y. N., Lynch, P. M., Lazaro, C., Navin, N. E., Scheet, P. A., Hawk, E. T., Capella, G. and Vilar, E. (2017). "Mutational Heterogeneity in APC and KRAS Arises at the Crypt Level and Leads to Polyclonality in Early Colorectal Tumorigenesis." *Clin Cancer Res*.
Gentleman, R. C., Carey, V. J., Bates, D. M., Bolstad, B., Dettling, M., Dudoit, S., Ellis, B., Gautier, L., Ge, Y., Gentry, J., Hornik, K., Hothorn, T., Huber, W., Iacus, S., Irizarry, R., Leisch, F., Li, C., Maechler, M., Rossini, A. J., Sawitzki, G., Smith, C., Smyth, G., Tierney, L., Yang, J. Y. and Zhang, J. (2004). "Bioconductor: open software development for computational biology and bioinformatics." *Genome Biol* **5**(10): R80.
Gerstung, M., Beisel, C., Rechsteiner, M., Wild, P., Schraml, P., Moch, H. and Beerenwinkel, N. (2012). "Reliable detection of subclonal single-nucleotide variants in tumour cell populations." *Nat Commun* **3**: 811.
Giannakis, M., Hodis, E., Jasmine Mu, X., Yamauchi, M., Rosenbluh, J., Cibulskis, K., Saksena, G., Lawrence, M. S., Qian, Z. R., Nishihara, R., Van Allen, E. M., Hahn, W. C., Gabriel, S. B., Lander, E. S., Getz, G., Ogino, S., Fuchs, C. S. and Garraway, L. A. (2014). "RNF43 is frequently mutated in colorectal and endometrial cancers." *Nat Genet* **46**(12): 1264-1266.
Giglia, M. D. and Chu, D. I. (2016). "Familial Colorectal Cancer: Understanding the Alphabet Soup." *Clin Colon Rectal Surg* **29**(3): 185-195.
Goddard, E. T., Hill, R. C., Barrett, A., Betts, C., Guo, Q., Maller, O., Borges, V. F., Hansen, K. C. and Schedin, P. (2016). "Quantitative extracellular matrix proteomics to study mammary and liver tissue microenvironments." *The International Journal of Biochemistry & Cell Biology* **81**(Part A): 223-232.
Goentoro, L. and Kirschner, M. W. (2009). "Evidence that fold-change, and not absolute level, of beta-catenin dictates Wnt signaling." *Mol Cell* **36**(5): 872-884.
Grady, W. M. and Carethers, J. M. (2008). "Genomic and epigenetic instability in colorectal cancer pathogenesis." *Gastroenterology* **135**(4): 1079-1099.
Graham, T. A., Humphries, A., Sanders, T., Rodriguez-Justo, M., Tadrous, P. J., Preston, S. L., Novelli, M. R., Leedham, S. J., McDonald, S. A. and Wright, N. A. (2011). "Use of methylation patterns to determine expansion of stem cell clones in human colon tissue." *Gastroenterology* **140**(4): 1241-1250.e1241-1249.
Graham, T. A., McDonald, S. A. and Wright, N. A. (2011). "Field cancerization in the GI tract." *Future Oncol* **7**(8): 981-993.
Grau, R., Punzon, C., Fresno, M. and Iniguez, M. A. (2006). "Peroxisome-proliferator-activated receptor alpha agonists inhibit cyclo-oxygenase 2 and vascular endothelial growth factor transcriptional activation in human colorectal carcinoma cells via inhibition of activator protein-1." *Biochem J* **395**(1): 81-88.

Greaves, L. C., Elson, J. L., Nooteboom, M., Grady, J. P., Taylor, G. A., Taylor, R. W., Mathers, J. C., Kirkwood, T. B. and Turnbull, D. M. (2012). "Comparison of mitochondrial mutation spectra in ageing human colonic epithelium and disease: absence of evidence for purifying selection in somatic mitochondrial DNA point mutations." *PLoS Genet* **8**(11): e1003082.
Greaves, L. C., Preston, S. L., Tadrous, P. J., Taylor, R. W., Barron, M. J., Oukrif, D., Leedham, S. J., Deheragoda, M., Sasieni, P., Novelli, M. R., Jankowski, J. A., Turnbull, D. M., Wright, N. A. and McDonald, S. A. (2006). "Mitochondrial DNA mutations are established in human colonic stem cells, and mutated clones expand by crypt fission." *Proc Natl Acad Sci U S A* **103**(3): 714-719.
Greaves, M. and Maley, C. C. (2012). "Clonal evolution in cancer." *Nature* **481**(7381): 306-313.
Groden, J., Thliveris, A., Samowitz, W., Carlson, M., Gelbert, L., Albertsen, H., Joslyn, G., Stevens, J., Spirio, L., Robertson, M. and et al. (1991). "Identification and characterization of the familial adenomatous polyposis coli gene." *Cell* **66**(3): 589-600.
Groulx, J.-F., Gagné, D., Benoit, Y. D., Martel, D., Basora, N. and Beaulieu, J.-F. (2011). "Collagen VI is a basement membrane component that regulates epithelial cell–fibronectin interactions." *Matrix Biology* **30**(3): 195-206.
Guo, H., Zeng, W., Feng, L., Yu, X., Li, P., Zhang, K., Zhou, Z. and Cheng, S. (2017). "Integrated transcriptomic analysis of distance-related field cancerization in rectal cancer patients." *Oncotarget* **8**(37): 61107-61117.
Gustavson, M. D., Crawford, H. C., Fingleton, B. and Matrisian, L. M. (2004). "Tcf binding sequence and position determines beta-catenin and Lef-1 responsiveness of MMP-7 promoters." *Mol Carcinog* **41**(3): 125-139.
Gutierrez-Gonzalez, L., Deheragoda, M., Elia, G., Leedham, S. J., Shankar, A., Imber, C., Jankowski, J. A., Turnbull, D. M., Novelli, M., Wright, N. A. and McDonald, S. A. (2009). "Analysis of the clonal architecture of the human small intestinal epithelium establishes a common stem cell for all lineages and reveals a mechanism for the fixation and spread of mutations." *J Pathol* **217**(4): 489-496.
Gutierrez-Gonzalez, L., Graham, T. A., Rodriguez-Justo, M., Leedham, S. J., Novelli, M. R., Gay, L. J., Ventayol-Garcia, T., Green, A., Mitchell, I., Stoker, D. L., Preston, S. L., Bamba, S., Yamada, E., Kishi, Y., Harrison, R., Jankowski, J. A., Wright, N. A. and McDonald, S. A. (2011). "The clonal origins of dysplasia from intestinal metaplasia in the human stomach." *Gastroenterology* **140**(4): 1251-1260.e1251-1256.
Hafner, C., Toll, A., Fernandez-Casado, A., Earl, J., Marques, M., Acquadro, F., Mendez-Pertuz, M., Urioste, M., Malats, N., Burns, J. E., Knowles, M. A., Cigudosa, J. C., Hartmann, A., Vogt, T., Landthaler, M., Pujol, R. M. and Real, F. X. (2010). "Multiple oncogenic mutations and clonal relationship in spatially distinct benign human epidermal tumors." *Proc Natl Acad Sci U S A* **107**(48): 20780-20785.
Halama, N., Michel, S., Kloor, M., Zoernig, I., Benner, A., Spille, A., Pommerencke, T., von Knebel, D. M., Folprecht, G., Luber, B., Feyen, N., Martens, U. M., Beckhove, P., Gnjatic, S., Schirmacher, P., Herpel, E., Weitz, J., Grabe, N. and Jaeger, D. (2011). "Localization and density of immune cells in the invasive margin of human colorectal cancer liver metastases are prognostic for response to chemotherapy." *Cancer Res* **71**(17): 5670-5677.
Halberg, R. B. and Dove, W. F. (2007). "Polyclonal tumors in the mammalian intestine: are interactions among multiple initiated clones necessary for tumor initiation, growth, and progression?" *Cell Cycle* **6**(1): 44-51.

Hamm, A., Prenen, H., Van Delm, W., Di Matteo, M., Wenes, M., Delamarre, E., Schmidt, T., Weitz, J., Sarmiento, R., Dezi, A., Gasparini, G., Rothe, F., Schmitz, R., D'Hoore, A., Iserentant, H., Hendlisz, A. and Mazzone, M. (2016). "Tumour-educated circulating monocytes are powerful candidate biomarkers for diagnosis and disease follow-up of colorectal cancer." *Gut* **65**(6): 990-1000.
Hanahan, D. and Weinberg, Robert A. (2011). "Hallmarks of Cancer: The Next Generation." *Cell* **144**(5): 646-674.
Hao, H. X., Jiang, X. and Cong, F. (2016). "Control of Wnt Receptor Turnover by R-spondin-ZNRF3/RNF43 Signaling Module and Its Dysregulation in Cancer." *Cancers (Basel)* **8**(6).
Hao, H. X., Xie, Y., Zhang, Y., Charlat, O., Oster, E., Avello, M., Lei, H., Mickanin, C., Liu, D., Ruffner, H., Mao, X., Ma, Q., Zamponi, R., Bouwmeester, T., Finan, P. M., Kirschner, M. W., Porter, J. A., Serluca, F. C. and Cong, F. (2012). "ZNRF3 promotes Wnt receptor turnover in an R-spondin-sensitive manner." *Nature* **485**(7397): 195-200.
Hao, X., Luo, H., Krawczyk, M., Wei, W., Wang, W., Wang, J., Flagg, K., Hou, J., Zhang, H., Yi, S., Jafari, M., Lin, D., Chung, C., Caughey, B. A., Li, G., Dhar, D., Shi, W., Zheng, L., Hou, R., Zhu, J., Zhao, L., Fu, X., Zhang, E., Zhang, C., Zhu, J.-K., Karin, M., Xu, R.-H. and Zhang, K. (2017). "DNA methylation markers for diagnosis and prognosis of common cancers." *Proceedings of the National Academy of Sciences*.
Hao, X., Tomlinson, I., Ilyas, M., Palazzo, J. P. and Talbot, I. C. (1997). "Reciprocity between membranous and nuclear expression of beta-catenin in colorectal tumours." *Virchows Arch* **431**(3): 167-172.
Harada, N., Tamai, Y., Ishikawa, T., Sauer, B., Takaku, K., Oshima, M. and Taketo, M. M. (1999). "Intestinal polyposis in mice with a dominant stable mutation of the beta-catenin gene." *Embo j* **18**(21): 5931-5942.
Hardwick, J. P., Osei-Hyiaman, D., Wiland, H., Abdelmegeed, M. A. and Song, B.-J. (2009). "PPAR/RXR Regulation of Fatty Acid Metabolism and Fatty Acid ω-Hydroxylase (CYP4) Isozymes: Implications for Prevention of Lipotoxicity in Fatty Liver Disease." *PPAR Research* **2009**: 952734.
Hawthorn, L., Lan, L. and Mojica, W. (2014). "Evidence for field effect cancerization in colorectal cancer." *Genomics* **103**(2-3): 211-221.
Hay, E. D. (1993). "Extracellular matrix alters epithelial differentiation." *Current Opinion in Cell Biology* **5**(6): 1029-1035.
Hayes, C. J., Dowling, C. M., Dwane, S., McCumiskey, M. E., Tormey, S. M., Anne Merrigan, B., Coffey, J. C., Kiely, P. A. and Dalton, T. M. (2016). "Extracellular matrix gene expression profiling using microfluidics for colorectal carcinoma stratification." *Biomicrofluidics* **10**(5): 054124.
He, L., Chinnery, P. F., Durham, S. E., Blakely, E. L., Wardell, T. M., Borthwick, G. M., Taylor, R. W. and Turnbull, D. M. (2002). "Detection and quantification of mitochondrial DNA deletions in individual cells by real-time PCR." *Nucleic Acids Res* **30**(14): e68.
He, X. C., Zhang, J., Tong, W. G., Tawfik, O., Ross, J., Scoville, D. H., Tian, Q., Zeng, X., He, X., Wiedemann, L. M., Mishina, Y. and Li, L. (2004). "BMP signaling inhibits intestinal stem cell self-renewal through suppression of Wnt-beta-catenin signaling." *Nat Genet* **36**(10): 1117-1121.
Heath, J. P. (1996). "Epithelial cell migration in the intestine." *Cell Biol Int* **20**(2): 139-146.

Heino, J. and Kapyla, J. (2009). "Cellular receptors of extracellular matrix molecules." *Curr Pharm Des* **15**(12): 1309-1317.
Helleday, T. (2010). "Homologous recombination in cancer development, treatment and development of drug resistance." *Carcinogenesis* **31**(6): 955-960.
Henry, L. R., Lee, H. O., Lee, J. S., Klein-Szanto, A., Watts, P., Ross, E. A., Chen, W. T. and Cheng, J. D. (2007). "Clinical implications of fibroblast activation protein in patients with colon cancer." *Clin Cancer Res* **13**(6): 1736-1741.
Herlihy, A. E. and de Bruin, R. A. (2017). "The Role of the Transcriptional Response to DNA Replication Stress." *Genes (Basel)* **8**(3).
Hernandez, C., Barrachina, M. D., Cosin-Roger, J., Ortiz-Masia, D., Alvarez, A., Terradez, L., Nicolau, M. J., Alos, R., Esplugues, J. V. and Calatayud, S. (2014). "Progastrin represses the alternative activation of human macrophages and modulates their influence on colon cancer epithelial cells." *PLoS One* **9**(6): e98458.
Herszenyi, L., Hritz, I., Lakatos, G., Varga, M. Z. and Tulassay, Z. (2012). "The behavior of matrix metalloproteinases and their inhibitors in colorectal cancer." *Int J Mol Sci* **13**(10): 13240-13263.
Herszenyi, L., Sipos, F., Galamb, O., Solymosi, N., Hritz, I., Miheller, P., Berczi, L., Molnar, B. and Tulassay, Z. (2008). "Matrix metalloproteinase-9 expression in the normal mucosa-adenoma-dysplasia-adenocarcinoma sequence of the colon." *Pathol Oncol Res* **14**(1): 31-37.
Hinz, B., Celetta, G., Tomasek, J. J., Gabbiani, G. and Chaponnier, C. (2001). "Alpha-smooth muscle actin expression upregulates fibroblast contractile activity." *Mol Biol Cell* **12**(9): 2730-2741.
Hokari, R., Kurihara, C., Nagata, N., Aritake, K., Okada, Y., Watanabe, C., Komoto, S., Nakamura, M., Kawaguchi, A., Nagao, S., Urade, Y. and Miura, S. (2011). "Increased expression of lipocalin-type-prostaglandin D synthase in ulcerative colitis and exacerbating role in murine colitis." *Am J Physiol Gastrointest Liver Physiol* **300**(3): G401-408.
Horvat, M. and Stabuc, B. (2011). "Microsatellite instability in colorectal cancer." *Radiology and Oncology* **45**(2): 75-81.
Hu, B., Castillo, E., Harewood, L., Ostano, P., Reymond, A., Dummer, R., Raffoul, W., Hoetzenecker, W., Hofbauer, G. F. and Dotto, G. P. (2012). "Multifocal epithelial tumors and field cancerization from loss of mesenchymal CSL signaling." *Cell* **149**(6): 1207-1220.
Hughes, L. A., Khalid-de Bakker, C. A., Smits, K. M., van den Brandt, P. A., Jonkers, D., Ahuja, N., Herman, J. G., Weijenberg, M. P. and van Engeland, M. (2012). "The CpG island methylator phenotype in colorectal cancer: progress and problems." *Biochim Biophys Acta* **1825**(1): 77-85.
Humphries, A., Cereser, B., Gay, L. J., Miller, D. S. J., Das, B., Gutteridge, A., Elia, G., Nye, E., Jeffery, R., Poulsom, R., Novelli, M. R., Rodriguez-Justo, M., McDonald, S. A. C., Wright, N. A. and Graham, T. A. (2013). "Lineage tracing reveals multipotent stem cells maintain human adenomas and the pattern of clonal expansion in tumor evolution." *Proceedings of the National Academy of Sciences* **110**(27): E2490-E2499.
Humphries, A. and Wright, N. A. (2008). "Colonic crypt organization and tumorigenesis." *Nat Rev Cancer* **8**(6): 415-424.
Ikeda, K., Iyama, K., Ishikawa, N., Egami, H., Nakao, M., Sado, Y., Ninomiya, Y. and Baba, H. (2006). "Loss of expression of type IV collagen alpha5 and alpha6 chains in colorectal cancer associated with the hypermethylation of their promoter region." *Am J Pathol* **168**(3): 856-865.

Inomata, M., Ochiai, A., Akimoto, S., Kitano, S. and Hirohashi, S. (1996). "Alteration of beta-catenin expression in colonic epithelial cells of familial adenomatous polyposis patients." *Cancer Res* **56**(9): 2213-2217.
Ireland, H., Houghton, C., Howard, L. and Winton, D. J. (2005). "Cellular inheritance of a Cre-activated reporter gene to determine Paneth cell longevity in the murine small intestine." *Dev Dyn* **233**(4): 1332-1336.
Isella, C., Terrasi, A., Bellomo, S. E., Petti, C., Galatola, G., Muratore, A., Mellano, A., Senetta, R., Cassenti, A., Sonetto, C., Inghirami, G., Trusolino, L., Fekete, Z., De Ridder, M., Cassoni, P., Storme, G., Bertotti, A. and Medico, E. (2015). "Stromal contribution to the colorectal cancer transcriptome." *Nat Genet* **47**(4): 312-319.
Ishiguro, K., Yoshida, T., Yagishita, H., Numata, Y. and Okayasu, T. (2006). "Epithelial and stromal genetic instability contributes to genesis of colorectal adenomas." *Gut* **55**(5): 695-702.
Issa, J. P. (2000). "CpG-island methylation in aging and cancer." *Curr Top Microbiol Immunol* **249**: 101-118.
Issa, J. P., Ahuja, N., Toyota, M., Bronner, M. P. and Brentnall, T. A. (2001). "Accelerated age-related CpG island methylation in ulcerative colitis." *Cancer Res* **61**(9): 3573-3577.
Jackson, L., Wahli, W., Michalik, L., Watson, S. A., Morris, T., Anderton, K., Bell, D. R., Smith, J. A., Hawkey, C. J. and Bennett, A. J. (2003). "Potential role for peroxisome proliferator activated receptor (PPAR) in preventing colon cancer." *Gut* **52**(9): 1317-1322.
Jacob, S. and Praz, F. (2002). "DNA mismatch repair defects: role in colorectal carcinogenesis." *Biochimie* **84**(1): 27-47.
Janda, C. Y., Waghray, D., Levin, A. M., Thomas, C. and Garcia, K. C. (2012). "Structural basis of Wnt recognition by Frizzled." *Science* **337**(6090): 59-64.
Jass, J. R., Whitehall, V. L., Young, J. and Leggett, B. A. (2002). "Emerging concepts in colorectal neoplasia." *Gastroenterology* **123**(3): 862-876.
Jenkins, M. A., Hayashi, S., O'Shea, A. M., Burgart, L. J., Smyrk, T. C., Shimizu, D., Waring, P. M., Ruszkiewicz, A. R., Pollett, A. F., Redston, M., Barker, M. A., Baron, J. A., Casey, G. R., Dowty, J. G., Giles, G. G., Limburg, P., Newcomb, P., Young, J. P., Walsh, M. D., Thibodeau, S. N., Lindor, N. M., Lemarchand, L., Gallinger, S., Haile, R. W., Potter, J. D., Hopper, J. L. and Jass, J. R. (2007). "Pathology features in Bethesda guidelines predict colorectal cancer microsatellite instability: a population-based study." *Gastroenterology* **133**(1): 48-56.
Jimenez-Marin, A., Collado-Romero, M., Ramirez-Boo, M., Arce, C. and Garrido, J. J. (2009). "Biological pathway analysis by ArrayUnlock and Ingenuity Pathway Analysis." *BMC Proc* **3 Suppl 4**: S6.
Jiricny, J. and Marra, G. (2003). "DNA repair defects in colon cancer." *Curr Opin Genet Dev* **13**(1): 61-69.
Jorgensen, M. L., Young, J. M. and Solomon, M. J. (2015). "Optimal delivery of colorectal cancer follow-up care: improving patient outcomes." *Patient Relat Outcome Meas* **6**: 127-138.
Jung, B., Gomez, J., Chau, E., Cabral, J., Lee, J. K., Anselm, A., Slowik, P., Ream-Robinson, D., Messer, K., Sporn, J., Shin, S. K., Boland, C. R., Goel, A. and Carethers, J. M. (2009). "Activin signaling in microsatellite stable colon cancers is disrupted by a combination of genetic and epigenetic mechanisms." *PLoS One* **4**(12): e8308.
Junttila, M. R. and de Sauvage, F. J. (2013). "Influence of tumour micro-environment heterogeneity on therapeutic response." *Nature* **501**(7467): 346-354.

Junttila, M. R., Mao, W., Wang, X., Wang, B. E., Pham, T., Flygare, J., Yu, S. F., Yee, S., Goldenberg, D., Fields, C., Eastham-Anderson, J., Singh, M., Vij, R., Hongo, J. A., Firestein, R., Schutten, M., Flagella, K., Polakis, P. and Polson, A. G. (2015). "Targeting LGR5+ cells with an antibody-drug conjugate for the treatment of colon cancer." *Sci Transl Med* **7**(314): 314ra186.
Kadowaki, T., Wilder, E., Klingensmith, J., Zachary, K. and Perrimon, N. (1996). "The segment polarity gene porcupine encodes a putative multitransmembrane protein involved in Wingless processing." *Genes Dev* **10**(24): 3116-3128.
Kalluri, R. (2016). "The biology and function of fibroblasts in cancer." *Nat Rev Cancer* **16**(9): 582-598.
Kalluri, R. and Zeisberg, M. (2006). "Fibroblasts in cancer." *Nat Rev Cancer* **6**(5): 392-401.
Kanehisa, M. and Goto, S. (2000). "KEGG: kyoto encyclopedia of genes and genomes." *Nucleic Acids Res* **28**(1): 27-30.
Kang, H., Salomon, M. P., Sottoriva, A., Zhao, J., Toy, M., Press, M. F., Curtis, C., Marjoram, P., Siegmund, K. and Shibata, D. (2015). "Many private mutations originate from the first few divisions of a human colorectal adenoma." *J Pathol* **237**(3): 355-362.
Kemper, K., Prasetyanti, P. R., De Lau, W., Rodermond, H., Clevers, H. and Medema, J. P. (2012). "Monoclonal antibodies against Lgr5 identify human colorectal cancer stem cells." *Stem Cells* **30**(11): 2378-2386.
Kessenbrock, K., Plaks, V. and Werb, Z. (2010). "Matrix metalloproteinases: regulators of the tumor microenvironment." *Cell* **141**(1): 52-67.
Kessenbrock, K., Wang, C.-Y. and Werb, Z. (2015). "Matrix metalloproteinases in stem cell regulation and cancer." *Matrix biology : journal of the International Society for Matrix Biology* **0**: 184-190.
Kessenbrock, K., Wang, C. Y. and Werb, Z. (2015). "Matrix metalloproteinases in stem cell regulation and cancer." *Matrix Biol* **44-46**: 184-190.
Kheirelseid, E. A. H., Miller, N., Chang, K. H., Curran, C., Hennessey, E., Sheehan, M. and Kerin, M. J. (2013). "Mismatch repair protein expression in colorectal cancer." *Journal of Gastrointestinal Oncology* **4**(4): 397-408.
Kim, D., Pertea, G., Trapnell, C., Pimentel, H., Kelley, R. and Salzberg, S. L. (2013). "TopHat2: accurate alignment of transcriptomes in the presence of insertions, deletions and gene fusions." *Genome Biology* **14**(4): R36-R36.
Kim, H., Jen, J., Vogelstein, B. and Hamilton, S. R. (1994). "Clinical and pathological characteristics of sporadic colorectal carcinomas with DNA replication errors in microsatellite sequences." *Am J Pathol* **145**(1): 148-156.
Kim, J. Y., Siegmund, K. D., Tavare, S. and Shibata, D. (2005). "Age-related human small intestine methylation: evidence for stem cell niches." *BMC Med* **3**: 10.
Kim, K. A., Kakitani, M., Zhao, J., Oshima, T., Tang, T., Binnerts, M., Liu, Y., Boyle, B., Park, E., Emtage, P., Funk, W. D. and Tomizuka, K. (2005). "Mitogenic influence of human R-spondin1 on the intestinal epithelium." *Science* **309**(5738): 1256-1259.
Kim, K. M. and Shibata, D. (2002). "Methylation reveals a niche: stem cell succession in human colon crypts." *Oncogene* **21**(35): 5441-5449.
Kim, K. M. and Shibata, D. (2004). "Tracing ancestry with methylation patterns: most crypts appear distantly related in normal adult human colon." *BMC Gastroenterol* **4**: 8.
Kim, P. K. and Hettema, E. H. (2015). "Multiple Pathways for Protein Transport to Peroxisomes." *Journal of Molecular Biology* **427**(6): 1176-1190.

Kim, T.-H., Escudero, S. and Shivdasani, R. A. (2012). "Intact function of Lgr5 receptor-expressing intestinal stem cells in the absence of Paneth cells." *Proceedings of the National Academy of Sciences* **109**(10): 3932-3937.
Kim, T. H., Saadatpour, A., Guo, G., Saxena, M., Cavazza, A., Desai, N., Jadhav, U., Jiang, L., Rivera, M. N., Orkin, S. H., Yuan, G. C. and Shivdasani, R. A. (2016). "Single-Cell Transcript Profiles Reveal Multilineage Priming in Early Progenitors Derived from Lgr5(+) Intestinal Stem Cells." *Cell Rep* **16**(8): 2053-2060.
Kinzler, K. W. and Vogelstein, B. (1996). "Lessons from hereditary colorectal cancer." *Cell* **87**(2): 159-170.
Kiraly, O., Gong, G., Olipitz, W., Muthupalani, S. and Engelward, B. P. (2015). "Inflammation-induced cell proliferation potentiates DNA damage-induced mutations in vivo." *PLoS Genet* **11**(2): e1004901.
Kirchberger, S., Royston, D. J., Boulard, O., Thornton, E., Franchini, F., Szabady, R. L., Harrison, O. and Powrie, F. (2013). "Innate lymphoid cells sustain colon cancer through production of interleukin-22 in a mouse model." *J Exp Med* **210**(5): 917-931.
Klampfer, L. (2011). "Cytokines, inflammation and colon cancer." *Curr Cancer Drug Targets* **11**(4): 451-464.
Klupp, F., Neumann, L., Kahlert, C., Diers, J., Halama, N., Franz, C., Schmidt, T., Koch, M., Weitz, J., Schneider, M. and Ulrich, A. (2016). "Serum MMP7, MMP10 and MMP12 level as negative prognostic markers in colon cancer patients." *BMC Cancer* **16**: 494.
Knudson, A. G., Jr. (1971). "Mutation and cancer: statistical study of retinoblastoma." *Proc Natl Acad Sci U S A* **68**(4): 820-823.
Koch, M., Beckhove, P., op den Winkel, J., Autenrieth, D., Wagner, P., Nummer, D., Specht, S., Antolovic, D., Galindo, L., Schmitz-Winnenthal, F. H., Schirrmacher, V., Büchler, M. W. and Weitz, J. (2006). "Tumor Infiltrating T Lymphocytes in Colorectal Cancer: Tumor-Selective Activation and Cytotoxic Activity In Situ." *Annals of Surgery* **244**(6): 986-993.
Koelzer, V. H., Canonica, K., Dawson, H., Sokol, L., Karamitopoulou-Diamantis, E., Lugli, A. and Zlobec, I. (2016). "Phenotyping of tumor-associated macrophages in colorectal cancer: Impact on single cell invasion (tumor budding) and clinicopathological outcome." *Oncoimmunology* **5**(4): e1106677.
Koi, M., Tseng-Rogenski, S. S. and Carethers, J. M. (2018). "Inflammation-associated microsatellite alterations: Mechanisms and significance in the prognosis of patients with colorectal cancer." *World J Gastrointest Oncol* **10**(1): 1-14.
Koo, B. K., Spit, M., Jordens, I., Low, T. Y., Stange, D. E., van de Wetering, M., van Es, J. H., Mohammed, S., Heck, A. J., Maurice, M. M. and Clevers, H. (2012). "Tumour suppressor RNF43 is a stem-cell E3 ligase that induces endocytosis of Wnt receptors." *Nature* **488**(7413): 665-669.
Koo, B. K., Stange, D. E., Sato, T., Karthaus, W., Farin, H. F., Huch, M., van Es, J. H. and Clevers, H. (2011). "Controlled gene expression in primary Lgr5 organoid cultures." *Nat Methods* **9**(1): 81-83.
Korinek, V., Barker, N., Morin, P. J., van Wichen, D., de Weger, R., Kinzler, K. W., Vogelstein, B. and Clevers, H. (1997). "Constitutive transcriptional activation by a beta-catenin-Tcf complex in APC-/- colon carcinoma." *Science* **275**(5307): 1784-1787.
Kortlever, R. M., Sodir, N. M., Wilson, C. H., Burkhart, D. L., Pellegrinet, L., Brown Swigart, L., Littlewood, T. D. and Evan, G. I. (2017). "Myc Cooperates with

Ras by Programming Inflammation and Immune Suppression." *Cell* **171**(6): 1301-1315.e1314.
Korzeniewski, B. (2001). "Theoretical studies on the regulation of oxidative phosphorylation in intact tissues." *Biochim Biophys Acta* **1504**(1): 31-45.
Kosinski, C., Li, V. S., Chan, A. S., Zhang, J., Ho, C., Tsui, W. Y., Chan, T. L., Mifflin, R. C., Powell, D. W., Yuen, S. T., Leung, S. Y. and Chen, X. (2007). "Gene expression patterns of human colon tops and basal crypts and BMP antagonists as intestinal stem cell niche factors." *Proc Natl Acad Sci U S A* **104**(39): 15418-15423.
Kostova, E., Slaninka-Miceska, M., Labacevski, N., Jakovski, K., Trojachanec, J., Atanasovska, E., Janevski, V., Jovanovik, R. and Janevska, V. (2014). "Expression of matrix metalloproteinases 2, 7 and 9 in patients with colorectal cancer." *Vojnosanit Pregl* **71**(1): 52-59.
Kozar, S., Morrissey, E., Nicholson, A. M., van der Heijden, M., Zecchini, H. I., Kemp, R., Tavare, S., Vermeulen, L. and Winton, D. J. (2013). "Continuous clonal labeling reveals small numbers of functional stem cells in intestinal crypts and adenomas." *Cell Stem Cell* **13**(5): 626-633.
Kramer, A., Green, J., Pollard, J., Jr. and Tugendreich, S. (2014). "Causal analysis approaches in Ingenuity Pathway Analysis." *Bioinformatics* **30**(4): 523-530.
Kretzschmar, K. and Clevers, H. (2017). "Wnt/ β -catenin signaling in adult mammalian epithelial stem cells." *Developmental Biology* **428**(2): 273-282.
Kuijper, A., Buerger, H., Simon, R., Schaefer, K. L., Croonen, A., Boecker, W., van der Wall, E. and van Diest, P. J. (2002). "Analysis of the progression of fibroepithelial tumours of the breast by PCR-based clonality assay." *J Pathol* **197**(5): 575-581.
Kulis, M. and Esteller, M. (2010). "DNA methylation and cancer." *Adv Genet* **70**: 27-56.
Kuo, Y. C., Su, C. H., Liu, C. Y., Chen, T. H., Chen, C. P. and Wang, H. S. (2009). "Transforming growth factor-beta induces CD44 cleavage that promotes migration of MDA-MB-435s cells through the up-regulation of membrane type 1-matrix metalloproteinase." *Int J Cancer* **124**(11): 2568-2576.
Kwong, L. N. and Dove, W. F. (2009). "APC and its modifiers in colon cancer." *Adv Exp Med Biol* **656**: 85-106.
Lamlum, H., Ilyas, M., Rowan, A., Clark, S., Johnson, V., Bell, J., Frayling, I., Efstathiou, J., Pack, K., Payne, S., Roylance, R., Gorman, P., Sheer, D., Neale, K., Phillips, R., Talbot, I., Bodmer, W. and Tomlinson, I. (1999). "The type of somatic mutation at APC in familial adenomatous polyposis is determined by the site of the germline mutation: a new facet to Knudson's 'two-hit' hypothesis." *Nat Med* **5**(9): 1071-1075.
Lamlum, H., Papadopoulou, A., Ilyas, M., Rowan, A., Gillet, C., Hanby, A., Talbot, I., Bodmer, W. and Tomlinson, I. (2000). "APC mutations are sufficient for the growth of early colorectal adenomas." *Proc Natl Acad Sci U S A* **97**(5): 2225-2228.
Lamprecht, S., Schmidt, E. M., Blaj, C., Hermeking, H., Jung, A., Kirchner, T. and Horst, D. (2017). "Multicolor lineage tracing reveals clonal architecture and dynamics in colon cancer." *Nat Commun* **8**(1): 1406.
Landskron, G., De la Fuente, M., Thuwajit, P., Thuwajit, C. and Hermoso, M. A. (2014). "Chronic Inflammation and Cytokines in the Tumor Microenvironment." *Journal of Immunology Research* **2014**: 19.
Langlands, A. J., Almet, A. A., Appleton, P. L., Newton, I. P., Osborne, J. M. and Nathke, I. S. (2016). "Paneth Cell-Rich Regions Separated by a Cluster of Lgr5+

Cells Initiate Crypt Fission in the Intestinal Stem Cell Niche." *PLoS Biol* **14**(6): e1002491.
Langmead, B. and Salzberg, S. L. (2012). "Fast gapped-read alignment with Bowtie 2." *Nat Methods* **9**(4): 357-359.
Lawrie, L. C., Dundas, S. R., Curran, S. and Murray, G. I. (2004). "Liver fatty acid binding protein expression in colorectal neoplasia." *Br J Cancer* **90**(10): 1955-1960.
Lechner, S., Müller-Ladner, U., Renke, B., Schölmerich, J., Rüschoff, J. and Kullmann, F. (2003). "Gene expression pattern of laser microdissected colonic crypts of adenomas with low grade dysplasia." *Gut* **52**(8): 1148-1153.
Lee, S. J., Park, S. S., Cho, Y. H., Park, K., Kim, E. J., Jung, K. H., Kim, S. K., Kim, W. J. and Moon, S. K. (2008). "Activation of matrix metalloproteinase-9 by TNF-alpha in human urinary bladder cancer HT1376 cells: the role of MAP kinase signaling pathways." *Oncol Rep* **19**(4): 1007-1013.
Lee, S. J., Park, S. S., Lee, U. S., Kim, W. J. and Moon, S. K. (2008). "Signaling pathway for TNF-alpha-induced MMP-9 expression: mediation through p38 MAP kinase, and inhibition by anti-cancer molecule magnolol in human urinary bladder cancer 5637 cells." *Int Immunopharmacol* **8**(13-14): 1821-1826.
Lee, S. R. and Han, J. (2017). "Mitochondrial Nucleoid: Shield and Switch of the Mitochondrial Genome." *Oxid Med Cell Longev* **2017**: 8060949.
Leedham, S. J., Graham, T. A., Oukrif, D., McDonald, S. A., Rodriguez-Justo, M., Harrison, R. F., Shepherd, N. A., Novelli, M. R., Jankowski, J. A. and Wright, N. A. (2009). "Clonality, founder mutations, and field cancerization in human ulcerative colitis-associated neoplasia." *Gastroenterology* **136**(2): 542-550.e546.
Leedham, S. J., Rodenas-Cuadrado, P., Howarth, K., Lewis, A., Mallappa, S., Segditsas, S., Davis, H., Jeffery, R., Rodriguez-Justo, M., Keshav, S., Travis, S. P., Graham, T. A., East, J., Clark, S. and Tomlinson, I. P. (2013). "A basal gradient of Wnt and stem-cell number influences regional tumour distribution in human and mouse intestinal tracts." *Gut* **62**(1): 83-93.
Leivonen, S. K., Chantry, A., Hakkinen, L., Han, J. and Kahari, V. M. (2002). "Smad3 mediates transforming growth factor-beta-induced collagenase-3 (matrix metalloproteinase-13) expression in human gingival fibroblasts. Evidence for cross-talk between Smad3 and p38 signaling pathways." *J Biol Chem* **277**(48): 46338-46346.
Lengauer, C., Kinzler, K. W. and Vogelstein, B. (1998). "Genetic instabilities in human cancers." *Nature* **396**(6712): 643-649.
Leoz, M. L., Carballal, S., Moreira, L., Ocana, T. and Balaguer, F. (2015). "The genetic basis of familial adenomatous polyposis and its implications for clinical practice and risk management." *Appl Clin Genet* **8**: 95-107.
Leslie, A., Carey, F. A., Pratt, N. R. and Steele, R. J. (2002). "The colorectal adenoma-carcinoma sequence." *Br J Surg* **89**(7): 845-860.
Levine, A. J., Phipps, A. I., Baron, J. A., Buchanan, D. D., Ahnen, D. J., Cohen, S. A., Lindor, N. M., Newcomb, P. A., Rosty, C., Haile, R. W., Laird, P. W. and Weisenberger, D. J. (2016). "Clinicopathological risk factor distributions for MLH1 promoter region methylation in CIMP positive tumors." *Cancer epidemiology, biomarkers & prevention : a publication of the American Association for Cancer Research, cosponsored by the American Society of Preventive Oncology* **25**(1): 68-75.
Lewis, A., Segditsas, S., Deheragoda, M., Pollard, P., Jeffery, R., Nye, E., Lockstone, H., Davis, H., Clark, S., Stamp, G., Poulsom, R., Wright, N. and Tomlinson, I. (2010). "Severe polyposis in Apc(1322T) mice is associated with

submaximal Wnt signalling and increased expression of the stem cell marker Lgr5." *Gut* **59**(12): 1680-1686.
Li, L. T., Jiang, G., Chen, Q. and Zheng, J. N. (2015). "Ki67 is a promising molecular target in the diagnosis of cancer (review)." *Mol Med Rep* **11**(3): 1566-1572.
Li, S. K. and Martin, A. (2016). "Mismatch Repair and Colon Cancer: Mechanisms and Therapies Explored." *Trends Mol Med* **22**(4): 274-289.
Li, V. S. and Clevers, H. (2012). "In vitro expansion and transplantation of intestinal crypt stem cells." *Gastroenterology* **143**(1): 30-34.
Li, V. S., Ng, S. S., Boersema, P. J., Low, T. Y., Karthaus, W. R., Gerlach, J. P., Mohammed, S., Heck, A. J., Maurice, M. M., Mahmoudi, T. and Clevers, H. (2012). "Wnt signaling through inhibition of beta-catenin degradation in an intact Axin1 complex." *Cell* **149**(6): 1245-1256.
Li, Y., Park, J. S., Deng, J. H. and Bai, Y. (2006). "Cytochrome c oxidase subunit IV is essential for assembly and respiratory function of the enzyme complex." *J Bioenerg Biomembr* **38**(5-6): 283-291.
Li, Y. Q., Roberts, S. A., Paulus, U., Loeffler, M. and Potten, C. S. (1994). "The crypt cycle in mouse small intestinal epithelium." *J Cell Sci* **107 (Pt 12)**: 3271-3279.
Liang, B., Li, C. and Zhao, J. (2016). "Identification of key pathways and genes in colorectal cancer using bioinformatics analysis." *Med Oncol* **33**(10): 111.
Lin, J., Goto, Y., Murata, H., Sakaizawa, K., Uchiyama, A., Saida, T. and Takata, M. (2011). "Polyclonality of BRAF mutations in primary melanoma and the selection of mutant alleles during progression." *Br J Cancer* **104**(3): 464-468.
Lin, S.-H., Raju, G. S., Huff, C., Ye, Y., Gu, J., Chen, J.-S., Hildebrandt, M. A. T., Liang, H., Menter, D. G., Morris, J., Hawk, E., Stroehlein, J. R., Futreal, A., Kopetz, S., Mishra, L. and Wu, X. (2018). "The somatic mutation landscape of premalignant colorectal adenoma." *Gut* **67**(7): 1299.
Liu, M., Li, Y., Chen, L., Chan, T. H., Song, Y., Fu, L., Zeng, T. T., Dai, Y. D., Zhu, Y. H., Li, Y., Chen, J., Yuan, Y. F. and Guan, X. Y. (2014). "Allele-specific imbalance of oxidative stress-induced growth inhibitor 1 associates with progression of hepatocellular carcinoma." *Gastroenterology* **146**(4): 1084-1096.
Liu, Y., Xia, T., Jin, C., Gu, D., Yu, J., Shi, W., Zhang, K. E., Zhang, L., Ye, J. and Li, L. (2016). "FOXP3 and CEACAM6 expression and T cell infiltration in the occurrence and development of colon cancer." *Oncol Lett* **11**(6): 3693-3701.
Logan, C. Y. and Nusse, R. (2004). "The Wnt signaling pathway in development and disease." *Annu Rev Cell Dev Biol* **20**: 781-810.
Lopez-Garcia, C., Klein, A. M., Simons, B. D. and Winton, D. J. (2010). "Intestinal stem cell replacement follows a pattern of neutral drift." *Science* **330**(6005): 822-825.
Lord, C. J. and Ashworth, A. (2012). "The DNA damage response and cancer therapy." *Nature* **481**(7381): 287-294.
Lorenc, Z., Waniczek, D., Lorenc-Podgórska, K., Krawczyk, W., Domagała, M., Majewski, M. and Mazurek, U. (2017). "Profile of Expression of Genes Encoding Matrix Metallopeptidase 9 (MMP9), Matrix Metallopeptidase 28 (MMP28) and TIMP Metallopeptidase Inhibitor 1 (TIMP1) in Colorectal Cancer: Assessment of the Role in Diagnosis and Prognostication." *Medical Science Monitor : International Medical Journal of Experimental and Clinical Research* **23**: 1305-1311.
Love, M. I., Huber, W. and Anders, S. (2014). "Moderated estimation of fold change and dispersion for RNA-seq data with DESeq2." *Genome Biol* **15**(12): 550.

Lu, B., Xu, J., Lai, M., Zhang, H. and Chen, J. (2006). "A transcriptome anatomy of human colorectal cancers." *BMC Cancer* **6**: 40.
Lu, P., Takai, K., Weaver, V. M. and Werb, Z. (2011). "Extracellular matrix degradation and remodeling in development and disease." *Cold Spring Harb Perspect Biol* **3**(12).
Luebeck, E. G. and Moolgavkar, S. H. (2002). "Multistage carcinogenesis and the incidence of colorectal cancer." *Proc Natl Acad Sci U S A* **99**(23): 15095-15100.
Luo, F., Brooks, D. G., Ye, H., Hamoudi, R., Poulogiannis, G., Patek, C. E., Winton, D. J. and Arends, M. J. (2009). "Mutated K-ras(Asp12) promotes tumourigenesis in Apc(Min) mice more in the large than the small intestines, with synergistic effects between K-ras and Wnt pathways." *Int J Exp Pathol* **90**(5): 558-574.
Luo, Y., Wong, C. J., Kaz, A. M., Dzieciatkowski, S., Carter, K. T., Morris, S. M., Wang, J., Willis, J. E., Makar, K. W., Ulrich, C. M., Lutterbaugh, J. D., Shrubsole, M. J., Zheng, W., Markowitz, S. D. and Grady, W. M. (2014). "Differences in DNA methylation signatures reveal multiple pathways of progression from adenoma to colorectal cancer." *Gastroenterology* **147**(2): 418-429.e418.
Lustig, B., Jerchow, B., Sachs, M., Weiler, S., Pietsch, T., Karsten, U., van de Wetering, M., Clevers, H., Schlag, P. M., Birchmeier, W. and Behrens, J. (2002). "Negative feedback loop of Wnt signaling through upregulation of conductin/axin2 in colorectal and liver tumors." *Mol Cell Biol* **22**(4): 1184-1193.
Maiorano, D., Lutzmann, M. and Mechali, M. (2006). "MCM proteins and DNA replication." *Curr Opin Cell Biol* **18**(2): 130-136.
Markowitz, S., Wang, J., Myeroff, L., Parsons, R., Sun, L., Lutterbaugh, J., Fan, R. S., Zborowska, E., Kinzler, K. W., Vogelstein, B. and et al. (1995). "Inactivation of the type II TGF-beta receptor in colon cancer cells with microsatellite instability." *Science* **268**(5215): 1336-1338.
Martincorena, I., Roshan, A., Gerstung, M., Ellis, P., Van Loo, P., McLaren, S., Wedge, D. C., Fullam, A., Alexandrov, L. B., Tubio, J. M., Stebbings, L., Menzies, A., Widaa, S., Stratton, M. R., Jones, P. H. and Campbell, P. J. (2015). "Tumor evolution. High burden and pervasive positive selection of somatic mutations in normal human skin." *Science* **348**(6237): 880-886.
Martinelli, E., Morgillo, F., Troiani, T. and Ciardiello, F. (2017). "Cancer resistance to therapies against the EGFR-RAS-RAF pathway: The role of MEK." *Cancer Treat Rev* **53**: 61-69.
Marusyk, A., Tabassum, D. P., Altrock, P. M., Almendro, V., Michor, F. and Polyak, K. (2014). "Non-cell-autonomous driving of tumour growth supports sub-clonal heterogeneity." *Nature* **514**(7520): 54-58.
McAlpine, C. A., Barak, Y., Matise, I. and Cormier, R. T. (2006). "Intestinal-specific PPARgamma deficiency enhances tumorigenesis in ApcMin/+ mice." *Int J Cancer* **119**(10): 2339-2346.
McCole, D. F. (2014). "IBD candidate genes and intestinal barrier regulation." *Inflamm Bowel Dis* **20**(10): 1829-1849.
McCole, D. F. (2014). "IBD Candidate Genes and Intestinal Barrier Regulation." *Inflammatory bowel diseases* **20**(10): 1829-1849.
McLean, M. H., Murray, G. I., Stewart, K. N., Norrie, G., Mayer, C., Hold, G. L., Thomson, J., Fyfe, N., Hope, M., Mowat, N. A., Drew, J. E. and El-Omar, E. M. (2011). "The inflammatory microenvironment in colorectal neoplasia." *PLoS One* **6**(1): e15366.

Melzer, C., von der Ohe, J., Lehnert, H., Ungefroren, H. and Hass, R. (2017). "Cancer stem cell niche models and contribution by mesenchymal stroma/stem cells." *Molecular Cancer* **16**(1): 28.
Menon, A. G., Janssen-van Rhijn, C. M., Morreau, H., Putter, H., Tollenaar, R. A., van de Velde, C. J., Fleuren, G. J. and Kuppen, P. J. (2004). "Immune system and prognosis in colorectal cancer: a detailed immunohistochemical analysis." *Lab Invest* **84**(4): 493-501.
Mercado-Lubo, R. and McCormick, B. A. (2010). "The interaction of gut microbes with host ABC transporters." *Gut Microbes* **1**(5): 301-306.
Meric-Bernstam, F. and Mills, G. B. (2012). "Overcoming implementation challenges of personalized cancer therapy." *Nat Rev Clin Oncol* **9**(9): 542-548.
Merlo, L. M., Pepper, J. W., Reid, B. J. and Maley, C. C. (2006). "Cancer as an evolutionary and ecological process." *Nat Rev Cancer* **6**(12): 924-935.
Merlos-Suarez, A., Barriga, F. M., Jung, P., Iglesias, M., Cespedes, M. V., Rossell, D., Sevillano, M., Hernando-Momblona, X., da Silva-Diz, V., Munoz, P., Clevers, H., Sancho, E., Mangues, R. and Batlle, E. (2011). "The intestinal stem cell signature identifies colorectal cancer stem cells and predicts disease relapse." *Cell Stem Cell* **8**(5): 511-524.
Merritt, A. J., Gould, K. A. and Dove, W. F. (1997). "Polyclonal structure of intestinal adenomas in ApcMin/+ mice with concomitant loss of Apc+ from all tumor lineages." *Proc Natl Acad Sci U S A* **94**(25): 13927-13931.
Middendorp, S., Schneeberger, K., Wiegerinck, C. L., Mokry, M., Akkerman, R. D., van Wijngaarden, S., Clevers, H. and Nieuwenhuis, E. E. (2014). "Adult stem cells in the small intestine are intrinsically programmed with their location-specific function." *Stem Cells* **32**(5): 1083-1091.
Milholland, B., Auton, A., Suh, Y. and Vijg, J. (2015). "Age-related somatic mutations in the cancer genome." *Oncotarget* **6**(28): 24627-24635.
Miquel, C., Jacob, S., Grandjouan, S., Aime, A., Viguier, J., Sabourin, J. C., Sarasin, A., Duval, A. and Praz, F. (2007). "Frequent alteration of DNA damage signalling and repair pathways in human colorectal cancers with microsatellite instability." *Oncogene* **26**(40): 5919-5926.
Miyaki, M., Konishi, M., Kikuchi-Yanoshita, R., Enomoto, M., Igari, T., Tanaka, K., Muraoka, M., Takahashi, H., Amada, Y., Fukayama, M. and et al. (1994). "Characteristics of somatic mutation of the adenomatous polyposis coli gene in colorectal tumors." *Cancer Res* **54**(11): 3011-3020.
Miyazono, K., Kamiya, Y. and Morikawa, M. (2010). "Bone morphogenetic protein receptors and signal transduction." *J Biochem* **147**(1): 35-51.
Mo, A., Jackson, S., Varma, K., Carpino, A., Giardina, C., Devers, T. J. and Rosenberg, D. W. (2016). "Distinct Transcriptional Changes and Epithelial-Stromal Interactions Are Altered in Early-Stage Colon Cancer Development." *Mol Cancer Res* **14**(9): 795-804.
Montgomery, R. K., Carlone, D. L., Richmond, C. A., Farilla, L., Kranendonk, M. E., Henderson, D. E., Baffour-Awuah, N. Y., Ambruzs, D. M., Fogli, L. K., Algra, S. and Breault, D. T. (2011). "Mouse telomerase reverse transcriptase (mTert) expression marks slowly cycling intestinal stem cells." *Proc Natl Acad Sci U S A* **108**(1): 179-184.
Morin, P. J., Sparks, A. B., Korinek, V., Barker, N., Clevers, H., Vogelstein, B. and Kinzler, K. W. (1997). "Activation of beta-catenin-Tcf signaling in colon cancer by mutations in beta-catenin or APC." *Science* **275**(5307): 1787-1790.

Mowat, A. M. and Agace, W. W. (2014). "Regional specialization within the intestinal immune system." *Nat Rev Immunol* **14**(10): 667-685.
Mroue, R. and Bissell, M. J. (2013). "Three-dimensional cultures of mouse mammary epithelial cells." *Methods Mol Biol* **945**: 221-250.
Muffler, S., Stark, H. J., Amoros, M., Falkowska-Hansen, B., Boehnke, K., Buhring, H. J., Marme, A., Bickenbach, J. R. and Boukamp, P. (2008). "A stable niche supports long-term maintenance of human epidermal stem cells in organotypic cultures." *Stem Cells* **26**(10): 2506-2515.
Mukaida, N. and Sasaki, S. (2016). "Fibroblasts, an inconspicuous but essential player in colon cancer development and progression." *World Journal of Gastroenterology* **22**(23): 5301-5316.
Murthy, S., Ryan, A. J. and Carter, A. B. (2012). "SP-1 regulation of MMP-9 expression requires Ser586 in the PEST domain." *Biochem J* **445**(2): 229-236.
Nagy, R., Sweet, K. and Eng, C. (2004). "Highly penetrant hereditary cancer syndromes." *Oncogene* **23**(38): 6445-6470.
Nakagawa, H., Liyanarachchi, S., Davuluri, R. V., Auer, H., Martin, E. W., Jr., de la Chapelle, A. and Frankel, W. L. (2004). "Role of cancer-associated stromal fibroblasts in metastatic colon cancer to the liver and their expression profiles." *Oncogene* **23**(44): 7366-7377.
Nakamura, S.-i. and Kino, I. (1984). "Morphogenesis of Minute Adenomas in Familial Polyposis Coli2." *JNCI: Journal of the National Cancer Institute* **73**(1): 41-49.
Nancey, S., Holvoet, S., Graber, I., Joubert, G., Philippe, D., Martin, S., Nicolas, J. F., Desreumaux, P., Flourie, B. and Kaiserlian, D. (2006). "CD8+ cytotoxic T cells induce relapsing colitis in normal mice." *Gastroenterology* **131**(2): 485-496.
Nebert, D. W., Wikvall, K. and Miller, W. L. (2013). "Human cytochromes P450 in health and disease." *Philosophical Transactions of the Royal Society B: Biological Sciences* **368**(1612): 20120431.
Network, C. G. A. (2012). "Comprehensive molecular characterization of human colon and rectal cancer." *Nature* **487**(7407): 330-337.
Network, T. C. G. A. (2012). "Comprehensive Molecular Characterization of Human Colon and Rectal Cancer." *Nature* **487**(7407): 330-337.
Nicholson, A. M., Graham, T. A., Simpson, A., Humphries, A., Burch, N., Rodriguez-Justo, M., Novelli, M., Harrison, R., Wright, N. A., McDonald, S. A. and Jankowski, J. A. (2012). "Barrett's metaplasia glands are clonal, contain multiple stem cells and share a common squamous progenitor." *Gut* **61**(10): 1380-1389.
Nicholson, A. M., Olpe, C., Hoyle, A., Thorsen, A. S., Rus, T., Colombe, M., Brunton-Sim, R., Kemp, R., Marks, K., Quirke, P., Malhotra, S., Ten Hoopen, R., Ibrahim, A., Lindskog, C., Myers, M. B., Parsons, B., Tavare, S., Wilkinson, M., Morrissey, E. and Winton, D. J. (2018). "Fixation and Spread of Somatic Mutations in Adult Human Colonic Epithelium." *Cell Stem Cell* **22**(6): 909-918.e908.
Nicolas, P., Kim, K. M., Shibata, D. and Tavare, S. (2007). "The stem cell population of the human colon crypt: analysis via methylation patterns." *PLoS Comput Biol* **3**(3): e28.
Nieminen, T. T., O'Donohue, M. F., Wu, Y., Lohi, H., Scherer, S. W., Paterson, A. D., Ellonen, P., Abdel-Rahman, W. M., Valo, S., Mecklin, J. P., Jarvinen, H. J., Gleizes, P. E. and Peltomaki, P. (2014). "Germline mutation of RPS20, encoding a ribosomal protein, causes predisposition to hereditary nonpolyposis colorectal carcinoma without DNA mismatch repair deficiency." *Gastroenterology* **147**(3): 595-598.e595.

Nissinen, L. and Kahari, V. M. (2014). "Matrix metalloproteinases in inflammation." *Biochim Biophys Acta* **1840**(8): 2571-2580.
Nooteboom, M., Johnson, R., Taylor, R. W., Wright, N. A., Lightowlers, R. N., Kirkwood, T. B. L., Mathers, J. C., Turnbull, D. M. and Greaves, L. C. (2010). "Age-associated mitochondrial DNA mutations lead to small but significant changes in cell proliferation and apoptosis in human colonic crypts." *Aging Cell* **9**(1): 96-99.
Novelli, M., Cossu, A., Oukrif, D., Quaglia, A., Lakhani, S., Poulsom, R., Sasieni, P., Carta, P., Contini, M., Pasca, A., Palmieri, G., Bodmer, W., Tanda, F. and Wright, N. (2003). "X-inactivation patch size in human female tissue confounds the assessment of tumor clonality." *Proc Natl Acad Sci U S A* **100**(6): 3311-3314.
Novelli, M. R., Williamson, J. A., Tomlinson, I. P., Elia, G., Hodgson, S. V., Talbot, I. C., Bodmer, W. F. and Wright, N. A. (1996). "Polyclonal origin of colonic adenomas in an XO/XY patient with FAP." *Science* **272**(5265): 1187-1190.
Nowell, P. C. (1976). "The clonal evolution of tumor cell populations." *Science* **194**(4260): 23-28.
Oshima, C. T., Iriya, K. and Forones, N. M. (2005). "Ki-67 as a prognostic marker in colorectal cancer but not in gastric cancer." *Neoplasma* **52**(5): 420-424.
Otori, K., Konishi, M., Sugiyama, K., Hasebe, T., Shimoda, T., Kikuchi-Yanoshita, R., Mukai, K., Fukushima, S., Miyaki, M. and Esumi, H. (1998). "Infrequent somatic mutation of the adenomatous polyposis coli gene in aberrant crypt foci of human colon tissue." *Cancer* **83**(5): 896-900.
Overall, C. M. and Lopez-Otin, C. (2002). "Strategies for MMP inhibition in cancer: innovations for the post-trial era." *Nat Rev Cancer* **2**(9): 657-672.
Pages, F., Berger, A., Camus, M., Sanchez-Cabo, F., Costes, A., Molidor, R., Mlecnik, B., Kirilovsky, A., Nilsson, M., Damotte, D., Meatchi, T., Bruneval, P., Cugnenc, P. H., Trajanoski, Z., Fridman, W. H. and Galon, J. (2005). "Effector memory T cells, early metastasis, and survival in colorectal cancer." *N Engl J Med* **353**(25): 2654-2666.
Paiss, T., Wohr, G., Hautmann, R. E., Mattfeldt, T., Muller, M., Haeussler, J. and Vogel, W. (2002). "Some tumors of the bladder are polyclonal in origin." *J Urol* **167**(2 Pt 1): 718-723.
Pal, T., Permuth-Wey, J. and Sellers, T. A. (2008). "A review of the clinical relevance of mismatch-repair deficiency in ovarian cancer." *Cancer* **113**(4): 733-742.
Park, H. S., Goodlad, R. A. and Wright, N. A. (1995). "Crypt fission in the small intestine and colon. A mechanism for the emergence of G6PD locus-mutated crypts after treatment with mutagens." *Am J Pathol* **147**(5): 1416-1427.
Park, J.-I. and Kwak, J.-Y. (2012). "The Role of Peroxisome Proliferator-Activated Receptors in Colorectal Cancer." *PPAR Research* **2012**: 876418.
Parrinello, S., Coppe, J. P., Krtolica, A. and Campisi, J. (2005). "Stromal-epithelial interactions in aging and cancer: senescent fibroblasts alter epithelial cell differentiation." *J Cell Sci* **118**(Pt 3): 485-496.
Parsons, B. L. (2008). "Many different tumor types have polyclonal tumor origin: evidence and implications." *Mutat Res* **659**(3): 232-247.
Pei, H., Zhu, H., Zeng, S., Li, Y., Yang, H., Shen, L., Chen, J., Zeng, L., Fan, J., Li, X., Gong, Y. and Shen, H. (2007). "Proteome analysis and tissue microarray for profiling protein markers associated with lymph node metastasis in colorectal cancer." *J Proteome Res* **6**(7): 2495-2501.
Peifer, M. and Polakis, P. (2000). "Wnt signaling in oncogenesis and embryogenesis--a look outside the nucleus." *Science* **287**(5458): 1606-1609.

Pellegrinet, L., Rodilla, V., Liu, Z., Chen, S., Koch, U., Espinosa, L., Kaestner, K. H., Kopan, R., Lewis, J. and Radtke, F. (2011). "Dll1- and dll4-mediated notch signaling are required for homeostasis of intestinal stem cells." *Gastroenterology* **140**(4): 1230-1240.e1231-1237.
Pepino, M. Y., Kuda, O., Samovski, D. and Abumrad, N. A. (2014). "Structure-Function of CD36 and Importance of Fatty Acid Signal Transduction in Fat Metabolism." *Annual review of nutrition* **34**: 281-303.
Petz, M., Them, N., Huber, H., Beug, H. and Mikulits, W. (2012). "La enhances IRES-mediated translation of laminin B1 during malignant epithelial to mesenchymal transition." *Nucleic Acids Res* **40**(1): 290-302.
Pickup, M., Novitskiy, S. and Moses, H. L. (2013). "The roles of TGF[beta] in the tumour microenvironment." *Nat Rev Cancer* **13**(11): 788-799.
Pillaire, M. J., Selves, J., Gordien, K., Gourraud, P. A., Gentil, C., Danjoux, M., Do, C., Negre, V., Bieth, A., Guimbaud, R., Trouche, D., Pasero, P., Mechali, M., Hoffmann, J. S. and Cazaux, C. (2010). "A 'DNA replication' signature of progression and negative outcome in colorectal cancer." *Oncogene* **29**(6): 876-887.
Pino, M. S. and Chung, D. C. (2010). "THE CHROMOSOMAL INSTABILITY PATHWAY IN COLON CANCER." *Gastroenterology* **138**(6): 2059-2072.
Pino, M. S. and Chung, D. C. (2010). "The chromosomal instability pathway in colon cancer." *Gastroenterology* **138**(6): 2059-2072.
Pires, E., Sung, P. and Wiese, C. (2017). "Role of RAD51AP1 in homologous recombination DNA repair and carcinogenesis." *DNA Repair* **59**: 76-81.
Ponder, B. A., Schmidt, G. H., Wilkinson, M. M., Wood, M. J., Monk, M. and Reid, A. (1985). "Derivation of mouse intestinal crypts from single progenitor cells." *Nature* **313**(6004): 689-691.
Potten, C. S. (1998). "Stem cells in gastrointestinal epithelium: numbers, characteristics and death." *Philos Trans R Soc Lond B Biol Sci* **353**(1370): 821-830.
Powell, D. W., Pinchuk, I. V., Saada, J. I., Chen, X. and Mifflin, R. C. (2011). "Mesenchymal cells of the intestinal lamina propria." *Annu Rev Physiol* **73**: 213-237.
Powell, S. M., Zilz, N., Beazer-Barclay, Y., Bryan, T. M., Hamilton, S. R., Thibodeau, S. N., Vogelstein, B. and Kinzler, K. W. (1992). "APC mutations occur early during colorectal tumorigenesis." *Nature* **359**(6392): 235-237.
Prall, F., Duhrkop, T., Weirich, V., Ostwald, C., Lenz, P., Nizze, H. and Barten, M. (2004). "Prognostic role of CD8+ tumor-infiltrating lymphocytes in stage III colorectal cancer with and without microsatellite instability." *Hum Pathol* **35**(7): 808-816.
Prasetyanti, P. R., Zimberlin, C. D., Bots, M., Vermeulen, L., Melo Fde, S. and Medema, J. P. (2013). "Regulation of stem cell self-renewal and differentiation by Wnt and Notch are conserved throughout the adenoma-carcinoma sequence in the colon." *Mol Cancer* **12**(1): 126.
Preston, S. L., Wong, W. M., Chan, A. O., Poulsom, R., Jeffery, R., Goodlad, R. A., Mandir, N., Elia, G., Novelli, M., Bodmer, W. F., Tomlinson, I. P. and Wright, N. A. (2003). "Bottom-up histogenesis of colorectal adenomas: origin in the monocryptal adenoma and initial expansion by crypt fission." *Cancer Res* **63**.
Preston, S. L., Wong, W. M., Chan, A. O., Poulsom, R., Jeffery, R., Goodlad, R. A., Mandir, N., Elia, G., Novelli, M., Bodmer, W. F., Tomlinson, I. P. and Wright, N. A. (2003). "Bottom-up histogenesis of colorectal adenomas: origin in the monocryptal adenoma and initial expansion by crypt fission." *Cancer Res* **63**(13): 3819-3825.
Prizment, A. E., Vierkant, R. A., Smyrk, T. C., Tillmans, L. S., Nelson, H. H., Lynch, C. F., Pengo, T., Thibodeau, S. N., Church, T. R., Cerhan, J. R., Anderson, K.

E. and Limburg, P. J. (2017). "Cytotoxic T Cells and Granzyme B Associated with Improved Colorectal Cancer Survival in a Prospective Cohort of Older Women." *Cancer Epidemiol Biomarkers Prev* **26**(4): 622-631.
Proietti, S., Cucina, A., Minini, M. and Bizzarri, M. (2017). "Melatonin, mitochondria, and the cancer cell." *Cell Mol Life Sci*.
Puccini, A., Berger, M. D., Naseem, M., Tokunaga, R., Battaglin, F., Cao, S., Hanna, D. L., McSkane, M., Soni, S., Zhang, W. and Lenz, H. J. (2017). "Colorectal cancer: epigenetic alterations and their clinical implications." *Biochim Biophys Acta* **1868**(2): 439-448.
Quigley, D. A. and Kristensen, V. (2015). "Predicting prognosis and therapeutic response from interactions between lymphocytes and tumor cells." *Mol Oncol* **9**(10): 2054-2062.
Rasanen, K. and Vaheri, A. (2010). "Activation of fibroblasts in cancer stroma." *Exp Cell Res* **316**(17): 2713-2722.
Reissfelder, C., Stamova, S., Gossmann, C., Braun, M., Bonertz, A., Walliczek, U., Grimm, M., Rahbari, N. N., Koch, M., Saadati, M., Benner, A., Büchler, M. W., Jäger, D., Halama, N., Khazaie, K., Weitz, J. and Beckhove, P. (2015). "Tumor-specific cytotoxic T lymphocyte activity determines colorectal cancer patient prognosis." *The Journal of Clinical Investigation* **125**(2): 739-751.
Renuka, Agnihotri, N. and Bhatnagar, A. (2017). "Differential ratios of fish/corn oil ameliorated the colon carcinoma in rat by altering intestinal intraepithelial CD8(+) T lymphocytes, dendritic cells population and modulating the intracellular cytokines." *Biomed Pharmacother* **98**: 600-608.
Reya, T. and Clevers, H. (2005). "Wnt signalling in stem cells and cancer." *Nature* **434**(7035): 843-850.
Richter, C., Park, J. W. and Ames, B. N. (1988). "Normal oxidative damage to mitochondrial and nuclear DNA is extensive." *Proc Natl Acad Sci U S A* **85**(17): 6465-6467.
Ritsma, L., Ellenbroek, S. I. J., Zomer, A., Snippert, H. J., de Sauvage, F. J., Simons, B. D., Clevers, H. and van Rheenen, J. (2014). "Intestinal crypt homeostasis revealed at single-stem-cell level by in vivo live imaging." *Nature* **507**(7492): 362-365.
Ro, S. and Rannala, B. (2001). "Methylation patterns and mathematical models reveal dynamics of stem cell turnover in the human colon." *Proc Natl Acad Sci U S A* **98**(19): 10519-10521.
Ro, S. and Rannala, B. (2001). "Methylation patterns and mathematical models reveal dynamics of stem cell turnover in the human colon." *Proceedings of the National Academy of Sciences of the United States of America* **98**(19): 10519-10521.
Roose, J., Molenaar, M., Peterson, J., Hurenkamp, J., Brantjes, H., Moerer, P., van de Wetering, M., Destree, O. and Clevers, H. (1998). "The Xenopus Wnt effector XTcf-3 interacts with Groucho-related transcriptional repressors." *Nature* **395**(6702): 608-612.
Roseweir, A. K., McMillan, D. C., Horgan, P. G. and Edwards, J. (2017). "Colorectal cancer subtypes: Translation to routine clinical pathology." *Cancer Treat Rev* **57**: 1-7.
Rothenberg, M. E., Nusse, Y., Kalisky, T., Lee, J. J., Dalerba, P., Scheeren, F., Lobo, N., Kulkarni, S., Sim, S., Qian, D., Beachy, P. A., Pasricha, P. J., Quake, S. R. and Clarke, M. F. (2012). "Identification of a cKit(+) colonic crypt base secretory cell that supports Lgr5(+) stem cells in mice." *Gastroenterology* **142**(5): 1195-1205.e1196.

Rubin, H. (2011). "Fields and field cancerization: the preneoplastic origins of cancer: asymptomatic hyperplastic fields are precursors of neoplasia, and their progression to tumors can be tracked by saturation density in culture." *Bioessays* **33**(3): 224-231.
Rudling, R., Hassan, A. B., Kitau, J., Mandir, N. and Goodlad, R. A. (2006). "A simple device to rapidly prepare whole mounts of murine intestine." *Cell Prolif* **39**(5): 415-420.
Rupp, C., Scherzer, M., Rudisch, A., Unger, C., Haslinger, C., Schweifer, N., Artaker, M., Nivarthi, H., Moriggl, R., Hengstschlager, M., Kerjaschki, D., Sommergruber, W., Dolznig, H. and Garin-Chesa, P. (2015). "IGFBP7, a novel tumor stroma marker, with growth-promoting effects in colon cancer through a paracrine tumor-stroma interaction." *Oncogene* **34**(7): 815-825.
Ryser, M. D., Min, B. H., Siegmund, K. D. and Shibata, D. (2018). "Spatial mutation patterns as markers of early colorectal tumor cell mobility." *Proc Natl Acad Sci U S A* **115**(22): 5774-5779.
Saleh, H. A., Jackson, H. and Banerjee, M. (2000). "Immunohistochemical expression of bcl-2 and p53 oncoproteins: correlation with Ki67 proliferation index and prognostic histopathologic parameters in colorectal neoplasia." *Appl Immunohistochem Mol Morphol* **8**(3): 175-182.
Salk, J. J., Salipante, S. J., Risques, R. A., Crispin, D. A., Li, L., Bronner, M. P., Brentnall, T. A., Rabinovitch, P. S., Horwitz, M. S. and Loeb, L. A. (2009). "Clonal expansions in ulcerative colitis identify patients with neoplasia." *Proc Natl Acad Sci U S A* **106**(49): 20871-20876.
Samudio, I., Harmancey, R., Fiegl, M., Kantarjian, H., Konopleva, M., Korchin, B., Kaluarachchi, K., Bornmann, W., Duvvuri, S., Taegtmeyer, H. and Andreeff, M. (2010). "Pharmacologic inhibition of fatty acid oxidation sensitizes human leukemia cells to apoptosis induction." *J Clin Invest* **120**(1): 142-156.
San Roman, A. K., Jayewickreme, C. D., Murtaugh, L. C. and Shivdasani, R. A. (2014). "Wnt secretion from epithelial cells and subepithelial myofibroblasts is not required in the mouse intestinal stem cell niche in vivo." *Stem Cell Reports* **2**(2): 127-134.
Sancho, E., Batlle, E. and Clevers, H. (2004). "Signaling pathways in intestinal development and cancer." *Annu Rev Cell Dev Biol* **20**: 695-723.
Sangiorgi, E. and Capecchi, M. R. (2008). "Bmi1 is expressed in vivo in intestinal stem cells." *Nat Genet* **40**(7): 915-920.
Sansom, O. J., Reed, K. R., Hayes, A. J., Ireland, H., Brinkmann, H., Newton, I. P., Batlle, E., Simon-Assmann, P., Clevers, H., Nathke, I. S., Clarke, A. R. and Winton, D. J. (2004). "Loss of Apc in vivo immediately perturbs Wnt signaling, differentiation, and migration." *Genes Dev* **18**(12): 1385-1390.
Sasaki, N., Sachs, N., Wiebrands, K., Ellenbroek, S. I., Fumagalli, A., Lyubimova, A., Begthel, H., van den Born, M., van Es, J. H., Karthaus, W. R., Li, V. S., Lopez-Iglesias, C., Peters, P. J., van Rheenen, J., van Oudenaarden, A. and Clevers, H. (2016). "Reg4+ deep crypt secretory cells function as epithelial niche for Lgr5+ stem cells in colon." *Proc Natl Acad Sci U S A* **113**(37): E5399-5407.
Sato, T. and Clevers, H. (2013). "Growing self-organizing mini-guts from a single intestinal stem cell: mechanism and applications." *Science* **340**(6137): 1190-1194.
Sato, T., Stange, D. E., Ferrante, M., Vries, R. G., Van Es, J. H., Van den Brink, S., Van Houdt, W. J., Pronk, A., Van Gorp, J., Siersema, P. D. and Clevers, H. (2011). "Long-term expansion of epithelial organoids from human colon, adenoma, adenocarcinoma, and Barrett's epithelium." *Gastroenterology* **141**(5): 1762-1772.

Sato, T., van Es, J. H., Snippert, H. J., Stange, D. E., Vries, R. G., van den Born, M., Barker, N., Shroyer, N. F., van de Wetering, M. and Clevers, H. (2011). "Paneth cells constitute the niche for Lgr5 stem cells in intestinal crypts." *Nature* **469**(7330): 415-418.
Sato, T., Vries, R. G., Snippert, H. J., van de Wetering, M., Barker, N., Stange, D. E., van Es, J. H., Abo, A., Kujala, P., Peters, P. J. and Clevers, H. (2009). "Single Lgr5 stem cells build crypt-villus structures in vitro without a mesenchymal niche." *Nature* **459**(7244): 262-265.
Satoh, K., Yachida, S., Sugimoto, M., Oshima, M., Nakagawa, T., Akamoto, S., Tabata, S., Saitoh, K., Kato, K., Sato, S., Igarashi, K., Aizawa, Y., Kajino-Sakamoto, R., Kojima, Y., Fujishita, T., Enomoto, A., Hirayama, A., Ishikawa, T., Taketo, M. M., Kushida, Y., Haba, R., Okano, K., Tomita, M., Suzuki, Y., Fukuda, S., Aoki, M. and Soga, T. (2017). "Global metabolic reprogramming of colorectal cancer occurs at adenoma stage and is induced by MYC." *Proceedings of the National Academy of Sciences of the United States of America* **114**(37): E7697-E7706.
Saurer, L. and Mueller, C. (2009). "T cell-mediated immunoregulation in the gastrointestinal tract." *Allergy* **64**(4): 505-519.
Scadden, D. T. (2006). "The stem-cell niche as an entity of action." *Nature* **441**(7097): 1075-1079.
Schepers, A. G., Snippert, H. J., Stange, D. E., van den Born, M., van Es, J. H., van de Wetering, M. and Clevers, H. (2012). "Lineage tracing reveals Lgr5+ stem cell activity in mouse intestinal adenomas." *Science* **337**(6095): 730-735.
Scherz-Shouval, R., Santagata, S., Mendillo, M. L., Sholl, L. M., Ben-Aharon, I., Beck, A. H., Dias-Santagata, D., Koeva, M., Stemmer, S. M., Whitesell, L. and Lindquist, S. (2014). "The reprogramming of tumor stroma by HSF1 is a potent enabler of malignancy." *Cell* **158**(3): 564-578.
Schmittgen, T. D. and Livak, K. J. (2008). "Analyzing real-time PCR data by the comparative CT method." *Nat. Protocols* **3**(6): 1101-1108.
Schneikert, J., Vijaya Chandra, S. H., Ruppert, J. G., Ray, S., Wenzel, E. M. and Behrens, J. (2013). "Functional comparison of human adenomatous polyposis coli (APC) and APC-like in targeting beta-catenin for degradation." *PLoS One* **8**(7): e68072.
Schuijers, J., Junker, J. P., Mokry, M., Hatzis, P., Koo, B. K., Sasselli, V., van der Flier, L. G., Cuppen, E., van Oudenaarden, A. and Clevers, H. (2015). "Ascl2 acts as an R-spondin/Wnt-responsive switch to control stemness in intestinal crypts." *Cell Stem Cell* **16**(2): 158-170.
Schwartz, S., Jr., Yamamoto, H., Navarro, M., Maestro, M., Reventos, J. and Perucho, M. (1999). "Frameshift mutations at mononucleotide repeats in caspase-5 and other target genes in endometrial and gastrointestinal cancer of the microsatellite mutator phenotype." *Cancer Res* **59**(12): 2995-3002.
Schwitalla, S., Fingerle, A. A., Cammareri, P., Nebelsiek, T., Goktuna, S. I., Ziegler, P. K., Canli, O., Heijmans, J., Huels, D. J., Moreaux, G., Rupec, R. A., Gerhard, M., Schmid, R., Barker, N., Clevers, H., Lang, R., Neumann, J., Kirchner, T., Taketo, M. M., van den Brink, G. R., Sansom, O. J., Arkan, M. C. and Greten, F. R. (2013). "Intestinal tumorigenesis initiated by dedifferentiation and acquisition of stem-cell-like properties." *Cell* **152**(1-2): 25-38.
Schwitalle, Y., Kloor, M., Eiermann, S., Linnebacher, M., Kienle, P., Knaebel, H. P., Tariverdian, M., Benner, A. and von Knebel Doeberitz, M. (2008). "Immune response against frameshift-induced neopeptides in HNPCC patients and healthy HNPCC mutation carriers." *Gastroenterology* **134**(4): 988-997.

Sedelnikova, O. A. and Bonner, W. M. (2006). "GammaH2AX in cancer cells: a potential biomarker for cancer diagnostics, prediction and recurrence." *Cell Cycle* **5**(24): 2909-2913.
Selim, K. A., Abdelrasoul, H., Aboelmagd, M. and Tawila, A. M. (2017). "The Role of the MAPK Signaling, Topoisomerase and Dietary Bioactives in Controlling Cancer Incidence." *Diseases* **5**(2).
Seshagiri, S., Stawiski, E. W., Durinck, S., Modrusan, Z., Storm, E. E., Conboy, C. B., Chaudhuri, S., Guan, Y., Janakiraman, V., Jaiswal, B. S., Guillory, J., Ha, C., Dijkgraaf, G. J., Stinson, J., Gnad, F., Huntley, M. A., Degenhardt, J. D., Haverty, P. M., Bourgon, R., Wang, W., Koeppen, H., Gentleman, R., Starr, T. K., Zhang, Z., Largaespada, D. A., Wu, T. D. and de Sauvage, F. J. (2012). "Recurrent R-spondin fusions in colon cancer." *Nature* **488**(7413): 660-664.
Shahriyari, L. and Mahdipour-Shirayeh, A. (2017). "Modeling dynamics of mutants in heterogeneous stem cell niche." *Physical Biology* **14**(1): 016004.
Shaul, Y. D. and Seger, R. (2007). "The MEK/ERK cascade: From signaling specificity to diverse functions." *Biochimica et Biophysica Acta (BBA) - Molecular Cell Research* **1773**(8): 1213-1226.
Sheridan, B. S. and Lefrançois, L. (2010). "Intraepithelial Lymphocytes: To Serve and Protect." *Current gastroenterology reports* **12**(6): 513-521.
Shih, I. M., Wang, T. L., Traverso, G., Romans, K., Hamilton, S. R., Ben-Sasson, S., Kinzler, K. W. and Vogelstein, B. (2001). "Top-down morphogenesis of colorectal tumors." *Proc Natl Acad Sci U S A* **98**(5): 2640-2645.
Shih, I. M., Zhou, W., Goodman, S. N., Lengauer, C., Kinzler, K. W. and Vogelstein, B. (2001). "Evidence that genetic instability occurs at an early stage of colorectal tumorigenesis." *Cancer Res* **61**(3): 818-822.
Shimokawa, M., Ohta, Y., Nishikori, S., Matano, M., Takano, A., Fujii, M., Date, S., Sugimoto, S., Kanai, T. and Sato, T. (2017). "Visualization and targeting of LGR5+ human colon cancer stem cells." *Nature* **545**(7653): 187-192.
Shin, H. W., Choi, H., So, D., Kim, Y. I., Cho, K., Chung, H. J., Lee, K. H., Chun, Y. S., Cho, C. H., Kang, G. H., Kim, W. H. and Park, J. W. (2014). "ITF2 prevents activation of the beta-catenin-TCF4 complex in colon cancer cells and levels decrease with tumor progression." *Gastroenterology* **147**(2): 430-442.e438.
Si, Y., Liu, P., Li, P. and Brutnell, T. P. (2014). "Model-based clustering for RNA-seq data." *Bioinformatics* **30**(2): 197-205.
Siegel, R., Desantis, C. and Jemal, A. (2014). "Colorectal cancer statistics, 2014." *CA Cancer J Clin* **64**(2): 104-117.
Simons, B. D. and Clevers, H. (2011). "Strategies for homeostatic stem cell self-renewal in adult tissues." *Cell* **145**(6): 851-862.
Simons, C. C., Hughes, L. A., Smits, K. M., Khalid-de Bakker, C. A., de Bruine, A. P., Carvalho, B., Meijer, G. A., Schouten, L. J., van den Brandt, P. A., Weijenberg, M. P. and van Engeland, M. (2013). "A novel classification of colorectal tumors based on microsatellite instability, the CpG island methylator phenotype and chromosomal instability: implications for prognosis." *Ann Oncol* **24**(8): 2048-2056.
Sinicrope, F. A., Rego, R. L., Foster, N. R., Thibodeau, S. N., Alberts, S. R., Windschitl, H. E. and Sargent, D. J. (2008). "Proapoptotic Bad and Bid Protein Expression Predict Survival in Stages II and III Colon Cancers." *Clinical cancer research : an official journal of the American Association for Cancer Research* **14**(13): 4128-4133.

Slaughter, D. P., Southwick, H. W. and Smejkal, W. (1953). "Field cancerization in oral stratified squamous epithelium; clinical implications of multicentric origin." *Cancer* **6**(5): 963-968.
Smith, Q., Stukalin, E., Kusuma, S., Gerecht, S. and Sun, S. X. (2015). "Stochasticity and Spatial Interaction Govern Stem Cell Differentiation Dynamics." *Sci Rep* **5**: 12617.
Smith, R. J., Rao-Bhatia, A. and Kim, T. H. (2017). "Signaling and epigenetic mechanisms of intestinal stem cells and progenitors: insight into crypt homeostasis, plasticity, and niches." *Wiley Interdiscip Rev Dev Biol* **6**(5).
Snippert, H. J., Schepers, A. G., van Es, J. H., Simons, B. D. and Clevers, H. (2014). "Biased competition between Lgr5 intestinal stem cells driven by oncogenic mutation induces clonal expansion." *EMBO Rep* **15**(1): 62-69.
Snippert, H. J., van der Flier, L. G., Sato, T., van Es, J. H., van den Born, M., Kroon-Veenboer, C., Barker, N., Klein, A. M., van Rheenen, J., Simons, B. D. and Clevers, H. (2010). "Intestinal crypt homeostasis results from neutral competition between symmetrically dividing Lgr5 stem cells." *Cell* **143**(1): 134-144.
Sobecki, M., Mrouj, K., Colinge, J., Gerbe, F., Jay, P., Krasinska, L., Dulic, V. and Fisher, D. (2017). "Cell-Cycle Regulation Accounts for Variability in Ki-67 Expression Levels." *Cancer Res* **77**(10): 2722-2734.
Sottoriva, A., Kang, H., Ma, Z., Graham, T. A., Salomon, M. P., Zhao, J., Marjoram, P., Siegmund, K., Press, M. F., Shibata, D. and Curtis, C. (2015). "A Big Bang model of human colorectal tumor growth." *Nature genetics* **47**(3): 209-216.
Souza, R. F., Appel, R., Yin, J., Wang, S., Smolinski, K. N., Abraham, J. M., Zou, T. T., Shi, Y. Q., Lei, J., Cottrell, J., Cymes, K., Biden, K., Simms, L., Leggett, B., Lynch, P. M., Frazier, M., Powell, S. M., Harpaz, N., Sugimura, H., Young, J. and Meltzer, S. J. (1996). "Microsatellite instability in the insulin-like growth factor II receptor gene in gastrointestinal tumours." *Nat Genet* **14**(3): 255-257.
Souza-Mello, V. (2015). "Peroxisome proliferator-activated receptors as targets to treat non-alcoholic fatty liver disease." *World Journal of Hepatology* **7**(8): 1012-1019.
Srinivasan, T., Walters, J., Bu, P., Than, E. B., Tung, K. L., Chen, K. Y., Panarelli, N., Milsom, J., Augenlicht, L., Lipkin, S. M. and Shen, X. (2016). "NOTCH Signaling Regulates Asymmetric Cell Fate of Fast- and Slow-Cycling Colon Cancer-Initiating Cells." *Cancer Res* **76**(11): 3411-3421.
Stamataki, D., Holder, M., Hodgetts, C., Jeffery, R., Nye, E., Spencer-Dene, B., Winton, D. J. and Lewis, J. (2011). "Delta1 expression, cell cycle exit, and commitment to a specific secretory fate coincide within a few hours in the mouse intestinal stem cell system." *PLoS One* **6**(9): e24484.
Stamenkovic, I. (2003). "Extracellular matrix remodelling: the role of matrix metalloproteinases." *J Pathol* **200**(4): 448-464.
Stamp, C., Zupanic, A., Sachdeva, A., Stoll, E. A., Shanley, D. P., Mathers, J. C., Kirkwood, T. B. L., Heer, R., Simons, B. D., Turnbull, D. M. and Greaves, L. C. (2018). "Predominant Asymmetrical Stem Cell Fate Outcome Limits the Rate of Niche Succession in Human Colonic Crypts." *EBioMedicine* **31**: 166-173.
Stankevicius, V., Vasauskas, G., Noreikiene, R., Kuodyte, K., Valius, M. and Suziedelis, K. (2016). "Extracellular Matrix-dependent Pathways in Colorectal Cancer Cell Lines Reveal Potential Targets for Anticancer Therapies." *Anticancer Res* **36**(9): 4559-4567.

Starzynska, T., Bromley, M., Ghosh, A. and Stern, P. L. (1992). "Prognostic significance of p53 overexpression in gastric and colorectal carcinoma." *Br J Cancer* **66**(3): 558-562.
Stephens, P. J., Greenman, C. D., Fu, B., Yang, F., Bignell, G. R., Mudie, L. J., Pleasance, E. D., Lau, K. W., Beare, D., Stebbings, L. A., McLaren, S., Lin, M. L., McBride, D. J., Varela, I., Nik-Zainal, S., Leroy, C., Jia, M., Menzies, A., Butler, A. P., Teague, J. W., Quail, M. A., Burton, J., Swerdlow, H., Carter, N. P., Morsberger, L. A., Iacobuzio-Donahue, C., Follows, G. A., Green, A. R., Flanagan, A. M., Stratton, M. R., Futreal, P. A. and Campbell, P. J. (2011). "Massive genomic rearrangement acquired in a single catastrophic event during cancer development." *Cell* **144**(1): 27-40.
Stewart, J. B. and Chinnery, P. F. (2015). "The dynamics of mitochondrial DNA heteroplasmy: implications for human health and disease." *Nat Rev Genet* **16**(9): 530-542.
Stratton, M. R. (2011). "Exploring the genomes of cancer cells: progress and promise." *Science* **331**(6024): 1553-1558.
Subramanian, A., Tamayo, P., Mootha, V. K., Mukherjee, S., Ebert, B. L., Gillette, M. A., Paulovich, A., Pomeroy, S. L., Golub, T. R., Lander, E. S. and Mesirov, J. P. (2005). "Gene set enrichment analysis: A knowledge-based approach for interpreting genome-wide expression profiles." *Proceedings of the National Academy of Sciences* **102**(43): 15545-15550.
Subramanian, S., Madgula, V. M., George, R., Mishra, R. K., Pandit, M. W., Kumar, C. S. and Singh, L. (2003). "Triplet repeats in human genome: distribution and their association with genes and other genomic regions." *Bioinformatics* **19**(5): 549-552.
Sun, R., Hu, Z., Sottoriva, A., Graham, T. A., Harpak, A., Ma, Z., Fischer, J. M., Shibata, D. and Curtis, C. (2017). "Between-region genetic divergence reflects the mode and tempo of tumor evolution." *Nat Genet* **49**(7): 1015-1024.
Sun, X., Liu, S., Wang, D., Zhang, Y., Li, W., Guo, Y., Zhang, H. and Suo, J. (2017). "Colorectal cancer cells suppress CD4+ T cells immunity through canonical Wnt signaling." *Oncotarget* **8**(9): 15168-15181.
Tahara, T., Yamamoto, E., Madireddi, P., Suzuki, H., Maruyama, R., Chung, W., Garriga, J., Jelinek, J., Yamano, H. O., Sugai, T., Kondo, Y., Toyota, M., Issa, J. P. and Estecio, M. R. (2014). "Colorectal carcinomas with CpG island methylator phenotype 1 frequently contain mutations in chromatin regulators." *Gastroenterology* **146**(2): 530-538.e535.
Tajima, M., Wakita, D., Noguchi, D., Chamoto, K., Yue, Z., Fugo, K., Ishigame, H., Iwakura, Y., Kitamura, H. and Nishimura, T. (2008). "IL-6-dependent spontaneous proliferation is required for the induction of colitogenic IL-17-producing CD8+ T cells." *J Exp Med* **205**(5): 1019-1027.
Takane, K., Matsusaka, K., Ota, S., Fukuyo, M., Yue, Y., Nishimura, M., Sakai, E., Matsushita, K., Miyauchi, H., Aburatani, H., Nakatani, Y., Takayama, T., Matsubara, H., Akagi, K. and Kaneda, A. (2016). "Two subtypes of colorectal tumor with distinct molecular features in familial adenomatous polyposis." *Oncotarget* **7**(51): 84003-84016.
Takashima, S., Kadowaki, M., Aoyama, K., Koyama, M., Oshima, T., Tomizuka, K., Akashi, K. and Teshima, T. (2011). "The Wnt agonist R-spondin1 regulates systemic graft-versus-host disease by protecting intestinal stem cells." *J Exp Med* **208**(2): 285-294.
Takayama, T., Ohi, M., Hayashi, T., Miyanishi, K., Nobuoka, A., Nakajima, T., Satoh, T., Takimoto, R., Kato, J., Sakamaki, S. and Niitsu, Y. (2001). "Analysis of

K-ras, APC, and beta-catenin in aberrant crypt foci in sporadic adenoma, cancer, and familial adenomatous polyposis." *Gastroenterology* **121**(3): 599-611.
Takeda, N., Jain, R., LeBoeuf, M. R., Wang, Q., Lu, M. M. and Epstein, J. A. (2011). "Interconversion between intestinal stem cell populations in distinct niches." *Science* **334**(6061): 1420-1424.
Tan, S. H. and Barker, N. (2018). "Wnt Signaling in Adult Epithelial Stem Cells and Cancer." *Prog Mol Biol Transl Sci* **153**: 21-79.
Tanaka, K., Sano, K., Nakano, T., Yuba, K. and Kinoshita, M. (2007). "Suppression of alpha smooth muscle actin expression by IFN-gamma in established myofibroblast cell lines." *J Interferon Cytokine Res* **27**(10): 835-839.
Taylor, R. W., Barron, M. J., Borthwick, G. M., Gospel, A., Chinnery, P. F., Samuels, D. C., Taylor, G. A., Plusa, S. M., Needham, S. J., Greaves, L. C., Kirkwood, T. B. and Turnbull, D. M. (2003). "Mitochondrial DNA mutations in human colonic crypt stem cells." *J Clin Invest* **112**(9): 1351-1360.
Taylor, R. W., Taylor, G. A., Durham, S. E. and Turnbull, D. M. (2001). "The determination of complete human mitochondrial DNA sequences in single cells: implications for the study of somatic mitochondrial DNA point mutations." *Nucleic Acids Res* **29**(15): E74-74.
Taylor, R. W. and Turnbull, D. M. (2005). "Mitochondrial DNA mutations in human disease." *Nat Rev Genet* **6**(5): 389-402.
Teller, I. C. and Beaulieu, J. F. (2001). "Interactions between laminin and epithelial cells in intestinal health and disease." *Expert Rev Mol Med* **3**(24): 1-18.
Tetteh, P. W., Basak, O., Farin, H. F., Wiebrands, K., Kretzschmar, K., Begthel, H., van den Born, M., Korving, J., de Sauvage, F., van Es, J. H., van Oudenaarden, A. and Clevers, H. (2016). "Replacement of Lost Lgr5-Positive Stem Cells through Plasticity of Their Enterocyte-Lineage Daughters." *Cell Stem Cell* **18**(2): 203-213.
Thirlwell, C., Will, O. C., Domingo, E., Graham, T. A., McDonald, S. A., Oukrif, D., Jeffrey, R., Gorman, M., Rodriguez-Justo, M., Chin-Aleong, J., Clark, S. K., Novelli, M. R., Jankowski, J. A., Wright, N. A., Tomlinson, I. P. and Leedham, S. J. (2010). "Clonality assessment and clonal ordering of individual neoplastic crypts shows polyclonality of colorectal adenomas." *Gastroenterology* **138**(4): 1441-1454, 1454 e1441-1447.
Thliveris, A. T., Halberg, R. B., Clipson, L., Dove, W. F., Sullivan, R., Washington, M. K., Stanhope, S. and Newton, M. A. (2005). "Polyclonality of familial murine adenomas: analyses of mouse chimeras with low tumor multiplicity suggest short-range interactions." *Proc Natl Acad Sci U S A* **102**(19): 6960-6965.
Thliveris, A. T., Schwefel, B., Clipson, L., Plesh, L., Zahm, C. D., Leystra, A. A., Washington, M. K., Sullivan, R., Deming, D. A., Newton, M. A. and Halberg, R. B. (2013). "Transformation of epithelial cells through recruitment leads to polyclonal intestinal tumors." *Proceedings of the National Academy of Sciences* **110**(28): 11523-11528.
Thomas, G. (2000). "An encore for ribosome biogenesis in the control of cell proliferation." *Nat Cell Biol* **2**(5): E71-72.
Tian, H., Biehs, B., Warming, S., Leong, K. G., Rangell, L., Klein, O. D. and de Sauvage, F. J. (2011). "A reserve stem cell population in small intestine renders Lgr5-positive cells dispensable." *Nature* **478**(7368): 255-259.
Tlsty, T. D. (2001). "Stromal cells can contribute oncogenic signals." *Semin Cancer Biol* **11**(2): 97-104.

Tomasetti, C., Marchionni, L., Nowak, M. A., Parmigiani, G. and Vogelstein, B. (2015). "Only three driver gene mutations are required for the development of lung and colorectal cancers." *Proc Natl Acad Sci U S A* **112**(1): 118-123.
Torres, S., Bartolome, R. A., Mendes, M., Barderas, R., Fernandez-Acenero, M. J., Pelaez-Garcia, A., Pena, C., Lopez-Lucendo, M., Villar-Vazquez, R., de Herreros, A. G., Bonilla, F. and Casal, J. I. (2013). "Proteome profiling of cancer-associated fibroblasts identifies novel proinflammatory signatures and prognostic markers for colorectal cancer." *Clin Cancer Res* **19**(21): 6006-6019.
Totafurno, J., Bjerknes, M. and Cheng, H. (1987). "The crypt cycle. Crypt and villus production in the adult intestinal epithelium." *Biophys J* **52**(2): 279-294.
Tóth, B., Ben‐Moshe, S., Gavish, A., Barkai, N. and Itzkovitz, S. (2017). "Early commitment and robust differentiation in colonic crypts." *Molecular Systems Biology* **13**(1): 902.
Traverso, N., Ricciarelli, R., Nitti, M., Marengo, B., Furfaro, A. L., Pronzato, M. A., Marinari, U. M. and Domenicotti, C. (2013). "Role of Glutathione in Cancer Progression and Chemoresistance." *Oxidative Medicine and Cellular Longevity* **2013**: 10.
Tripathi, D. N. and Walker, C. L. (2016). "The peroxisome as a cell signaling organelle." *Curr Opin Cell Biol* **39**: 109-112.
Truninger, K., Menigatti, M., Luz, J., Russell, A., Haider, R., Gebbers, J. O., Bannwart, F., Yurtsever, H., Neuweiler, J., Riehle, H. M., Cattaruzza, M. S., Heinimann, K., Schar, P., Jiricny, J. and Marra, G. (2005). "Immunohistochemical analysis reveals high frequency of PMS2 defects in colorectal cancer." *Gastroenterology* **128**(5): 1160-1171.
Tsujino, T., Seshimo, I., Yamamoto, H., Ngan, C. Y., Ezumi, K., Takemasa, I., Ikeda, M., Sekimoto, M., Matsuura, N. and Monden, M. (2007). "Stromal myofibroblasts predict disease recurrence for colorectal cancer." *Clin Cancer Res* **13**(7): 2082-2090.
Umar, A., Boland, C. R., Terdiman, J. P., Syngal, S., de la Chapelle, A., Ruschoff, J., Fishel, R., Lindor, N. M., Burgart, L. J., Hamelin, R., Hamilton, S. R., Hiatt, R. A., Jass, J., Lindblom, A., Lynch, H. T., Peltomaki, P., Ramsey, S. D., Rodriguez-Bigas, M. A., Vasen, H. F., Hawk, E. T., Barrett, J. C., Freedman, A. N. and Srivastava, S. (2004). "Revised Bethesda Guidelines for hereditary nonpolyposis colorectal cancer (Lynch syndrome) and microsatellite instability." *J Natl Cancer Inst* **96**(4): 261-268.
Valencia, T., Kim, J. Y., Abu-Baker, S., Moscat-Pardos, J., Ahn, C. S., Reina-Campos, M., Duran, A., Castilla, E. A., Metallo, C. M., Diaz-Meco, M. T. and Moscat, J. (2014). "Metabolic reprogramming of stromal fibroblasts through p62-mTORC1 signaling promotes inflammation and tumorigenesis." *Cancer Cell* **26**(1): 121-135.
Valenta, T., Degirmenci, B., Moor, A. E., Herr, P., Zimmerli, D., Moor, M. B., Hausmann, G., Cantu, C., Aguet, M. and Basler, K. (2016). "Wnt Ligands Secreted by Subepithelial Mesenchymal Cells Are Essential for the Survival of Intestinal Stem Cells and Gut Homeostasis." *Cell Rep* **15**(5): 911-918.
Valkenburg, K. C., de Groot, A. E. and Pienta, K. J. (2018). "Targeting the tumour stroma to improve cancer therapy." *Nat Rev Clin Oncol* **15**(6): 366-381.
Van Acker, A., Louagie, E., Filtjens, J., Taveirne, S., Van Ammel, E., Kerre, T., Elewaut, D., Taghon, T., Vandekerckhove, B., Plum, J. and Leclercq, G. (2016). "The role of Ly49E receptor expression on murine intraepithelial lymphocytes in intestinal cancer development and progression." *Cancer Immunol Immunother* **65**(11): 1365-1375.

van de Wetering, M., Francies, H. E., Francis, J. M., Bounova, G., Iorio, F., Pronk, A., van Houdt, W., van Gorp, J., Taylor-Weiner, A., Kester, L., McLaren-Douglas, A., Blokker, J., Jaksani, S., Bartfeld, S., Volckman, R., van Sluis, P., Li, V. S., Seepo, S., Sekhar Pedamallu, C., Cibulskis, K., Carter, S. L., McKenna, A., Lawrence, M. S., Lichtenstein, L., Stewart, C., Koster, J., Versteeg, R., van Oudenaarden, A., Saez-Rodriguez, J., Vries, R. G., Getz, G., Wessels, L., Stratton, M. R., McDermott, U., Meyerson, M., Garnett, M. J. and Clevers, H. (2015). "Prospective derivation of a living organoid biobank of colorectal cancer patients." *Cell* **161**(4): 933-945.

van de Wetering, M., Oosterwegel, M., Dooijes, D. and Clevers, H. (1991). "Identification and cloning of TCF-1, a T lymphocyte-specific transcription factor containing a sequence-specific HMG box." *Embo j* **10**(1): 123-132.

van den Heuvel, M., Harryman-Samos, C., Klingensmith, J., Perrimon, N. and Nusse, R. (1993). "Mutations in the segment polarity genes wingless and porcupine impair secretion of the wingless protein." *Embo j* **12**(13): 5293-5302.

van der Flier, L. G. and Clevers, H. (2009). "Stem cells, self-renewal, and differentiation in the intestinal epithelium." *Annu Rev Physiol* **71**: 241-260.

Van der Flier, L. G., Sabates-Bellver, J., Oving, I., Haegebarth, A., De Palo, M., Anti, M., Van Gijn, M. E., Suijkerbuijk, S., Van de Wetering, M., Marra, G. and Clevers, H. (2007). "The Intestinal Wnt/TCF Signature." *Gastroenterology* **132**(2): 628-632.

van der Flier, L. G., van Gijn, M. E., Hatzis, P., Kujala, P., Haegebarth, A., Stange, D. E., Begthel, H., van den Born, M., Guryev, V., Oving, I., van Es, J. H., Barker, N., Peters, P. J., van de Wetering, M. and Clevers, H. (2009). "Transcription factor achaete scute-like 2 controls intestinal stem cell fate." *Cell* **136**(5): 903-912.

Van der Heiden, M. G., Cantley, L. C. and Thompson, C. B. (2009). "Understanding the Warburg effect: the metabolic requirements of cell proliferation." *Science* **324**(5930): 1029-1033.

van Es, J. H., Kirkpatrick, C., van de Wetering, M., Molenaar, M., Miles, A., Kuipers, J., Destree, O., Peifer, M. and Clevers, H. (1999). "Identification of APC2, a homologue of the adenomatous polyposis coli tumour suppressor." *Curr Biol* **9**(2): 105-108.

van Es, J. H., Sato, T., van de Wetering, M., Lyubimova, A., Yee Nee, A. N., Gregorieff, A., Sasaki, N., Zeinstra, L., van den Born, M., Korving, J., Martens, A. C. M., Barker, N., van Oudenaarden, A. and Clevers, H. (2012). "Dll1+ secretory progenitor cells revert to stem cells upon crypt damage." *Nat Cell Biol* **14**(10): 1099-1104.

van Es, J. H., van Gijn, M. E., Riccio, O., van den Born, M., Vooijs, M., Begthel, H., Cozijnsen, M., Robine, S., Winton, D. J., Radtke, F. and Clevers, H. (2005). "Notch/gamma-secretase inhibition turns proliferative cells in intestinal crypts and adenomas into goblet cells." *Nature* **435**(7044): 959-963.

VanDussen, K. L., Carulli, A. J., Keeley, T. M., Patel, S. R., Puthoff, B. J., Magness, S. T., Tran, I. T., Maillard, I., Siebel, C., Kolterud, A., Grosse, A. S., Gumucio, D. L., Ernst, S. A., Tsai, Y. H., Dempsey, P. J. and Samuelson, L. C. (2012). "Notch signaling modulates proliferation and differentiation of intestinal crypt base columnar stem cells." *Development* **139**(3): 488-497.

Varga, T., Czimmerer, Z. and Nagy, L. (2011). "PPARs are a unique set of fatty acid regulated transcription factors controlling both lipid metabolism and inflammation." *Biochim Biophys Acta* **1812**(8): 1007-1022.

Varga, T., Czimmerer, Z. and Nagy, L. (2011). "PPARs are a unique set of fatty acid regulated transcription factors controlling both lipid metabolism and inflammation()." *Biochimica et Biophysica Acta* **1812**(8): 1007-1022.
Varjosalo, M. and Taipale, J. (2008). "Hedgehog: functions and mechanisms." *Genes Dev* **22**(18): 2454-2472.
Veigl, M. L., Kasturi, L., Olechnowicz, J., Ma, A. H., Lutterbaugh, J. D., Periyasamy, S., Li, G. M., Drummond, J., Modrich, P. L., Sedwick, W. D. and Markowitz, S. D. (1998). "Biallelic inactivation of hMLH1 by epigenetic gene silencing, a novel mechanism causing human MSI cancers." *Proc Natl Acad Sci U S A* **95**(15): 8698-8702.
Vermeulen, L., De Sousa, E. M. F., van der Heijden, M., Cameron, K., de Jong, J. H., Borovski, T., Tuynman, J. B., Todaro, M., Merz, C., Rodermond, H., Sprick, M. R., Kemper, K., Richel, D. J., Stassi, G. and Medema, J. P. (2010). "Wnt activity defines colon cancer stem cells and is regulated by the microenvironment." *Nat Cell Biol* **12**(5): 468-476.
Vermeulen, L., Morrissey, E., van der Heijden, M., Nicholson, A. M., Sottoriva, A., Buczacki, S., Kemp, R., Tavare, S. and Winton, D. J. (2013). "Defining stem cell dynamics in models of intestinal tumor initiation." *Science* **342**(6161): 995-998.
Vermeulen, L. and Snippert, H. J. (2014). "Stem cell dynamics in homeostasis and cancer of the intestine." *Nat Rev Cancer* **14**(7): 468-480.
Verrecchia, F. and Mauviel, A. (2002). "Transforming Growth Factor-β Signaling Through the Smad Pathway: Role in Extracellular Matrix Gene Expression and Regulation." *Journal of Investigative Dermatology* **118**(2): 211-215.
Vigneri, P. G., Tirrò, E., Pennisi, M. S., Massimino, M., Stella, S., Romano, C. and Manzella, L. (2015). "The Insulin/IGF System in Colorectal Cancer Development and Resistance to Therapy." *Frontiers in Oncology* **5**: 230.
Vincan, E. (2004) "Frizzled/WNT signalling: the insidious promoter of tumour growth and progression." Frontiers in bioscience : a journal and virtual library **9**, 1023-1034 DOI: 10.2741/1311.
Vogelstein, B., Papadopoulos, N., Velculescu, V. E., Zhou, S., Diaz, L. A., Jr. and Kinzler, K. W. (2013). "Cancer genome landscapes." *Science* **339**(6127): 1546-1558.
Walther, V. and Alison, M. R. (2016). "Cell lineage tracing in human epithelial tissues using mitochondrial DNA mutations as clonal markers." *Wiley Interdiscip Rev Dev Biol* **5**(1): 103-117.
Walther, V. and Graham, T. A. (2014). "Location, location, location! The reality of life for an intestinal stem cell in the crypt." *J Pathol* **234**(1): 1-4.
Wang, G., Bonkovsky, H. L., de Lemos, A. and Burczynski, F. J. (2015). "Recent insights into the biological functions of liver fatty acid binding protein 1." *J Lipid Res* **56**(12): 2238-2247.
Wang, J., El-Masry, N., Talbot, I., Tomlinson, I., Alison, M. R. and El-Bahrawy, M. (2013). "Expression Profiling of Proliferation and Apoptotic Markers along the Adenoma-Carcinoma Sequence in Familial Adenomatous Polyposis Patients." *Gastroenterology Research and Practice* **2013**: 107534.
Wang, X., Bi, Z., Chu, W. and Wan, Y. (2005). "IL-1 receptor antagonist attenuates MAP kinase/AP-1 activation and MMP1 expression in UVA-irradiated human fibroblasts induced by culture medium from UVB-irradiated human skin keratinocytes." *Int J Mol Med* **16**(6): 1117-1124.
Wang, Y.-X. (2010). "PPARs: Diverse Regulators in Energy Metabolism and Metabolic Diseases." *Cell research* **20**(2): 124-137.

Wasan, H. S., Park, H. S., Liu, K. C., Mandir, N. K., Winnett, A., Sasieni, P., Bodmer, W. F., Goodlad, R. A. and Wright, N. A. (1998). "APC in the regulation of intestinal crypt fission." *J Pathol* **185**(3): 246-255.
Weaver, J. M. J., Ross-Innes, C. S., Shannon, N., Lynch, A. G., Forshew, T., Barbera, M., Murtaza, M., Ong, C. J., Lao-Sirieix, P., Dunning, M. J., Smith, L., Smith, M. L., Anderson, C. L., Carvalho, B., O'Donovan, M., Underwood, T. J., May, A. P., Grehan, N., Hardwick, R., Davies, J., Oloumi, A., Aparicio, S., Caldas, C., Eldridge, M. D., Edwards, P. A. W., Rosenfeld, N., Tavare, S. and Fitzgerald, R. C. (2014). "Ordering of mutations in preinvasive disease stages of esophageal carcinogenesis." *Nat Genet* **46**(8): 837-843.
Weisenberger, D. J., Siegmund, K. D., Campan, M., Young, J., Long, T. I., Faasse, M. A., Kang, G. H., Widschwendter, M., Weener, D., Buchanan, D., Koh, H., Simms, L., Barker, M., Leggett, B., Levine, J., Kim, M., French, A. J., Thibodeau, S. N., Jass, J., Haile, R. and Laird, P. W. (2006). "CpG island methylator phenotype underlies sporadic microsatellite instability and is tightly associated with BRAF mutation in colorectal cancer." *Nat Genet* **38**(7): 787-793.
Welch, H. G. and Black, W. C. (2010). "Overdiagnosis in cancer." *J Natl Cancer Inst* **102**(9): 605-613.
Wells, K. and Wise, P. E. (2017). "Hereditary Colorectal Cancer Syndromes." *Surg Clin North Am* **97**(3): 605-625.
White, B. D., Chien, A. J. and Dawson, D. W. (2012). "Dysregulation of Wnt/beta-catenin signaling in gastrointestinal cancers." *Gastroenterology* **142**(2): 219-232.
Wilhelm, F., Simon, E., Böger, C., Behrens, H.-M., Krüger, S. and Röcken, C. (2017). "Novel Insights into Gastric Cancer: Methylation of R-spondins and Regulation of LGR5 by SP1." *Molecular Cancer Research* **15**(6): 776.
Willert, K., Brown, J. D., Danenberg, E., Duncan, A. W., Weissman, I. L., Reya, T., Yates, J. R., 3rd and Nusse, R. (2003). "Wnt proteins are lipid-modified and can act as stem cell growth factors." *Nature* **423**(6938): 448-452.
Williams, E. D., Lowes, A. P., Williams, D. and Williams, G. T. (1992). "A stem cell niche theory of intestinal crypt maintenance based on a study of somatic mutation in colonic mucosa." *Am J Pathol* **141**(4): 773-776.
Wittig, B. M. and Zeitz, M. (2003). "The gut as an organ of immunology." *Int J Colorectal Dis* **18**(3): 181-187.
Woda, B. A., Forde, K. and Lane, N. (1977). "A Unicryptal Colonic Adenoma, the Smallest Colonic Neoplasm Yet Observed in a Non-polyposis Individual." *American Journal of Clinical Pathology* **68**(5): 631-632.
Wolfrum, C., Borrmann, C. M., Borchers, T. and Spener, F. (2001). "Fatty acids and hypolipidemic drugs regulate peroxisome proliferator-activated receptors alpha - and gamma-mediated gene expression via liver fatty acid binding protein: a signaling path to the nucleus." *Proc Natl Acad Sci U S A* **98**(5): 2323-2328.
Wong, J. J., Hawkins, N. J., Ward, R. L. and Hitchins, M. P. (2011). "Methylation of the 3p22 region encompassing MLH1 is representative of the CpG island methylator phenotype in colorectal cancer." *Mod Pathol* **24**(3): 396-411.
Wong, S. C., Lo, E. S., Lee, K. C., Chan, J. K. and Hsiao, W. L. (2004). "Prognostic and diagnostic significance of beta-catenin nuclear immunostaining in colorectal cancer." *Clin Cancer Res* **10**(4): 1401-1408.
Wong, W. M., Mandir, N., Goodlad, R. A., Wong, B. C. Y., Garcia, S. B., Lam, S. K. and Wright, N. A. (2002). "Histogenesis of human colorectal adenomas and hyperplastic polyps: the role of cell proliferation and crypt fission." *Gut* **50**(2): 212-217.

Wood, S. M., Gill, A. J., Brodsky, A. S., Lu, S., Friedman, K., Karashchuk, G., Lombardo, K., Yang, D. and Resnick, M. B. (2017). "Fatty acid-binding protein 1 is preferentially lost in microsatellite instable colorectal carcinomas and is immune modulated via the interferon gamma pathway." *Mod Pathol* **30**(1): 123-133.
Worthley, D. L., Giraud, A. S. and Wang, T. C. (2010). "Stromal Fibroblasts in Digestive Cancer." *Cancer Microenvironment* **3**(1): 117-125.
Wu, C. (2007). "Focal Adhesion: A Focal Point in Current Cell Biology and Molecular Medicine." *Cell Adhesion & Migration* **1**(1): 13-18.
Wu, G., Fang, Y. Z., Yang, S., Lupton, J. R. and Turner, N. D. (2004). "Glutathione metabolism and its implications for health." *J Nutr* **134**(3): 489-492.
Wu, M., Pastor-Pareja, J. C. and Xu, T. (2010). "Interaction between Ras(V12) and scribbled clones induces tumour growth and invasion." *Nature* **463**(7280): 545-548.
Xu, L., Wang, R., Ziegelbauer, J., Wu, W. W., Shen, R. F., Juhl, H., Zhang, Y., Pelosof, L. and Rosenberg, A. S. (2017). "Transcriptome analysis of human colorectal cancer biopsies reveals extensive expression correlations among genes related to cell proliferation, lipid metabolism, immune response and collagen catabolism." *Oncotarget* **8**(43): 74703-74719.
Xu, S., Khoo, S., Dang, A., Witt, S., Do, V., Zhen, E., Schaefer, E. M. and Cobb, M. H. (1997). "Differential regulation of mitogen-activated protein/ERK kinase (MEK)1 and MEK2 and activation by a Ras-independent mechanism." *Mol Endocrinol* **11**(11): 1618-1625.
Yadav, N., Kumar, S., Marlowe, T., Chaudhary, A. K., Kumar, R., Wang, J., O'Malley, J., Boland, P. M., Jayanthi, S., Kumar, T. K. S., Yadava, N. and Chandra, D. (2015). "Oxidative phosphorylation-dependent regulation of cancer cell apoptosis in response to anticancer agents." *Cell Death & Disease* **6**(11): e1969.
Yamagishi, H., Kuroda, H., Imai, Y. and Hiraishi, H. (2016). "Molecular pathogenesis of sporadic colorectal cancers." *Chinese Journal of Cancer* **35**: 4.
Yamamoto, H., Sawai, H. and Perucho, M. (1997). "Frameshift somatic mutations in gastrointestinal cancer of the microsatellite mutator phenotype." *Cancer Res* **57**(19): 4420-4426.
Yamazaki, T., Kanda, T., Sakai, Y. and Hatakeyama, K. (1999). "Liver fatty acid-binding protein is a new prognostic factor for hepatic resection of colorectal cancer metastases." *J Surg Oncol* **72**(2): 83-87.
Yan, K. S., Janda, C. Y., Chang, J., Zheng, G. X. Y., Larkin, K. A., Luca, V. C., Chia, L. A., Mah, A. T., Han, A., Terry, J. M., Ootani, A., Roelf, K., Lee, M., Yuan, J., Li, X., Bolen, C. R., Wilhelmy, J., Davies, P. S., Ueno, H., von Furstenberg, R. J., Belgrader, P., Ziraldo, S. B., Ordonez, H., Henning, S. J., Wong, M. H., Snyder, M. P., Weissman, I. L., Hsueh, A. J., Mikkelsen, T. S., Garcia, K. C. and Kuo, C. J. (2017). "Non-equivalence of Wnt and R-spondin ligands during Lgr5+ intestinal stem-cell self-renewal." *Nature* **545**(7653): 238-242.
Yang, L., Tang, H., Kong, Y., Xie, X., Chen, J., Song, C., Liu, X., Ye, F., Li, N., Wang, N. and Xie, X. (2015). "LGR5 Promotes Breast Cancer Progression and Maintains Stem-Like Cells Through Activation of Wnt/beta-Catenin Signaling." *Stem Cells* **33**(10): 2913-2924.
Yao, H., Li, P., Venters, B. J., Zheng, S., Thompson, P. R., Pugh, B. F. and Wang, Y. (2008). "Histone Arg Modifications and p53 Regulate the Expression of OKL38, a Mediator of Apoptosis." *The Journal of Biological Chemistry* **283**(29): 20060-20068.
Yatabe, Y., Tavaré, S. and Shibata, D. (2001). "Investigating stem cells in human colon by using methylation patterns." *Proceedings of the National Academy of Sciences* **98**(19): 10839-10844.

Yen, T. H., Chen, Y., Fu, J. F., Weng, C. H., Tian, Y. C., Hung, C. C., Lin, J. L. and Yang, C. W. (2010). "Proliferation of myofibroblasts in the stroma of renal oncocytoma." *Cell Prolif* **43**(3): 287-296.
Young, M. A., Daly, C. S., Taylor, E., James, R., Clarke, A. R. and Reed, K. R. (2018). "Subtle Deregulation of the Wnt-Signaling Pathway Through Loss of Apc2 Reduces the Fitness of Intestinal Stem Cells." *Stem Cells* **36**(1): 114-122.
Zdunek, M., Silbiger, S., Lei, J. and Neugarten, J. (2001). "Protein kinase CK2 mediates TGF- β ;1-stimulated type IV collagen gene transcription and its reversal by estradiol1." *Kidney International* **60**(6): 2097-2108.
Zeki, S., Graham, T. A. and McDonald, S. A. (2012). "Utilizing DNA mutations to trace epithelial cell lineages in human tissues." *Methods Mol Biol* **916**: 289-301.
Zhan, T., Rindtorff, N. and Boutros, M. (2017). "Wnt signaling in cancer." *Oncogene* **36**(11): 1461-1473.
Zhang, Q. W., Liu, L., Gong, C. Y., Shi, H. S., Zeng, Y. H., Wang, X. Z., Zhao, Y. W. and Wei, Y. Q. (2012). "Prognostic significance of tumor-associated macrophages in solid tumor: a meta-analysis of the literature." *PLoS One* **7**(12): e50946.
Zhang, Y., Sime, W., Juhas, M. and Sjolander, A. (2013). "Crosstalk between colon cancer cells and macrophages via inflammatory mediators and CD47 promotes tumour cell migration." *Eur J Cancer* **49**(15): 3320-3334.
Zheng, J. (2012). "Energy metabolism of cancer: Glycolysis versus oxidative phosphorylation (Review)." *Oncol Lett* **4**(6): 1151-1157.
Zhong, X., Chen, B. and Yang, Z. (2018). "The Role of Tumor-Associated Macrophages in Colorectal Carcinoma Progression." *Cellular Physiology and Biochemistry* **45**(1): 356-365.
Zou, W. (2006). "Regulatory T cells, tumour immunity and immunotherapy." *Nat Rev Immunol* **6**(4): 295-307.

9 Appendix

Primer	Sequence 5' to 3'	Position
MTL1-F	AAAGCACATACCAAGGCCAC	9397
MTL1-R	TTGGCTCTCCTTGCAAAGTT	1873
FRAG1-F	TATCCGCCATCC CATACATT	15195
FRAG1-R	AATGTTGAGCCGTAGATGCC	9777

Table 9.1: Primer sequences for mtDNA PCR for frozen samples.

			Crypts/sections				Total #crypts across all sections			
Sample	**# adenomas**	**# serial sectons cut on LCM**	**# crypts/ adenoma**	**# crypts/ zone 1**	**# crypts/ zone 2**	**# crypts/ zone 3**	**# crypts/ adenoma**	**# crypts/ zone 1**	**# crypts/ zone 2**	**# crypts/ zone 3**
FAP1	Adenoma 1	6	25	22	14	15	150	132	84	90
	Adenoma 2	3	5	12	17	19	15	36	51	57
	Adenoma 3	8	15	18	13	18	120	144	104	144
FAP2	Adenoma 1	3	10	30	22	24	30	90	66	72
	Adenoma 2	8	33	46	32	21	264	368	256	168
FAP3	Adenoma 1	7	15	13	15	15	115	104	115	116
	Adenoma 2	6	22	11	14	11	116	67	65	51
	Adenoma 3	5	12	28	28	20	51	140	140	100
FAP4	Adenoma 1	4	10	2	5	7	40	8	20	28
	Adenoma 2	8	16	14	10	15	128	112	80	120

Table 9.2: Number of crypts laser capture microdissected in each zone.

Primer	Sequence 5' to 3'
Gapdh	TTGTGGAAGGGCTCATGACC
	TCTTCTGGGTGGCAGTGATG
Pold2	CATGGAAGACCACTTAGAGATCC
	TTGTAGAAGGGGTAGCACCCTA
Pold3	CAGCTGTATCTAGAAAACATAGACGAG
	GCTTAGCCACTTGTAAGTCACG
Pold4	TGGCAGTATGGGCCTTGTA
	AGGGTGTGCCTTCAACACTT
Pole	CGCTGCACAACATGATGAA
	GAATGATGCGATTGAAGTTGG
Mcm4	CCTTTTAATGCGTTGAAGACAA
	CGGAATCAGCTGTGATGTTC
Mcm6	ACCTGTACCACAATCTCTGCAC
	CACCGCGTTTTACTTCATCA
Mlh1	TTGAAAGTCTCAGTAAAGAATGTGC
	GGAGCCAGGCATGTCACT
Msh6	CAGCTGGCAGTGTGTGATG
	GATAAATAAGCCTCATGCACCTC
Bax	AGTGTCTCCGGCGAATTG
	CCACGTCAGCAATCATCCT
Casp6	TGAAATGCTTTAACGACCTCAG
	GTGGCTTGAAGTCGACACCT
Tnf-α	CTGTAGCCCACGTCGTAGC
	TTTGAGATCCATGCCGTTG
MMP9	AGACGACATAGACGGCATCC
	TCGGCTGTGGTTCAGTTGT
Col4a1	TGGCACAAAAGGGACGAG
	GGCCAGGAATACCAGGAAGT
Col6a2	GTACCCAGGCATCTTCTCCA
	AAGAGTCCCCCAATCAGGAG
Col9a1	CGCTTGTGTGCTGCTCAA
	TCTATGCCCGGAACTCCA
TLR4	GGACTCTGATCATGGCACTG
	CTGATCCATGCATTGGTAGGT
c-Fos	GGGACAGCCTTTCCTACTACC
	AGATCTGCGCAAAAGTCCTG
c-Jun	TGATCATCCAGTCCAGCAAT
	TTGGGGCACAAGAACTGG

Table 9.3: Primer sequences for qRT-PCR.

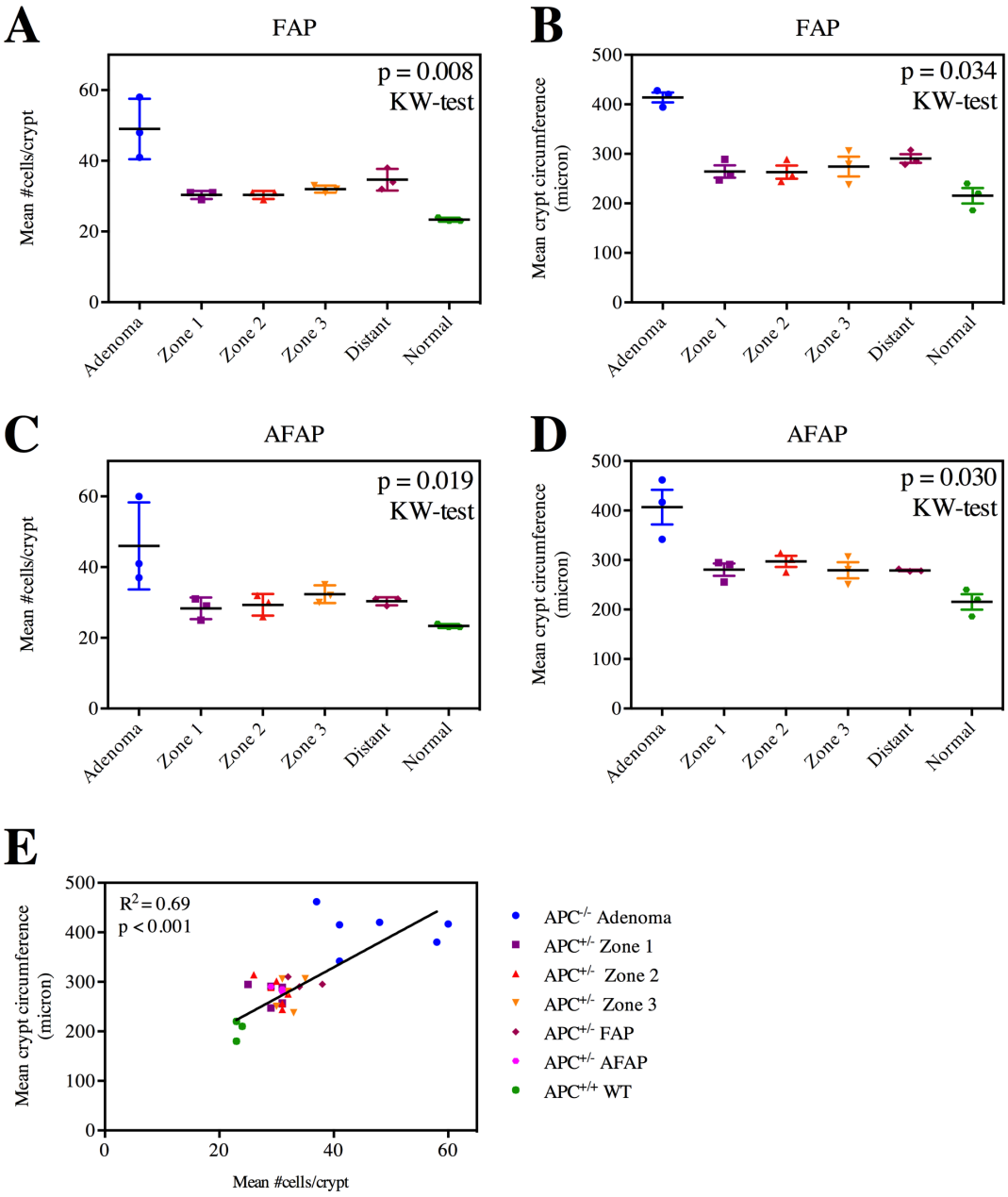

Figure 9.1: Mean cell number and mean circumference per crypt.
Average number of cells per crypt circumference was counted for FAP (A) and AFAP (C) patients, as well as the crypt circumference for FAP (B) and AFAP (D) patients measured manually in H&E sections of adenomatous colonic crypts, non-dysplastic crypts in zone 1 – 3, distant non-dysplastic crypts, and non-dysplastic colonic crypts in normal tissue sections. Each point on the graph represents the average number of cells (A, C) and the average crypt circumference (B, D) in one patient, which was obtained by analysing at least 20 representative crypts. The line within each count represents the mean. A) Kruskal-Wallis: p = 0.008. B) Kruskal-Wallis: p = 0.034, C) Kruskal-Wallis: p = 0.019, D) Kruskal-Wallis: p = 0.03. E) shows the correlations between the number of cells and the mean circumference per crypt.